STRUCTURE AND FUNCTION OF COLICIN A/CAI AND PUTP STUDIED BY SITE DIRECTED SPIN LABELING EPR SPECTROSCOPY

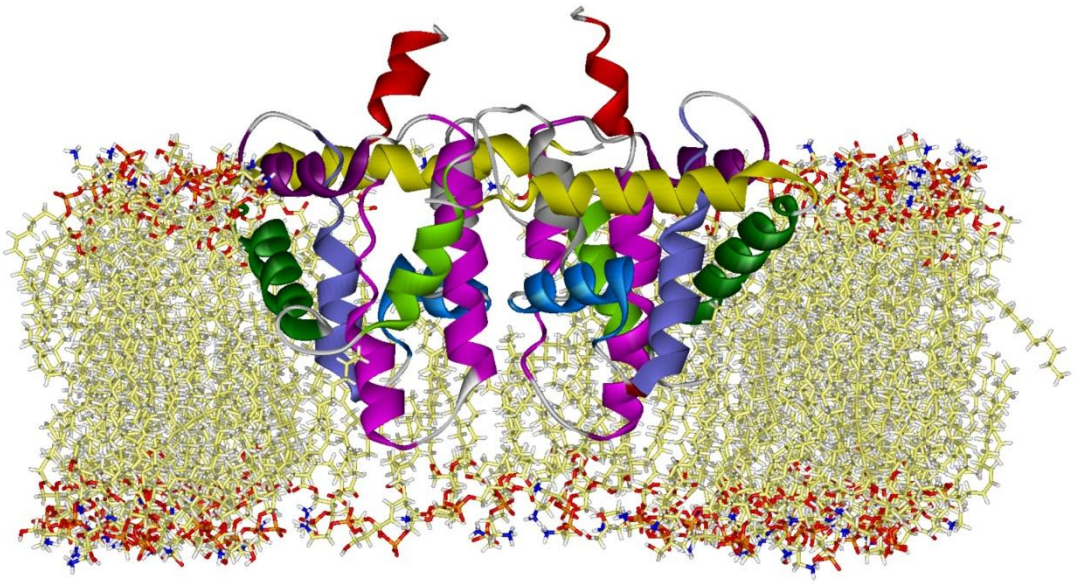

STRUCTURE AND FUNCTION OF COLICIN A/CAI AND PUTP STUDIED BY SITE DIRECTED SPIN LABELING EPR SPECTROSCOPY

Dissertation

submitted for the degree of
Dr. rer. nat. (Doctor of Natural Sciences)
in the Department of Biology
University of Osnabrueck, Germany

by

Dipl.-Biol. Sabrina Dunkel

from Georgsmarienhütte

UNIVERSITÄT OSNABRÜCK

September

2014

Contents

Abbrevations

AA	Acrylamide
APS	Ammoniumpersulfate
ATP	Adenosin-5'-triphosphate
BCA	Bicinchoninacid
BSA	Bovine Serum Albumin
CL	Cardiolipin
CMC	Critical micelle concentration
Cryo-EM	Cryo-electron microscopy
Cw	Continuous wave
DEER	Double Electron-Electron Resonance
DMSO	Dimethylsulfoxide
DTT	1, 4-Dithio-DL-threitol
EDTA	Ethylenediaminetetra-acetic acid
eL	Extracellular Loop
eL4	Extracellular Loop
ELDOR	Electron Double Resonance
EPR	Electron paramagnetic resonance
Ev	Eigenvector
Fig	Figure
FPLC	Fast performance liquid chromatography
FRET	Fluorescence/Förster resonance energy transfer
FTIR	Fourier transform infrared spectroscopy
GdHCl	Guanidinium Hydrochloride
i	Immobile component
iL	Intracellular Loop
IM	Inner membrane
IPTG	Isopropyl-β-D-thiogalactopyranosid
kDA	Kilo dalton
LB	Lysogeny Broth, "Luria broth" media
LMV	Large multilamellar vesicles
LUV	Large unilamellar vesicles
m	Mobile component
MD	Molecular dynamics
MG	Molten globule
MMM	Mulitiscale Modeling of Macromolecules

MTS	Methanethiosulphonate
MW	Molecular weight
MWC	Molecular weight cut off
NaPi	Sodium phosphate
Ni-EDDA	Nickel ethylene diamine diacetic acid
NMR	Nuclear magnetic resonance
NTA	Nitrilotriacetidacid
OD	Optical density
PAGE	Polyacrylamide gel electrophoresis
PAP	loading buffer
PC	1-palmitoyl-2-stearoyl-(5-doxyl)-*sn*-glycero-3-phosphocholine
PCR	Polymerase-chain reaction
PDB	Protein data bank
PEP	Phosphoenolpyruvate
P_i	Anorganic phosphate
Pmf	Proton motive force
PMSF	Phenylmethylsulfonylfluoride
POPE	1-palmitoyl-2-oleoyl-sn-glycero-3-phosphoethanolamine
POPG	1-palmitoyl-2-oleoyl-sn-glycero-3-phosphoglycerol
POPS	1-palmitoyl-2-oleoyl-sn-glycero-3-phosphoserine
rec-mem-ColA	Reconstituted membrane-bound colicin A
R1	Spin-labeled side chain (MTSSL)
RT	Room temperature
rpm	Rounds per minute
Sa	Doxyl-stearic acids
SDS	Natriumdodecylsulfate
SDSL	Site-directed spin labeling
sol-ColA	Water soluble colicin A
SSS	Na^+/solute symporter
SSSF	Sodium solute symporter family
TCA	Trichloroacetic acid
TEA	Tetraethylammonium
TEMED	N, N, N', N'-Tetramethylethylendiamine
TEMPO	2,2,6,6-Tetramethyl-1-piperidinyloxy
TM	Transmembrane domain

Tris	Tris (hydroxymethyl) aminomethan
Triton-X-100	Polyethylenglycol-mono [p-(1,1,3,3-tetramethyl-butyl)-phenyl]-ether
UV	ultra violet
WT	Wild type cells

CHAPTER 1
Introduction and Motivation

1. Introduction and Motivation

Proteins are biological macromolecules and one of the major constituents of living cells. They are vital for all kinds of life and perform a vast array of functions, being responsible for a cell's structure, the catalysis of chemical reactions, and are used for energy conversion, signal delivery within and between cells, and the transport of other molecules (for example nutrients) from one location to another, the latter especially across biological membranes. Furthermore, some organisms, like for example bacteria, use proteins to kill other cells, to increase their own probability to survive.

Proteins are linear polymers consisting of one or more amino acid chains. All existing proteins are different in their sequence of amino acids, which is genetically encoded and determines the protein's properties by means of the "folding" of the protein into a specific three-dimensional structure. Detailed knowledge about a protein's structure and its dynamics is therefore a necessary condition to understand the functionality of a protein.

There is a variety of methods to gain structural information, like X-ray crystallography (Drenth, 1999), Nuclear Magnetic Resonance (NMR) spectroscopy (Wagner et al., 1992) and cryo-electron microscopy (cryo-EM) (Henderson, 2004). However, by far not all existing proteins can be subjected to those methods due to methodological limitations. Furthermore, even if structural information about a protein can be obtained with one of them, it has always to be questioned if the structure determined properly reflects the properties of the protein within its natural environment, the cell. For example most of the available protein structures (≈ 90 %) in the protein database (http://www.rcsb.org/pdb/) have been determined by X-ray crystallography. However, this experiment is mostly limited by the recovery of biomolecules in crystals and furthermore restricts the natural flexibility of the proteins (Fernandez et al., 2003). Moreover, crystal packing effects, i.e. contacts between the proteins in the crystals – being necessary for crystal formation but not present in cells – can alter the protein's structure and lead to severe misinterpretation of the data concerning protein function. At present protein structures determined by Nuclear Magnetic Resonance (NMR) techniques constitute roughly nine percent of all available structures. The disadvantage of this method concerns the size limitation for the protein under investigation. Although sophisticated isotope labeling techniques have been established to overcome this drawback, this methodology is still limited to proteins of the size of a few ten kilo Daltons. Furthermore, for both of these methods relatively large amounts of the protein are necessary - a limitation that often hampers investigations especially on mammalian proteins that cannot be produced in large amounts. Finally, cryo-electron microscopy (cryo-EM), which is also applicable to very large proteins or protein complexes and does not require very large amounts, has the disadvantage of a limited resolution of ca. 0.5-0.8 nm, yielding information about a proteins overall fold, but not about molecular details necessary to understand its function. Finally, also the possibility to predict a protein's structure (and function) directly from its primary sequence should be mentioned here, although its applicability and reliability are still very much

limited. Most of the currently used approaches for *in silico* structure prediction therefore rely on comparison with proteins of known structure on the basis of their primary sequence – an approach called 'homology modeling'. A number of algorithms have been developed to identify the largest possible contiguous identical or similar portions in the amino acid sequence of the proteins (Needleman et al., 1970) (Waterman, 1984) (Taylor et al., 1989). Programs such as FASTA (Pearson 1990) (Pearson and Lipman, 1988) and SWISS-PROT (Bucher and Bairoch, 1994) (Boeckmann et al., 2003) have been created that implement these algorithms. One recent example – being of special relevance for this thesis - for homology modeling is a model for the sodium/proline symporter PutP based on the crystal structure of the bacterial Na^+/galactose symporter vSGLT (Olkhova et al., 2010). Very important in this context is that the structural predictions from such computational methods are verified by experimental methods. Fortunately, *vice versa* experimental data, for example distances between specific points in the primary sequence or information about side chain specific local properties like motional freedom or polarity, can be used to assist *in silico* modeling.

Two biophysical methods are particularly suited to provide structural constraints: Fluorescence / Förster Resonance Energy Transfer (FRET) (Chattopadhyay et al., 2010) (Heuck and Johnson, 2002) and site-directed spin labeling (SDSL) in combination with Electron Paramagnetic Resonance (EPR) spectroscopy. The FRET method uses so called chromophores, and is a very potent tool to study proteins based on the opportunity to determine the distance between two chromophores and the possibility to operate under physiological conditions, for example at biological temperatures, like room and elevated temperatures, important for the study of proteins from thermophilic organisms (Grohmann et al., 2010), or even *in vivo* (Wouters et al., 2001). However, fluorescence labels are often large and comprise a long linker for protein attachment to minimize disturbance of the protein structure. Labeling of proteins for FRET measurements is complicated by the fact that usually two different (donor and acceptor) molecules have to be attached at the two label positions. Furthermore, the pair of chromophores to be chosen for the respective experiment depends on distance that should be measured, requiring at least knowledge about the expected distance range. Finally, due to the relatively large aromatic moieties which comprise the interacting dipoles in this method, difficulties arise for interpretation of the distance data in terms of molecular structure because of the uncertainties in localization of the points in between the distance is actually determined by the experiment. Consequently, the resolution in terms of structure of this technique is generally lower compared to X-ray crystallography and NMR spectroscopy (Hemminga et al., 2007).

Alternatively, cw- and pulse electron paramagnetic resonance (EPR) spectroscopy in combination with site directed spin labeling can be applied to analyze protein structures and conformational changes (Altenbach et al., 1990). The method provides structural and dynamic information also under physiological conditions and this approach is applicable to soluble molecules as well as membrane bound proteins either being solubilized in detergent or embedded in a lipid bilayer. Especially the fact that EPR experiments can be easily performed also on lipid-reconstituted samples – contrary to most other structural techniques (see above) – render SDSL EPR spectroscopy a highly valuable tool for studying

membrane proteins. With the help of various EPR methods it is possible to get a wealth of information about the environment, the protein structure, structural changes and the corresponding functionality. Especially, analogous to FRET, EPR allows also the determination of inter-residue distances using doubly labeled proteins in order to generate three-dimensional models of proteins with largely unknown structure (Hemminga et al., 2007 /2011). Compared to FRET the SDSL EPR method has two major advantages. First, the spin label side chain can be relatively small, further minimizing disturbance of the labeled proteins' local structure, but also simplifying interpretation of inter spin-distances between two spin labels. In addition, due to location of the label in closer proximity to the protein backbone it reports with higher spatial resolution on the proteins local properties. Second, in EPR spectroscopy the paramagnetic centers between which distance measurements have to be performed can be identical, simplifying also protein labeling itself.

SDSL EPR has already been widely used to generate three dimensional protein structure models. As mentioned above, the method is particularly suitable for investigations of membrane proteins, like for example the sodium/proline symporter PutP (Hilger et al., 2007), bacteriorhodopsin (Altenbach et al., 1990) and the lactose permease (Voss et al., 1996/1997). Examples of soluble proteins comprise e.g. HSp16.5, a small heat-shock protein (Koteiche et al., 2005), αA-crystallin (Koteiche et al., 1998) and fibril-forming proteins like α-synuclein (Der-Sarkissian et al., 2003) (Drescher et al., 2008). Furthermore, this method emerged as a powerful tool for investigating protein function and dynamics, nicely exemplified by the detailed analyses of the archaebacterial phototaxis-mediating SRII/HtrII complex by SDSL EPR spectroscopy (Klare et al., 2007) (Klare et al., 2011) (Bordignon et al., 2005) (Bordignon and Steinhoff, 2007), and protein-protein interactions. Examples for the latter are studies on the homodimeric protein MnmE (Boehme et al., 2010), the homotrimer Glt_{PH} (Hänelt et al., 2013) and also comprise protein-nucleic acid interactions, like investigations on the dimeric transcriptional repressor LexA in complex with DNA (Butala et al., 2011).

In this work 3 different proteins are subjected to investigations on their structural, dynamic and functional properties by SDSL EPR spectroscopy, combined with *in silico* structure prediction and modeling: the pore-forming bacterial toxin colicin A in its membrane-bound form and its corresponding immunity protein Cai, and the Na^+/proline symporter PutP, all from *E. coli*. These systems and the motivations for studying them in this work are briefly described in the following paragraphs.

1.1 Structure of the colicin A pore-forming domain in *E. coli* lipids

Pore-forming proteins play a central role in many biological functions (Pugsley, 1984). These toxins belong to a special class of proteins, which are secreted as water-soluble proteins and insert into the cell membrane of attacked cells to open pores (Cramer, 1995) (Panchal, 2002) (Smarda and Smajs, 1998).
The analysis of bacterial toxins like those of the colicin family first of all provides an additional basis for understanding microbial defense mechanisms in general. Secondly, colicins are only active against specific other bacterial strains, and analyzing the mechanistic bases for this specificity can provide essential information for designing antibiotics (Panchal, 2002). Furthermore, some studies reported that colicins can selectively kill tumor cells (Smarda et al., 2001) (Fuska et al., 1979) (Walker et al., 2004). Finally, the structural motif of colicin pore-forming domains is also present in other pore-forming toxins (PFTs) like Diphtheria toxin, Bax or Aerolysin. Members of the Bcl-2-family - like Bax – comprise a major part of a cell's apoptotic machinery and it has been shown that they can act as tumor suppressors (Strasser et al., 2000). The property of e.g. Bax to permeabilize biological membranes gives rise for potential medical applications, like cancer chemotherapy dependent on programmed cell death (Strasser et al., 2000). Nevertheless, despite intense research in the past decades for none of the pore forming proteins mentioned above comprehensive and unambiguous structural information exist yet for their membrane bound states.

Colicin A (ColA) is a plasmid-encoded water-soluble pore-forming toxin produced by certain *E. coli* strains (Cascales et al., 2007). The protein kills unprotected cells of related strains by inserting specific helical segments of the pore-forming subdomain into the cytoplasmic membrane to form voltage-dependent ion channels. The crystal structure of the soluble form of the pore-forming domain has been solved, but detailed structural data for the membrane-bound channel, in the closed as well as in the open state, is still missing. In the present study, previous *in vitro* investigations by site-directed spin labeling and EPR spectroscopy (Pulagam et al., 2008) (Pulagam and Steinhoff, 2013) (Boehme et al., 2009) (Savitsky et al., 2004) have been substantially extended, including mobility, polarity, accessibility and inter spin distance measurements. In addition, inter spin distances measurement under *in vivo* conditions have been performed. This part of the work aims at a better understanding of the structural features of the membrane bound closed channel state of colicin A.

1.2 Structure of the colicin A pore-forming domain under influence of the immunity protein Cai. The topology of the colicin A/Cai complex

The protein Cai protects colicin A producing cells against the cytotoxic activity of its corresponding colicin. The immunity protein is an integral inner membrane protein that diffuses in the membrane and interacts with the helices of the pore-forming domain of colicin A to prevent it from opening the voltage-

dependent ion channel. Information about the immunity protein Cai is very limited, and consequently the mechanism for Cai action is still obscure. In general, two possibilities to prevent opening of the colicin A channel can be envisioned: either by stabilisation of the ColA closed channel state, or by inducing a conformation of colicin not competent for channel opening. In the present study the influence of Cai on colicin A is investigated by mobility, polarity and inter-spin distance measurements on spin labeled ColA in the presence of Cai as well as on Cai labeled at it's native cysteine residues to gain more insights into this poorly understood protein-protein interaction.

1.3 Structure and functional dynamics of Extracellular Loop 4 eL4 of the *E. coli* Na^+/proline symporter PutP

PutP is an integral membrane protein located in the cytoplasmic membrane of *E. coli*, being responsible for the coupled transport of Na^+ and proline in a 1:1 stoichiometry. It belongs to the family of sodium solute symporters (SSS). The mediated proline uptake by PutP is part of anabolic and metabolic pathways. The functions of the PutP transporters are different. For example the Na^+/ proline transporter of *Bacillus subtilis* is involved in cell adaption to osmotic stress (Spiegelhalter and Bremer, 1998), PutP in *Helicobacter pylori* and *Staphylococcus aureus* presents an essential virulence factor which was shown by functional inactivation of respective genes which prevents stomach colonization by *H. pylori* (Kavermann et al., 2003). A dysfunction of human PutP homologues like the Na^+/ glucose cotransporter (SGLT1) and the sodium / iodide symporter (NIS) results in glucose-galactose malabsorption and in an iodide transport defect (Dohan et al., 2003) (Wright et al., 2007). Structural data for PutP is not available, but secondary structure predictions together with biochemical and biophysical analyse suggest a 13 transmembrane helix motif with the N-terminus facing the periplasm and the C-terminus facing the cytoplasm. Recently, a homology model has been developed based on the crystal structure of another member of this protein family, the Na^+/galactose symporter vSGLT of *Vibrio parahaemolyticus* (Olkhova et al., 2011). To refine the homology model, in this work the structural properties of the extracellular loop 4 (eL4) of PutP are investigated by EPR analyses of a series of spin labeled PutP variants comprising each individual loop position. Furthermore, possible conformational changes induced by the two substrates, sodium and proline, are investigated. Analyses of spin label mobility and polarity as well as accessibility to paramagnetic quenchers and inter spin distances measurements allow us to refine the present homology model, especially concerning the extent of α-helical segments.

1.4 Bibliography

Altenbach et al., 1990 — Altenbach, C., Marti, T., Khorana, H. and Hubbell, W. L. (1990) A Method to determine transmembrane protein structure: spin labeling of bacteriorhodopsin mutants. *Science* **248**:1088–1093

Boehme et al., 2009 — Boehme S, Pulagam L. P., Holterhues J, Ouchni F, Klare JP, Steinhoff H.-J. (2009) Topology of the amphipathic helices of the colicin A pore-forming domain in *E. coli* lipid membranes studied by pulse EPR. *Phys. Chem. Chem. Phys.* **31**:6770-6777

Bordignon et al., 2005 — Bordignon, E., Klare, J.P., Doebber, M. A., Wegener, A. A., Martell, S., Engelhard, M., and Steinhoff, H.-J. (2005) Structural analysis of a HAMP domain: the linker region of the photo transducer in complex with sensory rhodopsin II. *J. Biol. Chem.* **280:**38767–38775

Bordignon and Steinhoff, 2007 — Bordignon, E., and Steinhoff, H.-J. (2007) Membrane protein structure and dynamics studied by site-directed spin labeling ESR. In: ESR Spectroscopy in Membrane Biophysics, M.A. Hemming and L.J. Berliner, eds. (New York: Springer Science and Business Media), pp. 129–164.

Boeckmann et al., 2003 — Boeckmann B., Bairoch A., Apweiler R., Blatter M., Estreicher A., Gasteiger E., Martin M., Michoud K., O'Donovan C., Phan I., Pilbout S., and Schneider M. (2003) The SWISS-PROT protein knowledgebase and its supplement TrEMBL in 2003. *Nucleic. Acids. Res.* **31**:365-370

Bucher and Bairoch, 1994 — Bucher, P. and Bairoch, A. (1994) A generalized profile syntax for biomolecular sequence motifs and its function in automatic sequence interpretation. *In. Proc. Int. Conf. Intell. Syst. Mol. Biol.* 53-61

Butala et al., 2011 — Butala M., Klose D., Hodnik V., Rems A., Podlesek Z., Klare J.P., Anderluh G., Busby S.J., Steinhoff H.J., Zgur-Bertok D. (2011) Interconversion between bound and free conformations of LexA orchestrates the bacterial SOS response. *Nucleic Acids Res.* **39**:6546-57

Cascales et al., 2007 — Cascales, E. K. Buchanan S.K., Duché D., Kleanthous, C. Lloube's, R. Postle, K. Riley, M. Slatin, S. and Cavard, D. (2007) Colicin Biology. *Microbiol. Mol. Biol. Rev.* **71**:158-229

Chattopadhyay et al., 2010 — Chattopadhyay, A., Raghuraman, H. (2010) Application of fluorescence spectroscopy to membrane protein structure and dynamics. *Current Science* **87**:175-180

Cramer, 1995 — Cramer, W.A. (1995) Structure-function of the channel-forming colicins. *Annu. Rev. Biophys. Biomol. Struct.* **24**:611-641

Der-Sarkissian et al., 2003 — Der-Sarkissian, A., Jao, C.C., Chen, J., and Langen, R. (2003) Structural organization of a-synuclein fibrils studied by site-directed spin labeling. *J. Biol. Chem.* **278:**37530–37535

Dohan et al., 2003 — Dohan, O., A. De la Vieja, V. Paroder, C. Riedel, M. Artani, M. Reed, C. S. Ginter and N. Carrasco, (2003) The sodium/iodide Symporter (NIS): characterization, regulation, and medical significance. *Endocr. Rev.* **24**:48-77

Drenth, J. 1999 — Drenth, J. (1999) Principles of Protein X-Ray Crystallography, Springer-Verlag, Berlin

Drescher et al., 2008 — Drescher, M., Veldhuis, G., van Rooijen, B.D., Milikisyants, S., Subramaniam, V., and Huber, M. (2008) Antiparallel arrangement of the helices of vesicle-bound a-synuclein. *J. Am. Chem. Soc.* **130***:*7796–7797

Fernandez et al., 2003 — Fernandez, C., Wüthrich, K. (2003) NMR solution structure determination of membrane proteins reconstituted in detergent micelles. *FEBS Lett.* **555**:44-150

Fuska, 1979 — Fuska, J. (1979) Effect of colicin E3 on leukemia cells P388 in vitro. *Experientia* **35**:406-407

Grohman et al., 2010 — Grohmann, D., Klose, D., Klare, J.P., Kay, C.W.M., Steinhoff, H.-J., and Werner, F. (2010) RNA-binding to archaeal RNA polymerase subunits F/E: a DEER and FRET study. *J. Am. Chem. Soc.* **132**:5954–5955

Henderson, 2004 — Henderson, R. (2004) Realizing the potential of electron cryo-microscopy. *Q. Rev. Biophys*. **37**:3-13

Hemminga et al., 2007 — Hemminga, M.A., Jeschke, G., Strancar, J., Fajer, P.G., Brown, L., Song, L., Bordignon, E., Steinhoff, H.-J., Smirnova, T.I., Smirnov, A.I., Fajer, M.I., Sale, K.L., Nilges, M.J., Mattson, K., Belford, R.L., Freed, J.H., Stoll, S. and Schweiger, A. (2007) Biological Magnetic Resonance Vol. **27**: ESR Spectroscopy in Membrane Biophysics. Springer, 379 pp.

Heuck and Johnson, 2002 — Heuck, A.P., Johnson, A.E. (2002) Pore-forming protein structure analysis in membranes using multiple independent fluorescence techniques. *Cell Biochem. Biophys.* **36**:89-101

Hilger et al., 2007 — Hilger, D., Polyhach, Y., Padan, E., Jung, H. and Jeschke, G. (2007) High-resolution structure of a Na^+ /H^+ antiporter dimer obtained by pulsed electron paramagnetic resonance distance measurements. *Biophys. J.* **93** 3675–3683

Hänelt et al., 2013 — Hänelt, I., Wunnicke, D., Bordignon, E., Steinhoff, H.-J., and Slotboom, D.J. (2013) Conformational heterogeneity of the aspartate transporter GltPh. *Nat. Struct. Mol. Biol.* **20***:*201–214.

Kavermann et al., 2003 — Kavermann, H., Burns, B. P., Angermuller, K., Odenbreit, S., Fischer, W., Melchers, K., and Haas, R. (2003) Identification and characterization of *Helicobacter pylori* genes essential for gastric colonization. *J. Exp. Med.* **197**:813-822

Klare et al., 2007 — Klare, J.P., Chizhov, I., and Engelhard, M. (2007) Microbial rhodopsins: scaffolds for ion pumps, channels, and sensors. *Results. Probl. Cell. Differ.* **45**:73 – 122

Klare et al., 2011 — Klare J.P., Bordignon E., Engelhard M., Steinhoff H.J. (2011) Transmembrane signal transduction in archaeal phototaxis: The sensory rhodopsin II-transducer complex studied by electron paramagnetic resonance spectroscopy. *Eur. J. Cell. Biol.* **90**:731-739

Koteiche et al., 1998 — Koteiche, H.A, Benrengian, A.R., and Mchaourab, H.S. (1998) Identification of protein folding patterns using site-directed spin labeling. Structural characterization of a b-sheet and putative substrate binding regions in the conserved domain of an A-crystallin. *Biochem.* **37**:12681–12688

Koteiche et al., 2005 — Koteiche, H.A., Chiu, S., Majdoch, R.L., Stewart, P.L., and Mchaourab, H.S. (2005) Atomic models by cryo-EM and site-directed spin labeling: application to the N-terminal region of Hsp16.5. *Structure* **13**:1165 – 1171

Needleman et al., 1970 — Needleman, S. B. and W. C. D. (1970) A general method applicable to the search for similarities in the amino acids of two proteins. *J. Mol. Biol.* **48**:443-453

Olkhova et al., 2010 — Olkhova, E., Raba, M., Bracher, S., Hilger, D., and Jung, H. (2010) Homology Model of the Na^+/Proline Transporter PutP of *Escherichia coli* and Its Functional Implications. *J. Mol. Biol.* **406**:59-74

Panchal, 2002 — Panchal, R.G. (2002) Pore-forming proteins and their application in biotechnology. *Curr. Pharm. Biotechnol.* **3**:99-115

Pugsley, 1984 — Pugsley, A.P. (1984) The ins and outs of colicins. Part II. Lethal action, immunity and ecological implications. *Microbiol. Science* **1**:203-205

Pulagam et al., 2008 — Pulagam, L. P. and Steinhoff, H.-J. (2008) Conformation of the closed channel state of colicin A in proteoliposomes: an umbrella model, *J. Mol. Biol.* **378**:204-214

Pulagam and Steinhoff, 2013 — Pulagam LP, Steinhoff, H.J. (2013) Acidic pH-induced membrane insertion of colicin A into *E. coli* natural lipids probed by site directed spin labeling. *J. Mol.Biol.* **425**:1782-94

Pearson, 1990 — Pearson, W. R. (1990) Rapid and sensitive sequence comparison with FASTP and FASTA. *Methods Enzymol.* **183**:63-98

Pearson and Lipman, 1988 — Pearson, W. R. and Lipman, D. J. (1988) Improved tools for biological sequence comparison. *Proc. Natl. Acad. Sci.* USA, **85**:2444-2448

Smarda and Smajs, 1998 — Smarda, J. and Smajs, D. (1998) Colicins-exocellular lethal proteins of *Escherichia coli. Folia Microbiol. (Praha),* **43**:563-82

Smarda et al., 2001 — Smarda, J., Fialova, M. and Smarda, J. (2001) Cytotoxic effects of colicins E1 and E3 on v-myb-transformed chicken monoblasts. *Folia Biol. (Praha)* **47**:11-3

Spiegelhalter and Bremer, 1998 — Spiegelhalter, F. and Bremer E. (1998) Osmoregulation of the *opuE* proline transport gene from *Bacillus subtilis*: Contributions of the sigma A- and sigma B-dependent stress-responsive promoters. *Mol. Microbiol.* **29**:285-296

Strasser et al., 2000 — Strasser, A., O'Connor, L., and Dixit, V. M. (2000) Apoptosis signaling. *Biochem.* **69**:217–245

Savitsky et al., 2004 — Savitsky, A., Kühn, M., Duché, D., Möbius, K., and Steinhoff, H.-J. (2004) Spontaneous refolding of the pore-forming colicin A toxin upon membrane association as studied by x-band and w-band high field electron paramagnetic resonance spectroscopy. *J. Phys. Chem.* **108**:9541–9548

Taylor et al., 1989 — Taylor, W. R., and Orengo, C. A. (1989) Protein Structure Alignment. *J. Mol. Biol.* **208**:1-22

Voss et al., 1996 — Voss, J., He, M.M., Hubbell, W.L., and Kaback, H.R. (1996) Site-directed spin labeling demonstrates that transmembrane domain XII in the lactose permease of *Escherichia coli* is an α-helix. *Biochem.* **35**:12915–12918

Voss et al., 1997 — Voss, J., Hubbell, W.L., Hernandez-Borrell, J., and Kaback, H.R. (1997) Site-directed spin-labeling of transmembrane domain VII and the 4B1 antibody epitope in the lactose permease of *Escherichia coli*. *Biochem.* **36**:15055– 15061

Wagner et al., 1992 — Wagner, G., Hyberts, S.G. and Havel, T.F. (1992) NMR Structure Determination in Solution: a critique and comparison with X-ray crystallography. *Annu. Rev. Biophys. Biomol. Struct.* **21**:167–198

Walker, 2004 — Walker, D. (2004) Identification of the catalytic motif of the microbial ribosome inactivating cytotoxin colicin E3. *Protein Sci.* **13**:1603-1611

Waterman, 1984 — Waterman, M. (1984) General methods for sequence comparison. *Bull. Math. Biol.* **46**:473-500.

Wouters et al., 2001 — Wouters, F. S., Verveer, P. J., and Bastiaens, P. I. (2001) Imaging biochemistry inside cells. *Trends Cell Biol.* **11**:203–211

Wright et al., 2007 — Wright, E. M., Hirayama, B.A., and Loo, D. F. (2007) Active sugar transport in health and disease. *J. Intern. Med.* **261**:32-43

CHAPTER 2

Principles of SDSL EPR Spectroscopy

2. Principles of SDSL EPR Spectroscopy

To understand the biological function of biomacromolecules like proteins, knowledge about their molecular structures and their dynamics involved in their respective biological functions are required. As already mentioned in the beginning, most of the currently available protein structures have been determined by conventional methods like X-ray crystallography and NMR spectroscopy. The disadvantages of these methods are their limitations concerning the molecular weight for NMR spectroscopy and the protein amounts needed for X-ray crystallography. Furthermore, especially membrane proteins – comprising about 30 % of most organism's proteomes and being target for the majority of pharmaceuticals – often do not crystallize and the detergent- or membrane-environment also hampers structural investigations by solution NMR. Alternative methods to determine the structural properties of membrane proteins are cryo-electron microscopy (cryo-EM), solid-state NMR and EPR spectroscopy. In this work, the technique of cw - and pulse electron paramagnetic resonance (EPR) spectroscopy in combination with site directed spin labeling (SDSL) has been applied. This method has evolved in the past 20 years as a valuable tool to study protein structures and conformational changes (Altenbach et al., 1990). The advantage of using EPR is that the structural details and dynamics of a protein can be studied in its physiological environment. This method has become one of the most powerful tools to investigate proteins under more physiological conditions (Bordignon and Steinhoff, 2007), compared to e.g. X-ray crystallography. In the first part of this chapter the reader is provided with the necessary theoretical and technical background aspects of EPR spectroscopy. The principle of „Electron Paramagnetic Resonance"(EPR) or "Electron Spin Resonance"(ESR) spectroscopy is the absorption of electromagnetic radiation by a paramagnetic sample placed in a magnetic field. Consequently, only samples with unpaired electrons can be directly studied by the EPR method. With the exception of some metallo-proteins, most proteins have no unpaired electrons and therefore cannot be directly analysed. This problem can be overcome using a method called site-directed spin-labeling (SDSL) to introduce nitroxide spin labels (carrying a stable radical) at any desired site in a protein that has been developed by Wayne Hubbell and co-workers (Altenbach et al., 1989) (Altenbach et al., 1990) (Hubbell et al., 1994). This methodology is described in the second part of this chapter.

2.1 The free Electron Spin

A free electron represents an elementary particle which is characterized by an intrinsic angular momentum, the so called spin $\hat{\mathbf{S}}$ that is accompanied by a magnetic moment $\boldsymbol{\mu}_s$:

$$\boldsymbol{\mu_S} = -\boldsymbol{g_e}\frac{e\hbar}{2\boldsymbol{m_e}}\widehat{\boldsymbol{S}} = -\boldsymbol{g_e}\boldsymbol{\mu_B}\widehat{\boldsymbol{S}} \qquad \textbf{(2.1)}$$

In this equation, m_e is the mass of the free electron. The g-factor of the free electron is g_e= 2.00231. Furthermore, μ_B=9.27400915·10^{-24} JT^{-1}, is the Bohr magneton, $\hbar = h/(2\pi)$ = 1.054571726 ·10^{-34} J· s is the reduced Planck's constant and $\widehat{\boldsymbol{S}}$ is the spin vector with its components S_X, S_Y, S_Z. For a free electron in a homogeneous constant magnetic B-field B_0, for the electron spin vector two possible states with different energies exist. The spin is oriented either parallel (m_S = - ½) or *spin down*, or antiparallel (m_S = + ½) or *spin up* with respect to the external magnetic field. Thus, two distinct energy levels labeled by the spin projection quantum number m_S = ± ½ can be occupied. Consequently, according to the m_S states also two discrete values for the magnetic moment are possible:

$$\boldsymbol{\mu_{S,z}} = \pm\frac{\mathbf{1}}{\mathbf{2}}\boldsymbol{g_e}\boldsymbol{\mu_B} \qquad \textbf{(2.2)}$$

In an external homogeneous magnetic field along the z-axis of the laboratory coordinate system $\boldsymbol{B}_0$ = (0, 0, B_0) interacting with the magnetic moment $\boldsymbol{\mu_S}$ the resulting energies are:

$$\boldsymbol{E} = -\boldsymbol{\mu_S}\cdot\boldsymbol{B_0} = -\boldsymbol{\mu_z}\cdot\boldsymbol{B_0} \qquad \textbf{(2.3)}$$

and the only two energy levels available for the electron are:

$$\boldsymbol{E_\alpha} = +\frac{\mathbf{1}}{\mathbf{2}}\boldsymbol{g_e}\boldsymbol{\beta_e}\boldsymbol{B_0} \qquad \textbf{(2.4a)}$$

$$\boldsymbol{E_\beta} = -\frac{\mathbf{1}}{\mathbf{2}}\boldsymbol{g_e}\boldsymbol{\beta_e}\boldsymbol{B_0} \qquad \textbf{(2.4b)}$$

The resulting energy splitting of the electron spin level into two levels is called the *electron Zeeman effect* (Figure 2.1).

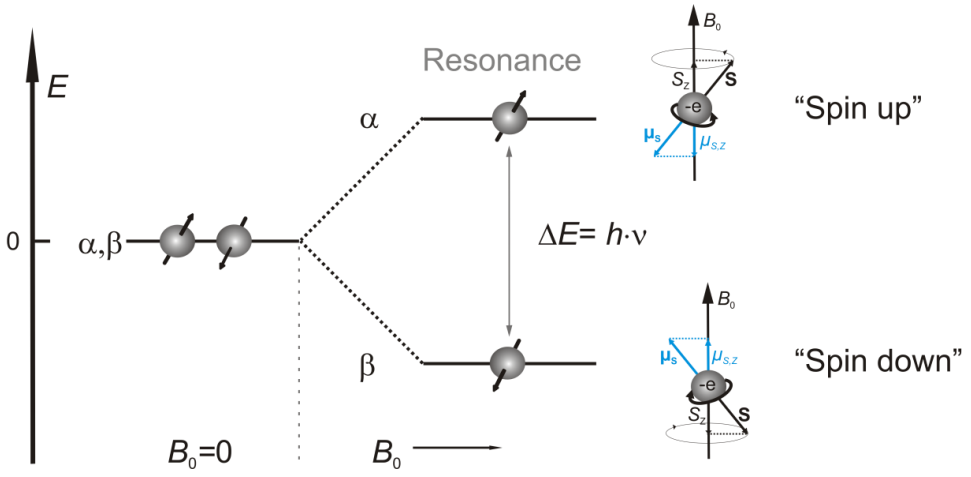

Figure 2.1: The electron Zeeman effect. The two spin states are described as α and β and are represented by arrows pointing up and down, respectively. Without an external B field ($B_0 = 0$) they have the same energy (the energy levels are *degenerate*). If the electron is placed in a magnetic field $B_0 \neq 0$, the two spins have different energy levels which are separated by ΔE. The figure was adopted from S. Boehme, PhD Thesis, 2010.

The Electron-Zeeman effect is the basis of EPR spectroscopy, where transitions of electrons between the two energy states are observed. In EPR spectroscopy such transitions are usually induced by microwave radiation. If the energy of the radiation, $h \cdot \nu$, provided by the applied field of frequency ν coincides with the energy difference ΔE between the two energy states, this phenomenon is called resonant absorption, and the resonance condition can be written as:

$$\boldsymbol{\Delta E = E_\alpha - E_\beta = g_e \mu_B B_0 = h \cdot \nu} \qquad \textbf{(2.5)}$$

2.2 The Spin Hamiltonian

The energy levels and the time evolution of their occupancies of a paramagnetic entity in the magnetic field *B* is described by the Hamilton operator or *Hamiltonian*. The total Hamiltonian describes the sum of the most important interactions of the free electron with its local environment. This includes the interaction of the electron spin $\hat{\mathbf{S}}$ with the external magnetic field, the magnetic moment from nuclear spins as well as from other electron spins, and the interaction between a nuclear spin and an external magnetic field. The total spin Hamiltonian including all possible interactions of the electron spin with its environment is:

$$\boldsymbol{\hat{\mathcal{H}}_S = \hat{\mathcal{H}}_{EZ} + \hat{\mathcal{H}}_{NZ} + \hat{\mathcal{H}}_{HF} + \hat{\mathcal{H}}_{ZFS} + \hat{\mathcal{H}}_{EXCH} + \hat{\mathcal{H}}_{DD} + \hat{\mathcal{H}}_{NQ} + \hat{\mathcal{H}}_{NN},} \qquad \textbf{(2.6)}$$

In Equ. 2.6, $\widehat{\mathcal{H}}_{EZ}$ describes the electron Zeeman interaction, $\widehat{\mathcal{H}}_{NZ}$ the nuclear Zeemann interaction, $\widehat{\mathcal{H}}_{HF}$ the hyperfine coupling between the electron and a nuclear spin, and $\widehat{\mathcal{H}}_{ZFS}$ the zero-field splitting for spin systems with $S > ½$. The zero-field interaction is caused by strong interactions between two unpaired electrons located in directly neighboring atom or even in the same atoms (this phenomenon is only of minor relevance for SDSL EPR since the unpaired electrons in spin labeled proteins usually do not come into so close proximity). $\widehat{\mathcal{H}}_{EXCH}$ and $\widehat{\mathcal{H}}_{DD}$ describe the Heisenberg exchange and dipole-dipole coupling between two electron spins. $\widehat{\mathcal{H}}_{NQ}$ reflects the nuclear quadrupole interactions for spins with nuclear spin quantum numbers $I > ½$, and $\widehat{\mathcal{H}}_{NN}$ the spin-spin interactions between pairs of nuclear spins. Also interactions described by $\widehat{\mathcal{H}}_{NQ}$ and $\widehat{\mathcal{H}}_{NN}$ usually do not contribute to the EPR spectra of proteins labeled with nitroxide spin labels (S =½, I = 1 (^{14}N)). Therefore they remain unconsidered in the following explanations.

2.2.1 Electron Zeeman interaction, $\widehat{\mathcal{H}}_{\mathbf{EZ}}$

This first term describes the interaction between the spin of a free electron and the external magnetic field. For electrons in molecular orbitals this interaction is an anisotropic interaction due to spin-orbit coupling, meaning that the magnetic moment of an electron spin bound to a molecule depends on the orientation of this electron spins in the molecule or on the orientation of the molecule in a magnetic field. This feature is indicated by the anisotropic $\underline{\boldsymbol{g}}$-tensor.

$$\widehat{\boldsymbol{H}}_{\boldsymbol{EZ}} = \frac{\boldsymbol{\mu_B}}{\hbar}\underline{\boldsymbol{g}}\widehat{\boldsymbol{S}}\boldsymbol{B_0} \qquad \textbf{(2.7)}$$

This equation describes the electron Zeeman interaction and $\underline{\boldsymbol{g}}$ describes the $\boldsymbol{g}$-tensor that has the following form:

$$\underline{\boldsymbol{g}} = \begin{pmatrix} \mathbf{g_{xx}} & \mathbf{0} & \mathbf{0} \\ \mathbf{0} & \mathbf{g_{yy}} & \mathbf{0} \\ \mathbf{0} & \mathbf{0} & \mathbf{g_{zz}} \end{pmatrix}$$

The typical g values for a MTS spin label are: g_{xx}≈ 2.0086, g_{yy}≈ 2.0066 and g_{zz}≈ 2.0023.

2.2.2 Nuclear Zeeman interaction, $\widehat{\mathcal{H}}_{\mathbf{NZ}}$

The nuclear Zeeman interaction describes the interaction of a nuclear spin with the external magnetic field B. This interaction becomes relevant for various EPR techniques like ESEEM spectroscopy and especially double resonance techniques (DEER or ENDOR), and is described by the Hamilton operator:

$$\widehat{\mathcal{H}}_{NZ} = -g_n \frac{\mu_B}{\hbar} \boldsymbol{B_0} \hat{I} \tag{2.8}$$

The nuclear magneton is defined by $\mu_N := \frac{e\hbar}{2m_P}$, $\hat{I}$ describes the nuclear spin operator and g_n the nuclear g-factor. The nuclear spin in a magnetic field B also reveals different energy states, and their quantization is defined through the magnetic quantum number of the nucleus $m_I = I, I - 1, \ldots, -I$.

2.2.3 Hyperfine interaction, $\widehat{\mathcal{H}}_{\mathbf{HF}}$

The hyperfine interaction characterizes the interaction between the electron spin $\widehat{\boldsymbol{S}}$ and the nuclear spin $\widehat{\boldsymbol{I}}$. This contribution is given by:

$$\widehat{\mathcal{H}}_{\mathbf{HF}} = \widehat{\boldsymbol{S}}\, \boldsymbol{A}\, \widehat{\boldsymbol{I}}_k \tag{2.9}$$

Here, $\boldsymbol{A}$ is the hyperfine tensor which is composed of two different parameters: (i) the anisotropic part and (ii) the isotropic part or Fermi contact interaction:

$$\widehat{\mathcal{H}}_{\mathbf{HF}} = \widehat{\mathcal{H}}_{\mathbf{HF,aniso}} + \widehat{\mathcal{H}}_{\mathbf{HF,iso}} \tag{2.10}$$

The anisotropic part of the hyperfine interaction arises from dipolar interaction between the nuclear and the electron spin, where the isotropic contribution results from a non-zero probability of the presence of the electron at the nucleus.

The hyperfine interaction leads to an energy splitting of the resonance lines and the energy levels from the Electron Zeeman interaction. With the system properties for a nitroxide spin label (S = ½, I = 1) and the quantum mechanical selection rules ($\Delta m_S = \pm 1$, $\Delta m_I = 0$) the energy differences for the three allowed EPR transitions are (Figure 2.2):

$$\begin{aligned}
\boldsymbol{m_I = 1} \quad &\rightarrow \quad \boldsymbol{E_1 = h\nu_1 = g_{\vartheta,\varphi}\beta_e B_0 + A_{\vartheta,\varphi}} \\
\boldsymbol{m_I = 0} \quad &\rightarrow \quad \boldsymbol{E_0 = h\nu_0 = g_{\vartheta,\varphi}\beta_e B_0} \\
\boldsymbol{m_I = -1} \quad &\rightarrow \quad \boldsymbol{E_{-1} = h\nu_{-1} = g_{\vartheta,\varphi}\beta_e - A_{\vartheta,\varphi}},
\end{aligned} \tag{2.11}$$

and the respective resonance positions can be determined by:

$$\begin{aligned}
\boldsymbol{B_{0(m_I=1)}} &= \frac{\boldsymbol{h\nu_1 - A_{\vartheta,\varphi}}}{\boldsymbol{\beta_e g_{\vartheta,\varphi}}} \\
\boldsymbol{B_{0(m_I=0)}} &= \frac{\boldsymbol{h\nu_0}}{\boldsymbol{\beta_e g_{\vartheta,\varphi}}} \\
\boldsymbol{B_{0(m_I=-1)}} &= \frac{\boldsymbol{h\nu_{-1} + A_{\vartheta,\varphi}}}{\boldsymbol{\beta_e g_{\vartheta,\varphi}}}
\end{aligned} \tag{2.12}$$

Here $g_{\vartheta,\varphi}$ and $A_{\vartheta,\varphi}$ are the g and A values for a given orientation of the B-field with respect to the molecular frame of the nitroxide, where the x-axis is oriented along the N-O bond and the z-axis perpendicular to the ring system (Fig. 2.3 and 2.9).

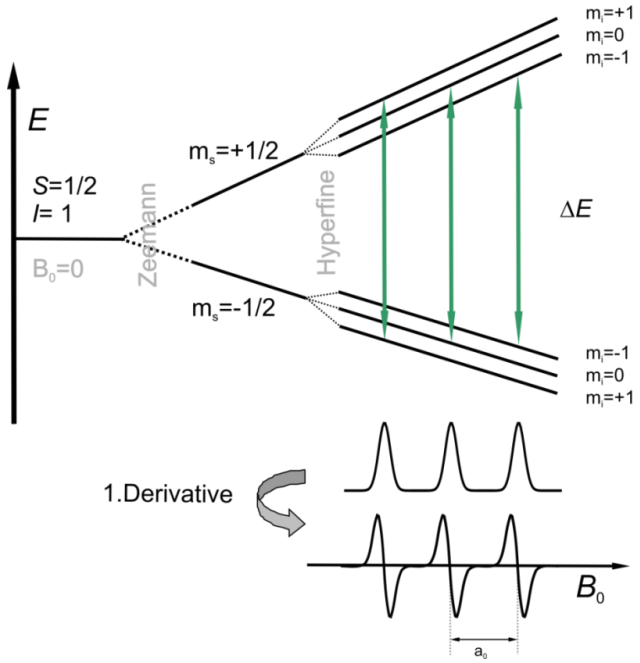

Figure 2.2: Schematic demonstration for the hyperfine interaction for a nitroxide radical (S = ½ and I = 1) as function of the magnetic field. Three resonance fields for three transitions can be identified. The two energy levels from the electron Zeeman interaction split in six energy levels. Caused by the selection rules for the allowed transitions ($\Delta m_I = 0$ and $\Delta m_S = \pm 1$), three EPR transitions can be measured with the resulting absorption signals. The resulting first derivative EPR spectrum is shown at the bottom. The apparent hyperfine splitting is designated by a_0. The Figure was adopted from J. Holterhues, PhD Thesis, 2009.

2.2.4 Dipole-Dipole interaction, $\widehat{\mathcal{H}}_{\mathbf{DD}}$

The systems considered previously describe the situation concerning a single unpaired electron. Therefore, in the following a system with two unpaired electrons that interact by exchange coupling and dipole-dipole coupling are described. The interaction energy of the two interacting magnetic dipoles $\boldsymbol{\mu}_1$ and $\boldsymbol{\mu}_2$ with the corresponding distance vector **r** between them is:

$$\boldsymbol{E} = \frac{\boldsymbol{\mu_0}}{\boldsymbol{4\pi}}\left(\frac{\boldsymbol{\mu_1}\cdot\boldsymbol{\mu_2}}{\boldsymbol{r^3}} - \frac{\boldsymbol{3(\mu_1\cdot r)(\mu_2\cdot r)}}{\boldsymbol{r^5}}\right) \qquad \textbf{(2.13)}$$

The dipole-dipole interaction is described by the following Hamiltonian equation by use of the correspondence principle:

$$\widehat{\mathcal{H}}_{DD} = \frac{\mu_0}{2h} g_1 g_2 \beta_e^{\,2} \left(\frac{\hat{S}_1 \cdot \hat{S}_2}{r_{12}^{\,3}} - \frac{3(\hat{S}_1 \cdot r_{12})(\hat{S}_2 \cdot r_{12})}{r_{12}^{\,5}} \right) = \hat{S} \underline{D} \hat{S} \qquad (2.14)$$

where $\hat{\mathbf{S}}$ indicates the group spin $\left(\hat{\mathbf{S}} = \hat{\mathbf{S}}_1 + \hat{\mathbf{S}}_2\right)$ composed of the two spin operators $\hat{\mathbf{S}}_1$ and $\hat{\mathbf{S}}_2$. g_1 and g_2 are the g-values of the two electron spins. The parameter $\underline{\boldsymbol{D}}$ denotes the dipole-dipole coupling tensor (Arthur Schweiger and Gunnar Jeschke, 2001). The dipolar interaction between the two electrons $\underline{\boldsymbol{D}}$ is proportional to the inter-spin distance r^{-3}. Therefore, quantification of the dipolar interaction allows determination of the distance between two paramagnetic centers.

2.2.5 Heisenberg spin exchange

The Heisenberg spin exchange is another electron-electron interaction. Spin exchange becomes significant if the inter-spin distance of the unpaired electrons is very small (≈ 0.8 nm) (Rabenstein et al., 1995), which occurs with a finite probability for the electrons at the same location and overlapping of the electron orbitals. The exchange interaction is described by the Hamilton equation:

$$\widehat{\mathcal{H}}_{EXCH} = -2J\hat{S}_1\hat{S}_2 \qquad (2.15)$$

Contrarily to the cubic distance dependence of the dipolar interaction described before, the Heisenberg exchange interaction of radicals in solution is supposed to fall approximately exponentially (Jeschke, 1998). Consequently, it is possible to obtain information about the distance *r* by determining the exchange coupling ***J***. Furthermore, exchange interaction is the underlying mechanism that can be used to determine spin label accessibilities to rapidly relaxing paramagnetic species exchanging with the unpaired electrons of protein-attached spin labels.

2.3 Site-directed spin labeling (SDSL) EPR Spectroscopy

In this work various EPR methods are used in order to obtain structural information and to study conformational changes of the pore-forming toxin colicin A upon interaction with membranes, the colicin A immunity protein Cai and the sodium-symporter PutP. With the help of nitroxide spin labeled proteins fundamental types of information can be obtained by this method like (i) the spin label mobility, (ii) the

accessibility towards paramagnetic quencher molecules, (iii) the polarity of the spin label environment, and (iiii) the inter-spin distance, the distance between two nitroxides. In the following sections the site-directed spin labeling approach is described (2.3.1) and it will be shown how the above mentioned information can be obtained from continuous wave (cw) EPR spectra of spin labeled proteins (2.3.2-2.3.6). Pulsed EPR spectroscopy, namely the Double Electron-Electron Resonance (DEER) experiment, that has been used in this work to determine inter spin distances in the distance range from ~ 1.5-5 nm, will be introduced and described in chapter 2.4.

2.3.1 The MTS spin label

The most widely used spin label molecule in EPR studies referenced in chapter 1 is the methanethiosulfonate spin label (MTSSL,1-oxyl-2,2,5,5-Tetramethylpyrrolin-3-methyl) methanethiosulfonate spin label) (Figure 2.3). The unpaired electron giving rise for the EPR signal is located at the nitroxide group in the heterocyclic ring of the label. *Spin labeling* is based on the specificity of the label reagent for reaction with the sulfhydryl group of a cysteine residue, either naturally present or site-specifically introduced via *site-directed* mutagenesis (Altenbach et al., 1990) (Hubbell and Altenbach, 1994) (Todd et al., 1998). Incubation of the purified protein with MTSSL causes reaction of the sulfhydryl group of cysteine side chains with MTSSL by formation of a disulfide bond. The resulting side chain is abbreviated as R1. Although a variety of different sulfhydryl-specific spin labels is available nowadays, the most commonly used label is MTSSL due to its small side chain size and its dynamic properties. Its molecular volume is in the range of that of amino acids like phenylalanine or trypthophane, and its flexible linker (see Figure 2.3 B) minimizes disturbances of the proteins secondary structure. Numerous spin labeling studies have shown that the proteins biological activity is usually preserved in the presence of R1 (Czogalla et al., 2007) (Mchaourab et al., 1996). The chemical structure of the MTS spin label bound to a protein *via* a cysteine side chain is shown in Figure 2.3.

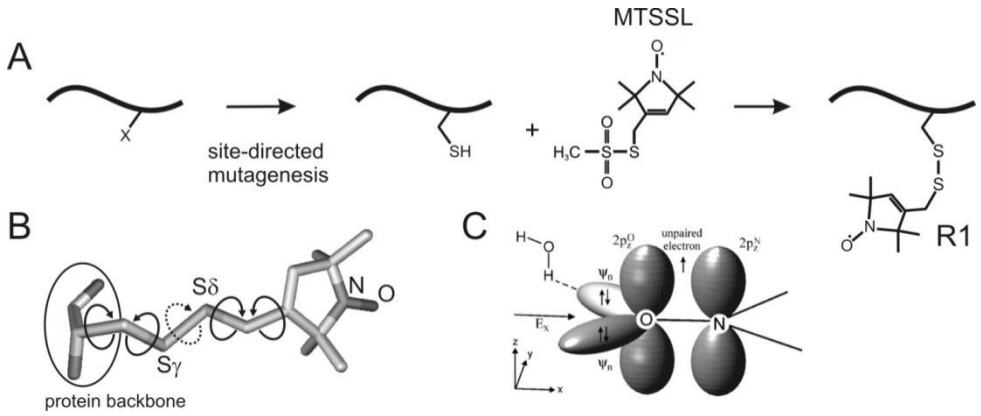

Figure 2.3: Site-directed spin labeling: (A) after replacing the residue of interest by cysteine using site-directed mutagenesis, reaction of the MTS spin label with the sulfhydryl group of the cysteine yields the spin label side chain R1. (B) Structure of R1 side chain. Rotatable bonds are indicated. The S-S bond displays a significantly higher energy barrier for rotation, as indicated by the dotted arrow (modified from Klare, 2013). (C) Electronic structure of the N-O bond in an external electric field E_x (reflecting the environmental polarity) and with one H-bond formation in the molecular frame (x, y, z). The unpaired electron is located in the partially overlapping p_z orbitals. The superposition of the oxygen 2s, $2p_x$ and $2p_y$ orbitals results in the non-bonding lone pair orbitals Ψn. Figure taken from Plato et al., 2002.

The paramagnetic characteristics of the MTS spin label are defined by the partial overlapping of the $2p_z$ orbitals of the oxygen and nitrogen atoms in which the unpaired electron is localized in the resulting π orbital of the nitroxide moiety.

2.3.2 Spin label side chain mobility

The EPR spectral shape at room temperature reflects the reorientational motion of the spin label side chain, for details see (Berliner, 1976) (Berliner, 1979) (Berliner and Reuben, 1989). To characterize the effects on the EPR spectral features the term "mobility " is used, which can be quantified by the *rotational correlation time* (Hemminga et al., 2007). The *rotational correlation time* describes the time for a molecule in motion, at which its orientation is not anymore correlated with its initial orientation. Three important parameters contribute to the overall motion of a spin label attached to a protein: (i) the motion of the protein, (ii) protein backbone dynamics and (iii) and the motion of the spin label itself. The resulting mobility of the R1 side chain can be derived from the spectral line shape of the EPR spectrum as can be seen in Figure 2.4, where simulated EPR spectra calculated for different rotational correlation times are shown.

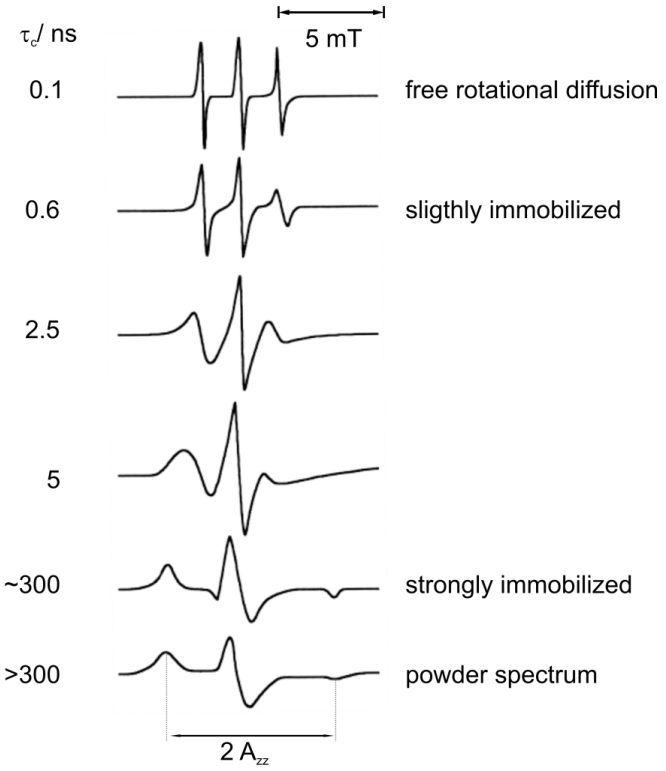

Figure 2.4: Simulated cw X-band EPR nitroxide spectra calculated for different rotational correlation times τ_C. Isotropic spectra as in case of free rotational diffusion (small τ_C values) show three distinct lines (top). Larger τ_C values are accompanied by spectral broadenings reflecting g and A anisotropies. In the case of correlation times above 300 ns corresponding to complete spin label immobilization, the spectra are called *powder spectra*. Figure adopted from Radzwill, PhD Thesis, 2001.

Spectra arising from spin label side chains showing a high degree of mobility, i.e. small rotational correlation times (τ_C), are characterized by three narrow lines (low-, middle- and high field line of the hyperfine splitting) and a small apparent hyperfine splitting (Figure 2.4, top). If the mobility of the side chain is more restricted by stronger interactions of the nitroxide with neighboring side chains or backbone atoms, the corresponding cw EPR spectra (Figure 2.4, spectra for rotational correlation times from 0.6 to 5 ns) display an increased apparent hyperfine splitting, smaller amplitudes and larger line widths. In the case of full immobilization (τ_C > 300 ns) a so-called *powder spectrum* (Figure 2.4, bottom) is observed. From the observed dynamics of an MTS spin label side chain conclusions can be drawn about its location and its surroundings within the protein it is attached to. For example, R1 side chains located in the protein interior are more restricted than those located in loop regions. Furthermore, periodical variations in spin label mobility can provide means to identify secondary structure elements, especially in the case of α-helices. Although the relation between the EPR spectral line shape and nitroxide dynamics is complex, the mobility can be quantitatively assessed by two so called mobility parameters, the line width of the center line (ΔH_0), and the spectral breadth or second moment of the spectra (H^2).

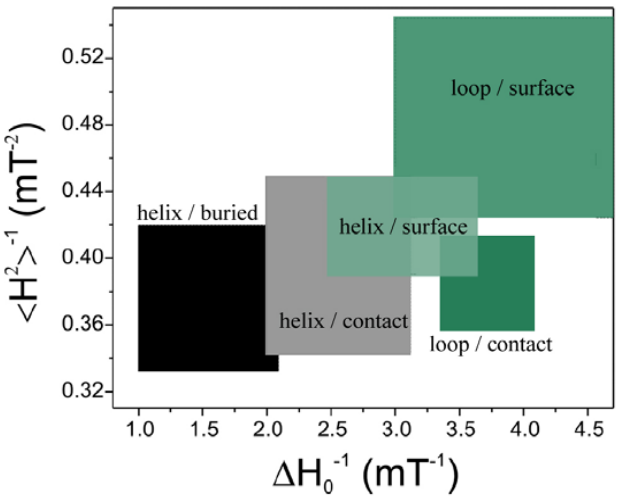

Figure 2.5: Classification of side chain localizations with regard to the protein structure by plotting the inverse spectral second moment versus the inverse central line width. These two semi empirical parameters were calculated from cw X-band EPR spectra at room temperature. Picture adopted from C. Abe, PhD Thesis, 2010 and modified from Bordignon et al., 2007.

It has been shown that these two parameters are correlated with the structure of the spin label binding site environment (Hubbell et al., 1996) (Mchaourab et al., 1996). For example, a plot of the mobility parameter ΔH_0^{-1} against the residue number reveals secondary structure elements through the periodic variation of the mobility as the spin label sequentially samples surface, tertiary, or buried sites. Furthermore, it is possible to perform a general classification of the side chain localization with regard to protein structure, by plotting the inverse of the central line width ΔH_0^{-1} and the inverse of the second moment $\langle H^2 \rangle^{-1}$ in a two-dimensional plot as shown in Figure 2.5.

2.3.3 Accessibility toward paramagnetic quencher molecules

Another tool to obtain structural information about a protein is determination of the spin label side chain accessibility towards paramagnetic quencher molecules. Paramagnetic probes exhibiting different solubilities in the different environments of the sample can be used to define the location of the R1 side chain with respect to the protein/water/membrane boundaries. The usual quencher components used for these types of experiments are water-soluble metal ion complexes like Ni-EDDA (Nickel ethylenediamine-diacetic acid) and hydrophobic molecules like molecular oxygen (O_2). The metal ions allow quantification of the spin label side chain accessibility from the aqueous environment, whereas molecular oxygen mainly concentrates in hydrophobic regions like the hydrophobic core of lipid membranes. Consequently a water exposed R1 side chain is associated with a high accessibility to Ni-EDDA and a smaller accessibility to oxygen. Contrarily, location of the nitroxide in a membrane bilayer

results in a higher accessibility to oxygen compared to Ni-EDDA. For a spin label located in the protein interior ("buried"), no or low accessibilities for both quencher probes are observed.

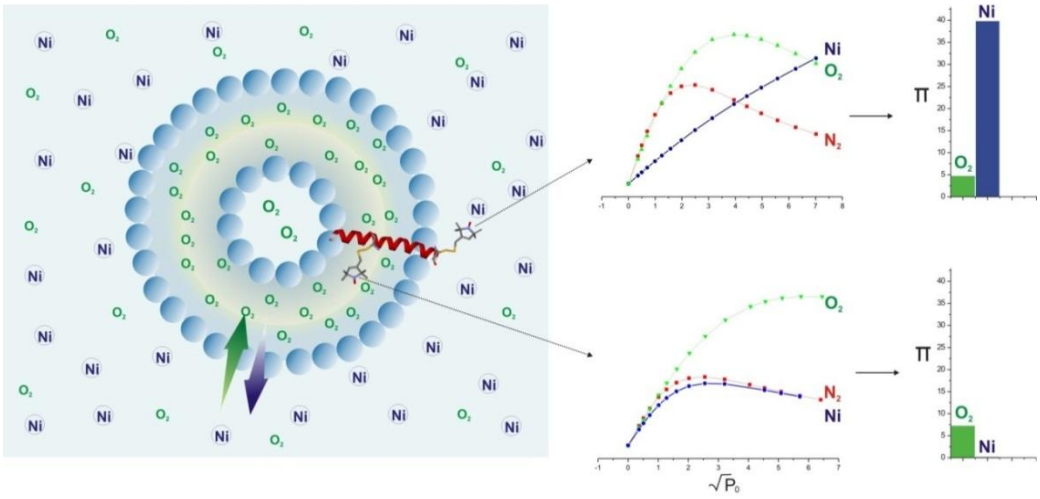

Figure 2.6: Accessibility of R1 side chains. Left: schematic illustration of the accessibility of the R1 side chain to the paramagnetic quenchers O_2 and Ni-EDDA. Due its hydrophobic nature the concentration of molecular oxygen is high in the hydrophobic regions of lipid membranes. Contrarily, the concentration of metal ion complexes like Ni-EDDA is higher in the aqueous environment. Right: typical saturation curves in the presence of the paramagnetic quencher molecules O_2 (green), Ni-EDDA (blue). The red curve shows the saturation behavior in the absence of collision reagents (fluxed with N_2). Figure adopted from L. Pulagam, PhD Thesis, 2007.

Collisions between the spin label and the diffusing exchange reagents are defined by their Heisenberg exchange frequency, W_{ex}. Most commonly, Heisenberg exchange rates are quantified using cw power saturation or saturation recovery measurements that allow measuring the spin-lattice relaxation time T_{1e} which is correlated to the Heisenberg exchange frequency W_{ex}:

$$\boldsymbol{W_{ex} = \Delta\left(\frac{1}{T_{1e}}\right)} \qquad \textbf{(2.16)}$$

In the case of cw power saturation measurements, which have been applied in this work, the dependency of the saturation behavior on the relaxation times is utilized to determine W_{ex}. The amplitude of the cw signal in dependency of the microwave power (peak to peak amplitude Y´ of the central resonance line obtained at different microwave power levels), exhibits a rise of the signal to a maximum followed by a decrease of the intensity (Figure 2.7). From this so called cw saturation curve (Figure 2.7), the parameter $P_{1/2}$, corresponding to the microwave power where the amplitude of the cw EPR spectrum is half of that, which would be obtained without any saturation (blue line in Figure 2.7) can be obtained. The corresponding saturation curves are analysed by fitting of the saturation curves with the equation:

$$Y' = \frac{I\sqrt{P}}{(1+(2^{\frac{1}{\epsilon}}-1)P/P_{1/2})} \quad \textbf{(2.17)}$$

Here, I is a scaling factor, and ε accounts for the homogeneity of saturation. The parameter $P_{1/2}$ can be extracted from the saturation curves by the program win power fit (Martin Kühn).

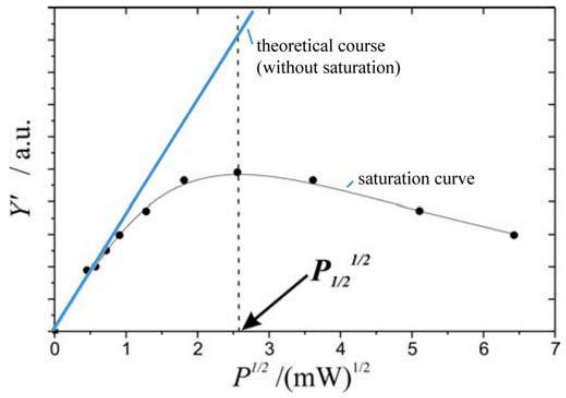

Figure 2.7: Plot of cw EPR signal amplitudes of the central line versus$\sqrt{P}$. The fit of the experimental data (black dots) with Equation 2.17 is shown as a black line. The theoretical behavior in the absence of saturation is shown in blue. Figure adopted from M. Doebber, PhD Thesis, 2009.

The $\boldsymbol{P_{1/2}}$ values reflect the relative collision frequencies and therefore the accessibility of the nitroxide towards the exchange reagent (Altenbach et al., 1989), but still also depend on the spin-spin relaxation time T_{2e}. To eliminate this dependency, the $\boldsymbol{P_{1/2}}$ values are divided by the spectra line widths ΔH_0 as a measure for T_{2e}^{-1}.

$$\Delta \boldsymbol{P'_{1/2}} = \frac{\boldsymbol{\Delta P_{1/2}}}{\boldsymbol{\Delta H_0}} = \frac{\boldsymbol{P_{1/2} - P^0_{1/2}}}{\boldsymbol{\Delta H_0}} \propto \boldsymbol{W_{ex}} \quad \textbf{(2.18a)}$$

Furthermore, to account for instrumental variability (for example resonator properties that influence saturation behavior), normalization of $\boldsymbol{\Delta P_{1/2}}$ with a reference sample - for example 2, 2-diphenyl-1-picrylhydrazyl (DPPH) powder diluted in KCl or TEMPO (2,2,6,6-Tetramethyl-1-piperidinyloxy, used in this study) - is performed to yield the dimensionless accessibility parameter π:

$$\boldsymbol{\pi} = \Delta \boldsymbol{P'_{1/2}} \frac{\boldsymbol{\Delta H_0(TEMPO)}}{\boldsymbol{P_{1/2}(TEMPO)}} = \boldsymbol{\alpha \cdot W_{ex}} \quad \textbf{(2.18b)}$$

$\boldsymbol{P_{1/2}}$ is the value in the presence and $\boldsymbol{P^0_{1/2}}$in absence of a collision reagent. The proportionality constant α, represents a cavity-dependent normalization factor. In this study a cavity with α = 1.87 s was used.

2.3.4 Immersion depth parameter Φ

Being of special interest for the topological characterization of membrane proteins, the immersion depth of the spin label side chain into a lipid bilayer can be quantified with the parameter (Φ) calculated from the accessibilities to O_2 and Ni-EDDA:

$$\Phi = \boldsymbol{ln}\left(\boldsymbol{W_{ex\,O_2}}\right)/\boldsymbol{ln}(\boldsymbol{W_{ex\,NiEDDa}}) \qquad \textbf{(2.19)}$$

Advantageously, this parameter exhibits only a weak dependency on the lipid composition of the bilayer (Hubbell et al., 1994). Extensive research concerning the immersion depth parameter Φ has been performed by Hubbell and coworkers (Altenbach et al., 1994) (Hubbell et al., 1994). In these studies the immersion depth parameter Φ has been experimentally determined for several spin labeling positions in bacteriorhodopsin (BR) as shown in Figure 2.8, allowing the determination of the distances of the R1 side chains with respect to the phospholipid head groups. In this plot of Φ versus label position it becomes apparent that this parameter represents a linear function of the distance from the lipid bilayer head groups with its maximum value in the middle of the bilayer.

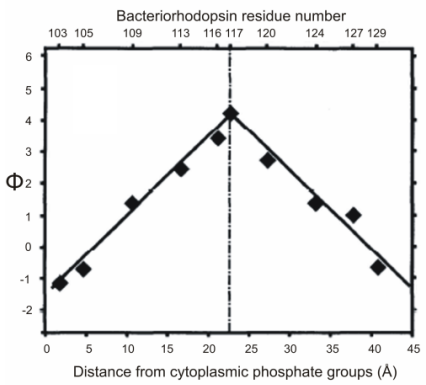

Figure 2.8: Immersion depth parameter Φ calculated from the collision frequencies (Ni-EDDA and O_2) obtained with BR mutants labeled with MTSSL at the positions indicated on the top y axis. The bilayer center is indicated by the dashed line, and the distances from the cytoplasmic phosphate head groups corresponding to the respective spin label side chain positions were determined from the BR structure. Figure adopted from Hubbell et al., 1994.

2.3.5 Polarity measurements

The polarity of the spin label environment influences the hyperfine coupling tensor element A_{zz}. The strength of the hyperfine interaction depends on the electron densities at the nitrogen and the oxygen atom of the nitroxide moiety, respectively, which in turn is affected by the polarity of the immediate spin label side chain environment, i.e. the electron density distribution for the unpaired electron is shifted between the two atoms depending on the local electric field. In a polar environment the stronger electric field *E* shifts the density of the unpaired electron into the direction of the nitrogen atom, leading to an increased hyperfine coupling with the N-atom (see Figure 2.9 A). In contrast, in a nonpolar environment (i.e. a weaker *E* field) the electron density is shifted into the direction of the oxygen atom, resulting in decreased hyperfine coupling (Figure 2.9 B). The resulting hyperfine interaction is reflected in the apparent hyperfine splitting (A_{zz}) that can be directly determined from cw EPR spectra recorded at low temperatures (below 190 K), where spin labels attached to a protein are completely immobilized (Figure 2.10 A). The hyperfine coupling tensor element A_{zz} is expected to be large in a polar environment (~3.6-3.7 mT), whereas smaller values indicate an apolar environment (~3.3-3.4 mT).

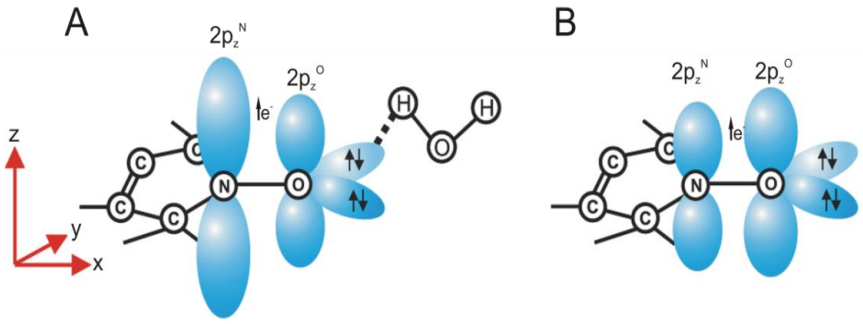

Figure 2.9: Schematic representation of localization of the electron density at the nitroxide group. The unpaired electron is shown as an arrow between the 2p orbitals of the nitrogen and oxygen in polar (A) and apolar (B) environment. (A) In a polar environment the oxygen forms a hydrogen bond and the electron density is shifted towards the nitrogen atom, indicated by the large 2p orbital at the nitrogen atom. (B) In a hydrophobic environment, the electron density in the 2p orbital of the nitrogen is decreased and shifted towards the oxygen atom of the nitroxide moiety. Figure adopted from J. Holterhues, PhD Thesis, 2009.

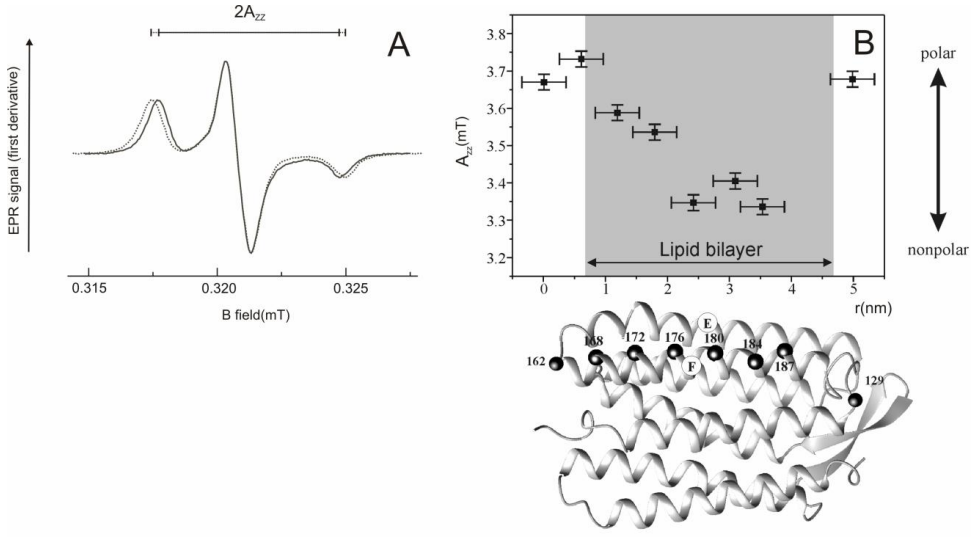

Figure 2.10: (A) Simulated X-band cw EPR powder spectrum reflecting the polarity of the nitroxide spin label environment. The resulting spectra of the MTSSL spin label are shown for a polar (dotted line) and nonpolar (continuous line) environment. Figure adopted from L. Pulagam, PhD Thesis, 2007. (B) Polarity parameters for helix F in BR. Shown are the A_{zz} values *versus* the spin label distance r from the lipid membrane surface. The profile reveals smaller A_{zz} values in the middle of the membrane bilayer and larger A_{zz} values near the lipid head groups. Figure adopted from Savitsky et al., 2004.

Determination of the environmental polarity of the R1 side chain allows obtaining structural and topological information about the protein under investigation. For example, spin labels located in the middle of the membrane reveal A_{zz} values of approximately 3.35 mT. In contrast, positions located close to the lipid head groups or the bulk water phase exhibit higher values like 3.6 mT. Thus, polarity measurements are a very useful to obtain information about the location of the side chains under investigation with respect to the membrane water interface. This is exemplified in Figure 2.10 B with a polarity profile forHelix F in BR. (Savitsky et al., 2004).

2.3.6 Inter Spin Distance measurements

Distances below ~ 2 nm between two spin label side chains can be determined from low temperature (below 190 K) cw EPR spectra, due to the fact that the dipolar interaction between two spins being < 2 nm apart leads to broadening of the EPR absorption lines (Altenbach et al., 2001) (Rabenstein et al., 1995) (Steinhoff et al., 1997). The magnetic dipole-dipole interaction between the magnetic moments $\boldsymbol{\mu_A}$ and $\boldsymbol{\mu_B}$ of spins A and B is proportional to r^{-3}, i.e., the strength of the dipole-dipole coupling increases with decreasing inter spin distance (see equation 2.13). The distance can be determined from the dipolar broadening of the EPR lines, where smaller distances lead to broader EPR spectra. Quantification of inter

spin distances can be achieved by a detailed line shape analysis of EPR spectra of frozen protein samples - or alternatively of proteins in solutions of high viscosity (Steinhoff et al., 1991).

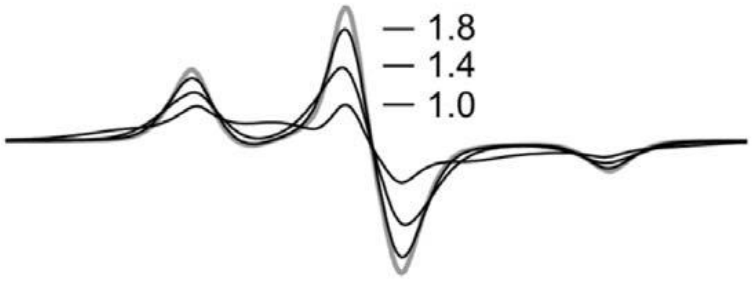

Figure 2.11: Influence of the dipolar interaction on low temperature X-band cw EPR spectra. The spectra were simulated with different inter-spin distances exhibiting a Gaussian distribution. Grey: > 2 nm (no visible dipolar interaction), black: 1.8, 1.4 and 1.0 nm. Picture taken from Bordignon et al., 2007.

2.4 Pulsed EPR

In contrast to cw EPR, in pulsed EPR the samples are irradiated (in a constant external magnetic field) with short microwave pulses in the nanosecond time range. In the last decades various pulse sequences have been developed, like 2- and 3-pulse ESEEM, HYSCORE, Mims and Davies ENDOR, DEER, etc., providing a wide range of information about the system of interest, e.g. interactions between the electron spin and nuclear spins, but also other electron spins. Pulsed EPR methods for example expanded the measurable inter spin distance range from 2 nm up to ~8 nm (Borbat et al., 2007) (Pannier et al., 2000). The corresponding technique is described in the following section.

2.4.1 Distance measurements with DEER spectroscopy

Double Electron-Electron Resonance (DEER) spectroscopy, also named Pulsed ELectron DOuble Resonance (PELDOR) spectroscopy, has been applied in this work for the determination of inter spin label distance distributions within the proteins colicin A, Cai and PutP, and is described in the following. DEER spectroscopy allows the determination of distances in the range of ~2-8 nm. Using deuterated solvents and deuterated proteins nowadays distances even up to about 10 nm can be measured (Ward et al., 2010). The 4-pulse DEER experiment applied here has been developed in the late 1990's (Martin et al., 1998) (Pannier et al., 2000). The basis of this method is the selective excitation of two spin populations, A

and B, of dipolar interacting spin partners by using two different microwave frequencies, ν_A and ν_B. These two frequencies are called observer-frequency, ν_A, and pump-frequency, ν_B, respectively. With the observer-frequency the behavior of a spin ensemble of species A at its resonance frequency, ν_A, is examined. The polarization of the electron spin B is flipped by the pump pulse, exhibiting the frequency ν_B. The dipolar coupling effects between A and B spins are then observed as a modulation of the observer echo amplitude depending on the position of the pump pulse within the pulse sequence, and can be used to determine the strength of the dipolar coupling and eventually the distance distribution between the electrons spins.

The DEER experiment and the origin of the DEER signal

In the 4-pulse DEER experiment a refocused Hahn-echo sequence is applied at the observer frequency ν_A, as illustrated in Figure 2.12 A. Figure 2.12 B visualizes the way how the time-dependent DEER signal is modulated with the so-called dipolar frequency, i.e. the shift in resonance frequency corresponding to the interaction energy given in Eq. 2.20 (Chapter 2.3.6). The behavior of the *macroscopic magnetization* **M** of the sample (i.e. the sum of the magnetic moments divided by the volume) is depicted in a reference frame that is set to rotate with the Lamor frequency of the observer spins ω_L (*observe*), so that the observer spins processing with ω_L (*observe*) appear stationary in this frame (vector picture of the rotating frame). Before the pulse sequence is applied to the system, the macroscopic magnetization **M** of the observer spins is aligned along the z-axis (1). The first two pulses, $\pi/2$ and π (the standard Hahn echo sequence), applied at the observer frequency ν_A, are separated by the time τ_1. The first $\pi/2$ pulse (with orientation of the microwave B-field along the y-axis of the rotating coordinate system) turns the magnetization **M** of the observer spins (species A) into the xy-plane of the rotating frame (1→2). During the time τ_1 the spins "fan out" in the xy-plane (dephasing of the transversal magnetization), caused by a distribution of different local fields leading to slightly different Lamor frequencies for the spins within the samples (2→3). Consequently, the resulting macroscopic magnetization in the xy-plane (being the signal usually measured in pulsed EPR) decreases over time until the xy components of all spins cancel out each other and the signal has completely decayed. This process (and also the resulting signal) is called *Free Induction Decay* (FID). After the time τ_1 the following π-pulse flips the magnetization by 180°, i.e. the single magnetization vectors are mirrored with respect to the yz-plane. As all spins keep their velocity and direction of rotation in the xy-plane during this process, the macroscopic magnetization in the xy-plane, is recovered due to *rephasing* of the spins (3→4). After the time τ has elapsed, all components are aligned along the y-axis, leading to the detection of a (negative) spin-echo, the so called Hahn-echo, after the time $2\tau_1$, where τ_1 is the delay time between the two pulses (4→5).

Now a second π-pulse (at the pump pulse position **t** in Figure 2.12 A) is applied at the second (pump-) frequency ν_B (6→7). This pulse changes the magnetization of spin species B (pumped spins), causing a change of the local magnetic field at the observer spins A and consequently a shift of their Lamor frequencies by two times the dipolar frequency (7). After the time τ_2 a second π_y-pulse is applied (8) at the observer frequency, leading to a refocused (positive) echo at τ_2 after this pulse, as the magnetization of the

observer spins A is again flipped by 180°around the z-axis resulting in rephrasing of the magnetization vectors along the x-axis (9→10). The echo amplitude in dependence of the time t can be monitored at $2(\tau_1 + \tau_2)$ after the last pulse (see Figure 2.12). Variation of the relative pump pulse position given by t leads to different phase offsets of the refocused magnetization, as the Lamor frequency shift caused by the pump pulse occurs at different times, reflected in a modulation of the echo amplitude with the dipolar frequencies resulting from spin-spin interactions.

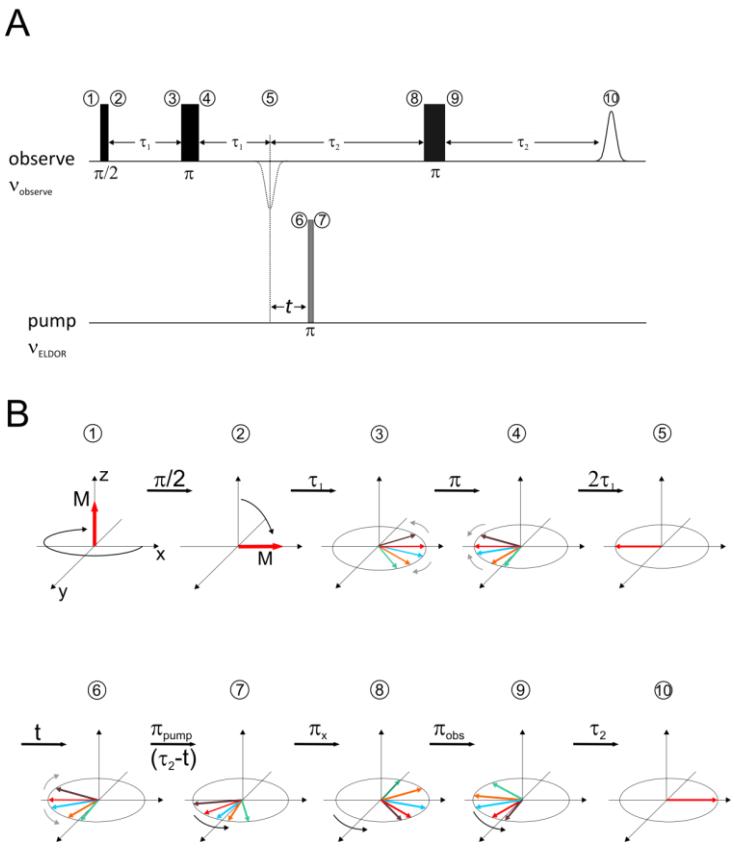

Figure 2.12: The DEER experiment. (A) Schematic representation of the four-pulse sequence. (B) Time evolution of the magnetization **M** in course of the DEER experiment. Figure adopted from S. Boehme, PhD Thesis, 2010.

The echo intensity resulting from a Hahn echo sequence is also determined by the temporal spacing between the two pulses. With increasing inter pulse delay a decrease of the echo intensity is observed. This is caused by the fact that in real EPR samples - due to local B-field fluctuations but also because of interactions of the electron spin with its environment, e.g. with nuclear spins, the spins do not keep their Lamor frequency over time. The time constant characterizing the decay of the echo intensity as function of the inter pulse delay is the so-called *phase memory time* T_m, comprising all effects causing echo dephasing, with the transverse relaxation time T_2 as one of its contributors (Jeschke,1998) (Schweiger et al., 2001). For interspin distance measurements the determination of T_m is important, as this time constant limits the maximum dipolar evolution time given by τ_2 (see Figure 2.12 A), and consequently the maximum accessible distance range - due to the r^3 dependency of the dipolar frequency and the prerequisite to cover

at least one oscillation of the latter with the dipolar evolution time for reliable determination of the frequency. The determination of T_m can be achieved by a 2 pulse Electron Spin Echo Envelope modulation (2pESEEM) experiment, which uses the Hahn-echo sequence ($\pi/2$ - τ_1 - π or $\pi/2$ - τ_1 - $\pi/2$). The spacing between the two pulses is varied to measure the exponential decay of the echo height due to dephasing over time.

Microwave pulses of finite length are always characterized by a certain bandwidth of excitation frequencies. For an optimal setup of the DEER experiment it is necessary to adjust the two excitation frequencies and pulse length in a way that overlaps between their excitation profiles are minimized or excluded. On the other hand, to optimize the signal intensity, it is important to excite as much spins as possible. In general, the choice for the pump frequency ν_B, is the frequency at which the EPR absorption spectrum reaches its maximum. The length of the π-pump pulse is usually set to 12 ns. In case of nitroxide spin labels, the observer frequency ν_A with a corresponding π-pump of 32 ns is set to the low field EPR maxima, which corresponds to a value between 65 up to 70 MHz larger than ν_B (see Figure 2.13).

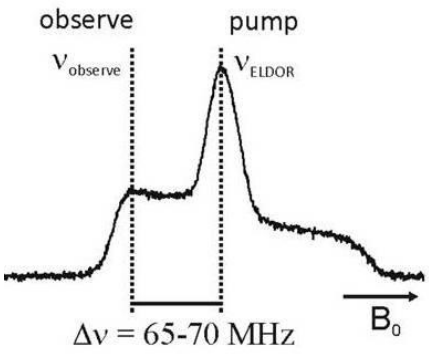

Figure 2.13: Setting of observer and pump pulse in the four-pulse DEER experiment on an echo detected field swept EPR spectrum of a nitroxide spin label bound to a protein.

Analysis of the DEER data

The echo amplitude at the time $2(\tau_1+\tau_2)$ depending on the time t (pump pulse position) represents the DEER signal. The total DEER signal intensity $\boldsymbol{V(t)}$ is composed of the local intra-molecular contribution $\boldsymbol{F(t)}$, called the form factor, and the background contribution $\boldsymbol{B(t)}$.

The overall DEER signal as function of the dipolar evolution time *t* can therefore be splitted in:

$$\boldsymbol{V(t) = V_{local}(t) \cdot V_{background}(t) = F(t) \cdot B(t)} \qquad \textbf{(2.20)}$$

Under the assumption that the background part arises from homogeneously distributed molecules it can be described by (Milov et al., 1997):

$$\boldsymbol{B(t) = exp(-kt^{D/3})} \qquad \textbf{(2.21)}$$

where D is the *dimensionality of the background* contribution. In case of frozen protein solutions, a three-dimensional distribution (D = 3) can be assumed, whereas membrane proteins in a lipid bilayer are most likely characterized by a two-dimensional distribution (D = 2) or a dimensionality between 2 and 3. Alternatively, the background contribution ***B (t)*** for doubly-labeled molecules can be determined experimentally from singly labeled species (Hilger et al., 2005) (Jeschke et al., 2006). The form factor ***F (t)*** (see Figure 2.14, panel A) appears as a damped oscillation with a frequency inversely proportional to the cube of the mean distance $\overline{r_{AB}}$ (see Equ. 2.13). The decay of the oscillation depends on the width of the inter spin distance distribution. With increasing width of the distance distribution the decay becomes faster, because ***F (t)*** is then a superposition of Lamor frequencies from a wider interval. Incomplete excitation of the pumped spins results in the fact that ***F (t)*** decays to a non-zero value 1-Δ, where Δ is the so-called modulation depth. For dipolar evolution times > T_{dd}, where T_{dd} is the characteristic decay time describing where the oscillation has fully decayed, the signal is described by

$$\boldsymbol{V(t > T_{dd}) = (1 - \Delta)B(t)} \qquad \textbf{(2.22)}$$

Separation of ***V (t)*** into ***F (t)*** and ***B (t)*** as described in equation 2.20 can thus be performed by fitting the two parameters k and Δ in equations 2.21 and 2.22. The analysis of the DEER traces to obtain the inter-spin distance distributions and average numbers of interacting spins of the sample was performed with the program *DeerAnalysis2011* (Jeschke et al., 2006).

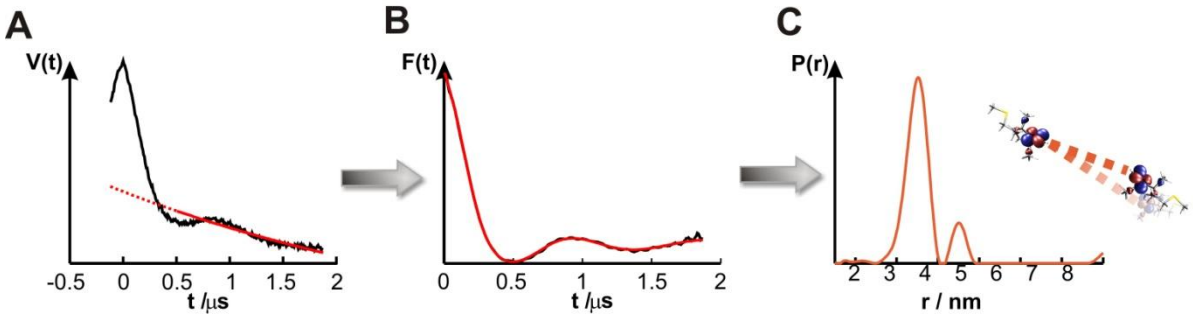

Figure 2.14: DEER. The double Electron-Electron Resonance: Determination of inter-spin distances and the respective probability distributions via a pump-probe pulse EPR. (A) A typical DEER signal ***V (t)*** and the exponentially decaying background part highlighted in red. (B) The resulting form factor ***F (t)*** after background correction (C) can be converted into a distance distribution ***P (r)***.

First, the program corrects the phase of the (complex) experimental data by minimizing the root mean square deviation of the imaginary part for the last three quarters of the data points. Next, a background correction according to the approach described in the previous paragraph of the phase corrected dipolar evolution data is performed. Background correction separates the signal $\boldsymbol{V(t)}$ into the dipolar evolution function $\boldsymbol{F(t)}$ (see Figure 2.14, panel A) and the background decay $\boldsymbol{B(t)}$. The quality of the background correction can be evaluated by inspection of the Fourier transform of the background corrected dipolar evolution data, the *Pake pattern* (Jeschke et al., 2006). If the background contribution $\boldsymbol{B(t)}$ to the DEER signal has been removed the resulting form factor $\boldsymbol{F(t)}$ (see Figure 2.14, panel B) can be translated in terms of distance distribution $\boldsymbol{P(r)}$ (see Figure 2.14, panel C). Determination of the distance distribution $\boldsymbol{P(r)}$ from the form factor $\boldsymbol{F(t)}$ is performed by Tikhonov regularization. A regularization method has been chosen as the solutions of this problem are not unique and also not stable with respect to artifacts and a poor signal to noise ratio, leading to variations and consequently uncertainties in the distance distributions. In Tikhonov regularization, the best compromise between the resolution of the distance distribution and noise suppression (smoothness) is seeked, judged by the regularization parameter α.
By minimizing the target function $\boldsymbol{G_\alpha(P)}$ the optimum distance distribution *P(r)* is then found and given by:

$$\boldsymbol{G_\alpha(P) = \|S(t) - F(t)\|^2 + \alpha \left\| \frac{d^2}{dr^2} P(r) \right\|^2} \qquad \textbf{(2.23)}$$

In this equation the first term describes the root mean square deviation between the simulated time-domain signal $\boldsymbol{S(t)}$ and the experimental background corrected DEER trace $\boldsymbol{F(t)}$. The second term described the second derivative of $\boldsymbol{P(r)}$ weighted by the regularization parameter α. The determination of a suitable α can be achieved based on the so called *L-curve criterion* (Jeschke et al., 2006). The L-curve represents the plot of the logarithm of the smoothness (Eq. 2.23, second term) against the logarithm of the mean square deviation between the simulated and experimental dipolar evolution function (Eq. 2.23, first term). This leads to a computed L-shaped curve and the simulated dipolar evolution function and the distance distribution can be inspected for all α values.

2.5 Bibliography

Abe, 2010 — Abe, C., (2010) Conformational changes of vinculin tail upon F-Actin and phospholipid binding studied by EPR spectroscopy, PhD Thesis, Universität Osnabrück.

Altenbach et al., 1990 — Altenbach, C., Marti, T., Khorana, H.G., and Hubbell, W.L. (1990) Transmembrane protein structure: spin labeling of bacteriorhodopsin mutants. *Science* **248**:1088–1092

Altenbach et al., 1989 — Altenbach C., Flitsch S.L., Khorana, H.G., Hubbell, W.L. (1989) Structural studies on transmembrane proteins, 2: spin labeling of bacteriorhodopsin mutants at unique cysteines. *Biochem.* **28**:7806-7812

Altenbach et al., 1994 — Altenbach C. and Hubbell, W. L. (1994) A collision gradient method to determine the immersion depth of nitroxides in lipid bilayers: Application to spin-labeled mutants of bacteriorhodopsin. *Proc. Natl. Acad. Sci.* **91**:1667–1671

Altenbach et al., 2001 — Altenbach, C., Oh, K.J., Trabanino, R.J., Hideg, and Hubbell, W.L. (2001) Estimation of Inter-Residue Distances in Spin Labeled Proteins at Physiological Temperatures: Experimental Strategies and Practical Limitations. *Biochem.* **40**:15471-15482

Berliner, 1976 — Berliner, L.J. (1976) Spin labeling: Theory and application. Academic Press Inc., London.

Berliner, 1979 — Berliner, L.J. (1979) Spin labeling II: Theory and application. Academic Press Inc., London.

Berliner and Reuben, 1989 — Berliner, L.J., and Reuben, J. (1989) Biological magnetic resonance-Vol.8: Spin labeling theory and applications. Plenum Press, New York.

Borbat et al., 2007 — Borbat P.P and Freed J.H. (2007) Pros and Cons Of Pulse Dipolar ESR: DQC and DEER, EPR Newsletter **17**:21-32

Bordingon and Steinhoff, 2007 — Bordignon E., and Steinhoff, H.-J. (2007) ESR spectroscopy in membrane biophysics, in: M.A. Hemminga, L.J. Berliner (Eds.), Biological Magnetic Resonance, Vol. 27, Springer, Heidelberg, pp. 129–164

Boehme, 2010 — S. Boehme (2010) Structural and functional analysis of the MnmE/GiDA protein complex studied by EPR spectroscopy, PhD Thesis, Universität Osnabrück.

Czogalla et al., 2007 — Czogalla, A., Pieciul, A., Jezierski, A., and Sikorski, A.F. (2007) Attaching a spin to a protein site-directed spin labeling in structural biology 1. *Acta Biochim. Pol.* **54**:235-244

Doebber, 2009 — Doebber, M. (2009) EPR Analysis of a Two-State Conformational Equilibrium in an *N. pharaonis* HAMP Domain, PhD Thesis, Universität Osnabrück.

Hemminga et al., 2007 — Hemminga, M.A., Jeschke, G., Strancar, J., Fajer, , Brown, L, Song, L., Bordignon, E., Steinhoff, H.-J., Smirnova, T.I, Smirnov, A.I., Fajer, M.I., Sale, K.L., Nilges, M.J., Mattson, K., Belford, R.L., Freed, J.H., Stoll, S.and Schweiger. A. (2007) *Biological Magnetic Resonance* - Vol. 27: ESR Spectroscopy in Membrane Biophysics. Springer Science and Business Media.

Hilger et al., 2005 — Hilger, D., Jung, H., Padan, E., Wegener, C., Vogel, K.P., Steinhoff, H.-J and Jeschke, G. (2005) Assessing Oligomerisation of Membrane Proteins by Four-Pulse DEER: pH-Dependent Dimerisation of NhaA Na^+/H^+ Antiporter of *E. coli. Biophys. J.* **89**:1328-1338

Holterhues, 2009 — Holterhues, J. (2009) Analyse der Signalweiterleitung im spinmarkierten sensorischen Rhodopsin/Transducer-Komplex mittels zeitaufgelöster ESR-Spektroskopie, PhD Thesis, Universität Osnabrück.

Hubbell et al., 1994 — Hubbell, W.L., Altenbach, C. (1994) Investigation of structure and dynamics in membrane proteins using site-directed spin labeling. *Curr.Opin.Struct.Biol.* **4**:566-573

Hubbell et al., 1996 — Hubbell, W. L., McHaourab, H. S., Altenbach, C., and Lietzow, M.A. (1996) Watching proteins move using site-directed spin labeling. *Structure* **4**:779-783.

Jeschke et al., 2006 — Jeschke, G., Chechik, V., Ionita, P., Godt, A., Zimmermann H., Banham, J.E, Timmel, C.R, Hilger, D. and Jung, H. (2006) DeerAnalysis2006 - a comprehensive software package for analyzing pulsed ELDOR data. *Appl. Magn. Reson.* **30**:473-498

Jeschke, 1998 — Jeschke, G. (1998). Einführung in die ESR-Spektroskopie: Skript zur Vorlesung von H.W. Spieß gehalten von G. Jeschke. MPI für Polymerforschung, Mainz, Germany.

Klare, 2013 — Klare, J.P. (2013) Site-directed spin labeling EPR spectroscopy in protein research. *Biol. Chem.* **394**:1281-1300

Martin et al., 1998 — Martin, R.E., Pannier, M., Diederich, F., Gramlich, V., Hubrich, M., Spiess, H.W. (1998). *Angew. Chem. Int. Ed.* **37**:2833-2837

Mchaourab et al., 1996 — Mchaourab H.S, Lietzow M.A, Hideg K, Hubbell W.L. (1996) Motion of spin-labeled side chains in T4 lysozyme. Correlation with protein structure and dynamics. *Biochem.* **35**:7692-7704

Milov et al., 1997 — A. D. Milov and Tsvetkov, Y. D. (1997) Double electron-electron resonance in electron spin echo: Conformations of spin-labeled poly-4-vinilpyridine in glassy solutions. *Appl. Magn. Reson.* **12**:495–504

Pannier et al., 2000 — Pannier, M., Veit, S., Godt, A., Jeschke, G., and Spiess, H.W. (2000) Dead Time Free Measurement Of Dipole-Dipole Interactions Between Electron Spins. *J. Magn. Reson.* **142**:331-340

Plato et al., 2002 — Plato, M., Steinhoff H.-J., Wegener, C., Törring, J., Savitsky, A. and. Möbius, K. (2002) Molecular orbital study of polarity and hydrogen bonding effects on the g and hyperfine tensors of site directed NO spin labeled bacteriorhodopsin. *Mol. Phys.* **100**:3711–3721

Rabenstein et al., 1995 — Rabenstein, M. D., and Shin Y.-K. (1995) Determination of the distance between two spin labels attached to a macromolecule. *Proc. Natl. Sci.* **92**:8239–8344

Radzwill, 2001 — Radzwill, N. (2001) Bestimmung der Strukturänderungen der lichtgetriebenen Protonenpumpe Bakteriorhodopsin mittels zweifacher Spinmarkierung and ESR-Spektroskopie. PhD Thesis, Fakultät für Physik and Astronomie.

Savitsky et al., 2004 — Savitsky, A., Kühn, M., Duché, D., Möbius, K., and Steinhoff, H.-J. (2004) Spontaneous refolding of the pore-forming Colicin A toxin upon membrane association as studied by x-band and w-band highfield electron paramagnetic resonance spectroscopy. *J. Phys.Chem.* **108**:9541–9548

Schweiger et al., 2001 — Schweiger, A. and Jeschke G. (2001) Principles of Pulse Electron Paramagnetic Resonance. Oxford University Press, first ed.

Steinhoff et al., 1997 — Steinhoff, H.-J., Radzwill, N., Thevis, W., Lenz, V., Brandenburg, D., Antson, A., Dodson, G.G., and Wollmer, A. (1997) Determination of interspin distances between spin labels attached to insulin: comparison of electron paramagnetic resonance data with the X- ray structure. *Biophys. J.* **73**:3287–3298

Pulagam, 2007 — Pulagam L.P (2007) Structural analysis of colicin A: *in vitro, in vivo* and *in silico* studies, PhD Thesis, Universität Osnabrück

Ward et al., 2010 — Ward, R., Bowman, A., Sozudogru, E., El-Mkami, H., Owen-Hughes, T., and Norman, D.G. (2010) EPR distance measurements in deuterated proteins.*J. Magn. Reson.* **207**:164–167

CHAPTER 3

Structure of the colicin A pore-forming domain in *E. coli* lipids

3. Structure of the colicin A pore-forming domain in *E. coli* lipids

3.1 Introduction

3.1.1 Motivation

A mechanism of cytotoxicity by means of the formation of pores in cell membranes is found in many organisms. Pore-forming toxins are usually secreted as water-soluble proteins and insert into the cytoplasmatic membrane to open pores with different selectivities (Cramer et al., 1995) (Panchal et al., 2002) (Smarda et al., 1998). This distinctive feature is frequently regulated by physical and chemical factors, like the membrane potential or by ligand-binding. In case of the pore-forming toxins of Enterobacteriaceae family members, this bacteriocines form voltage gated pores in the bacterial plasma membranes (Lakey et al., 1994) (Pugsley et al., 1994). This pore is - in contrast to ion channels - less selective, i.e. ions and/or small organic molecules can pass the channel (Cramer et al., 1995).

Deeper knowledge about bacterial toxins like the colicins not only provides additional means for understanding microbial defense mechanisms in general. Moreover, medical applications like designing antibiotics based on the mechanisms colicins use to *selectively* kill certain bacteria, or the finding that colicins can selectively kill tumor cells (Smarda et al., 2001) (Fuska et al., 1979) (Walker et al., 2004), are discussed. In addition, the structural motif of colicin pore-forming domains is also present in other pore-forming toxins (PFTs) like Diphtheria toxin, Aerolysin or members of the Bcl-2-family - like Bax. Bcl-2-family proteins comprise a major part of a cell's apoptotic machinery, and it has been shown that they can act also as tumor suppressors (Strasser et al., 2000). Moreover, the property of e.g. Bax to permeabilize biological membranes again gives rise for potential medical applications, like cancer chemotherapy dependent on programmed cell death (Strasser et al., 2000).

3.1.2 Colicin A expression and release

Colicins belong to the class of bacteriocines that are synthesized by enterobacteria like *E. coli,* and are active against other *E. coli* strains (Smarda et al., 1998) (Lakey et al., 1994). The members of the colicin family are different in effectiveness and can kill their target either by nuclease activity or by forming pores in the cytoplasmatic membrane. This work is focused on ColA, a water-soluble toxin of 592 amino acids that kills unprotected cells by inserting specific helical segments into the cytoplasmatic membrane, thereby forming a voltage-dependent ion channel (Cascales et al., 2007 and references therein). A positive membrane potential of 40-60 mV (Lazdunski et al., 1998) (Martinez et al., 1983) opens this non-specific

channel and permits the efflux of inorganic and small organic ions. This leads to a depolarization of the membrane and affects the proton motive force by depletion of the ATP level.

Colicins are encoded by the so called Col-plasmids that vary widely in size and properties. Representative examples for such plasmids are pColE1 for colicin E and pColA for colicin A (Figure 3.1). Three of the genes are fully characterized and important for the colicin A mechanism of action (Lakey et al., 1994) (Cascales et al., 2007). The gene *caa* is responsible for colicin A activity itself. The gene *cal* encodes the lysis protein cal and plays an important role in the secretion of colicin A by cell lysis induced by the BRP protein (bacteriocine-release protein) to allow the release of colicin from the cell (van der Wal et al., 1995). Each colicin plasmid also encodes a specific immunity protein that is encoded by the gene *cai*, that protects the colicin-producing cell against its own cytotoxic activity (Lakey et al., 1994) (Cascales et al., 2007). The immunity protein Cai is a transmembrane protein and protects the producing cell against the cytotoxic activity only of its corresponding colicin (Pugsley et al., 1984).

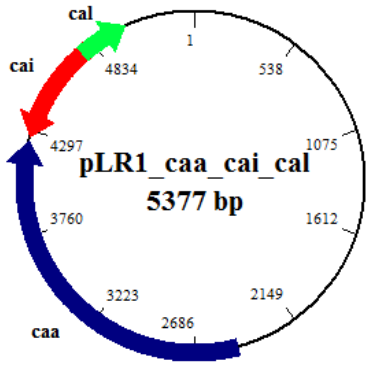

Figure 3.1: pColA plasmid pLR1 with arrangement of the genes *caa* (blue), *cal* (green) and *Cai* (red).

Expression of the two genes *caa* and *cal* in *E. coli* is strongly repressed by the LexA repressor, which is induced by the 'SOS' response (Pugsley et al., 1984), due to the presence of DNA-damaging agents or environmental factors like increasing population density and nutrient depletion (Lakey et al., 1994) (Pugsley et al., 1984). Damaged DNA - for example from UV-light or mitomycin C - causes activation of the inducer RecA and the activated form binds to the repressor protein LexA, which induces auto cleavage and release of the LexA repressor, allowing transcription of the operon. In contrast to the genes *caa* and *cal* the structural gene for the immunity protein Cai is located on a specific operon and is encoded on the antisense DNA-strand. Therefore, Cai expression is not dependent on the SOS-response, and the protein is continuously expressed at low levels (10^2 to 10^3 molecules per cell). For comparison, the number of colicin A molecules produced by a single cell reaches ~10^7 molecules (Zhang et al., 1993). Therefore, after induction colicin becomes the major protein of the cell. The bacteriocine release protein Cal is a – also highly expressed - small lipoprotein containing a signal peptide that remains stable and

accumulates in the cytoplasmic membrane after cleavage. Combined action of the accumulated signal peptides, the BRPs and phospholipase A causes the release of colicin A into the extracellular medium. In more detail, it could be shown that the BRPs activate phospholipase A that is located in the outer membrane (Cavard et al., 1997) (Pugsley et al., 1984) by dimerisation (Snijder et al., 1999) (Dekker et al., 1999). This causes a change in the phospholipid content, namely a decrease in phosphatidylethanolamine (PE) and an increase in lysophosphatidylethanolamine (lysoPE) and free fatty acid content (Pugsley et al., 1984), finally leading to membrane perturbance and the leakage of colicin A and other proteins. Furthermore, it could be shown that colicin A can affect the integrity of the outer membrane independently of phospholipase A (Howard et al., 1991). Colicins accumulate exclusively in the cytoplasm and it was suggested that release from the cytoplasm to the extracellular medium could be a one-step process (Cavard et al., 1981) (Luirink et al., 1991). Therefore it has also been proposed that the BRPs together with phospholipase A build trans-envelope pores through which colicin A and other proteins are able to pass (Luirink et al., 1991) (Cavard et al., 1992) (van der Wal et al., 1995). Nonetheless, for colicin A it was shown that it can also reach the outer membrane without the help of BRPs just by interaction with phospholipase A (Snijder et al., 1999). Phospholipase A forms a 12-stranded-β barrel which spans the membrane (Snijder et al., 1999), and it appears possible that phospholipase alone can also facilitate colicin A transport across the outer membrane (Cavard, 2002).

3.1.3 The solution structure of colicin A

Structural models for full-length pore-forming colicins are available for colicin B (Hilsenbeck et al., 2004), colicin N (Vetter et al., 1998) and colicin Ia (Wiener et al., 1997). Furthermore, structural data is available for the separated pore-forming domains of colicin A (Parker et al., 1989, 1992) and colicin E1 (Elkins et al., 1997). Due to the high sequence homology between colicins A and Ia (Figure 3.2 A) it can be expected that ColA exhibits the same structural features. According to this homology, the 592 amino acid protein ColA comprises three domains: The N-terminal translocation domain (T-domain), the central receptor binding domain (R-domain), and the C-terminal pore-forming domain (P-domain), as illustrated in Figure 3.2 B.

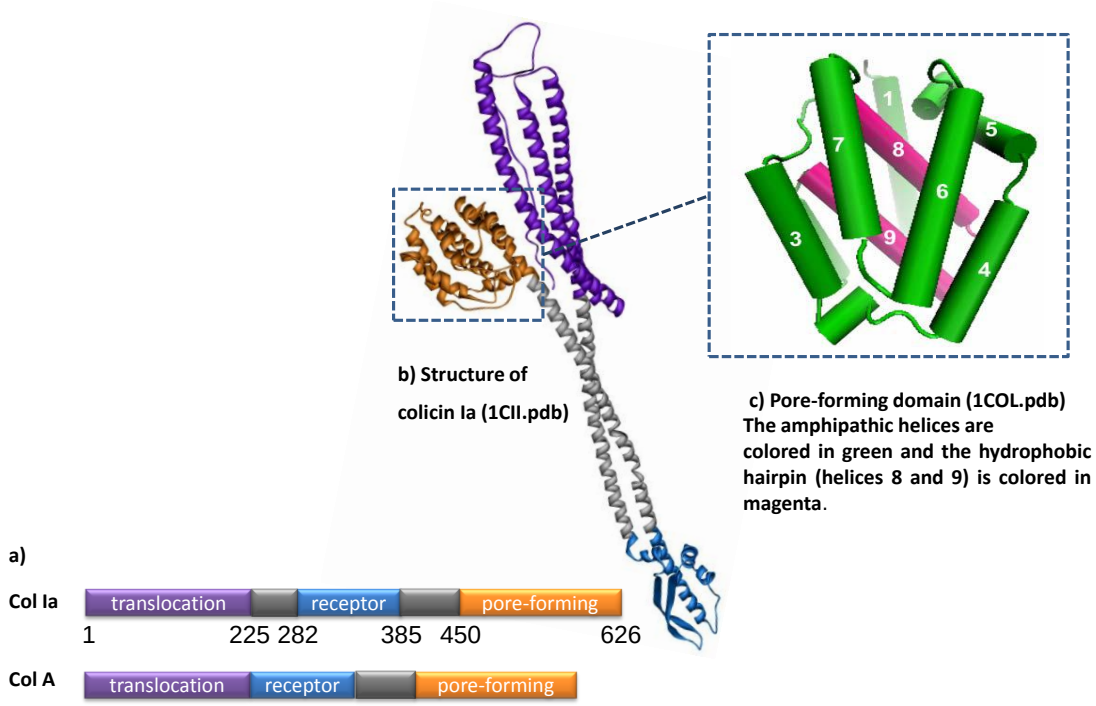

Figure 3.2: (a) The structural features of colicin A and Ia. (b) Ribbon structure of colicin Ia (1CII.pdb). The three individual domains are colored and named separately. (c) Schematic structure of pore-forming domain of colicin A (1COL.pdb). The amphipathic helices are colored in green and the hydrophobic hairpin (helices 8 and 9) is colored in magenta.

The ColA ion channel is formed by the C-terminal pore-forming domain. The available three dimensional structures of the soluble form of the pore-forming domains of colicins A, B, E1, Ia and N share the same architecture. The crystal structure of colicin A with 2.4 Å resolution was reported by Parker et al. (Parker et al., 1989 / 1992) and reveals a bundle of 10 alpha-helices as shown in Figure 3.2 C. The hydrophobic helices 8 and 9 comprise a hydrophobic hairpin that is surrounded by the other 8 amphipathic helices. The hydrophobic surfaces face towards the central hydrophobic core and the hydrophilic faces are exposed to the aqueous environment, rendering the protein soluble in water. The pore-forming domain of colicin A has 3 possible conformations (Cascales et al., 2007 and references therein): the water soluble form, the closed channel state and the open channel state and binding of colicin A to the membrane is irreversible. Since colicin channels are regulated by a voltage gating mechanism, the membrane bound-state of colicin A exist in an open and a closed channel state (Lakey et al., 1994) (Cramer et al., 1990). Nevertheless other unknown membrane bound conformations of the channel can't be excluded. The structure of the open channel state is at the moment completely unknown.

3.1.4 Colicin A interaction with target cells

Once released from the producing cell, the target of colicin A is the inner (cytoplasmic) membrane (IM) of other cells. The insertion of toxic proteins into membranes and subsequent channel formation is found for many toxins like diphtheria, tetanus and cholera toxins (Möbius et al., 2005) (Smarda et al., 1998) (Lakey et al., 1998) (Pugsley et al., 1984) (Smarda et al., 2001) (Fuska et al., 1979). All these molecules including the colicins have to overcome a major physical barrier to attack the target cells – the outer membrane. For translocation through the outer to the inner membrane colicins use either the TonB or the Tol-system. The Tol (for Tolerant) group of proteins is responsible for the energy independent import of colicins, whereas the TonB proteins mediate energy dependent import. Depending on these two import pathways colicins are classified into two groups:

1. **Group A** colicins which translocate through the Tol system like colicin A, E1-E9, K, L, N,

2. **Group B** colicins, which translocate through the Ton system like colicins B, D, Ia, Ib, M and V

The cell-killing mechanism of colicin A involves three functional steps. First, the receptor binding domain binds to the vitamin B12 receptor (BtuB) at the outer membrane surface. Next, translocation of the other two domains from the outer to the inner membrane takes place with the aid of the porin OmpF and the Tol system. Finally, the pore-forming domain inserts into the inner membrane to form a voltage-dependent ion channel. It has also been suggested that receptors like BtuB and OmpF can react as gated channels, where binding of the ligand opens this channel, allowing the ligands to pass (Lazdunski et al., 1998). Although the mechanism how colicins bind to their receptors and how they finally reach the inner membrane is still under lively debate, the major pathways are quite well known. Once colicin A is bound to the receptor BtuB, translocation across the membrane takes place through the second outer membrane protein OmpF, and based on the fact that colicin A uses these two proteins to traverse the membrane, it has been suggested these proteins must be localized in a close proximity to each other. Translocation itself is thought to take place *via* unfolding of the ColA translocation domain (Gouaux, 1997).
A-type colicins use the Tol-system that comprises the proteins TolA, TolB, TolQ, TolR and an outer membrane lipoprotein, Pal (Peptidoglycan associated lipoprotein). It is known that the periplasmatic protein TolB associates with Pal. Therefore it appears likely that the translocation of colicin starts with the interaction with TolB. The ColA-TolB interaction displaces the TolB-Pal interaction and thereby might promote an interaction of Pal with peptidoglycan (Lazdunski et al., 2000). Colicin interacts also with TolR and TolA, and it has been speculated that this step is followed by a further unfolding of the colicin polypeptide chain (Journet et al., 2001) (Lazdunski et al., 2000). Despite the fact that several studies have been carried out to unveil details of the translocation mechanism (Cascales et al., 2000), it is still largely unclear how translocation of the C-terminal cytotoxic pore-forming domain to the inner membrane takes place. One suggestion is, that interaction of phospholipids with the C-terminal cytotoxic domain induces a slow conformational change to reach the so called "molten globule" (MG) state, that allows passage of the

domain across the outer membrane (Lazdunski et al., 2000). Furthermore, it was proposed that colicin A does not pass the OmpF lumen (Bainbridge et al., 1998), but that it rather 'slides' down the side of OmpF (Lazzaroni et al., 2002) to reach contact with TolB (Zhang et al., 2009). In this proposed mechanism, first the translocation domain of ColA interacts with TolB in the periplasm and afterwards, due to higher affinity to the C-terminus of TolA (through β-barrel strand addition), with TolA (Zhang et al., 2009) (Li et al., 2012). This mechanism is based on the so called Brownian Ratcheting hypothesis (Journet et al., 2001) that states that the translocation domain moves through the periplasm by diffusion. Interactions with the Tol proteins putatively prevent colicin A from moving backwards.

Finally, the pore-forming domain inserts into the inner membrane to form a voltage-dependent ion channel. How channel formation of the colicins takes place is still largely unknown. Experimental evidences exist that in the first step, where the pore-forming domain reaches the inner membrane, positive charges on the domain surface induce a specific orientation relative to the membrane (Elkins et al., 1997). After binding to the membrane, it then inserts into the inner membrane – a process that has to be accompanied by large-scale conformational changes and/or partial unfolding of the domain (van der Goot et al., 1994) (Cramer et al., 1995) (Zakharov et al., 2002).

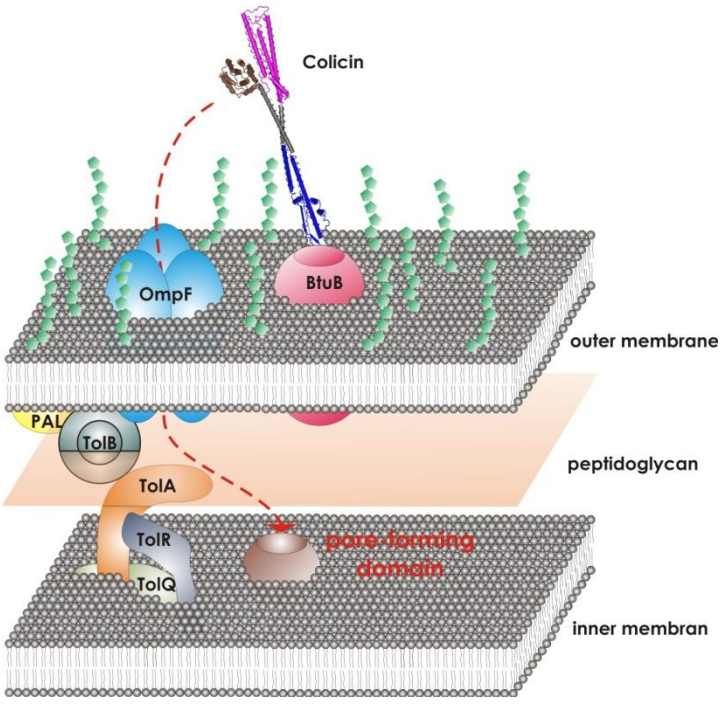

Figure 3.3: The colicin A translocation across the outer membrane. For details see text. Figure adopted from M. Sippach, Master Thesis, 2011.

Colicin channels are non-specific, allowing the passage of all ions including small organic molecules like glutathione and NAD^+ (for colicin E1) (Lakey et al., 1994) (Cramer et al., 1990) (Raymond et al., 1985). The efflux of ions through the channel results in high proton conductivity and consequently membrane depolarization. Colicin A channels can decrease the membrane potential from -165 to -85 mV (Cramer et

al., 1990), and the resulting depolarization disturbs the proton-motive force (pmf) that is required for ATP synthesis. Due to the reduced pmf and also the depleted phosphate pools, the level of ATP decreases rapidly, finally leading to cell death (Smarda et al., 1998) (Cramer et al., 1995).

3.1.5 Interaction of the pore forming domain of colicin A with membranes

In the absence of a transmembrane potential the channel appears in the closed conformation (Slatin et al., 2004) (Kienker et al., 1997). For the closed channel conformation two models have been proposed, the so called "Umbrella-model" see Figure 3.4 A) (Parker et al., 1992) and the "Penknife-model" (Lakey et al., 1991) (see Figure 3.4 B).

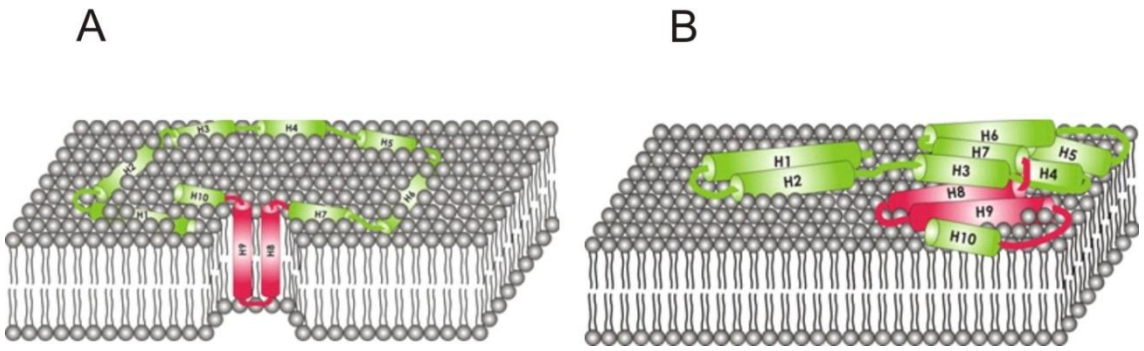

Figure 3.4: Models for the closed channel state of colicin A. (A) Umbrella model and (B) Penknife model. The colicin A pore-forming domain is illustrated in cartoon style embedded in a lipid bilayer. The amphipathic helices are colored in green and the hydrophobic hairpin (H8 and H9) is colored in red. (Figure adopted and modified from Cascales et al. 2007, M. Sippach, Bachelor Thesis, 2011).

The major difference between these two models concerns the orientation of the hydrophobic helical hairpin. In the "umbrella model" the hydrophobic hairpin adopts a transmembrane orientation and the amphipathic helices are located on the membrane surface. In contrast, in the "penknife model" all helices are located on the membrane surface. The closed channel state has been extensively studied by numerous groups using a variety of experimental approaches. Nevertheless, the topology of the closed channel state of pore-forming colicins is still obscure. For the closed channel state of colicin E1 the "umbrella model" was supported by data obtained with solid-state NMR (Kim et al., 1998), FRET (Tory et al., 1999), FTIR, EPR (Shin et al., 1993) and several biochemical techniques. For colicin A Parker et al., (1992) also proposed the "umbrella model", which was also supported by studies by González-Mañas et al. (1992) by the use of brominated phospholipids. Another study by Lakey et al. (1991) supports this notion by FRET assays. In addition analyzes with EPR measurements on ColA further support an arrangement of the helices of the channel domain according to the of the umbrella model (Pulagam et al., 2008) (Boehme et al., 2009). Contrarily, Lakey et al. (1991) proposed the "penknife model" in which the hydrophobic hairpin

and furthermore the amphipathic helices are orientated parallel to the membrane plane for colicin A. This idea was also supported by fluorescence experiments (Lakey et al., 1991), disulphide bond engineering experiments (Duché et al., 1994), neutron scattering (Jeanteur et al., 1994), proteolysis (Massotte et al., 1993), and by EPR experiments (Möbius et al., 2005). Consequently, discussion about the conformation of the closed channel state of colicin A is still controversial. One possible cause for the contradictory experimental results could be that for example a number of studies predicting the penknife model for the closed channel state have been performed using 100 % negatively charged lipids at low pH (~5) (Lakey et al., 1991) (Duché et al., 1999) (González-Mañas et al., 1993) (Lakey et al., 1992), a membrane composition that does not properly represent the *E. coli* inner membrane, that comprises approximately 70-75 % POPE, 20-25 % POPG and 5-10 % cardiolipin. In fact, it has been reported that the colicin E1 channel does not open in 100 % negatively charged lipids (Zakharov et al., 1996). A straightforward explanation for this finding is that the use of 100 % negatively charged lipids would significantly increase the strength of the electrostatic interactions of the above mentioned positively charged patch on the protein with the lipid surface. The artificially strong interaction between the positive amino acids and the negatively charged head groups thus might prevent helix-motions and therefore insertion of the hydrophobic helical hairpin into the membrane (Zakharov et al., 2002) (Lindeberg et al., 2000). Nevertheless, not all experimental contradictions are explainable by the use of inappropriate lipids.

Interestingly, studies by Tory et al. (1999) and Kienker et al. (1997/ 2000) on colicin E1 and colicin Ia revealed a thermodynamic equilibrium between two conformations according to the umbrella and the penknife model, and that this equilibrium depends on the type of colicin. According to these studies for colicin E1 the equilibrium is shifted toward the umbrella model, whereas for colicin Ia the penknife model structure is preferred. Such kind of thermodynamic equilibrium between structures according to the two models could also be possible for the closed channel state of colicin A, thereby providing another explanation for the contradictory results obtained so far. Furthermore, Prieto et al. (2011) suggested that one of these components could also be a 'precursor state' of the umbrella model structure. In such mechanism, first the colicin A pore-forming domain in its soluble form would be oriented with the hydrophobic hairpin parallel to the membrane plane the so called 'adsorbed state'. Then the hairpin undergoes conformational changes leading to a structure described by the penknife model - the 'precursor state' - and afterwards further conformational changes would change the orientation of the hydrophobic hairpin resulting in a structure according to the umbrella conformation (see Figure 3.5).

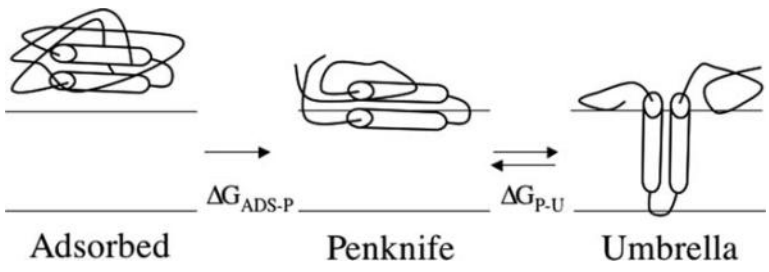

Figure 3.5: The mechanism of the colicin insertion adopted from Kienker et al. (1997).

In the presence of a positive membrane potential of 40-60 mV colicin channels change their structure to adopt an open conformation for which up to now no viable models exist. Nevertheless, experimental evidences exist, for example that helices 2 to 5 are translocated either completely (for colicin Ia), or at least partly across the inner membrane (Cascales et al., 2007). Moreover it has been reported that a trans negative potential drives the insertion of an amphipathic hairpin composed of helices 5-6 into the membrane to open the channel (Slatin et al., 2004).

For colicin A and Ia it was further reported that the first three helices can be eliminated without preventing channel opening (Nardi et al., 2001). The remaining helices should form a pore of approximately 7-10 Å, depending on the type of pore-forming colicin (for example colicin Ia: ~7 Å (Krasilnikov et al., 1998)). Interestingly, this pore diameter is much larger as for example that of tetrameric voltage-gated channels (Cascales et al., 2007). Data by Kienker et al. (1997/2000) and Slatin et al. (2004) revealed that tetraethylammonium (TEA) can pass the colicin A and Ia channels, and the authors state that this bulky cation might pass the channel in a different way than smaller ions do. Such behaviour was also proposed for peptides that form multimeric pores (Lin et al., 2000) (Matsuzaki, 1998) (Matsuzaki et al., 1996).

For colicin A a pore diameter of approximate 10 Å can be proposed based on electrophysiological experiments (Sippach, 2009). Furthermore, high proton selectivity (Kienker et al., 2002) and, interestingly and despite the large pore diameter, a small conductance for the colicin A channel similar to that of highly selective pores like gramicidin - a voltage gated tetrameric channel – has been reported (Cascales et al., 2007). Certainly, these observations are inconsistent with the assumption that only one colicin A molecule already forms a functional channel and is sufficient to depolarize the membrane. Although the vast majority of studies on colicin channels indicate a monomeric structure, the question remains, whether an ion channel with the above mentioned properties (esp. such a large pore diameter) can be formed by only two putative transmembrane segments (H8/H9). But even if involvement of more helices in pore formation is assumed, the formation of such a large pore remains inexplicable. Moreover, helices H8/H9 of the colicin A pore-forming domain appear to be even too short to span the membrane. Although it has been proposed based on EPR experiments, that during colicin E1 channel formation helix elongation of H4 should take place (Zakharov et al., 2002), explaining at least how full transmembrane segments could be formed, the overall size and architecture of the pore-forming domain further argue against a monomeric channel. Nevertheless, alternative models exist that protein-lipid interactions play a vital role in pore-formation and that the majority of the pore is formed by lipids rather than by the colicin A polypeptide itself (Cascales et al., 2007) (Zakharov et al., 2002). However, all observations concerning pore size and properties could also easily be explained if colicin channels are multimers. Indeed, a significant number of indications exist for colicin channels being oligomeric (Cavard, 2002) (Cavard, 2002 b) (Frenette et al., 1988). For example, colicin A has been shown to be expressed in various forms, many of them with higher molecular mass than a monomer, already suggesting the presence of multimers and oligomers (Cavard, 2002) (Cavard, 2002 b). Probably the best source of information is a publication that shows the oligomeric structure resolved by electron crystallographic analysis of two dimensional crystals

of the colicin Ia channel in lipid bilayer membranes (Greig et al., 2009), clearly revealing ring-like oligomers in the membrane, most likely in the form trimers of dimers (see Figure 3.6).

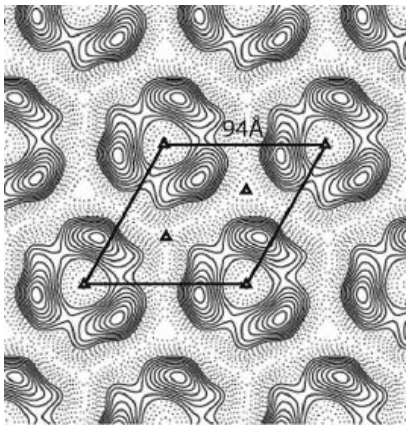

Figure 3.6: Oligomeric structure of colicin Ia channel in lipid bilayer membranes. The averaged projection density map is taken from (Greig et al., 2009, Figure 5). The colicin Ia protein forms oligomers most likely in form of trimers of dimers.

Interestingly, the structural motif of the colicin pore-forming domain is also present in other pore-forming toxins (PFTs) like Diphtheria toxin, Bax or Aerolysin. For these proteins dimerisation and oligomerisation could be observed and have been shown to be necessary for their function (Greig et al., 2009) (Antonsson et al., 2002) (Fivaz et al., 2001). Generally, PFTs are secreted as soluble monomers, like colicin A, diffuse to the membrane of the target cell and undergo a conformational change upon membrane binding (Walker et al., 1992 /1995). As an example, the pro-apoptotic Bcl-2-like protein Bax forms an oligomeric pore in the inner mitochondrial membrane, leading to membrane poration, release of cytochrome c and apoptosis (Kuwana et al., 2002). Members of the Bcl-2 protein family contain different so-called Bcl2 homology domains, BH1-BH4 (Gross et al. 1999) (Adams et al., 1998). The structure of monomeric Bax, which was solved by NMR (Suzuki et al., 2000) (McDonnell et al., 1999) (Chou et al., 1999) exhibits strong similarities to the pore-forming domain of the colicins and diphtheria toxin (Suzuki et al., 2000). Bax exhibits a globular fold of 9 alpha-helices, in which the hydrophobic helices 5 and 6 comprise the hydrophobic helical hairpin (helices 8 and 9 in colicins). Bax contains the Bcl-2 homology domains BH1, BH2 and BH3. The BH3 domain, located in helix 2 of Bax, seems to be required for its killing activity and for dimer formation (Wang et al., 1998), putatively linking dimerisation /oligomerisation with function. Remarkably, most members of the Bcl-2-family like Bax have been reported to form homo-and heterodimers. However, the structure of activated Bax, being responsible e.g. for cytochrome c release, is still not solved. It has been reported that the hydrophobic helices H5 and H6, and also H9 insert into the outer mitochondrial membrane (Nechushtan et al., 1999) (Annis et al., 2005). Another study reported four transmembrane domains for Bax, H1, H5, H6 and H9 (Garcia-Saez et al. 2004). A site-directed spin labeling study on the proteins Bax and Bid (Bleicken et al., 2009) supported that after activation of Bax by Bid the Bax-BH3-domains form an irreversible dimer. The authors

proposed that dimer-formation represents the nucleation event for formation of a larger oligomeric pore being able to conduct the exit of cytochrome c (Bleicken et al., 2009). Activation and membrane insertion by PFTs is thought to be a multistep process (Garcia-Saez et al. 2004). In this process pore-formation by Bax starts with the monomeric inactive protein that diffuses to the membrane. Afterwards it is oriented parallel to the membrane plane as an intermediate state. This is also proposed for colicin E1 (Zakharov et al., 2002). After Bax activation by Bid, dimer-formation takes place, leading to a precursor state before oligomerisation of dimers starts for the final pore-formation. Due to the strong similarities found between colicin A and Bax, this could also be applied to colicin A.

3.1.6 Aim of the work

Colicin A (ColA) is a plasmid-encoded water-soluble pore-forming toxin produced by *E. coli* (Cramer et al., 1995). The protein kills unprotected cells of related strains by inserting specific helical segments of the pore-forming subdomain into the cytoplasmic membrane to form voltage-dependent ion channels. The crystal structure of the soluble form of the pore-forming domain has been solved, but detailed structural data for the membrane-bound channel, in the closed as well as in the open state, is still missing. Currently, two models are discussed for the closed channel state, the "umbrella model" and the "penknife model". Previous EPR results (Pulagam et al., 2008) (Boehme et al., 2009) already provided evidence for the closed channel state to be in agreement with the previously suggested "umbrella model" (Panchal, 2002) (Lakey et al., 1994). Furthermore, in the literature the channel is widely assumed to be formed by a single pore-forming domain, although the channel properties, i.e. an inner pore diameter of at least 1 nm, are difficult to be explained in this way. Strong evidence for an oligomeric structure of the channel was already provided by an electron microscopy study on the closely related colicin Ia (Greig et al., 2009).

This work aims at a better understanding of the structural features of the membrane bound closed channel state of colicin A. In the present study, previous *in vitro* and in *silico* investigations by site-directed spin labeling and EPR spectroscopy (Pulagam et al., 2008) (Pulagam and Steinhoff, 2013) (Boehme et al., 2009) (Savitsky et al., 2004) have been substantially extended, including mobility, polarity, accessibility and inter spin distance measurements of additional mutants to clarify the following issues. First, what does the membrane bound state of colicin A look like? Second, does an equilibrium exist between two protein conformations in the closed channel state? And finally, does the pore forming domain act as a monomer or as an oligomer under *in vitro* and *in vivo* conditions?

3.2 Material and Methods

If not mentioned separately, all chemicals and reagents used were purchased from the following manufacturers. AppliChem (Darmstadt) , Avanti Polar Lipids Inc. (Alabaster, USA), BioRad Laboratories GmbH (Munich, Germany), Carl Roth GmbH + Co. KG (Karlsruhe, Germany), Eppendorf AG (Hamburg, Germany), Fermentas GmbH (St. Leon-Roth, Germany), GE Healthcare Europe GmbH (Munich, Germany), Merck KGaA (Darmstadt, Germany), Millipore GmbH (Eschborn, Germany), NEB GmbH (Frankfurt am Main, Germany), Qiagen GmbH (Hilden, Germany), Roche Diagnostics GmbH (Mannheim, Germany, Whatman GmbH (Dassel, Germany).

3.2.1 Bacterial strains and plasmids

Table 3.1 summarizes the bacterial strains with their respective genetic properties used in this work.

Table 3.1: *E. coli* strains used in this work with their respective genotypes.

***E.coli* strains**	**Genotype**
E. coli DH5α	F- *f80dlacZM15 D(lacZYA argF)U169* Hanahan (1983) *deo*R *phoA supE44 hsdr17(rK-, mK+) recA1endA1 gyrA96l- thi-1 relA1*
E. coli K12 C600	*F- thr leu thi lac tonA sup*E
E.coli Origami	*⊿(ara-leu)7697 ⊿lacX74 ⊿phoA Pvu*II *pho*R *araD139 ahpC galE galK rpsL* F'[*lac*$^{+}$ *lacI*^{q} *pro] gor522*::Tn*10 trxB* (Str^{R}, Tet^{R})

All colicin A mutants were encoded on the plasmid pLR1, carrying an Amp^{R} resistance. Single-site mutations to introduce cysteine residues for spin labeling were carried out with the oligonucleotides given in Table 3.2.

Table 3.2: Oligonucleotides used in this work (Primer), MWG Biotech (Ebersberg)

Name	Sequenz (5`-3`)	Function
pLR1_caa_for1	CGT TGT CCC GTT AGT GCT TCA TTG	sequencing primer
pLR1_caa_rev1	GAG CAT CAC GGT TAG CCA CTG	sequencing primer
pLR1_caa_for2	TGA TGC TCT GAA TAG CCA ATT GTC T	sequencing primer
pLR1_caa_rev2	GTT AAC AAC AGC CGG AAG GCC TG	sequencing primer
pLR1_Cai_for	GCA GAA TAG ATA AAC AAT TGC TGC ATA	sequencing primer
ColA_16Cys_for	TCTAGAAAAATGTAGTGAACTGATTGCT	mutagenesis primer
ColA_16Cys_rev	AGCTCCCGCTCATCTTTGGC	mutagenesis primer
ColA_77Cys_for	GAA AAT TAA TAA G TGT GAC AGA GAT GCT C	mutagenesis primer
ColA_77Cys_rev	ATG GCC GGG TTG GCC GTG ATT	mutagenesis primer
ColA_126Cys_for	ATT GAG GGG TAT TGT ACC GGG AAC TGG	mutagenesis primer
ColA_126Cys_rev	GCT CTT CTC GCG AAC CTT CTC	mutagenesis primer
ColA_182Cys_for	GCT AGC CGC G TGC GTT GGC GCC	mutagenesis primer
ColA_182Cys_rev	AGG ATC CCG GCG ATA CCA ACA G	mutagenesis primer
ColA_187Cys_for	GTT GTT GGC GCC TTA TGT GAT GAT AAG TTT GCA G	mutagenesis primer
ColA_187Cys_rev	CGC GGC TAG CAG GAT CCC GGC GAT AC	mutagenesis primer

3.2.2 Molecular biology techniques

3.2.2.1 Cloning and mutagenesis

The plasmid pLR1 encoding wild-type (wt) ColA was used as a template for a site-directed mutagenesis Kit (Finnzymes) to introduce Cys codons into the open reading frame for single and double cysteine mutants in the *caa* gene at different positions. The following pLR1 plasmids in *Escherichia coli* K-12 C600 with the *caa* gene carrying single cysteine mutations have been prepared:

Single mutants: T15R1, L19R1, I26R1, K33R1, A42R1, S62R1, I66R1, A77R1, A91R1, F105R1, V115R1, E126R1, W140R1, A150R1, S155R1, G166R1, A169R1, G176R1, A181R1, V182R1, V183R1, G184R1, I187R1, A192R1 and E198R1.
Double mutants: L19R1/I187R1, A42R1/I187R1, S62R1/I187R1, A91R1/I187R1, V115R1/I187R1, A91R1/G184R1, A91R1/V115R1, L19R1/A42R1, I26R1/A77R1, A77R1/W140R1, A77R1/S155R1, W140R1/A150R1, I26R1/A192R1, I26R1/E126R1and K33R1/E198R1

All colicin A mutants except T15R1, I66R1, A77R1, V182R1, I187R1, I26R1/A77R1, A77R1/W140R1 and A77R1/S155R1 were kindly provided by Dr. Denis Duché, Dr. Sabine Boehme and Dr. V. Lakshmi Padmavathi, Pulagam (see Table 3.7 in the appendix of chapter 3).

3.2.2.2 Polymerase chain reaction (PCR)

Site directed mutagenesis was performed using a Phusion site-directed mutagenesis kit (Finnzymes, Thermo Fisher) as recommended by the manufacturer. For this purpose, point mutations are created by designing a mismatch in the primer. The PCR reaction was performed using the PCR sprint thermal cycler (Thermo Scientific). The PCR reaction mixture and the thermo-cycling conditions were chosen as recommended by the manufacturer.

3.2.2.3 DNA sequencing

After mutagenesis the DNA sequence of the plasmid constructs for each mutant was verified by DNA sequencing (Seqlab).

3.2.2.4 Preparation of competent *E. coli* cells and transformation

To prepare $CaCl_2$ chemically competent *E.coli* K12 C600 cells the method of Sambrook et al., 1989 was used and followed by standard transformation protocols (Finnzymes; NEB).

3.2.2.5 Isolation of plasmid DNA from *E. coli*

For the isolation of plasmid DNA, 5 ml *E.coli* overnight culture (120 rpm, 37°C in LB medium, see 3.2.3) was cultivated and the „QIAprep Spin Miniprep Kit“ (Qiagen, Hilden) was used as recommended by the manufacturer.

3.2.3 Media and cultivation conditions

3.2.3.1 Growth media for *E. coli* cells

Cultivation of *E. coli* cells was performed in rich medium, LB (Lysogeny Broth, "Luriabroth") with 10 g/L bacto-tryptone (Difco, Detroit, USA), 5 g/L yeast extract and 10 g/L NaCl (Sambrook et al., 1989) at 37°C under aerobic conditions. To select for cells carrying pLR1 plasmids, the medium was supplemented with ampicillin to a final concentration of 100 mg/ml. For agar plates 15 g/L Bacto-Agar was added before autoclaving.

3.2.3.2 Expression and cultivation conditions

Growth of the bacterial cultures was followed by determining the optical density (OD) of the medium at 600 nm wavelength. *E. coli* K12 C600 cells were transformed with the pLR1-wt plasmid DNA or with pLR1 plasmids carrying *caa* genes with single or double cysteine mutations. *E. coli* cells were cultivated overnight in LB medium containing ampicillin (100 mg/ml) at 37°C. Subsequently, the cells were inoculated with the overnight culture to obtain an optical density OD_{600} = 0.1, and further cultivated at 37°C. The heterologous overexpression of colicin A was induced by the addition of mitomycin C (300 ng/ml) when the cultures reached an optical density of OD_{600} = 0.5 - 0.7, and grown until the optical density starts to decrease. For cell harvesting the culture medium was centrifuged at 4500 rpm at 4°C for 20 min, using a Sorvall centrifuge equipped with a SLA 3000 rotor.

3.2.4 General analytical and biochemical techniques

3.2.4.1 Protein separation

Based on the mechanism of action and the translocation pathway of colicin A described in chapter 3.1 it has to be expected that a significant amount of colicin A is incorporated into the inner membranes of the cultured cells. In previous protocols for colicin A protein separation, only the supernatant (colicin A released into the medium) was used. The protocol was optimized such that colicin A was *additionally purified from isolated E. coli membranes*. According to the previous protocol recombinant cysteine mutants were expressed as described in 3.2.3.2. The cells were harvested at 4500 rpm for 20 min at 4°C by a Sorvall centrifuge equipped with a SLA 3000 rotor. Proteins in the isolated supernatant were precipitated with ammonium sulphate (243 g/L) at 4°C for 1 h and afterwards sedimented at 4200 rpm at 4°C for 45 min. For the isolation of colicin A from *E. coli* membranes the corresponding cell pellet after harvesting was resuspended in a small volume of supernatant and treated with lysozyme (0.5 mg/ml), DNase and 0.5 mM PMSF. Subsequently, cells were disrupted by sonification and solubilized with 2 % DDM overnight at 4°C. Afterwards, the crude extract was centrifuged for 20 min at 4500 rpm and 4°C to separate the cell

debris. The supernatant was then added to the 'external' colicin A supernatant prior to protein precipitation with ammonium sulphate. After centrifugation the pellet was resuspended in 10 mM sodium phosphate buffer, pH 6.8 and dialyzed overnight against 10 L buffer (10 mM sodium phosphate, pH 6.8) to remove the remaining ammonium sulphate.

3.2.4.2 Protein purification *via* Fast Protein Liquid Chromatography (FPLC): cation exchange

The dialyzed protein-solution was centrifuged for 45 min, 4°C at 15000 rpm and the supernatant was loaded onto a Hitrap SP FF column - a cation exchange column. A FPLC system (Pharmacia) was used (4°C). First, the column was equilibrated with buffer A (10 mM sodium potassium buffer, pH 6.8, 1 mM EDTA) at a flow rate of 5 ml/minute. Afterwards, the protein was applied to the column at a flow rate of 4 ml/minute. The protein bound to the column was eluted by a 0 - 400 mM NaCl gradient. Elution of the protein was monitored at 280 nm by an UV detector. 5 ml were collected and in the fractions containing protein the presence of colicin A was verified by SDS-PAGE electrophoresis. Fractions containing colicin A were pooled and concentrated (see 3.2.4.6) for further purification *via* size exclusion chromatography.

3.2.4.3 Protein purification Fast Protein Liquid Chromatography (FPLC): size exclusion

For size exclusion chromatography 500 µl of the concentrated and pooled eluates from the cation exchange column were loaded on a gel filtration column Superdex 200 MR. 10/30 (Amersham Pharmacia Biotech) and purified based on their size with 0.5 ml/minute flow rate of 10 mM sodium potassium buffer, pH 6.8. Elution of the protein was monitored at 280 nm by an UV detector. The protein fractions were concentrated and stored at -80°C in liquid nitrogen for further use.

3.2.4.4 SDS-Polyacrylamide Gel Electrophoresis (PAGE)

For the electrophoretic analyses of proteins under denaturing conditions the method by Schägger et al., (1987) was used with a 4 % stacking and a 10 % resolving gel. The proteins were diluted in PAP (50 mM Tris/Hcl, pH 6.8, 2 % SDS, 10 % glycerol, 5 % mercaptoethanol, 0.1 % bromphenolblue) and gel electrophoresis was performed in a MINI Vertical Dual Plate Electrophoresis Unit (BioRad). For transfer through the stacking gel phase, 100 V were applied for 15 min. Separation was carried out at 160 V for 45-60 min. Visualization of proteins was performed by means of Coomassie Brilliant Blue staining developed by Sambrook et al., 1989. For this purpose, the SDS-gels were incubated in a staining solution (0.25 % Coomassie Brilliant Blue G-250, 50 % (v/v) methanol, 10 % TCA) for 1 to 16 h, followed by destaining of the gels using 5 % (v/v) methanol and 7.5 % acetic acid.

Table 3.3: Buffer and solutions for SDS-Page

	Stacking gel	**Resolving gel**
acrylamide (48 % AA / 1,5 % BisAA)	1 ml	6.1 ml
gel buffer	3 ml	10 ml
glycerol 87 % (v/v)		3.25 ml
H_2O_{dd}	8 ml	10.65 ml
TEMED 10 %	10 µl	10 µl
APS 10 %	100 µl	100 µl

3.2.4.5 Preparation of whole cell lysates for SDS-Page

Test expressions have been carried out in 5 ml cultures at 37°C like described in 3.2.3.2. For analysis *via* SDS Page test samples were taken at different times during the growth phase. Samples were also taking prior to induction at an OD_{600} of approximately 0.5. At the same time protein expression was induced by adding mitomycin C. After induction samples were taken in 30 min intervals. According to Neidhardt et al. (1990), for *E. coli* an OD_{600} of 1 corresponds to about 160 µg of protein per 1 ml of cell culture. Consequently, the test samples contained ~ 20 - 50 µg protein. After centrifugation for 2 - 3 min at 13000 x g the cell pellets were resuspended in 25 µl 1-fold PAP, incubated for 5 min at 100°C and then analysed by SDS Page.

3.2.4.6 Concentration of colicin A by ultrafiltration

To concentrate the purified colicin A in solution a membrane filtration technique was used. Centrifugal filter devices with a MWC (molecular weight cutoff) of 30 kDa (Amicon/Millipore, Carringtwohill, Co. Cork, Ireland; Vi-Vascience, Lincoln, USA) were used. The membranes in the filter devices were saturated two times with BSA in a concentration of 1 mg /ml to prevent aggregation of colicin A on the membrane. To remove loosely bound BSA and prevent contamination of the colicin A solutions, the filters were washed two times with buffer (50 mM sodium potassium buffer, pH 6.8) prior to application of the colicin A samples.

3.2.4.7 Determination of protein concentrations

To measure the protein concentration of colicin A in solution the absorption of the protein was determined at 280 nm with an UV-VIS spectrophotometer (UV-2450, Shimadzu Corporation, Kyoto, Japan) and applying Lambert-Beer's law. The extinction coefficients of the proteins were calculated with the Expasy tool *protparam* (web.expasy.org/protparam/) (ε = 51910 $M^{-1}cm^{-1}$).

3.2.4.8 Site-directed spin labeling (SDSL)

For labeling with the MTS spin label ((1-oxy-2,2,5,5-tetramethyl-pyrrolinyl-3-methyl) methanethiosulfonate, see 2.3.1) freshly prepared 1 M DTT (Sigma-Aldrich, Munich, Germany) stock solution was added to purified colicin A to a final concentration of 10 mM, and incubated overnight at 4°C. DTT was removed by exchanging the buffer 5 times with 50 mM potassium phosphate buffer (pH 6.8) by using 30 K BSA saturated Amicon Ultra-4 centrifugal filter units (Millipore). Subsequently, a MTS spin label stock solution (100 mM in acetonitrile) was added to the protein solutions to reach a final MTSSL concentration of 1 mM, and incubated overnight at 4°C. Unbound spin label was removed by exchanging the buffer (10 mM potassium phosphate buffer pH 6.8) for 5 times and the spin-labeled colicin was concentrated (see 3.2.4.6) and stored at -80°C. For spin labeling of positions in colicin that appear buried in the soluble form the protein was labeled in an unfolded state and subsequently refolded. DTT was removed by exchanging the buffer 3 times with 50 mM potassium phosphate buffer containing 6 M guanidinium hydrochloride (GdHCl) (see 3.2.4.6). The MTS spin label stock solution (100 mM in acetonitrile) was added to a final concentration of 1 mM and incubated overnight at 4°C. Refolding of the protein after labeling and removal of unreacted spin label was achieved by exchanging the 50 mM potassium phosphate buffer stepwise with decreasing GdHCl concentrations (6 M down to 0.5 M), and subsequent incubation of the protein in 0.5 M GdHCl at 4°C overnight. Afterwards stepwise dilution was continued to reach final a GdHCl concentration < 0.05 M, and the spin-labeled colicin was concentrated (see 3.2.4.6) and stored at -80°C.

3.2.4.9 Viability tests

Functionality of the mutated and labeled colicin A constructs used in this work, i.e. the toxic activity towards wt *E. coli* cells, was tested using a so called *viability test* that is based on a plating method. For this technique for each mutant and for wt colicin A a stock solution with a concentration of 2 mg/ml ColA was prepared. 500 µl of an *E. coli* K12 C600 culture that has been incubated overnight at 37°C was placed on a LB agar plate and spread with glass spreader. The *E. coli* agar plates were treated with 1 µl of the above mentioned colicin A solutions in 5 different dilutions (from 10^0 up to 10^5, with the respective

buffer) and incubated overnight at 37°C. After incubation the diameter of the bacteria free areola was determined and compared to that of the colicin A wild-type.

3.2.4.10 Liposome preparation

For preparation of liposomes, native *E. coli* phospholipids (Polar Lipid Extract, 20 mg/ml dissolved in chloroform, (Avanti Polar Lipids, Alabaster, USA)), were used. First, chloroform was evaporated to dryness in a nitrogen flux. Subsequently, the dry lipids were hydrated in 50 mM potassium buffer, pH 6.8 to a final concentration of 20 mg/ml and sonicated until a homogeneous solution was obtained. The resulting suspension containing large multilamellar vesicles (LMVs) was subjected to 3 freeze-thaw cycles and finally stored at -80°C. Prior to use for reconstitution of colicin A variants, the LMV suspension was thawed slowly at room temperature and then extruded (Avanti Mini-Extruder, Avanti Polar Lipids, Alabaster, USA) 11 times through 400 nm polycarbonate filters (Whatman, Dassel, Germany) to form liposomes.

3.2.4.11 Detergent-mediated reconstitution

For protein reconstitution liposomes were first solubilized by stepwise addition of 0.1 % Triton X-100 (v/v, 50 mM NaPi, pH 6.8). The degree of solubilization was monitored by measuring the turbidity at a wavelength of 540 nm. After saturation with detergent, the liposomes were mixed with spin labeled colicin A in a molecular ratio of 1:500, and incubated by slowly seesawing for 30 min at RT. Afterwards the detergent was remove step-wise using pre-washed (50 mM NaPi, pH 6.8) detergent removal beads (Calbiosorbs, Calbiochem). For this purpose 5 times 40 mg/ml of half dry Calbiosorbs beads were added to the protein/liposome/detergent-mixture and incubated by slowly seesawing (15 min at room temperature, then 15 min, 30 min, overnight and for 1 h at 4°C. Each time the beads are replaced by fresh beads). After removing the beads, the solution was centrifuged for 1.5 h at 80,000 rpm and 4°C (Sorvall Discovery ultracentrifuge, Thermo Fisher). The resulting pellet was resuspended in 50 µl buffer (50 mM NaPi, pH 6.8), frozen in liquid nitrogen, subjected to 3 freeze-thaw cycles and finally stored at – 80°C. The protocol for detergent-mediated reconstitution is schematically depicted in Figure 3.7.

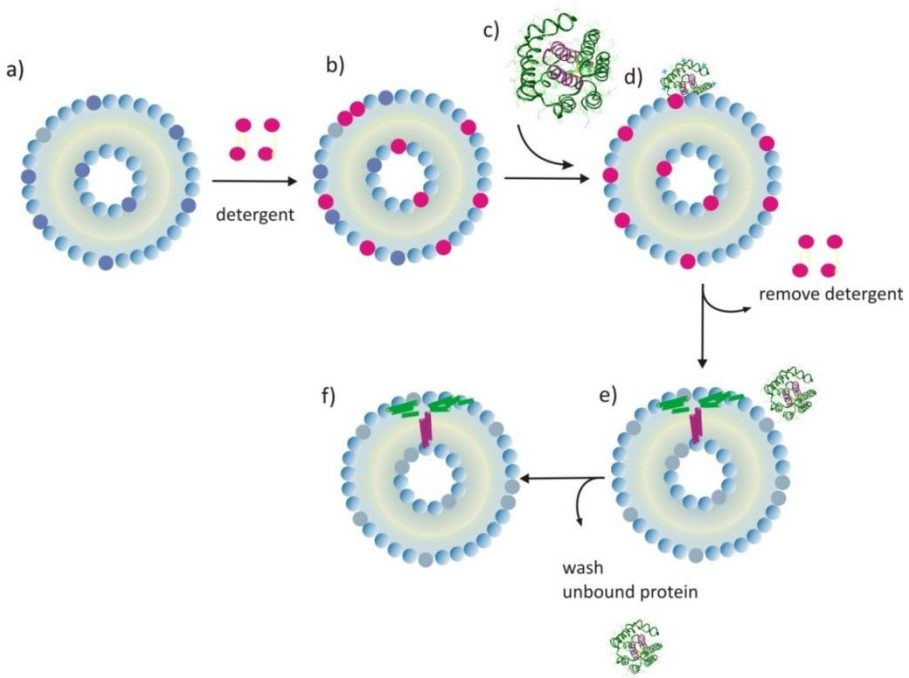

Figure 3.7: Schematic representation of the reconstitution method. (a) large unilamellar vesicles (b) detergent-destabilized liposomes (c) water-soluble spin-labeled colicin A (d) detergent solubilized liposomes and protein. The detergent is removed by detergent-adsorbing beads. (e) Resulting proteoliposomes with unbound protein and (f) resulting proteoliposomes. Figure adopted and modified from L. Pulagam, PhD Thesis, 2007.

3.2.4.12 Sample preparation for DEER measurements on live *E.coli* cells

100 ml *E. coli* Origami cell culture (LB medium) was cultivated overnight at 37°C. This culture was used to inoculate 100 ml LB medium to obtain an optical density OD_{600} = 0.1. The cultures were further grown at 37°C. At an OD_{600} = 0.5 the cells were harvested by centrifugation at 4500 rpm, for 15 min at 4°C (Beckmann coulter centrifuge Allegra-X-15R with SX4750A rotor). The cell pellets were resuspended in 2 ml 50 mM sodium phosphate buffer (pH 6.8), containing 0.2 % glucose and 0.3 mM KCl, and incubated on ice for 30 minutes. Afterwards the cells were harvested again by centrifugation and resuspended in 1 ml of the same buffer. To 100-200 µl cell suspension 2 mg/ml of spin-labeled colicin A was added. After incubation time < 2 minutes the cells were pelleted at 13000 rpm, 4°C for 1 minute. The cell pellet was washed two times with 100-200 µl 50 mM sodium phosphate buffer (pH 6.8), 0.2 % glucose and 0.3 mM KCl to remove unbound colicin A. Finally, the cell pellet was resuspended in 30 µl of the same buffer containing 20 % deuterated glycerol (glycerol-d_8, Sigma-Aldrich) and transferred into 3 mm (outer diameter) EPR quartz capillaries and immediately frozen in liquid nitrogen for the DEER measurements.

3.2.5 Cw EPR Methods

3.2.5.1 Mobility measurements

For analysis of the dynamics of the spin label side chains attached to colicin A room temperature (293 K) spectra were recorded using a home-made X-band (9.3–9.4 GHz) EPR spectrometer equipped with a dielectric resonator (MD5, Bruker Biospin). All spectra were obtained at 0.5 mW incident microwave power and 0.15 mT B-field modulation with 20 µl of sample volume in 0.9 mm (inner diameter) EPR glass capillaries. For direct comparison of the cw EPR spectra normalization of the spectra either to (i) the maximum amplitude of the EPR first derivative spectrum (all EPR spectra shown in this chapter have been normalized in this way), or (ii) to the area under the EPR absorption spectrum was carried out. The area under the absorption spectrum is directly proportional to the spin concentration in the sample and can be used to calculate the sample´s concentration when compared to the area integral of a reference spin probe (2,2,6,6-Tetramethyl-1-piperidinyloxy (TEMPO)) of known concentration.

$$\boldsymbol{C_{sl-sample} = \frac{Area_{sample} \cdot c_{sl-ref}}{Area_{reference}}} \qquad \textbf{(3.1)}$$

$c_{sl\text{-}sample}$ and $c_{sl\text{-}ref}$ are the spin concentrations of the colicin sample and the reference sample (100 µM TEMPO or TEMPOL), respectively. The spin labeling efficiency can be calculated if the protein concentration in the sample is known:

$$\boldsymbol{Labeling\ Efficiency = \frac{c_{sl-sample}}{c_{sample}}} \qquad \textbf{(3.2)}$$

For the analysis of the spin label mobility two semi-empirical mobility parameters, the width of the central line (ΔH_0^{-1}) and the spectral second moment ($<H^2>^{-1}$), were used (see chapter 2.3.2). The second moment and the central line width were calculated using the program *unispec* written by Christian Beier. In addition the central line width was also determined manually from the EPR spectrum.

3.2.5.2 Temperature dependent measurements

Temperature dependent cw EPR spectra were analysed in terms of an equilibrium between the two components with different mobilities present in the spectra at ambient temperature. The EPR spectra were recorded in the temperature range from 273 K to 303 K. The first derivatives of the spectra were normalized (see 3.2.5.1) and compared. The relative contributions of the two components were

determined by means of the amplitudes in the low field region. The logarithm of the ratio of the two components was then plotted *versus* the inverse of temperature to obtain the corresponding ΔG values for the transition between the conformational states characterized by the two spectral components from the resulting van´t Hoff plots.

3.2.5.3 Accessibility measurements

Accessibilities were determined for the collision reagents gaseous oxygen and NiEDDA (Ni(II)ethylenediamine diacetate). Measurements were carried out on a homebuilt cw EPR spectrometer equipped with a loop gap resonator. The B-field modulation was set to 0.15 mT. The applied microwave power was varied in the range from 0.1 to 50 mW. In order to change the main attenuator during the measurement a motor, controlled by the data acquisition software, was used. Gas permeable TPX (Polymethylpenten) capillaries (RototecSpintec GmbH, Biebesheim, Germany) were filled with 6.3 µl of sample solution and placed into the resonator. For reference measurements the sample was deoxygenated by fluxing the resonator permanently with nitrogen gas. In order to obtain accessibilities for oxygen, the nitrogen was replaced by 100 % O_2. For Ni-accessibility determination, 200 mM NiEDDA solution was added to the sample solution, leading to a final concentration of 20 mM NiEDDA. During the measurement the nitrogen gas flux was preserved. Before each experiment the sample was fluxed with the respective gas for at least 30 min. The amplitudes of the central resonance line were determined and W_{ex} was calculated using the program *powerfit* written by Martin Kühn (2003). The peak-to-peak line widths of the EPR central line and the corresponding amplitudes were obtained by fitting of a pseudo-Voigt function to the EPR central line. Then the calculated amplitudes were plotted versus the square root of the power, automatically done by the program *satfit*. To these data points a curve according to equation 2.17 in chapter 2.3.3 was fitted and the parameter $P_{1/2}$ was calculated. The accessibility parameters Π and W_{ex} were determined using equation 2.18. The cavity dependent normalization factor *a*, that is needed for the calculation of W_{ex} from Π, is $a = 1.87$ (Doebber, PhD Thesis 2009). The immersion depth parameter Φ was calculated using equation 2.19.

3.2.5.4 Polarity measurements

Low temperature (160 K) cw-EPR measurements have been carried out to determine the polarity of the spin label environment of colicin A R1 side chains using a homemade X-band EPR spectrometer equipped with a Bruker super high-Q cavity. The magnetic field was measured with a B-NM 12 B-field meter (Bruker Biospin). For stabilization of the sample temperature at 160 K a continuous flow cryostat Oxford ESR900 (Oxford Instruments, Oxfordshire, UK) and a temperature controller (ITC 4; Oxford Instruments) was used. All spectra were obtained at 0.2 mW microwave power and 0.24 mT B-field modulation amplitude. 40 µl of sample solution were filled into EPR quartz capillaries with 3 mm inner

diameter. The A_{zz} values as a measure of the environmental polarity were determined from a detailed line shape analysis using the program *Dipfit* developed by Steinhoff and coworkers (Steinhoff et al., 1997). This simulation program considers a Gaussian distribution of inter spin distances, variable contributions of singly spin-labeled protein and employs automated routines to determine best-fit parameters. Fit parameters for the double mutants were obtained by fitting of the EPR spectra obtained with the corresponding singly labeled protein samples.

3.2.6 Pulse EPR experiments

3.2.6.1 DEER-Double Electron-Electron Resonance

Pulse EPR experiments (DEER) were performed at X-band frequencies (9.3–9.4 GHz) with a Bruker Elexsys 580 spectrometer equipped with a Bruker Flexline split-ring resonator ER 4118X-MS3. 3 mm outer diameter EPR quartz capillaries were loaded with 25-50 µl of protein/liposome solution containing 20 % of deuterated glycerol. Temperature control was achieved using a continuous flow helium cryostat (ESR900; Oxford Instruments) regulated by an Oxford temperature controller ITC 503S. All measurements were performed using the four-pulse DEER sequence (Pannier et al., 2000):

$$\pi/2(\upsilon_{obs}) - \tau_1 - \pi\,(\upsilon_{obs}) - t' - \pi\,(\upsilon_{pump}) - (\tau_1 + \tau_2 - t') - \pi\,(\upsilon_{obs}) - \tau_2 - echo$$

For pulses at the observer frequency the ‹x› channels were used. A two-step phase cycling (+ ‹x›, - ‹x›) is performed on $\pi/2(\upsilon_{obs})$. Time t' is varied, whereas τ_1 and τ_2 are kept constant, and the dipolar evolution time is given by $t = t' - \tau_1$. Data were analysed only for $t > 0$. The resonator was over coupled to Q ~ 100; the pump frequency υ_{pump} was set to the center of the resonator dip and coincided with the maximum of the nitroxide EPR spectrum, whereas the observer frequency υ_{obs} was 67 MHz higher and coincided with the low field local maximum of the spectrum. All measurements were performed at a temperature of 50 K with observer pulse lengths of 16 ns for $\pi/2$ and 32 ns for π pulses and a pump pulse length of 12 ns. Deuterium modulation was averaged by adding traces at eight different τ_1 values, starting at $\tau_{1,0}$ = 400 ns and incrementing by $\Delta\tau_1$ = 56 ns. Analysis of the DEER traces was performed with the software Deer Analysis 2011 (Jeschke et al. 2006). Briefly, the phase corrected dipolar evolution data was background corrected assuming a homogeneous 2.4D background, and distance distributions were obtained by Tikhonov regularization with the regularization parameter α chosen based on the L curve criterion. For more details see chapter 2.4.

The number of coupled spins in a biomolecule can be determined from the modulation depth of the dipolar evolution function after background correction (Jeschke et al., 2009). The modulation depth Δ is given by the following equation:

$$\Delta = 1 - (1 - \lambda)^{N-1} \qquad \textbf{(3.3)}$$

where N describes the average number of interacting spins in the observed nanoobject and λ the fraction of spins excited by the pump pulse (inversion efficiency). For further details see Jeschke et al. (2009).

3.2.7 Molecular modeling of ColA

3.2.7.1 MD simulations

The experimentally obtained distance distributions for ColA embedded in the membrane were compared to the results of a MD-simulation. Molecular dynamic (MD) simulations were carried out by Dr. Johann Klare (University of Osnabrück) using the software package YASARA Structure. In brief, after incorporation of the dimer model into a membrane-bilayer containing PE and PG (74 % PEA, 26 % PGL) lipids, a 30 ns MD simulation with explicit water (PIP3P) at 298 K was carried out to provide information about the dynamics of the protein and the interactions between the individual atoms. The force field used (AMBER03) contains terms for the potential energies and pre-calculated force constants to calculate the total potential energy of the model at each step of the simulation. The total potential energy is based on inter atomic bonds, van der Waals and electrostatic interactions of the system. Thus it is possible to get insights and information about the motions of the different spin label side chains, considering the movement of all protein atoms.

3.2.7.2 The rotamer library analysis (RLA)

To improve the comparison of the experimental distances with available crystal structures, or in this case the manually constructedColA dimer model, possible orientations of R1 side chains and distances between these side chains attached at different helix positions are predicted by using a semi-dynamic structure model of the spin label. The dynamics of the R1 side chains are represented by a discrete set of possible rotational isomers, which is called rotamer library and is well described in (Polyhach and Jeschke, 2010), (Polyhach et al., 2011). To perform the rotamer analysis in this work, the program MMM 2013.2 (Multiscale Modeling of Macromolecules) from Y. Polyhach and G. Jeschke (ETH Zürich) was used. The conformational structures of the MTSSL (R1) were provided by a so called rotamer library, containing 210 R1 rotamer structures, which represent different variations of the dihedral angles of R1 attached to a single cysteine residue. The R1 structures can be attached to the respective cysteine position in the protein structure, and the resulting set of possible rotamers on the selected position is determined by calculating the probability of each particular rotamer to occur in the protein structure. The calculated probabilities are influenced by spatial restrictions of the R1 chain due to its local environment defined by other protein atoms. The free energy for each rotamer is computed by Van-der-Waals interactions between atoms of the protein and atoms of the label, by using a Lennard-Jones potential parameterized by an OPLS (optimized potentials for liquid simulations) force field. The energy E_k for the k-th rotamer of the library attached to the protein is calculated by:

$$E_k = \sum i \sum j 4\epsilon_{ij}\left[\left(\frac{\sigma_{ij}}{r_{ij}}\right)^{12} - \left(\frac{\sigma_{ij}}{r_{ij}}\right)^{6}\right] f_{ij} \quad \textbf{(3.4)}$$

where r_{ij} is the distance between the *i*-th atom of the spin label side chain and the *j*-th protein atom. $\epsilon_{ij} = (\epsilon_i \epsilon_j)^{1/2}$ is the interaction coefficient from the individual atom coefficients (extractable from the used force field), and $\sigma_{ij} = (\sigma_i \sigma_j)^{1/2}$ describes the effective radius from the van der Waals radii of the respective atoms. The parameter f_{ij} describes an energy scaling factor (forgive factor) and was set to 1 in the OPLS force field. Reducing the scaling factor reduces the energy penalty for atom clashes. Therefore, a certain amount of flexibility of the local spin label environment is mimicked.
The population parameter P_k for the *k*-th rotamer in the library attached to a certain protein position is calculated by weighting the determined energy E_k according to a Boltzmann distribution normalized by the partition function *Z*:

$$P_k = \frac{exp\left(-\frac{E_k}{k_B T}\right)}{Z} \quad \textbf{(3.5)}$$

k_B describes the Boltzmann constant, *T* the temperature, and the partition function *Z* is given by:

$$Z = \sum_k exp\left(-E_k / k_B T\right) \quad \textbf{(3.6)}$$

From the rotamer sets of two different residual positions all possible distance combinations are calculated and their intensities are weighted by the product of the populations of the considered rotamers

3.2.7.3 Graphical representations of protein structures

Preparation of graphical representations of protein structures in this work has been carried out with the following software packages; YASARA Structure (Krieger et al., 2002), Swiss PDB Viewer (http://spdbv.vital-it.ch/); Accelrys Viewer Lite 4.2 (www.accelrys.com), and UCSF Chimera 1.7 (Pettersen et al., 2004).

3.3 Results and Discussion

R1-labeled colicin A variants were investigated regarding side chain dynamics, accessibilities, polarity of the spin label microenvironment, and inter spin distances in the conformation colicin A adopts when reconstituted in liposomes prepared from *E. coli* polar lipid extracts (rec-mem-ColA) to obtain structural information about the membrane bound closed-channel state of the protein. The following questions are specifically addressed in this work:

a) What does the membrane bound state of colicin A look like, and can it be described by the current models, i.e. the 'umbrella' or the 'penknife' model?
b) Does an equilibrium exist between two protein conformations in the closed channel state exist?
a) Currently, colicin A is suggested to form a functional channel by means of a single protomer, although a significant number of indications exist for colicin channels being oligomeric. Consequently, the question is if the colicin A pore forming domain acts as a monomer or as an oligomer.

3.3.1 Sample preparation

3.3.1.1 Cloning and over-expression of colicin A

The plasmid pLR1, encoding the wild-type ColA, was used as a template to replace different residues by cysteine side chains to obtain single and double cysteine mutants. As described in Chapter 3.2.2.4, *E.coli* K12 C600 cells were transformed with the pLR1-wt plasmid DNA or with pLR1 variants carrying the cysteine mutations. Heterologous overexpression of colicin A was induced by the addition of mitomycin C (300 ng/ml) at an optical density of OD_{600} = 0.5-0.7 of the cell cultures, which were grown until the optical density started to decrease. To increase the yields of purified protein obtained from the cell cultures the existing protocols were optimized in an initial step (described chapter 3.2.4.1). For this purpose, first the extent of colicin A-production over time after induction was analysed in detail (see Figure 3.8).

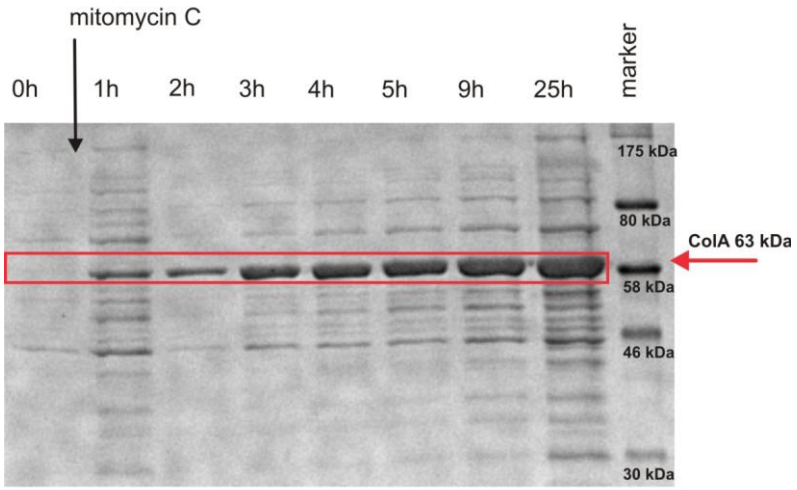

Figure 3.8: SDS-Page analysis of colicin A production in *E. coli* cells carrying the wt-plasmid pLR1. The samples were prepared as described in 3.2.4.4. The numbers given on the top of the gel indicate the time of cell culturing. The band corresponding to colicin A is marked in red. There is no colicin A production in the first hour before the expression was induced with 300 ng/ml mitomycin C.

The test expression reveals that the largest amount of colicin A is present after about 1 day of incubation at 37°C after induction. Consequently, it seems to be necessary to increase the incubation time from several hours as used in the present protocols to about 1 day. Noteworthy, in this experiment only the colicin A released into the extracellular medium was detected. Based on the translocation pathway of colicin A it has to be expected that a significant amount of colicin A is incorporated into the cell membranes. In order to test for this assumption, the amount of membrane bound colicin A was determined by means of the analysis of whole cell lysates by SDS-Page (see Figure 3.9).

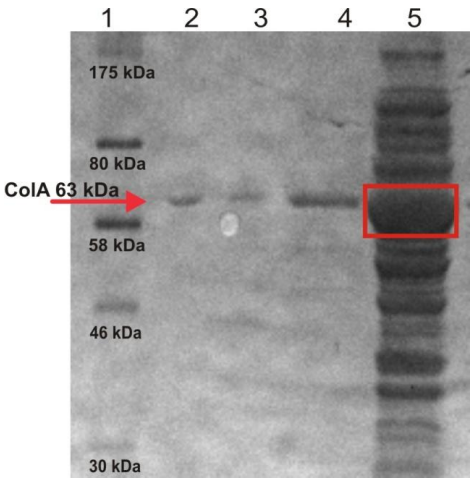

Figure 3.9: Colicin A whole cell lysates, analysed by SDS-PAGE. Lane 1: marker, lane 2 and 3: marker ColA, lane 4: supernatant fraction colicin A after 4 h, lane 5: membrane fraction colicin A after 4 h.

The analysis reveals that indeed a significant amount of colicin A can be detected in the membrane fraction. Compared to the amount of protein present in the supernatant fraction after 4 hours of incubation time it can be expected that the protein yield can be significantly increased if the membrane fraction is also used. Consequently, a new protocol for colicin A expression and separation was established that allows using both fractions of colicin A, as described in chapter 3.2.4. In brief, the cells were harvested after ~ 1 day to separate the supernatant and the cell pellet. The cell pellets were resuspended and disrupted by ultra sonication. Afterwards the solution was solubilized overnight with buffer containing the detergent DDM in a final concentration of 2 % to solubilize the membrane proteins. SDS-Page analysis (data not shown) confirmed that there was no remaining colicin A in the membrane fraction after solubilization. The proteins in the culture medium and those removed from the membrane fraction were collectively precipitated with ammonium sulfate (40 %) and dialyzed.

3.3.1.2 Purification

The first purification step was performed by ion exchange chromatography with a Hitrap SP column attached to a FPLC System (see chapter 3.2.4.2). The purification principle is based on the isoelectrical point of the protein. A pH value at which the protein carries no net charge is called the isoelectrical point, pI. At a pH value below this pI, the molecule will carry a positive charge and bind to the negatively charged surface of the polypropylene column.

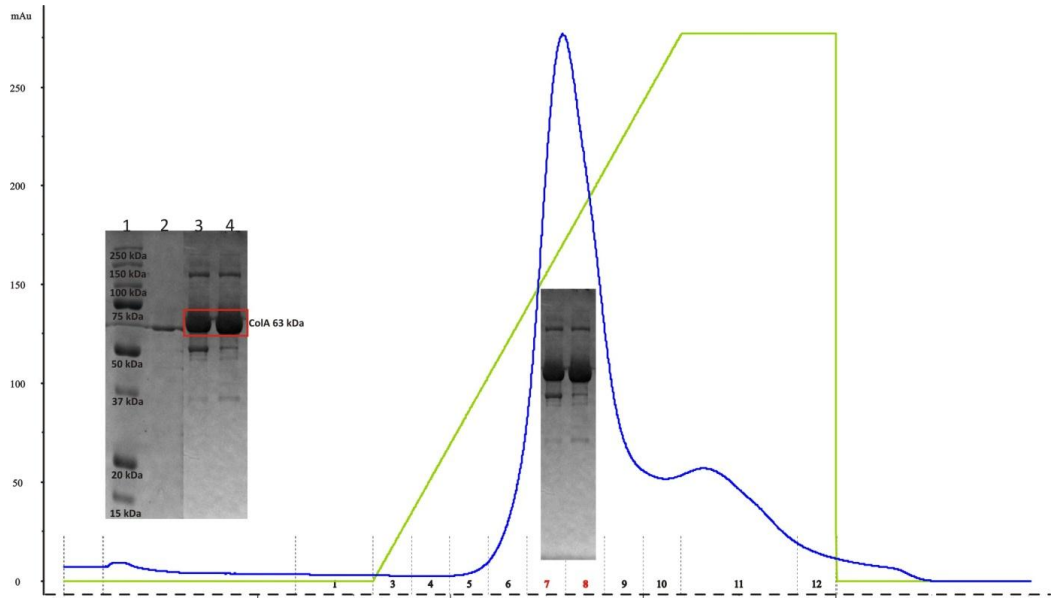

Figure 3.10: Cation exchange elution profile of colicin A mutant 150R1^{H8}. The protein fractions corresponding to this peak in the elution profile were collected and checked using SDS-Page, lane 1: marker, lane 2: marker ColA 63 kDa, lane 3: fraction F7 and lane 4: fraction F8. Blue line: protein peak at 280 nm, green line: sodium chloride continuous gradient from 0 to 400 mM.

After binding of colicin A to the ion exchange column, unbound proteins were washed out with buffer A (10 mM sodium potassium buffer, pH 6.8). Protein elution was obtained with a sodium chloride continuous gradient from 0 to 400 mM. The eluted protein was detected at 280 nm by an UV detector and the fractions were analysed by SDS-Page (Figure 3.10). The elution profile shown in Figure 3.10 represents an example for the purification of a colicin A single mutant (ColA-A150R1). Inspection of the SDS Page reveals a large amount of the selected mutant, judged based on the intensity of the corresponding band at a size of ~ 63 kDa. Moreover, bands with a higher molecular mass than 63 kDa (i.e. a colicin A monomer) could be observed. All colicin A variants used in this work exhibited the same behaviour during the expression and purification procedures. The appropriate fractions containing colicin A were pooled, concentrated and subjected to size exclusion chromatography. 500 µl samples from the cation exchange chromatography were loaded onto a gel filtration column Superdex 200 MR 10/30 (Amersham Pharmacia Biotech) that has been calibrated before, and purified based on their size with a 0.5 ml/minute flow rate of 10 mM sodium potassium buffer, pH 6.8. The resulting elution profile from the gel filtration column for ColA-A150R1 is shown in Figure 3.11.

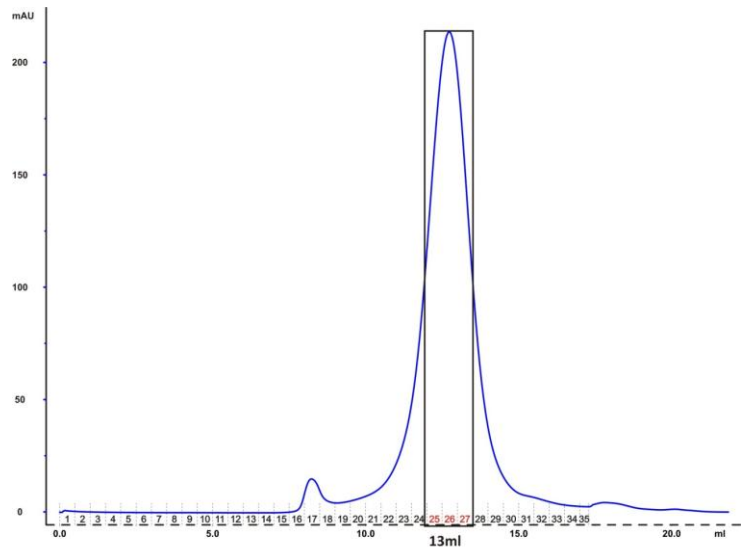

Figure 3.11: Size exclusion elution profile of colicin A mutant A150R1^{H8}.

According to the calibration of the gel filtration column, for colicin A with its size of ~ 63 kDa a retention volume of 13 ml was expected. Indeed, the major elution peak appeared at this retention volume as it can be seen in Figure 3.11. The appropriate fractions were pooled and concentrated for further use. The protein concentration of the purified colicin A samples was determined by UV-VIS spectroscopy (see 3.2.4.7). For wild-type colicin A a final yield of 0.12 mg protein/liter of cell culture was obtained based on the previous purification protocol. With the optimized protocol (see above and chapter 3.2.4) a yield 18 mg protein/liter of cell culture was obtained for wt colicin A. This corresponds to an increase of the protein yield by a factor of about 150. Consequently, all colicin A mutants used in this work have been prepared using the optimized protocol.

3.3.1.3 Spin labeling

Spin labeling of colicin A was carried out as described in chapter 3.2.4.8. In this work 25 single site mutants and 15 double mutants have been used. The single site mutants I26R1, K33R1, A42R1, S62R1, A91R1, F105R1, V115R1, S155R1, G166R1, A169R1, G176R1, A191R1, V183R1, G184R1 and A192R1 were also analysed in previous studies (Savitzky et al., 2004) (L. Pulagam, PhD Thesis, 2007) and (Pulagam et al., 2008), by means of mobility, polarity and accessibility measurements. However, all mutants were newly reconstituted and re-measured in this work. Furthermore, due to the limited number of label positions, where for example no labels have been positioned on H4 and H7, this study has been substantially extended. Already existing, but previously not analysed mutants (L19R1, E126R1, W140R1 and E198R1) and five new mutants (T15R1, I66R1, A77R1, V182R1 and I187R1) have been included, so that on each colicin A-helix at least one label is placed (see Figure 3.12). The double mutants A42C/I187C, S62C/I187C, A91C/I187C and V115C/I187C, for which inter-spin distances measurements have already been performed in a previous study by Boehme et al. (2009), were also freshly prepared and re-measured in this work (see table 3.7 ColA mutant list; appendix chapter 3).

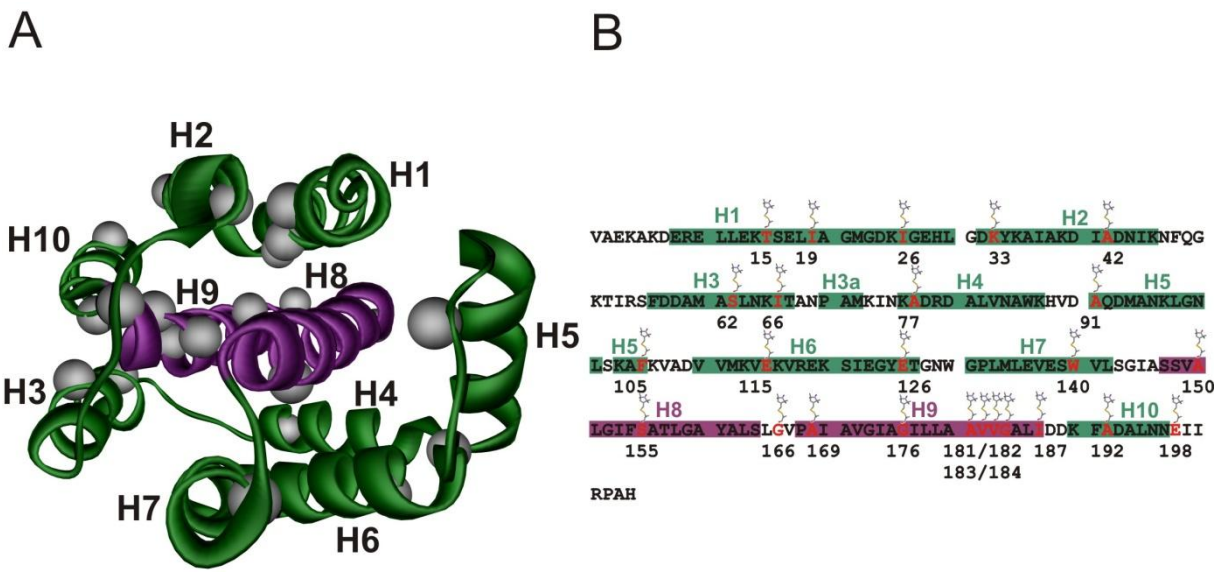

Figure 3.12: Spinlabel positions. (A) X-ray crystal structure of water-soluble pore-forming domain of colicin A (1COL.pdb) showing the positions where spin labels have been introduced (grey spheres at the Cα atom positions). The amphipathic helices are colored in green and the hydrophobic hairpin in magenta. (B) Amino acid sequence of the colicin A pore forming domain. The label positions are colored in red and the respective residue numbers are given.

The room temperature cw EPR spectra of the single site R1 mutants of colicin A in solution (soluble form, sol-ColA) are shown in Figure 3.13. In some of the spectra a residual amount of free (unbound) spinlabel is present, as deduced from the extremely mobile component present in the respective spectra. Examples are the spectra for positions $15R1^{H1}$ and $19R1^{H1}$. This residual amount of free spin label was tolerated in the samples, as extensive washing to remove the free label led to high losses of protein due to precipitation.

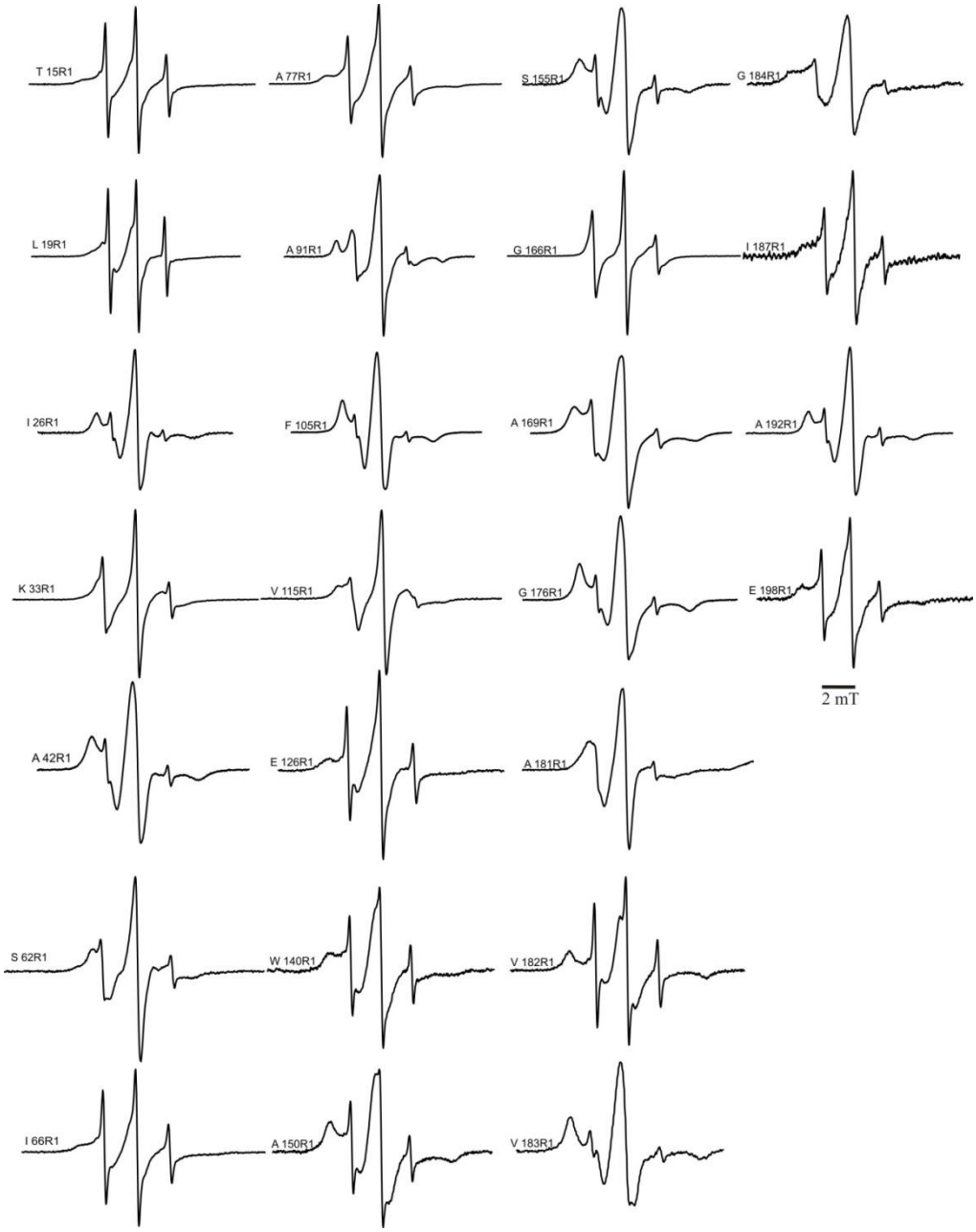

Figure 3.13: Room temperature EPR spectra of single R1 labeled sol-ColA. The spectra are normalized by their amplitudes.

3.3.1.4 Functional analysis of spin-labeled colicin A mutants

In order to test if the mutations of the respective side chains and binding of MTSSL influences the structure and function of the protein, an *in vivo* viability test was performed with each spin label mutant. *E.coli* K12 cells were treated with colicin A as described in chapter 3.2.4.9. Following incubation overnight at 37°C, the bacteria free areas were determined. As a control for the mutant activity wt-colicin A was used. Figure 3.14 shows the results of the viability test for three examples: colicin A-wt, A91R1^{H5} and G166R1$^{LoopH8\text{-}H9}$. As expected, cells treated with wt-colicin A did not survive even at 10,000-fold dilution, corresponding to a concentration of ~ 200 ng/ml (~ 3 nM), indicating the strong lethal interaction of colicin A with the cells. For the mutant A91R1^{H5} about the same functionality as for the wt could be observed (up to 10^4-fold dilution) although the bacteria-free areas appear to be about 10-15 % smaller.

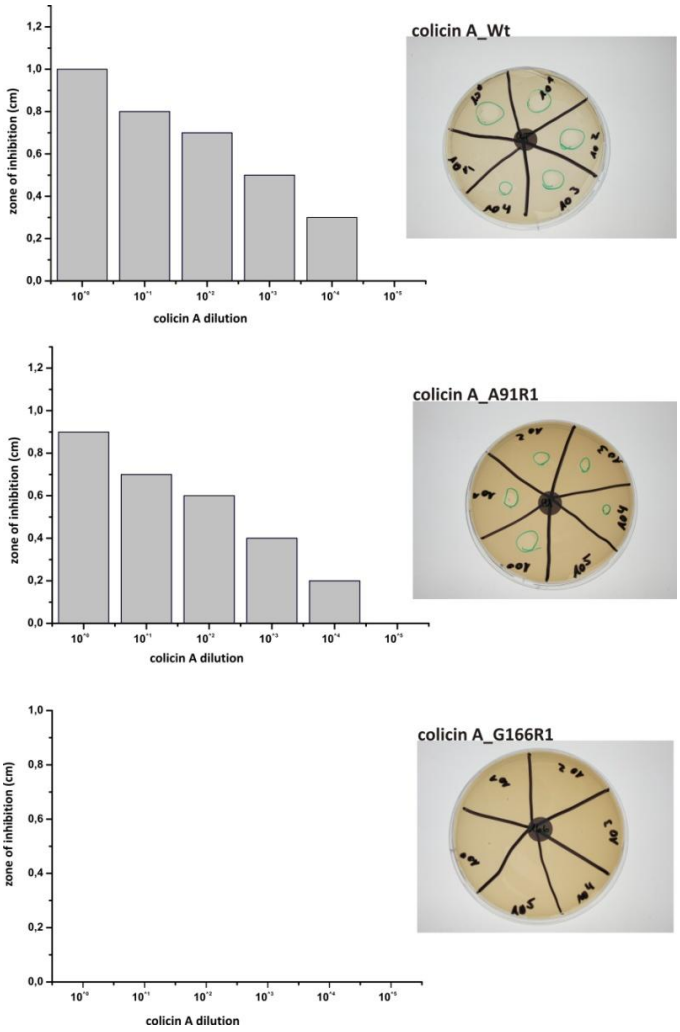

Figure 3.14: Viability of the cells with colicin A. (left) bacteria-free areas, determined from the agar plates treated with colicin A exhibiting the bacteria free areas measured by means of its diameter. The dilution factors for colicin A are given. As a control, the mutant activity of wt-colicin A was determined. (right) photographs of the corresponding plates.

In contrast, colicin A-G166R1$^{LoopH8/H9}$ treated *E. coli* cells survived without any indication of cell death, indicating complete functional impairment of colicin A with a spin label at this position, that is located in the loop between helices 8 and 9 on the protein surface of the soluble form, according to the crystal structure of the water soluble pore forming domain. Consequently, it can be concluded that residue G166 plays an important role either in membrane association, membrane insertion or the function of the channel. The viability test for the whole set of mutants (Table 3.4) reveals that all colicin A mutants except ColA-I19R1^{H1}, G166R1 and G184R1^{H9} were still active. It can be concluded that the structural and functional properties of all other mutants are preserved and that they can be analysed in terms of the colicin A structure in the membrane bound form.

Table 3.4: Influence of mutations in ColA on the pore-forming ability. Functionality of all spin labeled colicin A mutants was assayed by a viability test. The data is reported as the highest dilution of colicin A that still inhibits cell growth. (* ColA dilution from 2 mg/ml resulting in cell-free area in the viability test).

ColA mutant	**ColA dilution** *	**ColA mutant**	**ColA dilution***
Wt 5mg/ml	10^4	L19C/I187C	10^1
Wt 2mg/ml	10^3	A42C/I187C	10^0
T15C	10^2	S62C/I187C	10^1
L19C	no activity	A91C/I187C	10^3
I26C	10^4	V115C/I187C	10^2
K33C	10^2	A91C/G184C	10^4
A42C	10^2	A91C/V115C	10^4
S62C	10^4	L19C/A42C	10^1
I66C	10^2	I26C/A77C	10^4
A77C	10^3	A77C/W140C	10^3
A91C	10^4	A77C/S154C	10^2
F105C	10^3	W140C/A150C	10^4
V115C	10^5	I26C/A192C	10^2
E126C	10^4	I26C/E126C	10^4
W140C	10^3	K33C/E198C	10^4
A150C	10^3		
S155C	10^5		
G166C	no activity		
A169C	10^4		
G176C	10^5		
A181C	10^3		
V182C	10^4		
V183C	10^4		
G184C	no activity		
I187C	10^1		
A192C	10^5		
E198C	10^5		

3.3.1.5 Membrane model system for colicin A

The lipid environment of membrane proteins has been shown to play a major role in protein function and structure, e.g. for rhodopsin (Baldwin and Hubbell, 1985), or small multidrug resistances protein family members (Bay and Turner, 2013), (reviewed for example in Hunte and Richers, 2008). As already mentioned, for colicin E1 it was postulated that the use of 100 % negatively charged lipids prevents the pore-forming domain from inserting into the membrane (Zakharov et al., 2002) (Lindeberg et al., 2000). Moreover, the influence of the lipid composition becomes obvious from the studies on the colicin A closed channel state. As already described in more detail in chapter 3.1.5, some of the studies published so far support the umbrella model for the closed channel state, whereas other data support the penknife model - a controversy that might result from the use of lipid compositions with different influence on the interaction between colicin A and the membrane. In order to test if the lipid composition indeed influences membrane insertion of the colicin A pore forming domain, i.e. it influences the structural properties of the membrane bound state, for a first set of experiments a small subset of the single-site spin label mutants were selected to investigate the influence of different membrane compositions on their room temperature cw EPR spectra. Two positions have been chosen for this purpose: First, position $A181^{H9}$ on the hydrophobic hairpin that either inserts into the membrane or resides on the membrane surface, according to the umbrella - and penknife model, respectively. Second, a position on helix H6, $V115^{H6}$, has been selected as a number of models for membrane insertion postulate a transmembrane orientation of H6 and H7 in the *open* channel conformation. A non-native conformation of these two helices already in the *closed* channel state, thus preventing their membrane insertion, could explain an impaired channel function in for example 100 % negatively charged lipids. The most commonly used model systems for *E. coli* membranes are mixtures of either 1-palmitoyl-2-oleoyl-sn-glycero-3-phosphoethanolamine (POPE) and 1-palmitoyl-2-oleoyl-sn-glycero-3-phosphogylcerol (POPG) lipids, or POPE and 1-palmitoyl-2-oleoyl-sn-glycero-3-phosphoserine (POPS) lipids (see Figure 3.15). These phospholipid compositions are characterized by largely different properties in terms of the surface charges present on membranes prepared thereof. For example, phosphoethanolamine (PE) lipids have no net charge (but a strong dipole moment of the headgroup with a positive charge at the distal end), whereas the hydroxylated phospholipids phosphoglycerol (PG) and phosphoserine (PS) carry a negative charge. Native *E. coli* membranes predominantly consist of PG, cardiolipin (CL, being uncharged) and PS (i.e. approximately the composition of the lipid extract used for comparison) lipids, and consequently their surface is in total negatively charged without positive charges at the very surface from PE lipids (Yeaman et al., 2003). In this work, the influence of these two mixtures of *synthetic* lipids compared to an *E. coli* polar lipid extract has been examined by analysis of RT cw EPR spectra recorded for ColA-V115R1 and ColA-A181R1 reconstituted into liposomes.

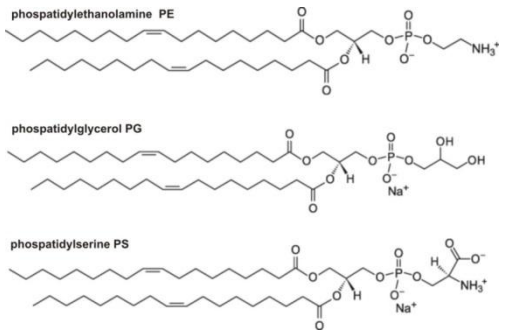

Figure 3.15: Chemical structure of common phospholipids. Source: Avanti polar lipids (http://www.avantilipids.com).

Figure 3.16 shows the room temperature X band cw EPR spectra of ColA-V115R1 reconstituted in *E. coli* polar lipid extract and different POPE/POPG mixtures (panel a), and ColA-A181R1 (panel b) using the lipid extract and different POPE/POPS compositions for liposome preparation and subsequent reconstitution. Comparison of the spectra reveals clear differences between the synthetic mixtures and the native lipids in almost all cases. Obviously, the motional freedom of spin label side chains located at the two positions under investigation is significantly affected by the lipid environment and it can be expected that the structure of the membrane bound colicin A also considerably differs between the samples. Nevertheless, lipid mixtures containing either 50 % or 75 % POPG and POPE seem to resemble the native lipid environment at least for position V115^{H6}, indicating that the PG content seems to be the major determinant for proper membrane insertion of colicin A.

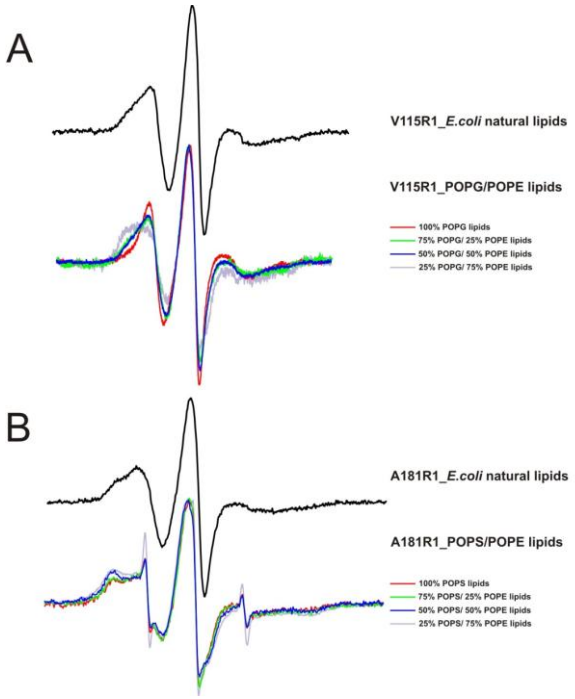

Figure 3.16: Cw-EPR room temperature spectra of the investigated singly labeled rec-mem-ColA mutant (A) V115R1^{H6} and (B) A181R1^{H9} in presence of different PS-lipid compositions.

A more detailed analysis of the influence of the membrane environment on the conformation and properties of colicin A has not been carried out, as this is beyond the focus of this work. Nevertheless, a detailed examination of the influence of membrane lipid composition is needed in the future for a better understanding of its influence on membrane interaction and insertion of colicin A and of membrane proteins in general. For example, cardiolipin is enriched in *E. coli* membranes (Koppelmann et al., 2001) (Yeaman et al., 2003) and suggested to be a key component determining the properties of such bilayers (Lopes et al., 2010), advising studies that examine its influence on ColA membrane insertion.

To exclude that in the structural studies described in the following a non-native conformation is observed, for all preparations of membrane bound spin labeled ColA in the present work an *E. coli* polar lipid extract was used for liposome preparation and reconstitution.

3.3.1.6 Reconstitution of colicin A

Once the functionality of the labeled colicin A mutants was verified, the proteins were reconstituted into liposomes prepared from *E. coli* natural lipids as described in the Materials and Methods section (3.2.4.10 and 3.2.4.11). The reconstitutions were carried out at a molar protein: lipid ratio of 1:500 unless stated otherwise in the following chapters. In order to verify that the protein is incorporated into the lipid membranes, the reconstituted samples were analysed by SDS-Page. After removing the detergent-adsorbing beads, the solution was centrifuged, unbound protein was removed by buffer exchange (→supernatant) and the supernatant as well as the membrane pellet resuspended in buffer was loaded on a SDS gel. Figure 3.17 shows a representative gel obtained with samples taken from reconstitutions of the colicin A mutants L19R1, V183R1, G184R1, I187R1 and E198R1. It is clearly visible that in all cases most of the ColA can be detected in the reconstituted pellet fractions compared to the protein content of the supernatant fractions. From the intensity of the protein bands on the gels high incorporation rates between 70-90 % were obtained for most of the preparations carried out in this work.

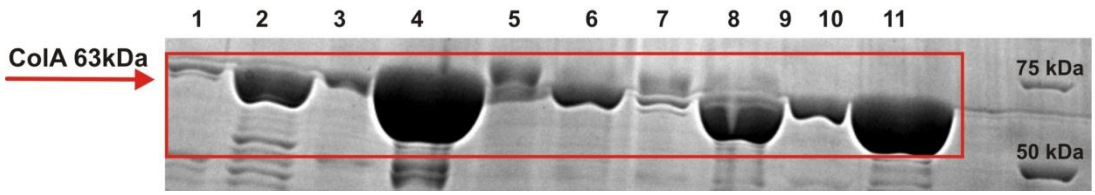

Figure 3.17: Reconstitution of colicin A in *E.coli* lipid membranes in a molar ratio of 1:500. Lane 1: supernatant ColA_L19R1, lane 2: liposomes ColA_L19R1, lane 3: supernatant ColA_V183R1, lane 4: liposomes ColA_V183R1, lane 5: supernatant ColA_G184R1, lane 6: liposomes ColA_G184R1, lane 7: supernatant ColA_I187R1, lane 8: liposomes ColA_I187R1, lane 9: supernatant ColA_E198R1, lane 10: liposomes ColA_E198R1, lane 11: marker (BioRad, Precision Plus Protein).

3.3.2 Spin label mobility measurements on singly labeled ColA

In a first set of experiments, room temperature X-band cw EPR spectra were recorded and analysed to investigate the dynamic properties of spin labels attached to reconstituted ColA single mutants (see chapter 2.3.2 for a description how the spin label dynamics are reflected in RT cw EPR spectra). The EPR spectra are shown in Figure 3.18. The spin label mutants can be – based on the observed spectral properties – categorized into three groups characterized by different spin label side chain mobilities: positions W140R1^{H7}, A150R1^{H8}, S155R1^{H8}, A169R1^{H9}, G176R1^{H9}, 192R1^{H10} and E198R1^{H10} are characterized by large apparent hyperfine splittings with a resolved high field hyperfine line indicating *strongly immobilized* positions due to strong tertiary interactions. Weaker interactions between the protein and the nitroxides result in decrease of the apparent hyperfine splitting and narrowing of the EPR line shapes. A corresponding *intermediate mobility* was found for K33R1^{H2}, A42R1^{H2}, S62R1^{H3}, A91R1^{H5}, F105R1^{H5}, V115R1^{H6}, A181R1^{H9}, V182R1^{H9} and V183R1^{H9}. Finally, *high mobilities*, i.e. the spin labels appear to be attached to very dynamic domains and most likely on the protein surface, are observed for T15R1^{H1}, I26R1^{H1}, I66R1^{H3}, A77R1^{H4} and E126R1^{H6}.

Strikingly, all the room temperature spectra of membrane bound colicin A reveal the presence of at least two spectral components characterized by different mobilities, indicating an equilibrium between two spin populations with different mobilities, as it has for example being reported for residue 165R1 in bacteriorhodopsin (Steinhoff et al., 2000) and for other membrane proteins like KcsA (Gross et al., 1999) and Rhodopsin (Altenbach et al., 1996) (Kroncke et al., 2010). In general, the presence of spin populations with different mobilties can arise from (i) different *spin label rotamer populations* separated by a large energy barrier due to strong tertiary interactions, or (ii) an equilibrium between *protein conformational states* leading to different spin label mobilities. In both cases, exchange between the populations/states is slow on the EPR timescale and both components are observed in RT cw EPR spectra. Under the assumption that ColA exhibits just one single conformation in its membrane bound state, the observed shape of the EPR spectra would therefore result from the presence of at least two spin label rotamer conformations. Nevertheless, although a protein conformational equilibrium for membrane bound ColA is rarely discussed in the present literature, the two spectral components could also arise from different protein conformations. Solely based on the cw room temperature measurements it is difficult to distinguish between these two possibilities, and this issue will be discussed later in more detail. Nevertheless, as it seems very unlikely that spin labels at *all* 26 positions in ColA – especially those exhibiting high mobilities, comprising about 20 % of the positions investigated – experience tertiary contacts that could cause the presence of rotamer populations in slow exchange. Thus the presence of a protein conformational equilibrium for membrane bound colicin A appears to be likely.

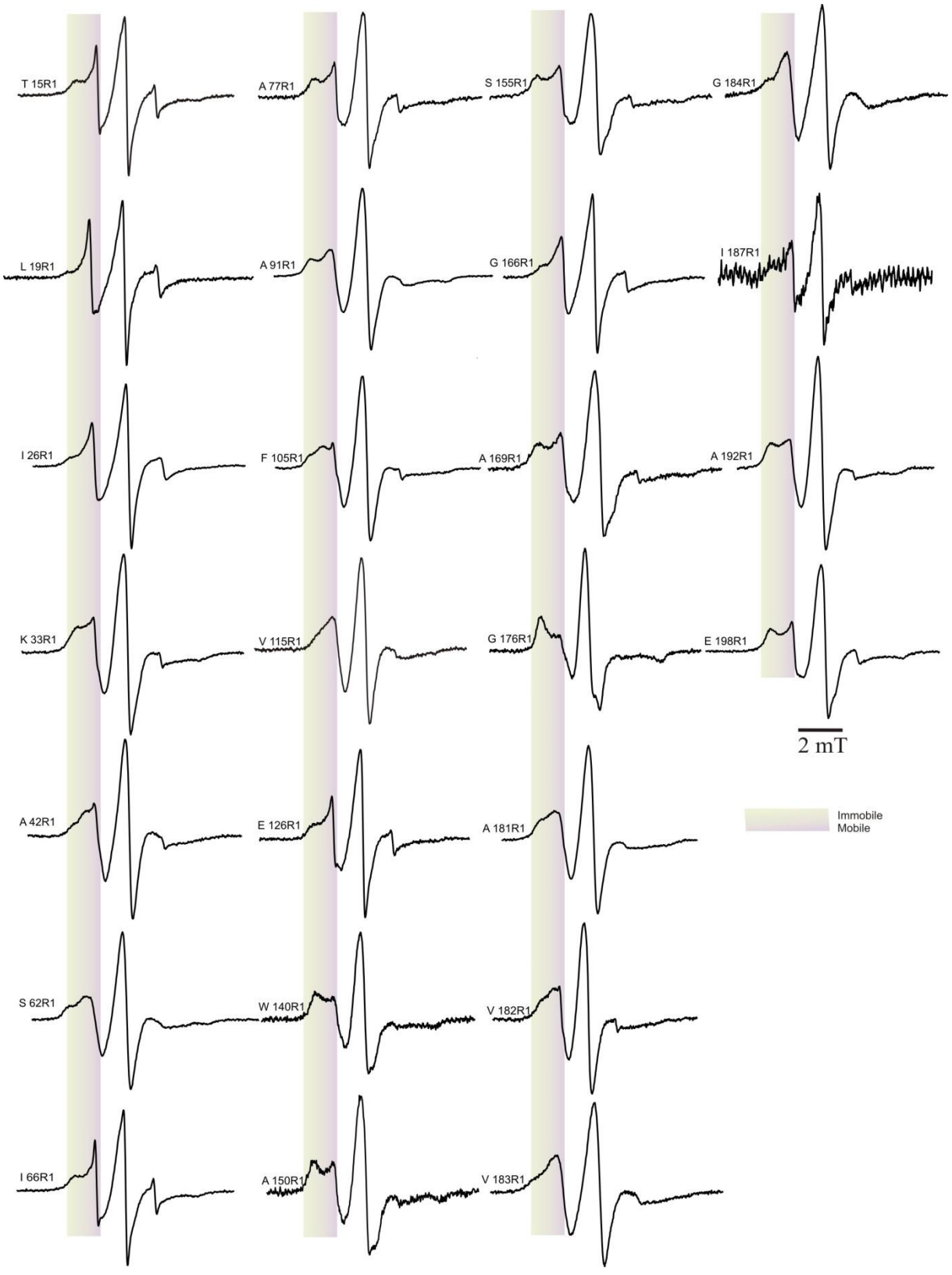

Figure 3.18: Room temperature EPR spectra of single R1 labeled rec-mem-ColA .The spectra were normalized by amplitude. Residue numbers are given for each spectrum. Bars are placed at the low field spectral line to highlight the mobile and immobile components.

The mobility of the R1 side chain can be analysed quantitatively by two semi-empirical mobility parameters, the inverse of the central line width (ΔH_0^{-1}), and the inverse of the second moment ($\langle H^2 \rangle^{-1}$), as described in chapter 2.3.2. Based on ΔH_0^{-1} (Figure 3.19) exceptional high mobilities ($\Delta H_0^{-1} > 3$ mT^{-1}) are observed for residues T15R1^{H1} and 26R1^{H1} on helix 1, I66R1^{H3} and for position 198R1^{H10} on Helix 10. Such high mobility values are a characteristic feature of spin labels located either on exposed helix surfaces or in loop regions. In contrast, strong immobilization ($\Delta H_0^{-1} < 2$ mT^{-1}), corresponding to R1 side chains that are buried in the protein interior, is only observed for residue 176R1^{H9}. All remaining residues exhibit intermediate mobilities ((2 mT^{-1} > ΔH_0^{-1} > 3 mT^{-1}), presumably arising from tertiary interactions, suggesting their location in contact regions between the ColA helices. The mobility values obtained for positions 19R1^{H1}, 166R1$^{LoopH8-H9}$ and 184R1^{H9} are not included in the analysis as labels at these positions have been shown to impair the colicin A channel functionality.

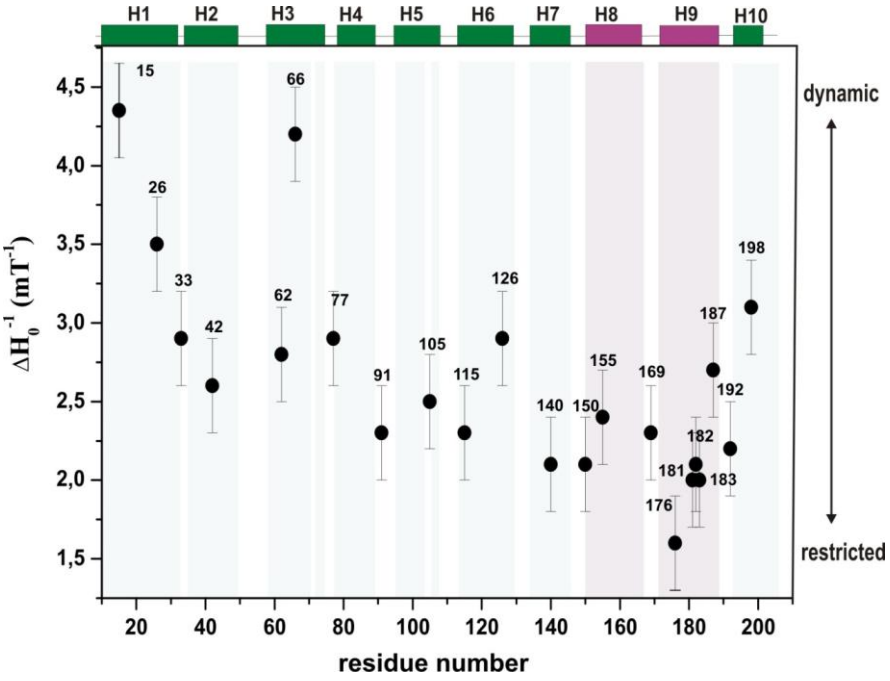

Figure 3.19: Plot of the inverse of the central line width (ΔH_0^{-1}) *versus* residue number for R1 attached to rec-mem-ColA, determined from the EPR spectra shown in Fig. 3.18 using the program *unispec*. The corresponding helices are indicated on the top of the plot. Amphipathic helices (H1-H7 and H10) are colored in green. The hydrophobic hairpin (H8 and H9) is shown in magenta.

The presence of at least two components characterized by different mobilities in all spectra obtained with spin labeled ColA complicates a meaningful analysis of the spin label dynamics. An evaluation of spin label side chain mobilities by means of the inverse central line width of RT cw spectra is intrinsically biased towards the mobile component in multi-component spectra as it dominates the central resonance line – and consequently ΔH_0^{-1} - due to its sharpness. In contrast, the value of the inverse second moment

(i.e. the inverse spectral breadth) is dominated by the immobile spectral component, and combined evaluation of both mobility parameters in a two-dimensional plot of the inverse spectral second moment ($\langle H^2 \rangle^{-1}$) *versus* the inverse central line width (ΔH_0^{-1}), allows classification of the localization of a spin label side chain with regard to protein structure according to Hubbell and Mchaourab (Hubbell et al., 1996) (Mchaourab et al., 1996, see chapter 2.3.2). However, for evaluation of the results described in the following it should be always kept in mind that due to the presence of at least two spectral components, that might arise from the presence of a protein conformational equilibrium, interpretation of the mobility values in terms of protein structure has to be conducted with caution.

The mobility map for the spin labeled ColA variants shown in Figure 3.20 reveals strong immobilisation as observed for R1 sides chains buried in the protein interior also only for residue 176R1^{H9}. Contrarily, very high mobility, being characteristic for highly dynamic loop/surface regions can only be found for position 26R1^{H1} that even does not exhibit the highest ΔH_0^{-1} value (~ 3.5 mT^{-1}, compared to > 4 mT^{-1} for T15R1^{H1} and I66R1^{H3}). T15R1^{H1} and I66R1^{H3} can be – despite their exceptional high ΔH_0^{-1} values rather categorized as located on a loop structure involved in tertiary contacts (loop/contact). All other positions investigated here seem to be located on helices that exhibit tertiary contacts to other helices.

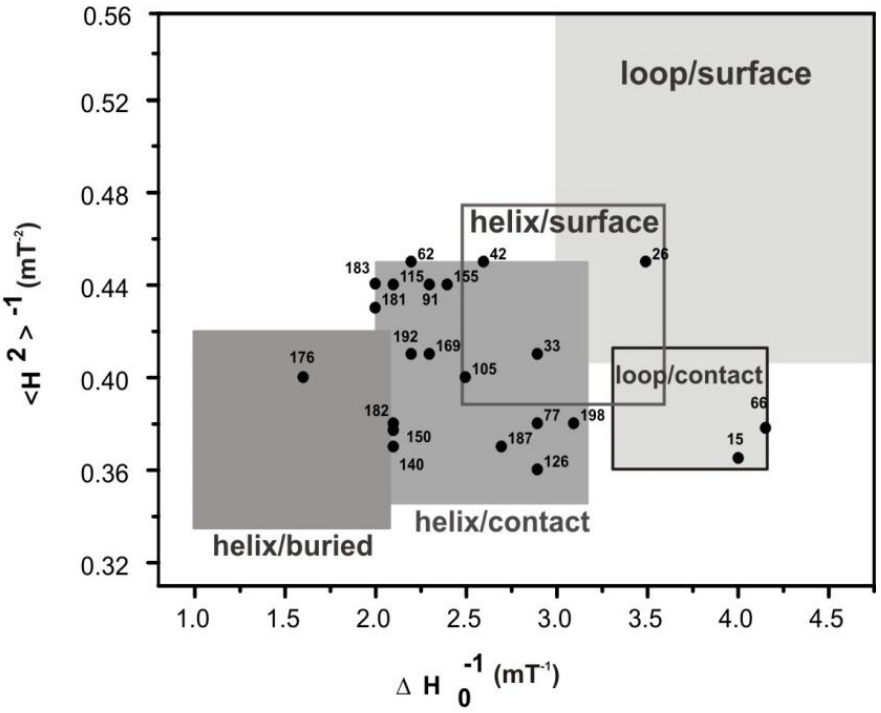

Figure 3.20: Classification of colicin A side chain localizations with regard to protein structure by plotting the inverse spectral second moment ($\langle H^2 \rangle^{-1}$) *versus* the inverse central line width (ΔH_0^{-1}). The parameters were calculated from the RT cw X-band EPR spectra shown in Figure 3.18.

In more detail, in the 2D plot two positions of the colicin A hydrophobic hairpin, 150R1^{H8} and 182R1^{H9}, as well as position 140R1^{H7} on helix 7 are located at the border between two areas, representing helix contact sites and helix buried sites. Consequently, spin label side chains at these positions have strong tertiary contacts and might even be partially buried in the protein interior, although a certain degree of

immobilization might also be attributed to contacts with either the lipid head groups or fatty acid chains of lipid molecules that are specifically bound to the protein. Nevertheless, in the spectra shown in Figure 3.18 the two spectral components (immobile and mobile) are clearly distinguish able for numerous positions throughout most of the helices, e.g. for 62R1^{H3}, 77R1^{H4}, 91R1^{H5}, 140R1^{H7}, 150R1^{H8}, 155R1^{H8}, 169R1^{H9}, 192R1^{H10} and 198R1^{H10}, and this observation has been found to be correlated with helices being involved in tertiary contacts (Kroncke et al., 2010). Although the results of this "basic" mobility analysis (no attempts have been made to perform a "multi-component analysis" of the spectra (see e.g. Budil et al., 1996, but possible reasons for the ubiquitous presence of at least two spectral components and how this could be analysed in more detail will be discussed later) provides only limited information about the structural features of this state of the protein, it already seems to rule out a model for the membrane bound state of ColA previously suggested. Based on a limited set of colicin A double spin label mutants (Boehme et al., 2009) and on a FRET study on the pore forming domain of colicin E1 (Lindeberg et al., 2000) (Zakharov and Cramer, 2002 b), a ring-like structure on the membrane surface formed by helices 1-7 and only H1 and H7 (and maybe also H6) being in contact with other helices, was proposed. The results obtained in the present study with a significantly larger set of spin label positions clearly indicate a more densly packed structure than previously suggested.

3.3.3 Polarity and accessibility measurements

The structural information on colicin A provided by the mobility analysis can be supplemented with polarity and accessibility measurements in order to specify the location of the respective helices with respect to the membrane. Accessibility measurements allow to distinguish between R1 side chains exposed to the lipid phase, to the aqueous phase or to the protein interior (see 2.3.3), and can be further used to determine the immersion depths of the label side chain in the membrane bilayer (see 2.3.4). Furthermore, determination of the R1 side chain's environmental polarity also provides information on its location in a protein/membrane/water system (see chapter 2.3.5).

For both, the accessibility and the polarity measurements on membrane bound colicin A, reference data has been obtained using *E. coli* polar lipid liposomes containing ca. 5 % stearic acid spin labeled at positions 5, 12 and 16 of its alkyl chain (5-, 12- or 16-doxyl-stearic acids, Sa5, Sa12 and Sa16, respectively) and 5-, 12 or 16-doxyl-Pc (Pc5, Pc12 and Pc16). As the location of the nitroxide group in the lipids relative to the phosphate head groups is known, they can serve for "calibration" of the accessibility data and especially for the immersion depth parameter calculated thereof. Furthermore, immersion depth values published for transmembrane helix D of bacteriorhodopsin, BR (Hubbell et al., 1994), were also used for calibration and comparison purposes.

3.3.3.1 Accessibility measurements

The quencher compounds used here are the water soluble metal complex Ni-EDDA (20 mM) and molecular oxygen (O_2). By virtue of its hydrophobic nature O_2 preferentially concentrates in hydrophobic regions, like the core of the lipid bilayer. In contrast Ni-EDDA is excluded from the core of lipid bilayers and is concentrated in the aqueous environment. The measurements were performed as described in chapter 3.2.5.3. Data analysis was performed using the program *powerfit* to calculate the Heisenberg exchange rates We_x values for Ni-EDDA and O_2.

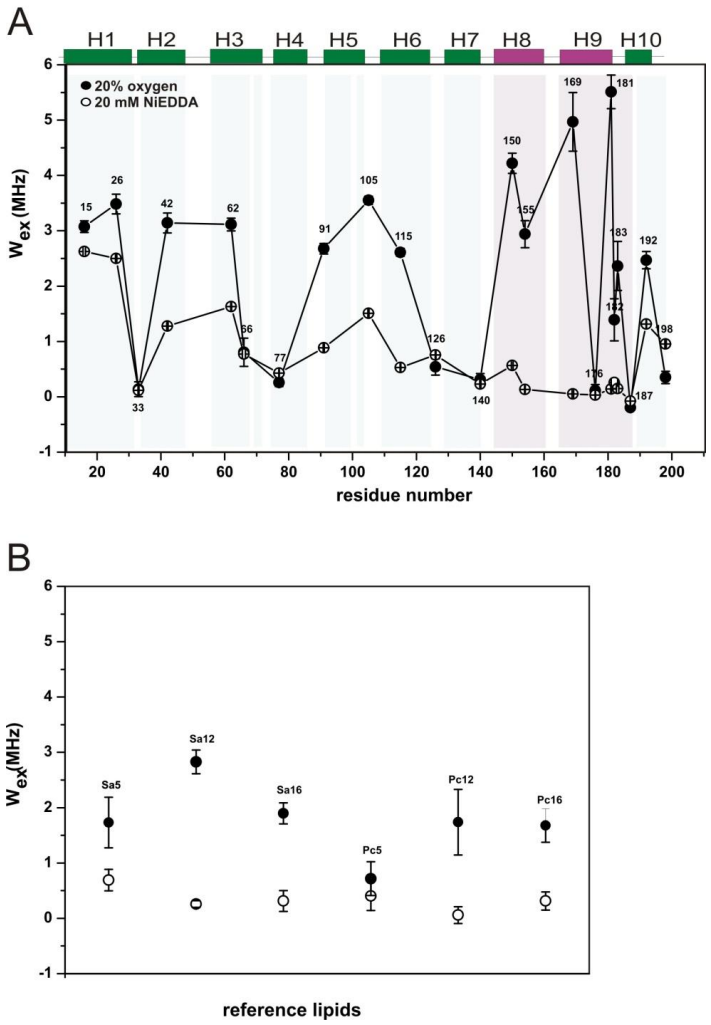

Figure 3.21: (A) Exchange rates (W_{ex}) of R1 side chains of the rec-mem-ColA for O_2 and Ni-EDDA. The W_{ex} values were determined in the presence of 20 mM Ni-EDDA (open circles) or equilibrated with 100% molecular oxygen calculated to 20 %, for comparison with published values obtained from samples equilibrated with air, (filled circles). (B) Exchange rates obtained from the labeled lipids.

The Heisenberg exchange frequencies W_{ex} for R1 side chains attached to rec-mem-ColA are shown in Fig. 3.21. The plot of W_{ex} *versus* residue number reveals higher overall exchange rates for O_2 compared to Ni-EDDA, although with some exceptions, indicating that most positions under investigation are located in the membrane rather than in the aqueous phase. For position $198R1^{H10}$ a significantly higher accessibility

for Ni-EDDA than for O_2 is observed, indicating its exposure to an aqueous environment. Spin labels at positions 15R1^{H1} and 26R1^{H2} exhibit a high accessibility for both quencher molecules, due to their high mobility (see 3.3.2) and a location in the polar head group region of the membrane. In contrast, residues 33R1^{H2}, 66R1^{H3}, 77R1^{H4}, 126R1^{H6}, 140R1^{H7}, 176R1^{H9} and 187R1^{H9} reveal neither significant accessibility towards O_2 or Ni-EDDA, a feature characteristic for side chains that are buried in the protein interior, also largely being in line with the observed restricted mobilities of spin labels attached at these sites. However, closer inspection of the results for positions 66R1^{H3}, 77R1^{H4} and 126R1^{H6} reveals a slightly higher accessibility for Ni-EDDA, whereas for buried residues slightly higher rates are expected for O_2 compared to Ni-EDDA due to the fact, that diffusion of Ni-EDDA within the protein interior is significantly stronger limited by its size compared to O_2. Consequently, these positions appear to be located more towards the aqueous environment than in the protein interior. The accessibility for the remaining residues 42R1^{H2}, 62R1^{H3}, 91R1^{H5}, 105R1^{H5}, 115R1^{H6}, 150R1^{H8}, 155R1^{H8}, 169R1^{H9}, 181R1^{H9}, 182R1^{H9}, 183R1^{H9} and 192R1^{H10} indicates higher exchange rates with oxygen and negligible exchange rates for Ni-EDDA, suggesting that these residues are located in the hydrophobic core of the membrane bilayer, like Sa12 and Sa16 (Figure 3.21 B). Strikingly, accessibility values corresponding to a location close to the headgroup region within the bilayer (Reference Sa5, Figure 3.21 B) are only observed for position 182 in the hydrophobic hairpin. Consequently, the results of the accessibility measurements reveal that more helices than only the hydrophobic hairpin are at least partly located in the hydrophobic part of the membrane and do not only lie in the head group region.

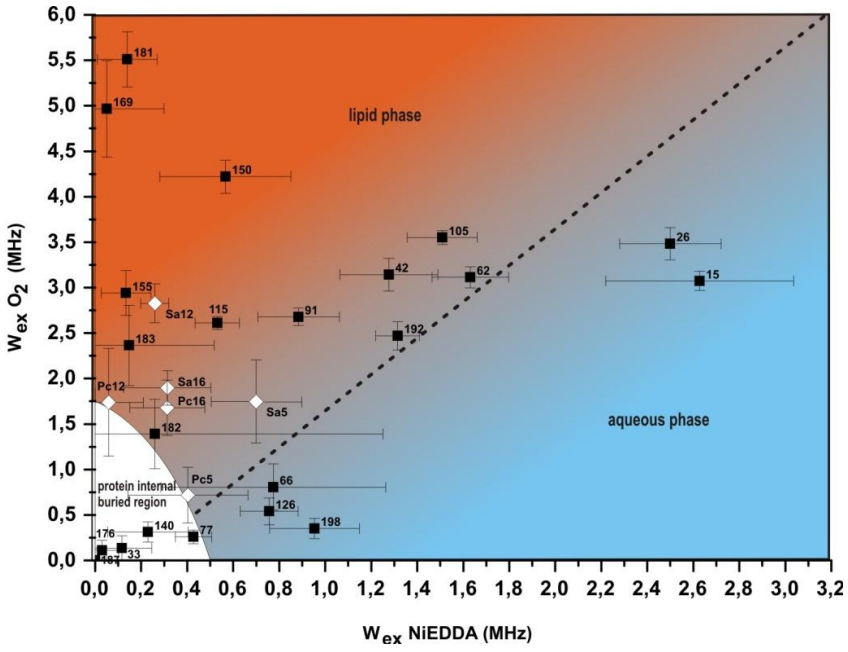

Figure 3.22: Accessibility map of the ColA R1 side chains (black squares) and for the labeled lipids (white diamonds). The plot is divided into three areas: protein internal or buried, aqueous phase and lipid phase. The boundaries between these areas are based on the studies by Wegener et al., 2000 and L.Pulagam, PhD Thesis, 2007.

In Figure 3.22 the W_{ex} values for O_2 are plotted against those for Ni-EDDA. Such kind of 2D *accessibility map* can be used to assess the relative location of the spin label side chain in a protein/lipid/water system more intuitively than a 1D plot versus residue number (Figure 3.21). According to this analysis positions A42R1^{H2}, S62R1^{H3}, A91R1^{H5}, F105R1^{H5}, E115R1^{H6}, A150R1^{H8}, S155R1^{H8}, A169R1^{H9}, A181R1^{H9}, V182R1^{H9}, V183R1^{H9} and A192R1^{H10} are exposed to the lipid phase. 15R1^{H1}, I26R1^{H2} and E198R1^{H10} are located in the aqueous phase. Residues located in the protein interior, characterized by low accessibilities for both quencher molecules, are K33R1^{H2}, I66R1^{H3}, A77R1^{H4}, E126R1^{H6}, W140R1^{H7}, G176R1^{H9} and I187R1^{H9}, wherein especially residues I66R1^{H3} and E126R1^{H6} are more exposed to the aqueous environment than to the protein interior, confirming the conclusions drawn from the "raw" exchange rates.

The *immersion depth* of a spin label side chain in a lipid bilayer can be determined by calculating the dimensionless immersion depth parameter Φ = ln (Π (O2)/ Π (Ni-EDDA)) from the collision frequencies towards the paramagnetic quenchers O_2 and Ni-EDDA. In Fig. 3.23 the immersion depth parameters determined for the spin labeled stearic acids and PC lipids are shown in comparison with the values that have been obtained for BR helix D (Hubbell et al., 1994). As the corresponding values for bacteriorhodopsin BR have been determined in the presence of 20 % molecular oxygen (sample equilibrated with air), the Π (O_2) values for the spin labeled lipids and for rec-mem-ColA in the following have been divided by the factor 5 to allow direct comparison. The range of immersion depth values indicating immersion of the label position into the hydrophobic core of the lipid bilayer is indicated in this Figure.

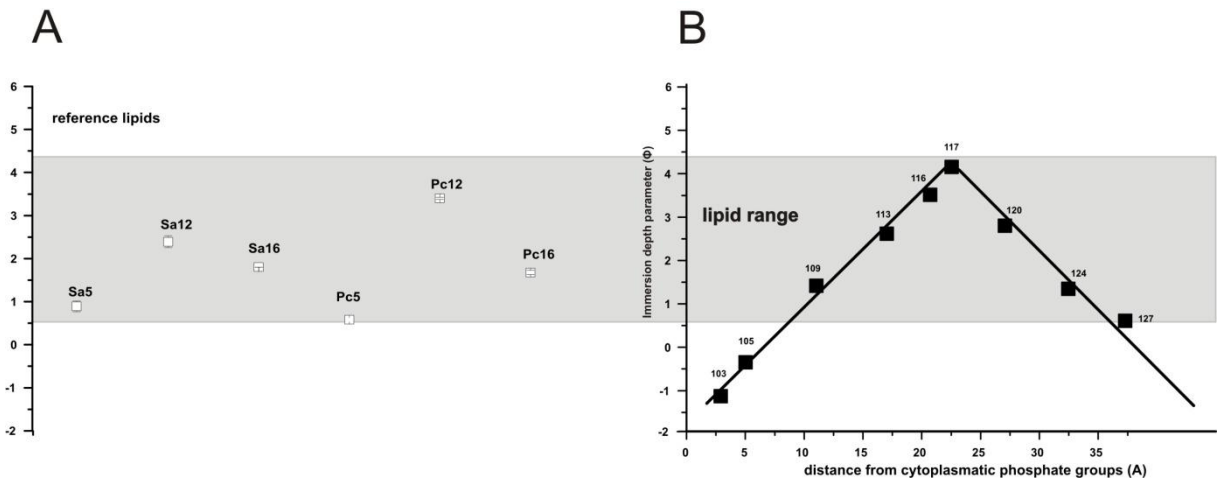

Figure 3.23: (A) Immersion depth calibration based on 5-, 12- or 16-doxyl-stearic acid and 5-, 12- or 16-doxyl-PC in *E. coli* polar Lipid extract. The immersion depth parameter Φ = ln (Π (O_2)/ Π (Ni-EDDA))is calculated from the Π values determined in the presence of 20 mM Ni-EDDA and 100 % oxygen, respectively. The Φ values and the corresponding distances from the lipid head groups obtained from an analysis for helix D of BR (Hubbell et al., 1994) are shown for comparison in panel (B) The corresponding values for bacteriorhodopsin BR have been determined in the presence of 20 % molecular oxygen (sample equilibrated with air). To allow a direct comparison, the Π (O_2) values for the spin labeled lipids have been divided by 5.

Comparison with the distances from the lipid headgroups obtained for the respective positions in BR helix 6 from its crystal structure shown in Fig. 3.23 panel B reveals that the values found for Sa5 and Pc5 approximately correspond to a distance of 0.8-1.1 nm from the lipid head groups. The nitroxides of Sa12 and Pc12 are located about 1.7-2.0 nm below the headgroup region and therefore closer to center of the lipid bilayer. As already observed for the W_{ex} (O_2) values for the spin labeled stearic acids and PC lipids (Figure 3.21 B and Figure 3.22), a nitroxide at the end of the alkyl chain (position 16) seems to be less deep inserted compared to Sa12 and Pc12. In principle, it should be expected that both the *n*-stearic acids and *n*-doxyl PCs demonstrate a linear dependency of Φ from the distances of the nitroxide to the phosphate head groups (Dalton et al., 1987) (Farahbakhsh et al., 1992). Nevertheless, comparison with BR helix 6 reveals distances of about 1.4-1.5 nm from the lipid head groups for Sa16 and Pc16. This behavior has also been observed in other studies (Caffrey and Feigenson, 1981) (Chattopadyhay and London, 1987) and is usually explained with the end of the alkyl chains bending towards the lipid headgroups. Contrarily, on a transmembrane helix (BR helix 6) the spin label side chains exhibit a significantly more rigid and better defined immersion depth in the lipid bilayer. According to the study by Hubbell et al. (1994), residues with Φ ~ 0 are located approximately 5Å from the phospholipid head groups and those with Φ ~ 4 close to the center of the bilayer.

The results of the immersion depth calculation for ColA are shown and compared to the results for BR (Hubbell et al., 1994) in Figure 3.24. It is apparent from this Figure that the hydrophobic hairpin deeply inserts into the hydrophobic core of the lipid bilayer, as all residues located on H8 and H9 exhibit Φ values between ~ 1.5 and 4.5. The highest immersion depth was obtained for position 169R1 (Φ ~ 4.5) in H9 that should consequently be located at the center of the bilayer. As expected for an orientation of the hairpin along the membrane normal, from position 150R1 in the beginning of H8 the immersion depth parameter Φ increases up to the maximum value found for 169R1 and subsequently decreases to the end of H9. For position 187R1 at the end of H9 no Heisenberg exchange frequencies could be determined and therefore no immersion depth was calculated. An exception represents position 176R1 on H9, for which a significantly lower Φ value of ~ 1 is observed. This indicates a transmembrane orientation of the hairpin, in which position 176 is located close to the headgroup region *on the other side of the membrane*. Consequently, the data obtained in the present study are in line with the umbrella model for the membrane bound state of colicin A. Previous EPR accessibility measurements for ColA (Pulagam et al., 2008) also supported the umbrella-model for the closed channel state in which the hydrophobic hairpin (H8/H9) exhibits a transmembrane orientation. Nevertheless, in the umbrella model the amphipathic helices H1-H7 are thought to be located close to the lipid/water interface. In contrast to this model the immersion depth values obtained for ColA indicate that also helices H2, H3, H5 and H6 are at least partially located in the hydrophobic part of the membrane and not only at the head group region, characterized by Φ values between ~ 1 and 2, corresponding to immersion depths in the hydrophobic core of ~ 1.0 - 1.5 nm.

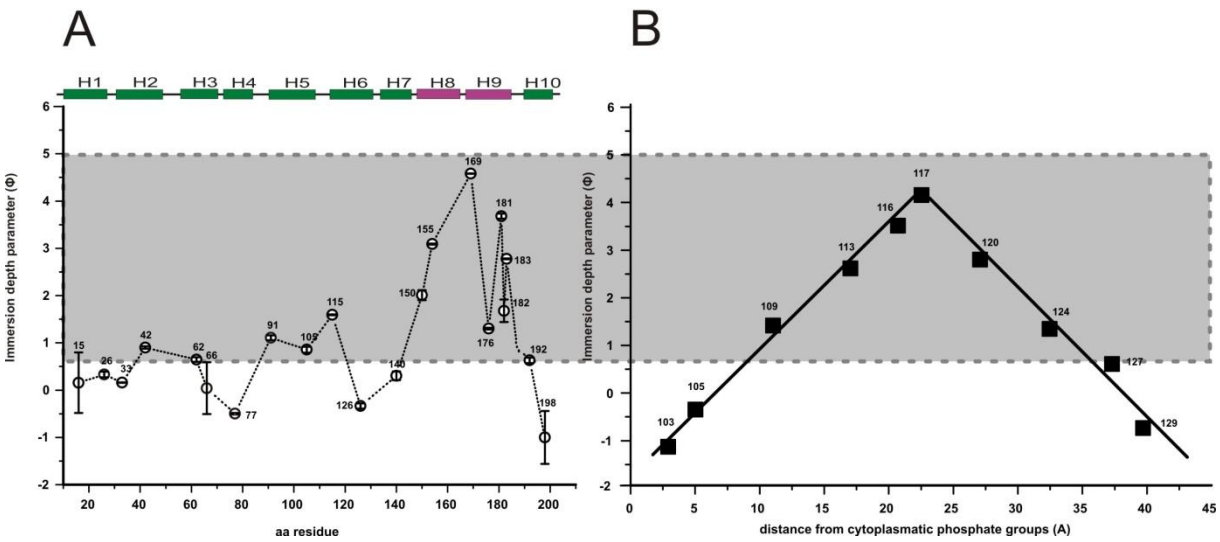

Figure 3.24: (A) The immersion depth parameter Φ determined by accessibility measurements for ColA. The range of obtained Φ values in case of ColA is indicated (B) Comparison to the results of spin labeled BR mutants adopted from (Hubbell et al., 1994).

In more detail, positions 42R1^{H2} and 105R1^{H5} exhibit Φ ~0.9 and 91R1^{H5} a value of ~1.1. These values have also been found for positions 109R1 and 127R1 in BR (Hubbell et al., 1994), that are located about 1 nm away from the headgroup region on opposite sides of the membrane bilayer. Even more deeply embedded in the bilayer core appears position 115R1^{H6} (Φ ~ 1.6) in the N-terminal part of H6, indicating a distance to the headgroup region of ~ 1.5 nm. Contrarily, for 126R1^{H6} at the C-terminal end of helix 6 a Φ value of -0.3 is observed, suggesting its location in the head group region. This observation can easily be explained if it is assumed that H5 appears to adopt an orientation tilted with respect to the membrane plane, with the N-terminal end protruding into the hydrophobic core of the membrane. Furthermore, also positions 62R1^{H3} and 192R1^{H10}, both exhibiting Φ values of ~ 0.7, seem to be inserted in the membrane rather than be located on top of it. The Φ values obtained for residues T15R1^{H1}, I26R1^{H1}, K33R1^{H2}, S62R1^{H3}, I66R1^{H3}, A77R1^{H4}, W140R1^{H7} and A192R1^{H10} are in the range of about -0.5 - 0.5, indicating their location in close vicinity to the lipid head groups. The data obtained for the BR mutants further show that immersion depth values below Φ = -1 indicate a fully water exposed orientation for nitroxides. Such values are only observed for position 198R1^{H10} in ColA, indicating its location in the bulk water region.

3.3.3.2 Polarity measurements

Low temperature (160 K) cw-EPR measurements were performed to determine the hyperfine coupling tensor element A_{zz}, thus providing a measure for the polarity of the microenvironment of the R1 side chains attached to ColA. This data can provide further information about the location of the respective helices with respect to the membrane, as the membrane/water system is characterized by a strong polarity gradient along the membrane normal. The A_{zz} value for nitroxides is expected to be large in a polar

environment like the bulk aqueous phase (~ 3.6 - 3.7 mT), whereas spin labels located in the middle of the bilayer – an apolar environment - are characterized by small A_{zz} values (~ 3.3 - 3.4 mT). Intermediate A_{zz} values indicate either location in the headgroup region of the lipid bilayer or a protein aqueous environment (Plato et al., 2002) The A_{zz} values determined from the low temperature spectra of reconstituted ColA (Figure 3.26) are shown in Fig. 3.25 *versus* residue number. Strikingly, all A_{zz} values observed for the ColA variants are in the range 3.4 – 3.6 mT, indicating their location either in the headgroup region of the lipid bilayer or surrounded by protein structures according to the course classification mentioned above. This seems to partly contradict the results from the accessibility measurements described in the previous chapter, as here clear indications for membrane insertion of the hydrophobic hairpin as well as for helices H2, H3, H5 and H6 have been obtained. Here, A_{zz} values that indicate at least vicinity to the hydrophobic membrane core (3.40 – 3.45 mT) are only observed for spin labels located at positions 33^{H2}, $169^{H8\text{-}H9}$, 176^{H9} and 183^{H9}.

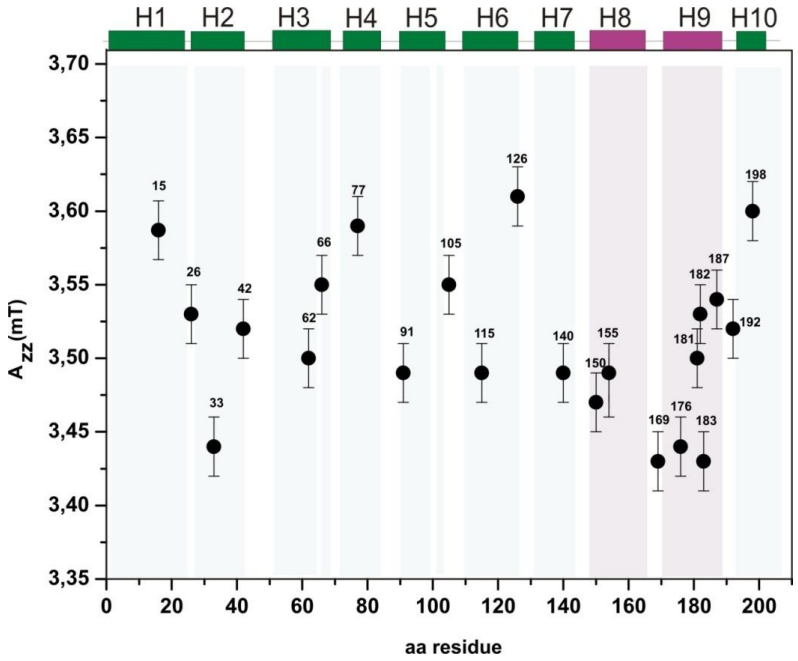

Figure 3.25: Hyperfine coupling tensor elements A_{zz} determined from the cw low-temperature spectra recorded for membrane-bound singly spin labeled ColA variants shown in Figure 3.26.

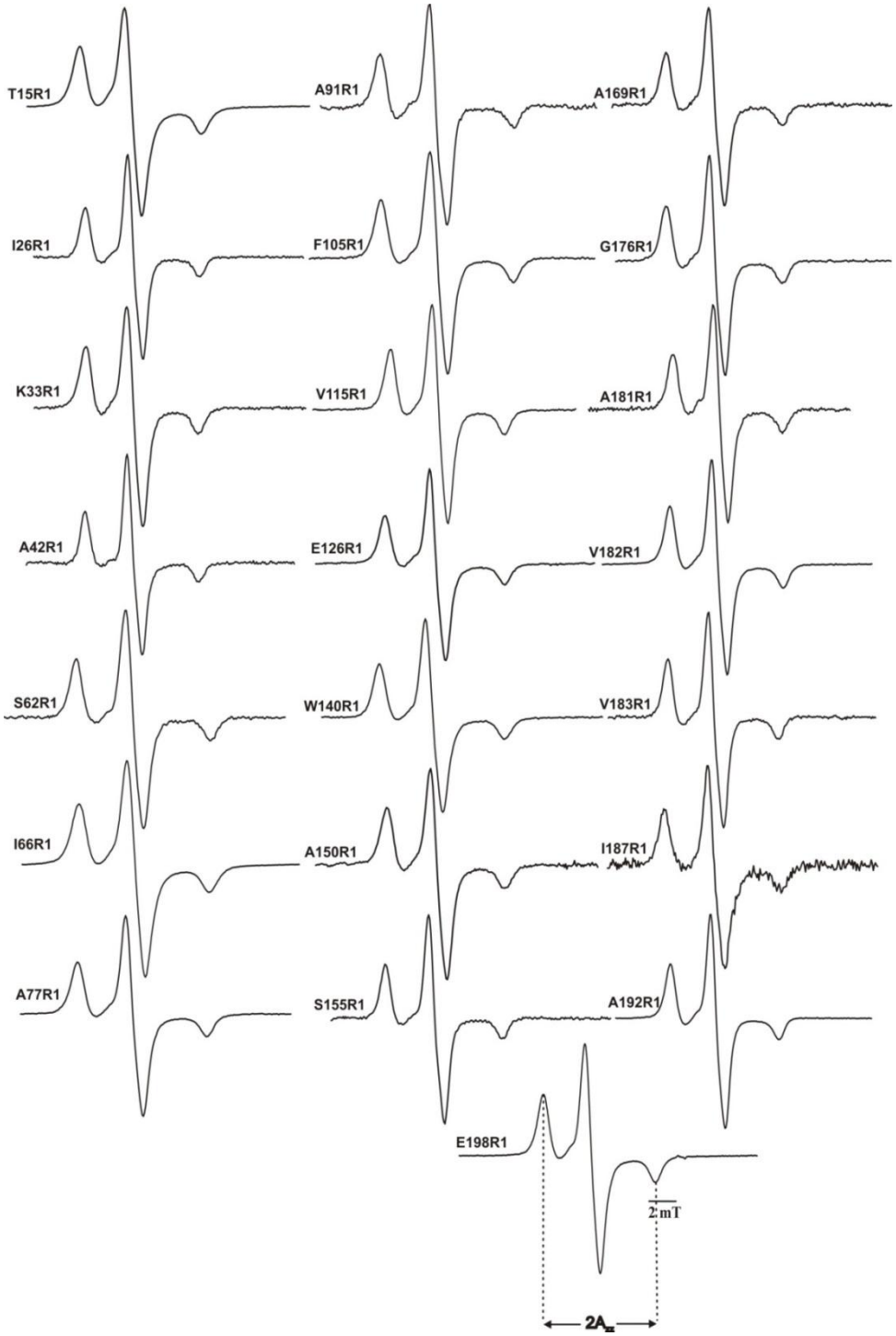

Figure 3.26: Low temperature (160 K) EPR spectra recorded for singly labeled colicin A reconstituted in liposomes. Residue numbers are given.

As for the accessibility and immersion depth values a much better correlation also of the polarity values with the other data is obtained, if reference values from systemsare used, where the location of the spin label side chain within the membrane bilayer is known. Polarity measurements with spin labeled stearic acids and PC lipids (the resulting values are shown in Figure 3.27 A) reveal that in case of Sa5PS and Pc5PS (close to the headgroup region) A_{zz} values of 3.46-3.47 mT are observed, being in line with an

intermediate polarity according to the coarse classification described before. The A_{zz} values for Sa12PS, Pc12PS, Sa16PS and Pc16PS are significantly smaller with values of approximately 3.32 mT obtained for the 12PS references and 3.24 mT for the 16PS references, indicating very apolar environment like it is found in the middle of the lipid bilayer. Nevertheless, we have to keep in mind that a direct comparison of the absolute A_{zz} values between the references and the samples is limited due to the different nitroxide moieties.

A more reliable reference in terms of the comparability of the systems under investigation is again a protein with known crystal structure, in this case bacteriorhodopsin. In Figure 3.27 B the results obtained by Savitsky et al. (2004) for BR helix F are shown, clearly indicating that unexpectedly high A_{zz} values of 3.5 – 3.6 can be found also for positions immersing 1-2 nm into the hydrophobic membrane core. Moreover, in a later study on positions of BR helix D, that are oriented towards the interior of the protein (Möbius et al., 2005), even A_{zz} values of 3.6 – 3.7 mT have been obtained for positions that are according to the crystal structure clearly located in the very middle of the lipid bilayer. BR is a light-driven proton pump comprising intra- and extracellular channels that connect the retinal moiety with the bulk aqueous phases. If spin labels are placed in these channels polarity values are obtained that would usually suggest their exposure to the bulk water phase. Colicin A also forms channels in lipid bilayers and even though the closed channel state is observed in most of the experiments performed in this study, this state might already exhibit a channel connecting the lipid bilayer core with the bulk phase. Consequently, it can be expected to find also for colicin A in the close channel state regions in the protein that are located deeply in the membrane, but appear to be exposed to a polar, aqueous environment, if the spin label side chain is located inside the channel.

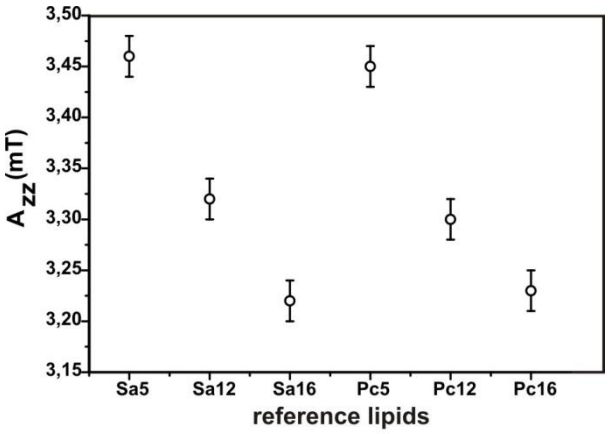

Figure 3.27 (A): Polarity (A_{zz}) values obtained for spin labeled lipids.

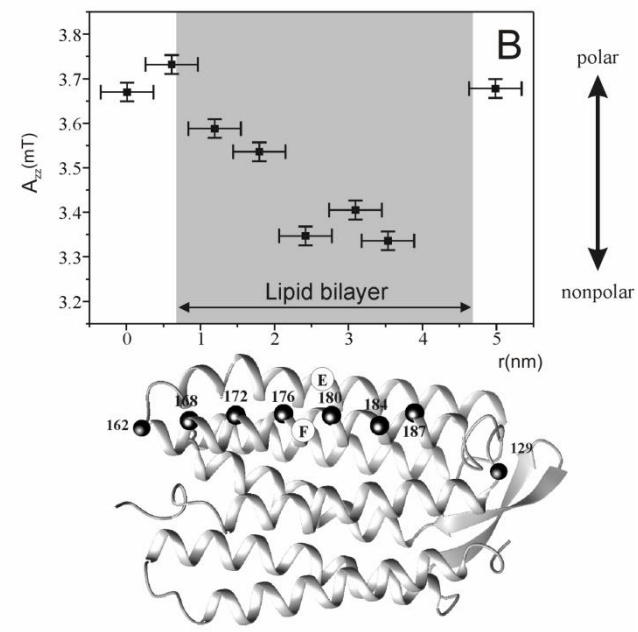

Figure 3.27 (B): Behavior of the A_{zz} values of nitroxides attached to the surface of the membrane-spanning helix F of BR with respect to the position of the labeled side chain within the lipid bilayer. Figure taken from Savitsky et al., 2004.

Noteworthy, the same arguments hold for investigations on the mobilities and accessibilities of spin labels placed in channel-forming proteins, and should always be kept in mind when analyzing such proteins by SDSL EPR spectroscopy or related techniques like fluorescence spectroscopy. Therefore, of course this has to be taken into account when interpreting the experimental results reported for colicin A in this work, and especially for the polarity values described in the following.

Low A_{zz} values between 3.43 and 3.44 mT are found for residues K33R1^{H2}, A169R1^{H9}, G176R1^{H9} and V183R1^{H9}, indicating their location close to the center of the lipid bilayer according to the values found for BR (Figure 3.27 B). For positions 169R1^{H9}, 176R1^{H9} and 183R1^{H9} these results are in agreement with the accessibility data, where 169R1^{H9} shows the highest penetration depth (Φ ~ 4.5, Figure 3.24). In contrast, the observed value for K33R1^{H2} (~ 3.44 mT) is not in line with the accessibility measurements, where it has been found that the collision rates are low for both quencher molecules, indicating a location of this spin label side chain in the protein interior. Combining both results therefore suggests, that K33R1^{H2} might be located in a slightly hydrophobic pocket within the protein, where it is shielded from the quencher molecules by other parts of the protein.

Contrarily, A_{zz} values of ~ 3.6 mT obtained for T15R1^{H1}, A77R1^{H4}, E126R1^{H6} and E198R1^{H10} suggest their location in a highly polar environment like the bulk water phase, what is also in agreement with the previous accessibility measurements that suggested a location of the nitroxides at these positions close to lipid head groups or bulk water region.

Combining the results from the accessibility and the polarity measurements described before, it can be assumed that the hydrophobic helical hairpin H8/H9 most likely adopts a transmembrane orientation like it is proposed in the umbrella model for the ColA closed channel state. Nevertheless, strong indications are found in this work that more colicin A helices are located within the membrane, as already suggested in other studies (Cascales, 2007). Based on the data obtained in this work H5 and H6, and also parts of H2, H3 and H10 appear to be embedded in the membrane, and only helices H1, H4 and H7 are located close to the head group region, being contradictory to *both* models for the closed channel state, the umbrella and the penknife model (Figure 3.4). However, keeping the existence of at least two spectral components in all RT cw EPR spectra in mind, it cannot be excluded that an equilibrium between at least two different conformational states is observed by the EPR measurements. This would - at least partly – explain some of the inconsistencies found between the mobility, the polarity and the accessibility data as described before. Consequently, the major question arises if the components observed in the cw EPR spectra reflect two spin label populations or indicate an equilibrium between protein conformations. This question will be discussed in the following section.

3.3.4 Analysis of the spectral two-component system of ColA

3.3.4.1 Influence of the temperature on the EPR spectral features

As already mentioned and clearly visible from Figure 3.18, all the room temperature cw spectra recorded for spin labeled colicin A reveal the presence of at least two spectral components characterized by different mobilities. Due to this fact it is hard to interpret the data described in the previous chapters, as it appears possible that a mixture of two or more conformational states is present in the samples investigated. In case of the mobility measurements, it is possible to differentiate between the two components by means of the two mobility parameters, where the inverse linewidth is dominated by the more mobile component, whereas the second moment reflects the influence of the more immobile component. In contrast, the accessibility measurements show the mixture of both components and the polarity measurements might be strongly biased towards the immobile component, as the experiments are performed in the frozen state.

The presence of two resolved components with different mobilities has already been observed for other proteins, for example it was reported for residue 165R1 of bacteriorhodopsin, which exhibits an equilibrium between two spin populations with different mobilities (Steinhoff et al., 2000), and for other membrane proteins like KcsA and rhodopsin (Kroncke et al., 2010). The major question is of course if in the case of colicin A these two components reflect either different protein populations in equilibrium or if the two components arise from two spin label rotamer populations on one protein structure (Mchaourab et al., 1996), although the probability that the two spectral components of *all* 22 rec-mem-ColA positions under investigation arise from different rotamer conformations appears very unlikely. In order to

characterize the two components in more detail, temperature dependent measurements have been performed with a subset of the colicin A spin label mutants. Cw EPR spectra were recorded in the temperature range from 273 K to 303 K for positions I26R1^{H1}, A77R1^{H4} and G176R1^{H9}. The selection has been made based on the proportions of the two spectral components in the spectra recorded at RT. For I26R1^{H1} and A77R1^{H4} the mobile component is dominating to different extents, whereas G176R1^{H9} exhibits a dominating immobile component. For a more detailed analysis also an *in vivo* non-functional sample like G166R1$^{LoopH8/H9}$ was examined. As obvious from the spectra shown in Figure 3.28, lowering the temperature leads to an increase of the immobile (i) component and a concomitant decrease of the mobile (m) component, thus shifting the equilibrium between the two conformations.

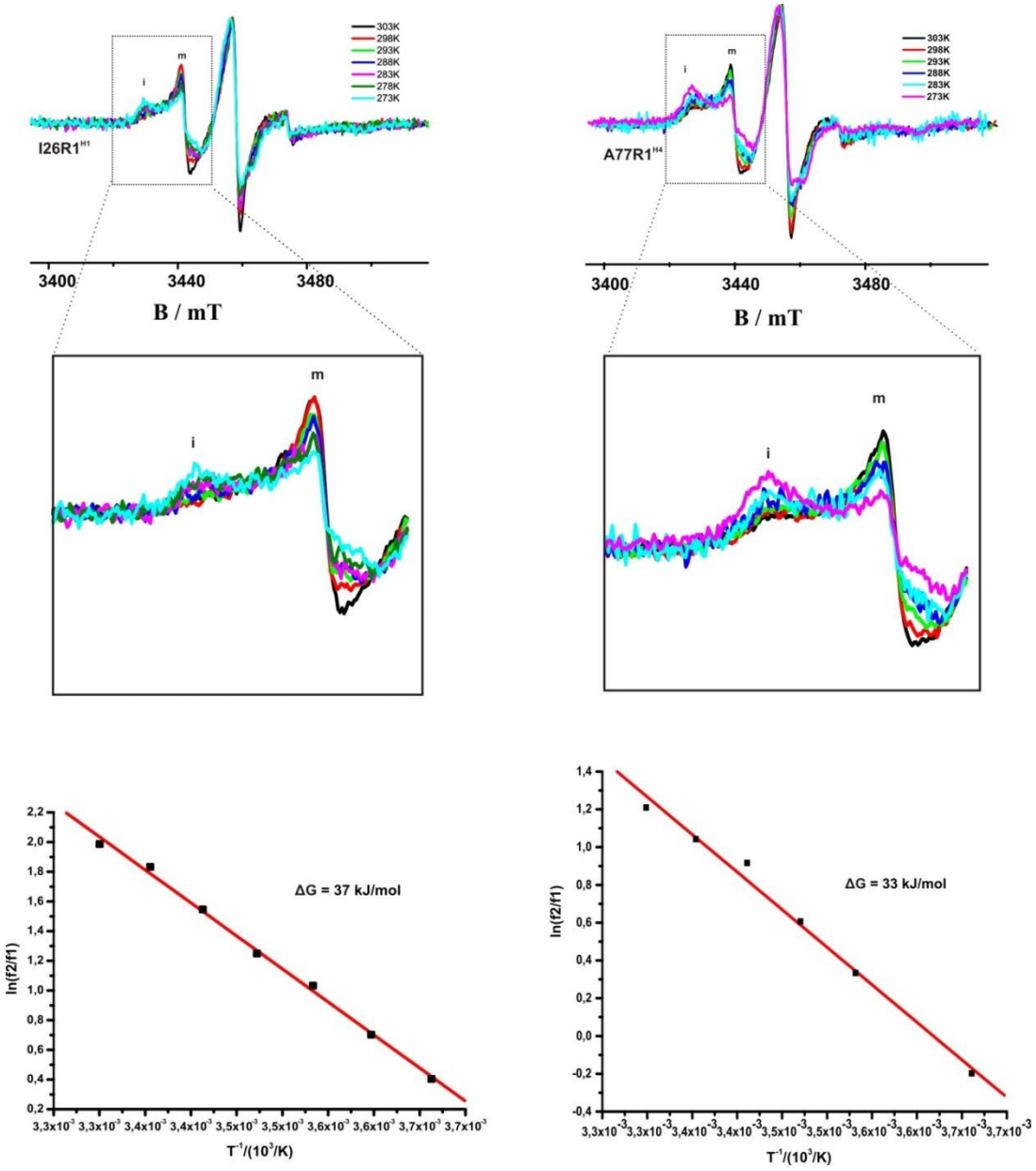

Figure 3.28 (A): Temperature dependent cw EPR spectra. The cw spectra were recorded from 273 K to 303 K and the corresponding van´t Hoff plots reveal the Gibbs enthalpies for transition between the different states.

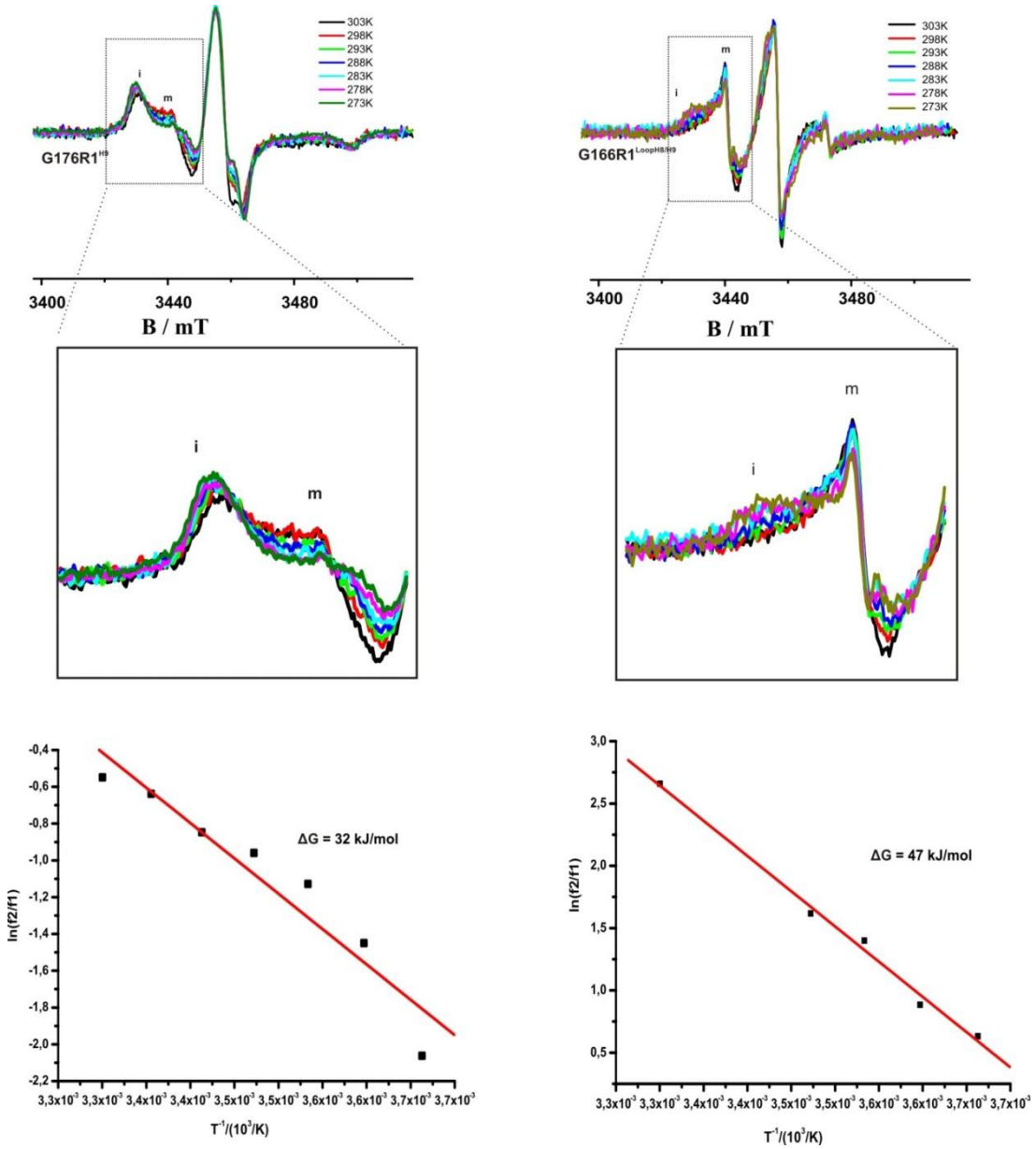

Figure 3.28 (B): Temperature dependent cw EPR spectra. The cw spectra were recorded from 273 K to 303 K and the corresponding van´t Hoff plots reveal the Gibbs enthalpies for transition between the different states.

To get insights into the thermodynamic properties of the observed equilibrium the temperature dependent spectra have been analysed by means of van't Hoff plots, revealing Gibbs enthalpies for 26R1^{H1} of ΔG = 37 kJ/mol (9 kcal/mol), for 77R1^{H4} ΔG =33 kJ/mol (8 kcal/mol) and for 176R1^{H9} ΔG = 32 kJ/mol (7.8 kcal/mol), whereas for the *in vivo* non-functional sample 166R1$^{LoopH8/H9}$ a value of ΔG = 47 kJ/mol (11.3 kcal/mol) was determined. This sample is indeed nonfunctional *in vivo* however it shows channel opening upon application of an electrical field in electrophysiological measurements (Sippach, 2009). This leads to the assumption that a mutation in 166R1$^{LoopH8/H9}$ has an influence on the *in vivo* protein translocation

pathway from the outer to the inner membrane. The study by Kroncke et al. (2010) revealed ΔG values of about 4 kcal/mol for different side chain rotamers. In more detail, Kroncke et al. stated that this value arises from the observed non-traditional hydrogen bond between a sulfur-atom of the disulfide bridge and the protein backbone, contributing approximately 2 kcal/mol (Barth et al., 2007) (Gu et al., 1999) (Scheiner et al., 2001) (Vargas et al., 2000), and the stability of the conformer in the crystal structure due to its buried surface area (~ 70 Å²), accounting for another 2 kcal/mol (Kroncke et al., 2010). Consequently, as significantly higher values of 8-9 kcal/mol are observed, the two spectral components in the case of colicin A could arise from different protein conformations rather than spin label side chain rotamers, being in line with what was also proposed by Tory et al. (1999) and Kienker et al. (1997/2000) for colicin E1 and colicin Ia. However, solely based on the temperature dependent measurements the existence of different spin label rotamer conformations can still not be excluded.

3.3.4.2 Influence of paramagnetic quenchers on the EPR spectral features

Another possibility to investigate the origin of two-component spectra is accessibility measurements. Usually, the saturation curves used to obtain the accessibility parameters Π or Heisenberg exchange rates W_{ex} are determined from the peak to peak amplitudes (I_{pp}) of the central resonance line as already described in chapter 2.3.3. Therefore, like already discussed in conjunction with the mobility measurements, the results are biased towards the mobile component in the EPR spectra. Consequently, if the saturation behavior of the two components in the low field peak is separately analysed, the results should reflect the accessibility of the spin label population being responsible for the immobile (i) and the mobile (m) component, respectively. This analysis has been performed for another subset of colicin A spin label mutants, $15R1^{H1}$, $26R1^{H1}$ and $33R1^{H1}$. Figure 3.29 A shows the saturation curves determined from the peak-to-peak amplitudes of the mobile (left) and the immobile (right) component of the low field EPR line (Y', vs. √P) of a nitroxide attached to position $15R1^{H1}$ in the presence of molecular oxygen.

As clearly visible from comparison of the two saturation curves shown in Figure 3.29 A, the two components exhibit a significantly different saturation behavior towards the paramagnetic quencher molecule oxygen. Experiments with the water-soluble quencher compound Ni-EDDA (data not shown) reveal a similar result. The same behavior is observed for the other two positions investigated here, $I26R1^{H1}$ and $K33R1^{H1}$ (data not shown). If the two components would arise from two spin label rotamer populations, they should exhibit the same saturation behavior, as the exchange between two spin-label conformations would be at least one order of magnitude faster than the exchange between two protein conformations. Furthermore, the $P_{1/2}$ values reflect the relative collision frequencies and therefore the accessibility of the nitroxide towards the exchange reagent (Altenbach et al., 1989), but still also depend on the spin-spin relaxation time T_{2e}. Calculation of the exchange rates (W_{ex}) in the presence of 20 mM NiEDDA (Figure 3.29 B) reveals differences between the mobile and immobile component for the 3

analysed positions in H1, caused by the fact that the two spectral components exhibit different T_{2e} relaxation times.

This observation indicates that indeed most likely a protein conformational equilibrium exists at least for helix 1 of colicin A. In order to characterize the conformational equilibrium in more detail, further experiments should be carried out, covering the whole colicin A molecule and using experimental techniques like saturation recovery experiments (Bridges et al., 2010), that will provide means to clearly differentiate between protein and spin label conformational equilibria. Unfortunately, at the time this work has been performed, this technique was not available in our group.

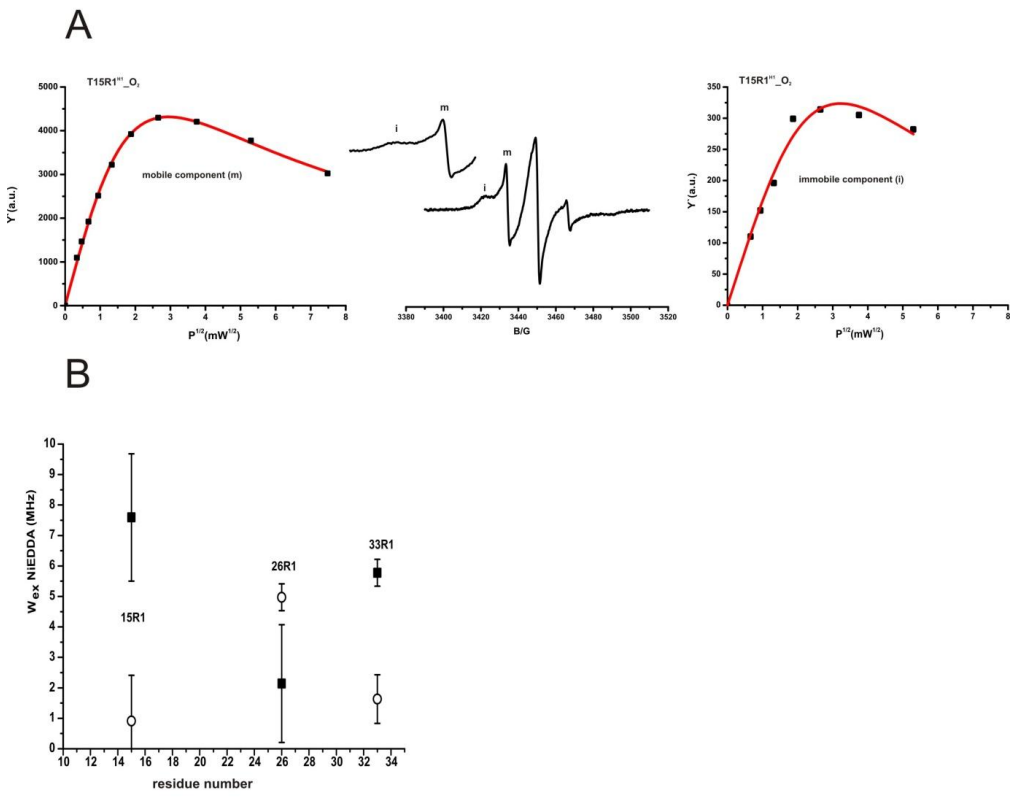

Figure 3.29: (A) Saturation curves determined from the two spectral components visible in the low field peak for ColA-T15R1^{H1} in the presence of oxygen. Left: Saturation behavior of the mobile component (m). In the middle the cw room temperature spectra for position T15R1^{H1} is given. Right: saturation curve of the immobile component. (B) Exchange rates (W_{ex}) for Ni-EDDA of the R1 side chains from the two spectral components in helix 1, black squares: mobile component, open circle: immobile component.

3.3.5 Conclusions from the cw EPR results

Colicin A under *in vitro* conditions has already been investigated concerning mobility, polarity and accessibility by L. Pulagam (L. Pulagam, PhD Thesis 2007) (Pulagam et al., 2008). The results obtained there suggested that the arrangement of the hydrophobic hairpin is perpendicular to the membrane plane and therefore suggested the umbrella model to be valid for the closed channel state. The results for the

amphiphatic helices revealed a location in the membrane-water interface and not only on the membrane surface (L. Pulagam, PhD Thesis, 2007). In the present work the *in vitro* investigations by Pulagam have been repeated and substantially extended by several additional mutants to analyse the ColA closed channel state (see table 3.7 ColA mutant list in appendix of chapter 3). Concerning the mobility and polarity measurements no differences between the recent and previous measurements have been observed, thus indicating reliable reproducibility of the data.

In summary, the cw EPR experiments performed to analyze the mobility, accessibility, membrane immersion depth and environmental polarity of spin labels attached to the ColA pore-forming domain reveal that the helical hairpin clearly inserts into the membrane. On first sight, this supports the umbrella model for the membrane bound closed-channel state. Contrary to this model, in which the remaining amphipathic helices lie (in a circular arrangement) on the membrane surface or are located in the headgroup region of the lipid bilayer, the results obtained here indicate that only helices H1 and H7, and partly helices H3 (66R1) and H10 (198R1) are most likely located on the membrane surface or in the aqueous phase. Clear indications, mainly from the accessibility and polarity data, have been found that at least parts of H2 (42R1), H3 (62R1), H6 (115R1) and H10 (192R1) are protruding into the hydrophobic part of the membrane. Moreover, helix H5 seems to be fully located in the hydrophobic membrane core. A clear statement about the exact orientation and location of H4 cannot be given here, as only one position at the N-terminus of this helix (77R1) has been investigated, indicating that it is located in the headgroup region. Nevertheless, it appears likely that the end of H4 is also protruding into the hydrophobic part of the membrane due to its connection to the membrane-embedded H5 *via* a short (three amino acids) linker. This supports the idea that colicin A contributes four (H5/H6 and H8/H9) rather than two (H8/H9) membrane segments in the membrane integrated closed-channel state. Furthermore, these results are in good agreement with previous studies on Col Ia (Slatin et al., 1994) in which the possible existence of an amphipathic hairpin beside the hydrophobic one predicted by the umbrella model for ColA, leading to four transmembrane segments for Col Ia was discussed.

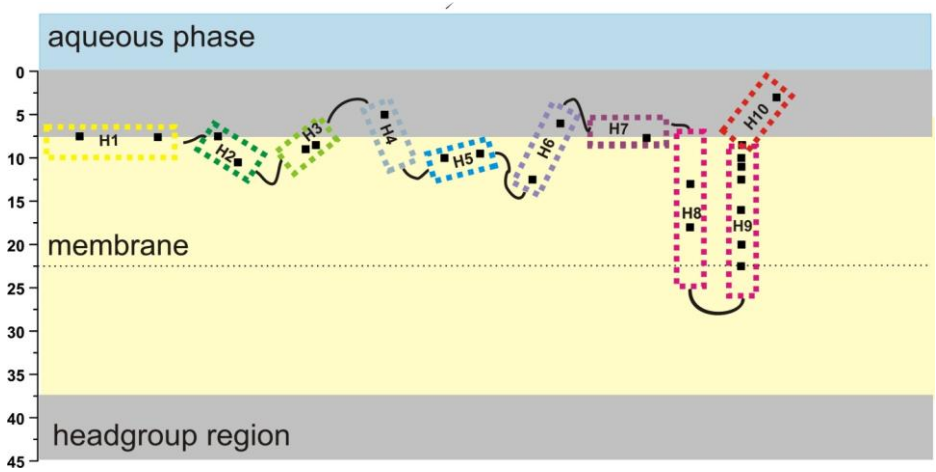

Figure 3.30: Putative topology model of the colicin A membrane-inserted closed channel state obtained from cw EPR experiments (mobility, accessibility and polarity measurements).

3.3.6 Inter spin distance determination by DEER

3.3.6.1 Assessing the oligomeric state of colicin A

As already mentioned in the introduction in chapter 3.1 numerous indications exist that colicin A might form oligomeric assemblies in its soluble form (Cavard, 2002) (Cavard, 2002 b) as well as in the membrane-bound state. Especially for the latter case – that is subject of this work – an oligomeric state forming the functional pore in *E. coli* membranes is widely discussed in the literature (see chapter 3.1.5), as formation of a voltage-gated channel by a single ColA molecule cannot explain the observed channel properties. Nevertheless, only a very limited number of experimental evidences exist up to date for the presence of ColA oligomers in membranes.

DEER spectroscopy provides means to detect protein-protein interactions and to assess the oligomerisation state of a protein. If dimerisation or oligomerisation of a protein brings spin labels attached at single sites on the protomers into a distance within the sensitivity range of the DEER experiment (~ 1.5 – 7 nm), information can be obtained about the *distance distribution between the labels and* the number of interacting label side chains (Bode et al., 2007) as described in chapter 3.2.6.1, further allowing to determine *the number of subunits in the oligomer*. Consequently, DEER spectroscopy was used in this work to investigate not only the topology of the protein in its membrane bound state but also to investigate if ColA channels in the membrane might be oligomeric.

3.3.6.2 Inter spin distance measurements on soluble colicin A in *vitro*

In a first set of experiments DEER distance measurements have been carried out with a 'random' subset of the single mutants comprising ColA-26R1^{H1}, 62R1^{H3}, 105R1^{H5}, 169R1^{H9} and 198R1^{H10} in aqueous solution. Indications for ColA oligomerisation already in the soluble state exist in the literature and have been found also in this work, as analysis of purified ColA by SDS PAGE gel electrophoresis revealed protein bands with significantly higher molecular weight (e.g. ~ 130 kDa) than a ColA monomer (63 kDa) (see chapter 3.3.1.2). The dipolar evolution functions for soluble ColA are shown in Figure 3.31. In all 5 cases the DEER data can be completely fitted with a background function (see chapter 2.4.1), indicating the absence of significant ColA oligomerisation in the soluble state.

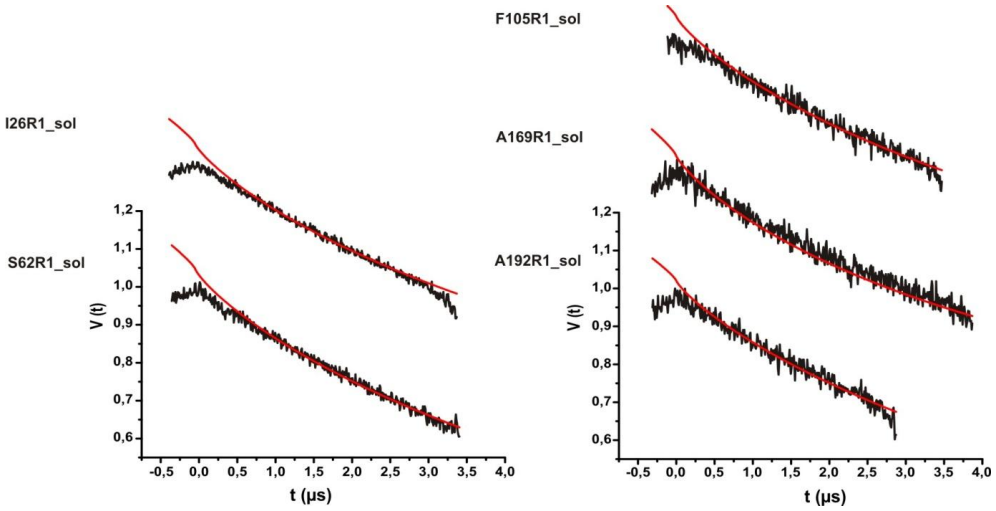

Figure 3.31: Dipolar evolution functions (black) and 3D background fits (red) obtained from DEER experiments on ColA-26R1^{H1}, 62R1^{H3}, 105R1^{H5}, 169R1^{H9} and 198R1^{H10} in the soluble state. The corresponding fits have been calculated with the program DeerAnalysis.

3.3.6.3 Inter spin distance measurements on reconstituted colicin A *in vitro*

DEER measurements of singly labeled ColA in the presence of *E. coli* polar lipid extract have been carried out to investigate a possible oligomerisation of colicin A upon membrane binding. Since it is well known that clustering of membrane proteins can be artificially induced by high protein: lipid ratios, in an initial set of experiments one colicin A single mutant, 77R1^{H4}, was chosen to investigate the possible influence of this parameter and to find optimized conditions for the reconstitutions and DEER experiments with the other single and double site mutants (i.e. maximizing protein concentrations in the samples to obtain a good signal-to-noise ratio in the DEER experiments, but not forcing oligomerisation). DEER data from ColA-77R1^{H4} were obtained for different protein to lipid ratios (1:500 – 1:5000) and the results of these experiments are shown in Figure 3.33 A. It is evident that at a high protein lipid ratio of 1:5000 the dipolar evolution data can be satisfactorily fitted with a background function as it has been observed also for the soluble form of ColA (see Figure 3.31), indicating the absence of oligomers. With increasing protein to lipid ratios a concomitant increase of the DEER modulation depth could be detected, i.e. dipolar modulations could be observed in the time traces, indicating a dipolar interaction caused by oligomerisation of colicin A in the membrane integrated state. The modulation depths and therefore the fraction of oligomeric colicin depend on the protein/lipid ratio. As it can be seen from the DEER traces and from a plot of the modulation depth *vs.* protein/lipid ratio (Figure 3.33 B), the modulation depths of the form factors (reflecting the fraction of dimers or oligomers) correlates with the protein/lipid ratio, as it would have to be expected assuming reversible association of ColA monomers to dimers or higher oligomers. From the titration curve a sigmoidal behaviour for the modulation depth as function of

concentration would be expected. Nevertheless, the poor signal to noise ratios obtained for especially the most lipid-diluted samples, that pose high uncertainties on the values obtained for the modulation depths, only a very coarse analysis of the binding constant (K_d) was carried out. Moreover, the reconstitution efficiencies also depend on the protein/lipid ratio and are prune to fluctuations, thus causing further hard-to-assess influences on the modulation depth values and their correlation with the protein/lipid ratio. A modulation depth of about 0.41 reflects 2 interacting spins (experimentally determined using a synthetic biradical) in the system and would correspond to 100 % of putative dimers. For ColA the highest modulation depth in the titration experiment (Fig. 3.33 B) was observed to be ~ 0.187 for a protein/lipid ratio of about 1:500, which would reflect ~ 46 % dimers or < 46 % higher oligomers. Thus, assuming dimerisation of ColA in membranes, the K_d can be estimated to approximately correspond to this ratio.

From the DEER experiments with ColA-77R1^{H4} reconstituted at different protein/lipid ratios it is obvious, that (a) *ColA does form oligomers in lipid bilayers*, and that (b) oligomerisation already occurs at a molar protein/lipid ratio of 1:2500, indicating that the detected oligomeric state is not forced by a high protein/lipid ratio. At this ratio for each colicin molecule – calculated based on an average surface area on the membrane per lipid molecule of 72 Å^2 (Luzzati, 1986), and taking both sides of the bilayer into account - a surface area of about 900 nm^2 is available, corresponding to a square of 30 by 30 nm (see Figure 3.33 C). The ColA pore forming domain in its soluble (globular) form has a diameter of ~ 5 nm, and even if the molecule partly unfolds upon membrane insertion, the mean distance between two ColA-pfds should not be below 15-20 nm. Thus, the observed oligomerisation of ColA has to be caused by a significant affinity of ColA protomers towards each other rather than by clustering due to high protein/lipid ratios.

Remarkably, cw data obtained for the samples, in particular mobility and environmental polarity of 77R1^{H4} (Figure 3.32 A) does not exhibit significant changes with varying protein/lipid ratios, although the ratio between the two spectral components in the spectra seems to exhibit a weak but not strictly systematic dependency on the protein/lipid ratio. These results suggests, taking the putative presence of two protein conformations in thermodynamic equilibrium into account (see 3.3.4), that both components seem to exist in the monomeric as well as in the oligomeric state. An assignment of the two components to the monomeric and oligomeric state, respectively, appears inappropriate as then one of the components should be absent at the lowest protein/lipid ratio (1:5000), where no oligomerisation could be detected by the DEER experiment.

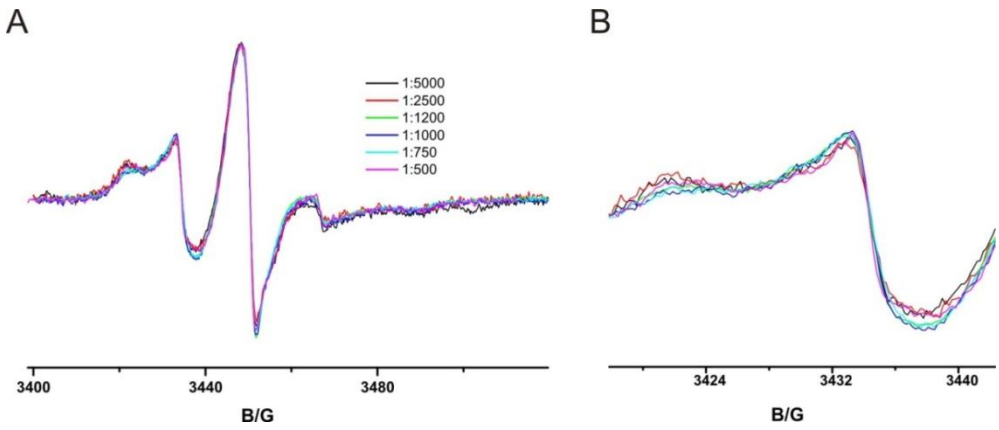

Figure 3.32 (A) Cw RT EPR spectra of ColA-77R1^{H4} reconstituted with different protein/lipid ratios. (B) close-up view of the low-field region of the spectra shown in panel (A), showing the two spectral components mentioned in the text.

Furthermore, with the help of the protein-lipid dilution DEER experiments on ColA-77R1^{H4} the dimensionality of the background contribution for analysis of the DEER data was determined. Normally membrane proteins in a lipid bilayer are most likely characterized by a two dimensional (2D) distribution. Nevertheless, at low protein/lipid ratios values between 2 and 3 might reflect the real spatial distribution – and therefore the necessary background correction - more appropriately. The program DeerAnalysis offers an option to fit the background dimensionality to the experimental traces (see manual of the program for details of the fitting approach), that was used to determine such value for each protein-lipid ratio. As it can be seen from the plot of these values *vs.* protein/lipid ratio (Figure 3.33 D), the background dimensionality decreases with increasing molar protein/lipid ratio up to 1:1000 to a value of 2.4 that is also observed for a protein/lipid ratio of 1:500.

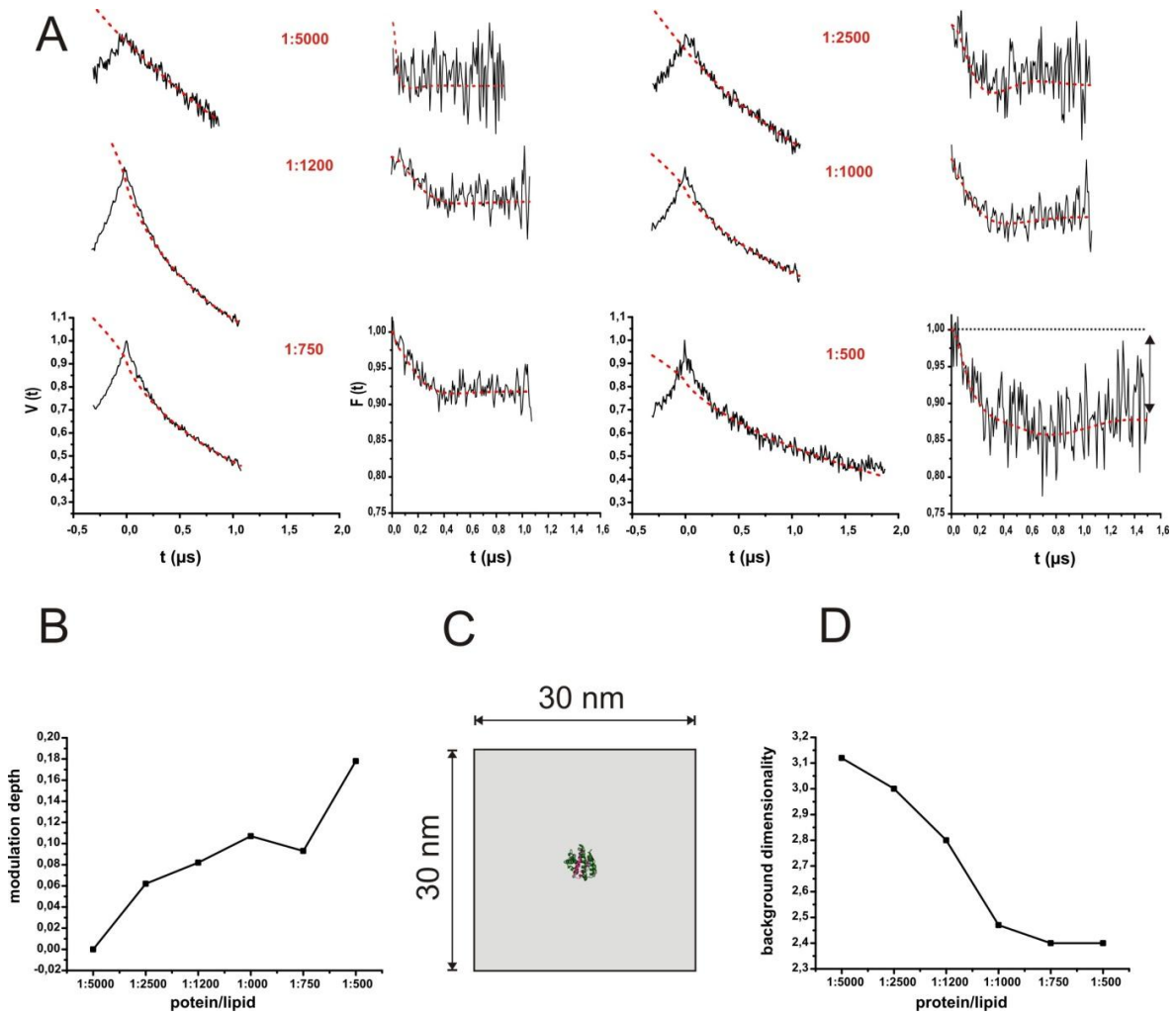

Figure 3.33: (A) DEER measurements for different molar protein to lipid ratios of the singly labeled colicin A mutant 77R1^{H4}. The modulation depth is indicated by the arrow in the form factor for the 1:500 dilution (B) modulation depth versus protein/lipid ratio (C) calculated surface area for ColA of about 900 nm^2 at lipid to protein ratio of 1:2500 (D) calculated background dimensionality for each protein-lipid ratio. For details see text.

In the next step, DEER experiments have then been performed on all singly labeled colicin A mutants reconstituted into lipid membranes. Inter-spin distances of less than 2 nm were determined by analysis of low temperature cw EPR spectra. Based on the results obtained in the "lipid dilution" experiments described above, for the reconstitutions a protein/lipid ratio of 1:500 has been chosen to maximize the spin concentration in the samples. The DEER analysis for all singly labeled variants of ColA in the membrane bound state is shown in Figure 3.34 A- D, with the background corrected dipolar evolution data (left panel) and the corresponding distance distributions (right panel). The analysis of DEER traces was performed using the software DeerAnalysis 2011 (Jeschke et al., 2006). Background correction of the dipolar evolution data was performed using a background dimensionality of 2.4 as determined from the lipid dilution experiments (see above). The distance distributions have been obtained by Tikhonov regularization.

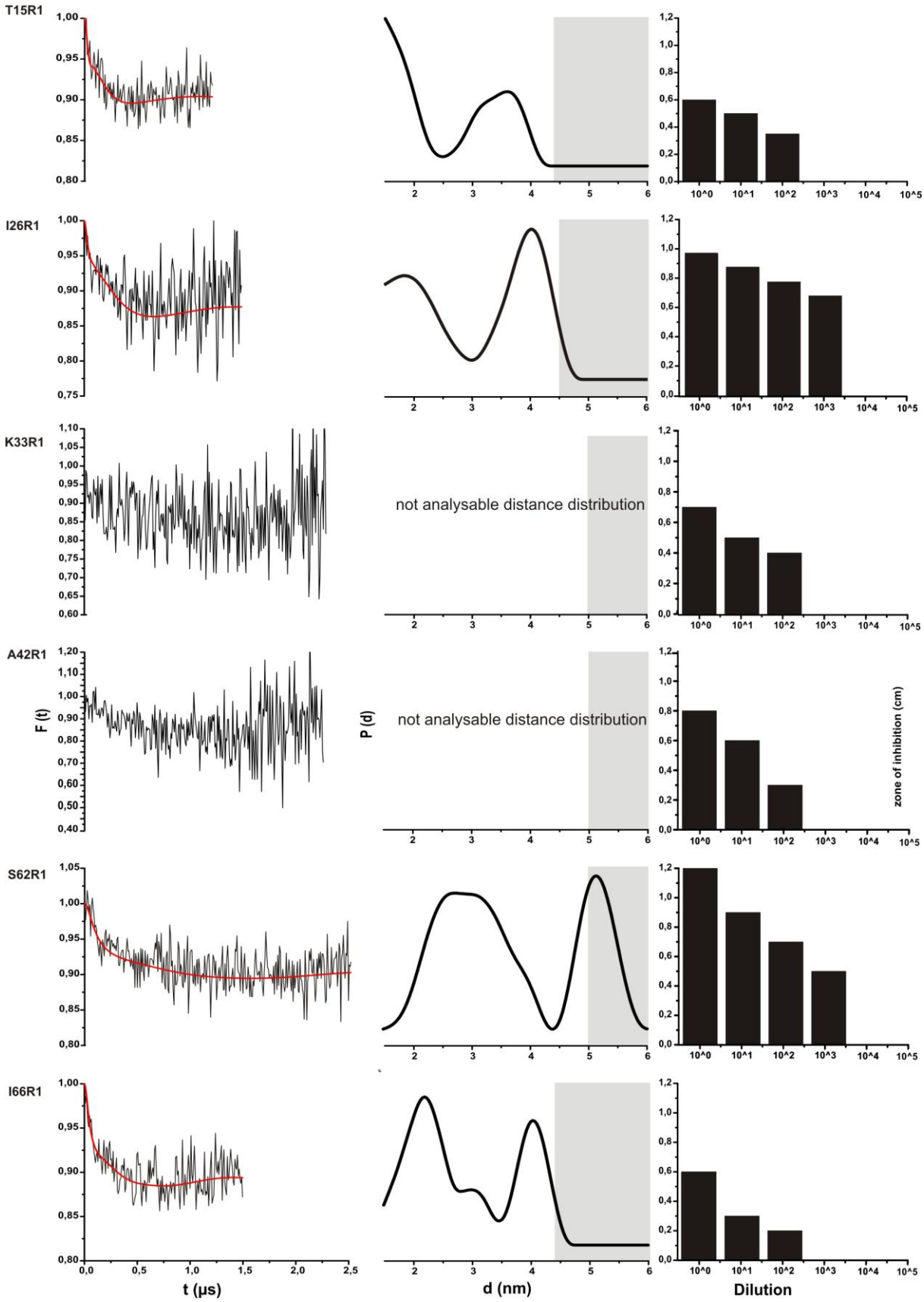

Figure 3.34 (A): DEER spectroscopy results of rec-mem ColA single mutants **H1-H3**. Left: dipolar evolution functions are shown as black lines and the corresponding fits calculated with DeerAnalysis indicated as red lines. Middle: the resulting DEER distance distribution obtained by Tikhonov regularization using DeerAnalysis. Right: viability test, the data is reported as the highest dilution of colicin A that still inhibits cell growth.

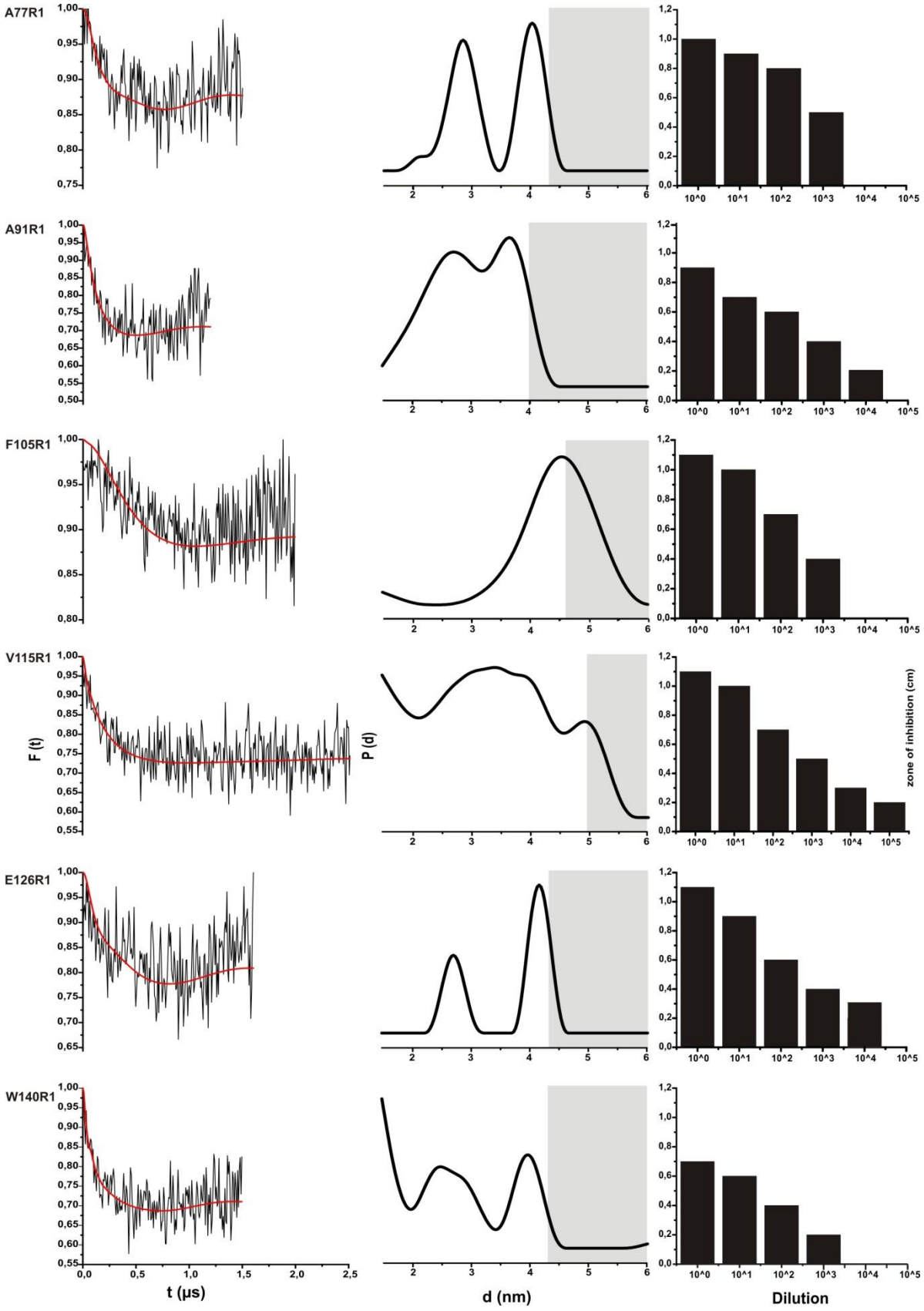

Figure 3.34 (B): DEER spectroscopy results of rec-mem ColA single mutants **H4-H7**. Left: dipolar evolution functions are shown as black lines and the corresponding fits calculated with DeerAnalysis indicated as red lines. Middle: the resulting DEER distance distribution obtained by Tikhonov regularization using DeerAnalysis. Right: viability test, the data is reported as the highest dilution of colicin A that still inhibits cell growth.

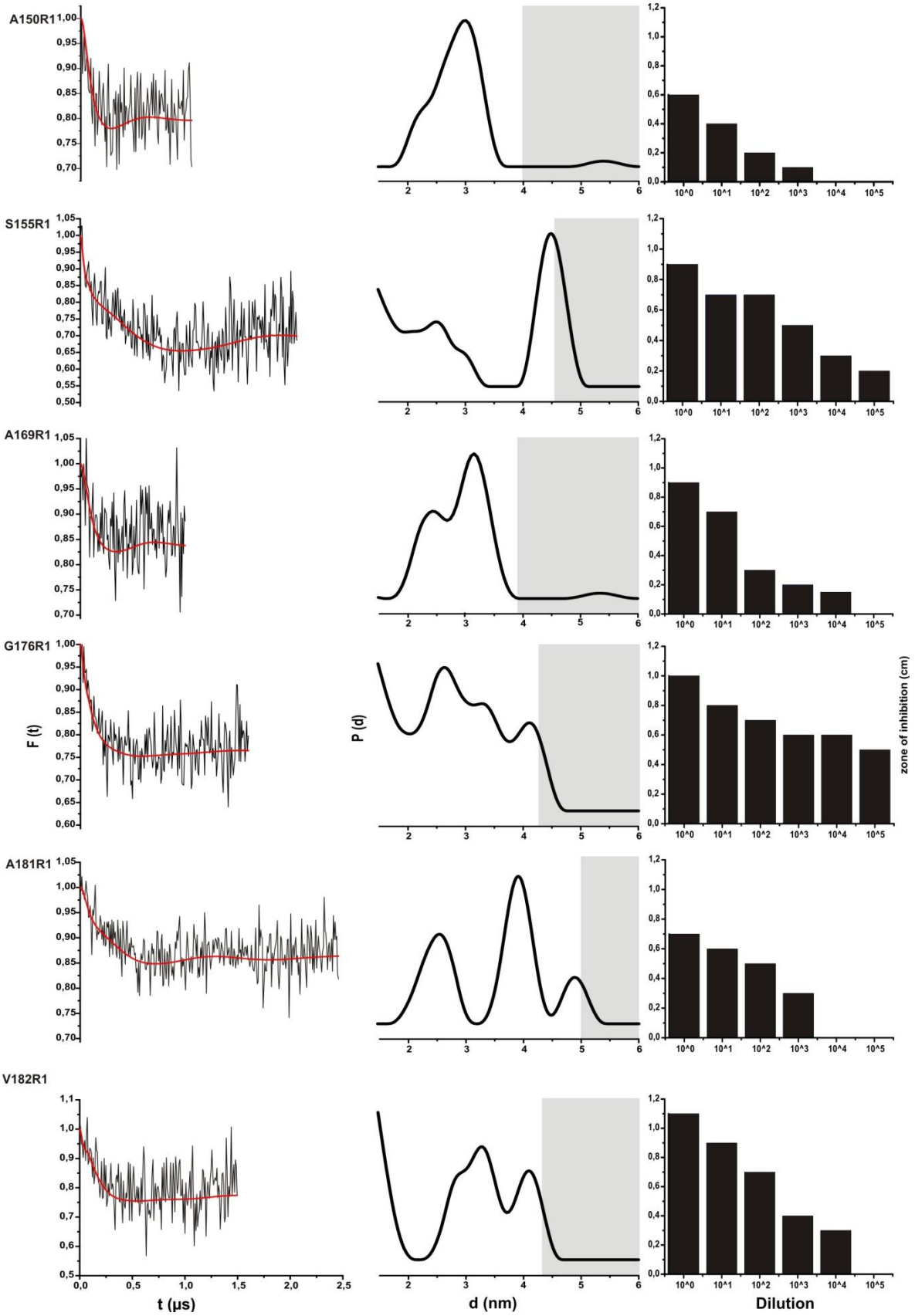

Figure 3.34 (C): DEER spectroscopy results of rec-mem ColA single mutants **H8-H9**. Left: dipolar evolution functions are shown as black lines and the corresponding fits calculated with DeerAnalysis indicated as red lines. Middle: the resulting DEER distance distribution obtained by Tikhonov regularization using DeerAnalysis. Right: viability test, the data is reported as the highest dilution of colicin A that still inhibits cell growth.

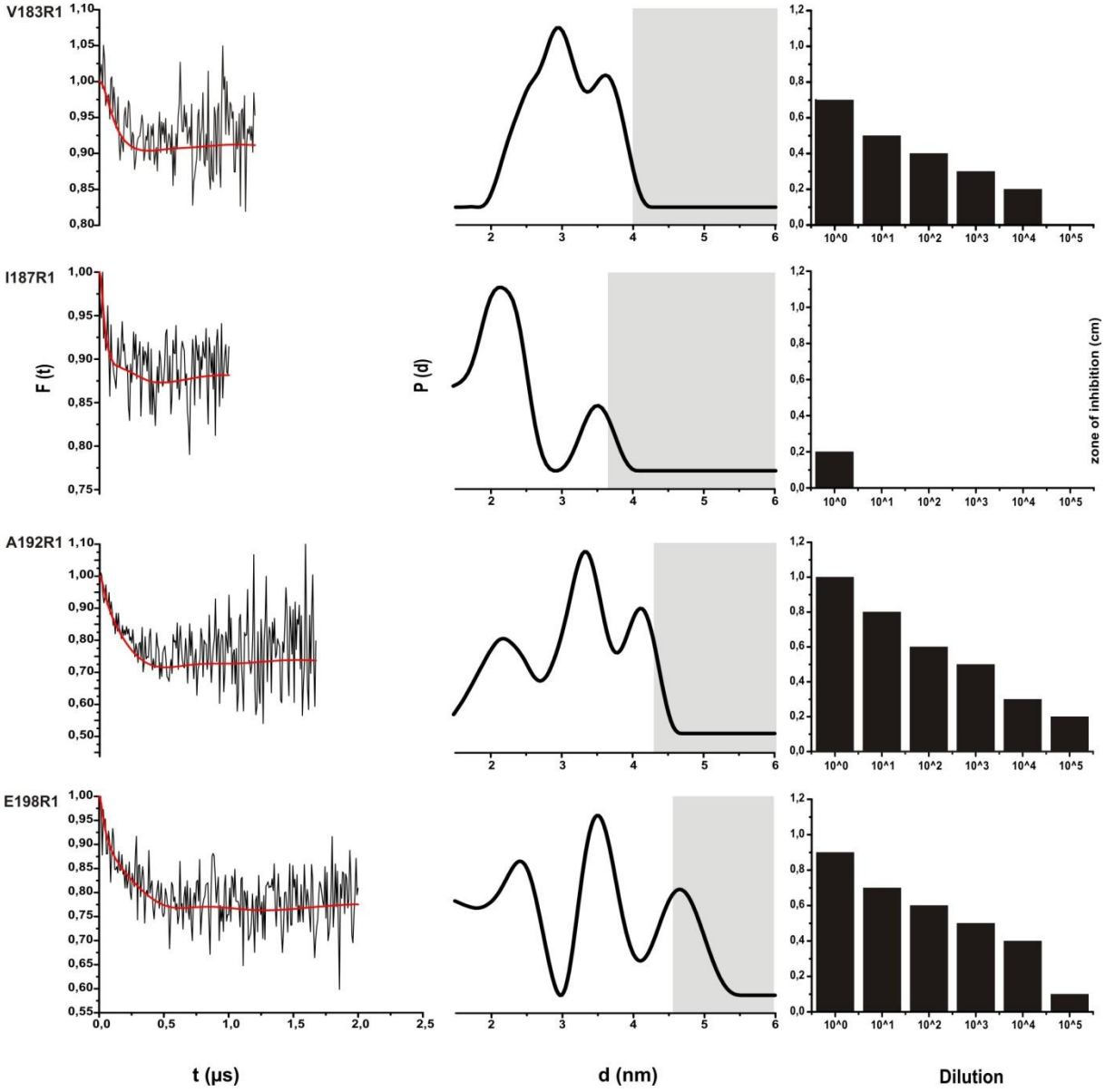

Figure 3.34 (D): DEER spectroscopy results of rec-mem ColA single mutants **H9-H10**. Left: dipolar evolution functions are shown as black lines and the corresponding fits calculated with DeerAnalysis indicated as red lines. Middle: the resulting DEER distance distribution obtained by Tikhonov regularization using DeerAnalysis. Right: viability test, the data is reported as the highest dilution of colicin A that still inhibits cell growth.

As obvious from Figure 3.34 A- D the DEER form factors (background corrected DEER data) for all label positions on the colicin A pore forming domain, except K33R1 and A42R1 exhibit dipolar modulations that can be translated into distance distributions. These findings clearly underline the assumption of oligomerisation in the membrane bound state of colicin A made before based on the lipid-dilution experiments on ColA-77R1^{H4}. The modulations depths of the form factors vary between < 0.1 – 0.3, corresponding to a number of interacting spins of 1.1 – 1.7. Taking the labeling efficiencies of the samples and the fact into account that even at the highest protein/lipid ratio used here the monomer-oligomer equilibrium might be still on the side of the monomers (see Figure 3.33 B, at a protein/lipid ratio

of 1:500 the observed modulation depth corresponds to ≥ 54 % monomers and ≤ 46 % oligomers), these values could be well in line with a dimeric or trimeric organization of colicin A in the membrane. Where distances < 2 nm are present in the DEER distance distributions, the low temperature cw EPR spectra (see 3.3.3.2) have been analysed in terms of dipolar broadening. Contributions below 2 nm in the distance distributions are consequently classified as (noise) artifacts, if the cw EPR spectra did not show indications for distances below 2 nm for the colicin A single mutants (see Figure 3.26). Furthermore, systematic variation of the background correction using the validation tool implemented in DeerAnalysis revealed that in several cases distance contributions > 4-4.5 might arise from an incorrect background correction that is complicated by the weak signal to noise ratio of some traces. Consequently, in such cases also the long distance contributions have been neglected. Table 3.5 summarizes the resulting mean distances obtained from the distance distributions shown in Figure 3.34 A-D.

Table 3.5: Results of the DEER distance measurements for ColA single mutants. Given are mean distances and modulation depths. If two distinct maxima are given in the distance distribution, the mean distances for both populations are given.

Label Position	Mean Distances (nm)	Modulation Depth
T15C^{H1}	**3.5**	**0.102**
I26C^{H1}	**2; 4**	**0.137**
K33C^{H2}	**>4.5**	**0.138**
A42C^{H2}	**>4.5**	**0.135**
S62C^{H3}	**3; >4**	**0.105**
I66C^{H3}	**2.3**	**0.116**
A77C^{H4}	**2.9,4**	**0.178**
A91C^{H5}	**3.5**	**0.274**
F105C^{H5}	**>4.5**	**0.084**
V115C^{H6}	**3.5**	**0.256**
E126C^{H6}	**4.2**	**0.195**
W140C^{H7}	**2.5; 4**	**0.293**
A150C^{H8}	**3**	**0.181**
S155C^{H8}	**2.5; >4**	**0.239**
A169C^{H9}	**2.8**	**0.162**
G176C^{H9}	**3**	**0.254**
A181C^{H9}	**3.9**	**0.148**
V182C^{H9}	**3.3**	**0.260**
V183C^{H9}	**3.2**	**0.080**
I187C^{H9}	**2.2**	**0.147**
A192C^{H10}	**3.2**	**0.227**
E198C^{H10}	**3.2**	**0.236**

For 33R1^{H2} and 42R1^{H2} the form factors in Figure 3.34 A, left panels, do not show clear modulations, leaving only possible distances > 4.5 nm (corresponding to the length of the DEER traces). The strong influence of noise in these samples (i.e. the high noise level) arises from their low spin concentrations that in turn are most likely caused by impaired membrane insertion. Furthermore, oligomerisation might also be hampered due to the impaired membrane insertion and/or disturbance of the protein-protein interface due to labeling. Both assumptions would also explain the observed low toxicity of these mutants (see Figure 3.34 A, right panel). Indeed, a weak correlation can be inferred from the data in Figure 3.34 between the toxicity of the mutant in the viability tests and the respective DEER modulation depth, i.e. the number of interacting spins and consequently the fraction of oligomeric ColA. This observation could be interpreted as an indication for the physiological relevance of oligomeric ColA in membranes

Most of the distance distributions obtained for the singly labeled ColA mutants are remarkably broad and often also at least bimodal. Broad distributions reflect either a high conformational flexibility of the R1 side chains and/or their point of attachment, meaning loop structures or disordered regions, or the superposition of distance distributions arising from the presence of two quite similar protein conformations in equilibrium. Bimodal distance distributions often reflect an equilibrium between two distinct protein conformations, but can also be caused by the presence of two discrete spin label rotamer populations. Nevertheless, the observed inter spin distance distributions for the ColA single R1 mutants provide further evidence for the presence of a protein conformational equilibrium for the closed channel state, as it has already been deduced from the presence of two components in the RT cw spectra (see 3.3.2). Interestingly, for positions that show strong spin label immobilization (see Figures 3.18, 3.20), e.g. for most label positions on helices H6, H7, H8 and H9, in most cases also more narrow distance distributions are observed. This further indicates that besides a protein conformational equilibrium for large regions of the ColA pore forming domain (H1-H5, H10) a higher conformational flexibility contributes to the width of the distance distributions. Strikingly, the mean distances in table 3.5 can be grouped in a similar way, with an average inter spin distance of 3.0 nm for positions on H6-H9, and 3.8 nm for H1-H5 and H10 (for this calculation, contributions > 4.0 and > 4.5 nm have been counted as 4.5 and 5.0 nm, respectively).

Thus, the results from the DEER measurements on ColA single R1 mutants identify a rigid "core" region comprising H6-H9 that inserts at least partly into the membrane (see results of the accessibility measurements in 3.3.3.1 and Figure 3.30) and also should at least partly comprise the dimerisation/trimerization interface. Contrarily, H1-H5 and H10 exhibit higher conformational flexibility and are characterized by inter spin distances being in average 0.8 nm larger than for the "core" region H6-H9, suggesting a circular (or similar) arrangement of these helices around the "oligomer (dimer) core" formed by two or more core regions H6-H9, and they are located in the headgroup region.

The DEER data presented up to this point provide clear evidence for an oligomeric pore under *in vitro* conditions and it could be shown that this oligomerisation has to result from a significant affinity of the ColA pore-forming domains in a membrane bilayer. The presence of solubilized oligomers in the samples

can be excluded as (i) oligomerisation in soluble form has been shown to be present only at detergent concentrations > 10 % (data not shown). The concentration used here was only 0.3 %. (ii) In the supernatant of the reconstitution no soluble protein was detectable (data not shown). Despite the fact that natural lipids (*E. coli* polar lipid extract, see chapter 3.3.1.5) have been used for all sample preparations for the DEER and cw experiments, the question arises if the oligomeric state could also be observed *in vivo*. In the next chapter it will be shown that oligomerisation of ColA also takes places in living *E. coli* cells.

3.3.6.4 DEER spectroscopy of colicin A *in vivo*

The DEER data obtained from spin labeled colicin A reconstituted into liposomes prepared from *E. coli* polar lipids shows that the protein oligomerises in the membrane bound state under in *vitro* conditions. It is well known that the conformation of a protein and also its dynamics strongly depend on the environmental conditions, for membrane proteins in particular the composition of the lipid bilayer including other membrane proteins, but also on the membrane potential, cytosolic as well as periplasmic pH etc. Consequently, experimental results obtained *in vitro* with a usually largely simplified system under investigation do not necessarily reflect the structure and dynamics of the protein *in vivo*. As clear experimental evidences for an oligomeric ColA pore are sparse besides this study, the question arises if oligomerisation of membrane bound colicin A occurs also under physiological conditions, i.e. when acting on living *E. coli* cells and inserting into the inner membrane of the cells. To answer this question, DEER distance measurements with singly spin labeled colicin A incubated with *E. coli* cells were performed. Unfortunately, investigations by SDSL EPR *in vivo* are complicated by several factors. The main limiting factor of SDSL EPR in living cells is the rapid signal decay due to the reductive conditions in the cells. Figure 3.35 shows an example, where MTSSL has been incubated with living Origami *E. coli* cells (L. Pulagam, PhD Thesis, 2007). The *E. coli* Origami strain, a mutant for thioredoxin reductase (*trxB*) and glutathione reductase (*gor*) was used in this study to reduce the rate of signal decay. In case of Origami cells with MTS spin label the EPR signal decreases with a half-time of about 5 minutes compared to about 2 minutes for a wt strain, which is attributed to the lack of *gor* and *trx*. Using this property, cw RT EPR measurements on spin labeled ColA acting on *E. coli* cells have been already reported (L. Pulagam PhD Thesis, 2007). Nevertheless, inter spin distance measurements with the DEER experiments ColA under *in vivo* conditions have not been successfully performed before.

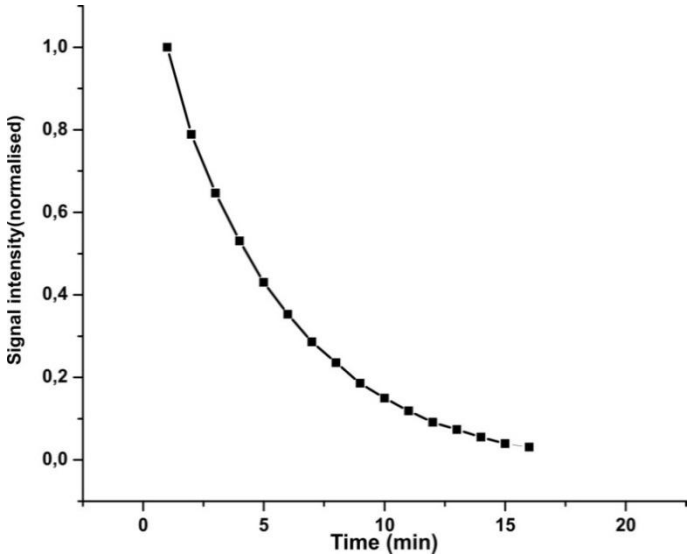

Figure 3.35: Free MTS spin label signal reduction upon incubation with living Origami *E. coli* cells. The signal intensities were derived from the amplitude of the central resonance line. The curves were normalized in relation to the maximal value. (Figure adopted and modified from L. Pulagam PhD Thesis, 2007.

The ColA mutant selected for these experiments is position 192R1^{H10}, for which the viability test showed unimpaired toxicity. The sample was prepared as described in chapter 3.2.4.12. Briefly, *E. coli* cells in the exponential growth phase were incubated for 2 min with 2 mg/ml of the spin labeled ColA mutant, then washed twice, resuspended in buffer and shock frozen in liquid nitrogen in EPR quartz capillaries.

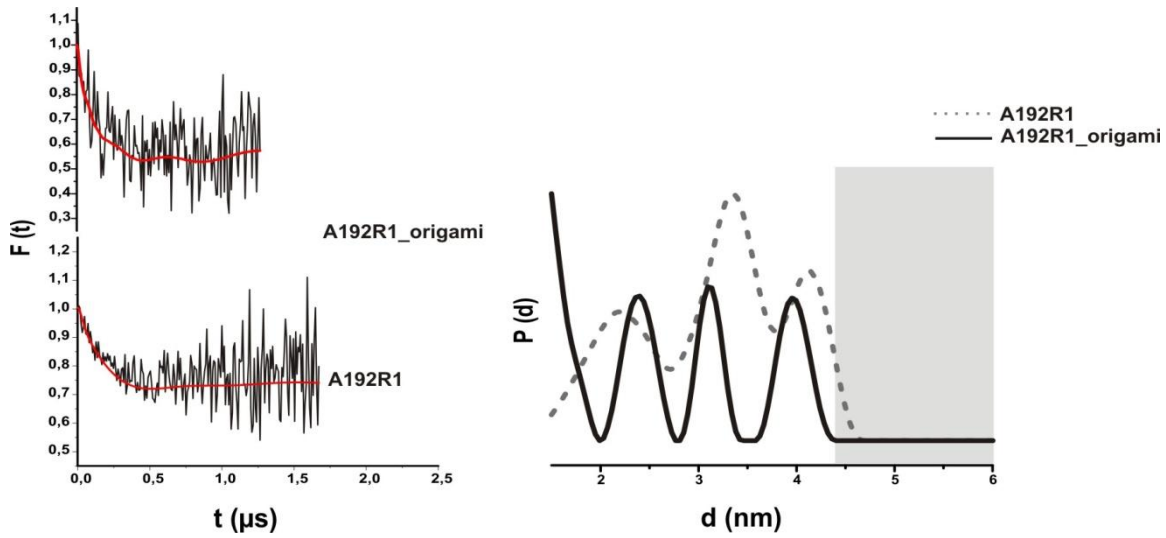

Figure 3.36: DEER spectroscopy results for sol-ColA single mutants incubated with *E.coli* Origami living cells (solid line) compared to the results obtained for the protein reconstituted in liposomes (dotted line). Left: dipolar evolution functions are shown in black and the corresponding fits calculated with DeerAnalysis indicated as red lines. Right: The resulting DEER distance distribution obtained from Tikhonov analysis.

For ColA-A192R1^{H4} the DEER traces for the protein in liposomes and incubated with *E. coli* cells exhibit very similar dipolar modulations that translate into similar distance distributions. This indicates that (i) the oligomerisation of ColA takes also place *in vivo*, and that (ii) the native conformational state of the protein seems to be generally preserved in the model system using *E. coli* polar lipid liposomes, although definite conclusions cannot be drawn from the DEER data due to the poor signal to noise ratio especially for the data obtained *in vivo*. Consequently, analysis of such dataset does not lead to a reliable distance distribution and the clear differences obvious from comparison with the data obtained for the mutant in liposomes cannot be taken as an indication for large structural differences between the protein *in vitro* and *in vivo*. Nevertheless, *the results of the DEER experiments performed on living cells clearly reveal that colicin A oligomerises in the membrane also under physiological conditions, in vivo*. Furthermore, reconstitution of ColA into liposomes does not seem to cause significant structural differences compared to the protein *in vivo*, although experiments have to be performed on all ColA spin label mutants to unequivocally identify the structure *in vivo*. It has also to be kept in mind that the observed differences could be caused mainly by the fact that in liposomes no membrane potential is present that could lead to opening of the ColA-channel pore. Consequently, in liposomes only the closed channel state should be observed, whereas in the *E. coli* inner membrane a significant fraction of protein should be frozen in the open channel state. Further *in vivo* DEER experiments have not been performed, as it is at the methologiocal limit with the labeling techniques used in this work. Improved labeling techniques (for example reduction resistant spin labels) for *in vivo* EPR are currently in the development in our group.

3.3.6.5 Determination of intramolecular inter spin distances in colicin A double mutants

In addition, to obtain distance constrains also for the single protomers in a potential colicin oligomer DEER experiments on doubly labeled ColA were performed. The double mutants selected for this study are almost randomly distributed over all helices of the pore forming domain. Two positions, I187R1^{H9} and A77R1^{H4}, have been combined with different other positions, thereby serving as "reference points" for topological mapping of the protein (see Figure 3.37 A). For the following double mutants reconstituted in liposomes DEER experiments have been performed: A42R1/I187R1, S62R1/I187R1, V115R1/I187R1, A91R1/V115R1, I26R1/A77R1, A77R1/W140R1, A77R1/S155R1, W140R1/A150R1, I26R1/A192R1, I26R1/E126R1 and K33R1/E198R1. As already mentioned the double mutants A42R1/I187R1, S62R1/I187R1, A91R1/I187R1 and V115R1/I187R1 have been already investigated by inter spin distances measurements in the study by Boehme et al., (2009) but were freshly prepared and re-measured in this work.

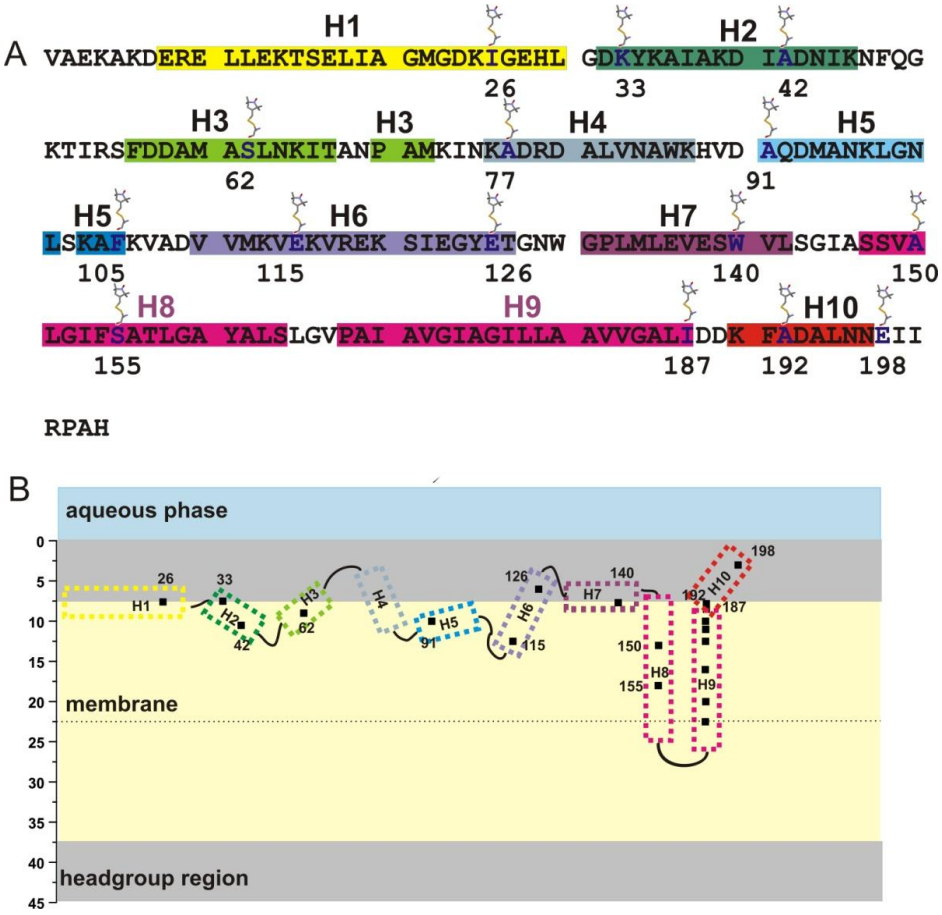

Figure 3.37: (A) Amino acid sequence of the colicin A pore forming domain. The label positions are colored in red and the respective residue number is given. (B) Colicin A double mutants depicted on the topological model derived from the results of the cw EPR experiments.

The results of the DEER analyses for the ColA doubly labeled variants are given in Figure 3.38 A-C. As the DEER experiments on singly labeled ColA described in the previous sections clearly revealed that colicin A oligomerises in the membrane, the distance distributions obtained for the doubly labeled samples consequently contain intramolecular as well as the previously observed intermolecular contributions, complicating data analysis in terms of the intramolecular distance constraints for modeling of the membrane bound state of ColA. To circumvent this problem for each double mutant datasets have been recorded, where 20 % spin labeled ColA was mixed and incubated with the unlabeled wt protein (80 %), a procedure called "spin dilution". In such samples the contributions from intermolecular spin spin interactions should be largely suppressed, as statistically only a low percentage of oligomers comprises spin labels on all ColA protomers in the complex. Comparison of these datasets with those obtained from fully labeled samples should then allow to separate inter- and intramolecular distances and to yield information about the possible arrangement of the helices in a colicin A oligomer.

In Figure 3.38 A-C the DEER results for the fully labeled ColA double mutants are shown as dotted black lines, and the data obtained from the corresponding spin-diluted samples are given as grey solid lines. In addition, for both preparations of each double mutant, low temperature cw-EPR measurements were performed to detect distances below 2 nm.

Fully labeled ColA-I26/A77R1$^{H1\text{-}H4}$ (dotted line) exhibits a distance distribution with a broad single distance peak ranging from 2-4 nm, containing the inter- and intramolecular distances, with a mean distance of about 3.4 nm. The inter-spin distances already determined for the two single mutants I26R1^{H1} and A77R1^{H4} at 2/4 nm and 4 nm, respectively, are reflected in the distance distribution. The spin diluted I26R1/A77R1-wt$^{H1\text{-}H4}$ sample (grey line) reveals an intramolecular distance distribution centered at 2.9 nm. The shoulder at ~ 2.3 nm most likely arises from noise artifacts at the beginning of the DEER trace and can most likely be neglected. This example shows how the intermolecular interactions are largely eliminated and the corresponding intramolecular distance can be determined. The intramolecular inter spin distances, i.e. distance constraints in the protomers in a ColA oligomer, obtained from this analysis are summarized in table 3.6 for all double mutants investigated here, including distances below 2 nm obtained from the cw experiments.

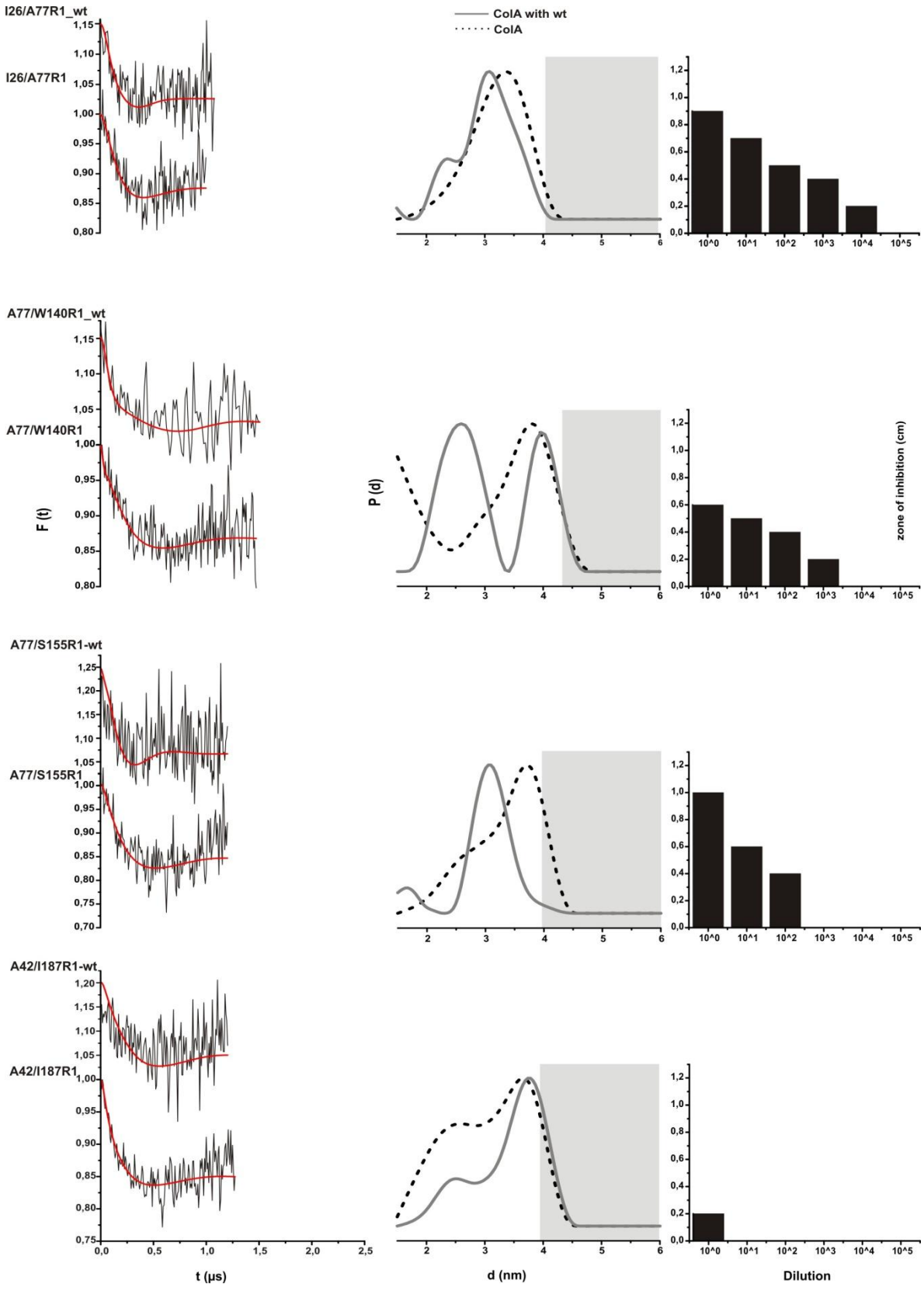

Figure 3.38 (A): DEER results of the rec-mem ColA double mutants. Left panel: The dipolar evolution functions are shown in black and the corresponding fits calculated with DeerAnalysis indicated as red lines. Center panel: The resulting DEER distance distributions obtained from Tikhonov regularization of the data in DeerAnalysis. Black dotted lines: fully labeled double mutants. Grey solid lines: datasets obtained with spin-diluted samples. Right panel: viability test, the data is reported as the highest dilution of colicin A that still inhibits cell growth.

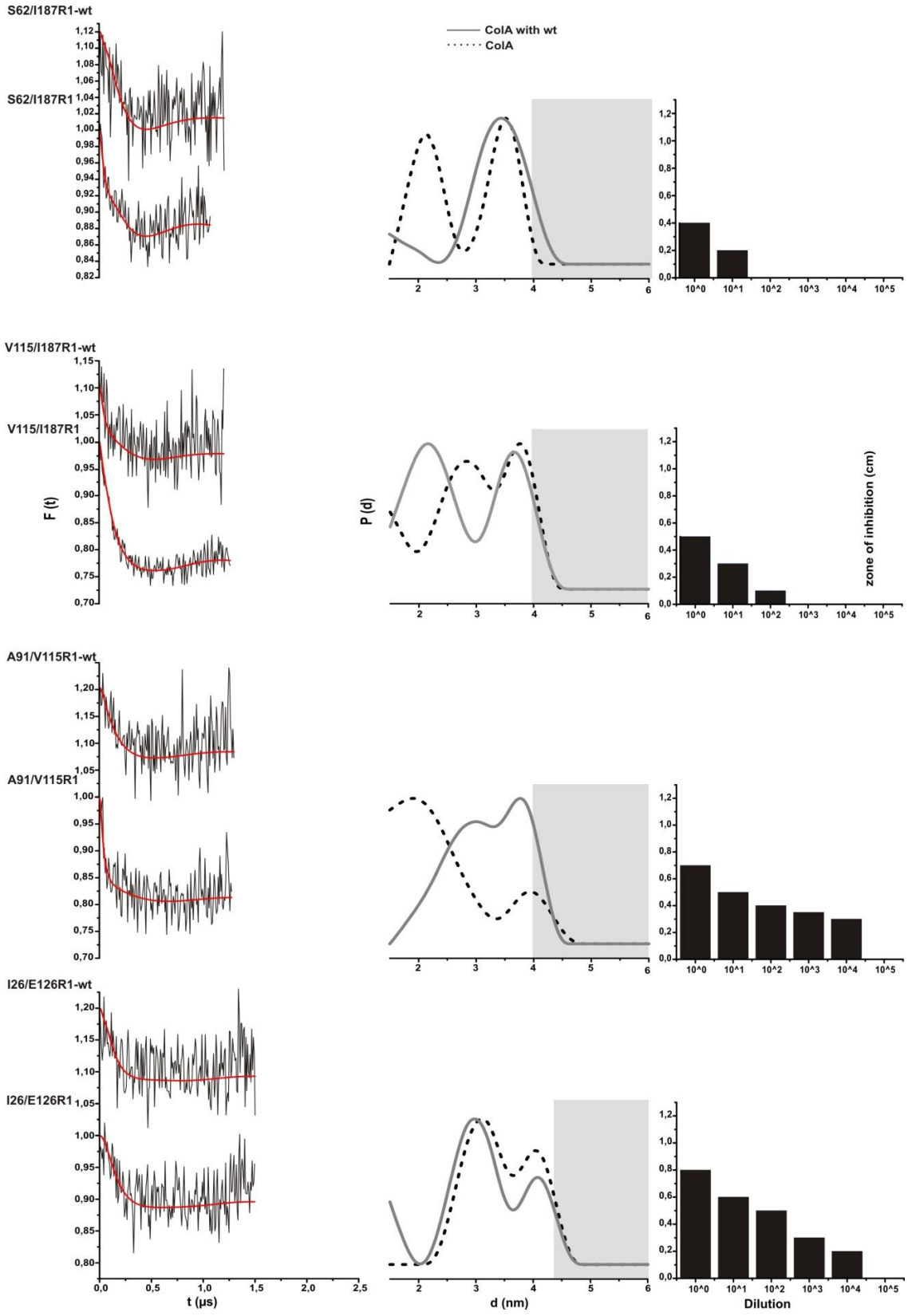

Figure 3.38 (B): DEER results of the rec-mem ColA double mutants. Left panel: The dipolar evolution functions are shown in black and the corresponding fits calculated with DeerAnalysis indicated as red lines. Center panel: The resulting DEER distance distributions obtained from Tikhonov regularization of the data in DeerAnalysis. Black dotted lines: fully labeled double mutants. Grey solid lines: datasets obtained with spin-diluted samples. Right panel: viability test, the data is reported as the highest dilution of colicin A that still inhibits cell growth.

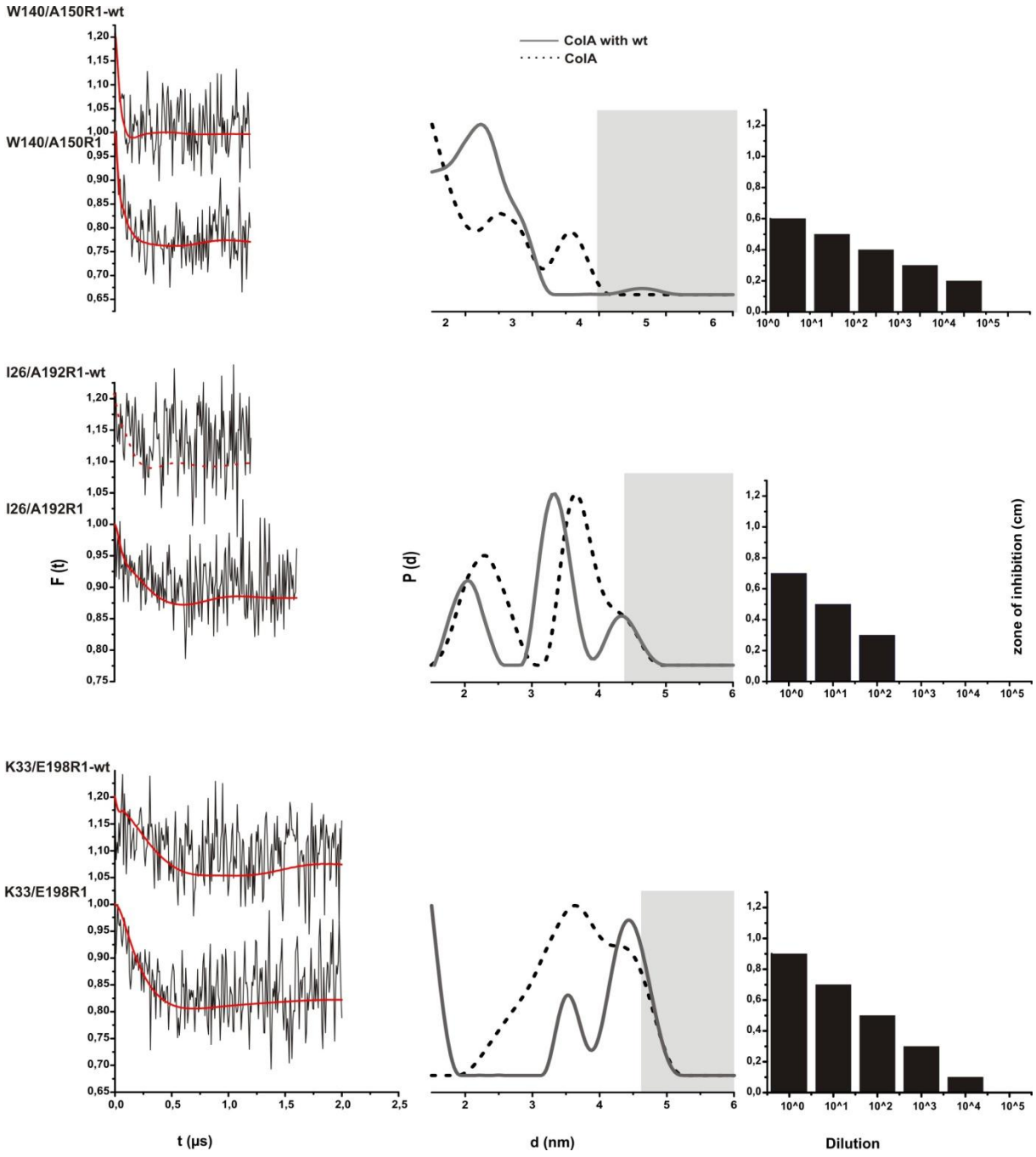

Figure 3.38 (C): DEER results of the rec-mem ColA double mutants. Left panel: The dipolar evolution functions are shown in black and the corresponding fits calculated with DeerAnalysis indicated as red lines. Center panel: The resulting DEER distance distributions obtained from Tikhonov regularization of the data in DeerAnalysis. Black dotted lines: fully labeled double mutants. Grey solid lines: datasets obtained with spin-diluted samples. Right panel: viability test, the data is reported as the highest dilution of colicin A that still inhibits cell growth.

The data reveals that the protomers in the membrane-inserted ColA oligomers exhibit a relatively compact fold in which the helices (assuming that the secondary structure is largely preserved upon membrane insertion of the protein) are densely packed, except for a distance > 4 nm found in between helices H2 and H10. Interestingly, for ColA-A42R1/I187R1$^{H2\text{-}H9}$ the DEER experiments reveal an intramolecular inter spin distance of about 3.9 nm and the cw data obtained from the spin diluted sample exhibits clear dipolar broadening resulting from an inter spin distance of 1.3 nm. It can be speculated that in this case the protein conformational equilibrium deduced from the presence of two components in the RT cw EPR spectra (see 3.3.2) is reflected in the overall bimodal distance distribution obtained for this sample.

Table 3.6: Intramolecular distances obtained by distance measurements on spin diluted samples.

ColA mutant	Distance by DEER (nm)	Distance by cw (nm)
I26R1/A77R1$^{H1\text{-}H4}$	**2.9**	**-**
I26R1/E126R1$^{H1\text{-}H6}$	**3.1**	**-**
I26R1/A192R1$^{H1\text{-}H10}$	**-**	**1.1**
K33R1/E198R1$^{H2\text{-}H10}$	**>4**	**-**
A42R1/I187R1$^{H2\text{-}H9}$	**3.9**	**1.3**
S62R1/I187R1$^{H3\text{-}H9}$	**3.5**	**-**
A77R1/W140R1$^{H4\text{-}H7}$	**2.5**	**-**
A77R1/S155R1$^{H4\text{-}H8}$	**3.1**	**-**
A91 R1/V115R1$^{H5\text{-}H6}$	**3.5**	**-**
V115R1/I187R1$^{H6\text{-}H8}$	**2.2**	**-**
W140R1/A150R1$^{H7\text{-}H8}$	**2.3**	**-**

3.3.7 A Model for the closed channel state of colicin A

3.3.7.1 The oligomeric state of the ColA pore-forming domain

In the previous chapters a wealth of data has been obtained that provides information about the structural properties of colicin A in the membrane bound state. The mobility, accessibility and polarity data obtained from cw EPR experiments (see chapters 3.3.2 - 3.3.5) has been already used to predict the immersion depth of the helical segments in the lipid bilayer as reflected in the topological model presented in Figure 3.30. Furthermore, the inter spin distance measurements described in chapter 3.3.6 clearly revealed that ColA does form oligomers in the membrane bound state, and corresponding experiments performed on live *E. coli* cells (chapter 3.3.6.4) confirmed that oligomerisation takes also place *in vivo*, i.e. is of physiological relevance. In this chapter, the results of the DEER experiments, providing intramolecular inter spin distance constraints for the protomers from analysis of the double mutants, and intermolecular distance constraints in the oligomer from the single mutants, will be combined with the knowledge obtained from the cw experiments to propose a molecular model for the closed channel state of colicin A.

Besides distance constraints and other topological data of course also *knowledge about the degree of oligomerisation* of colicin A in the membrane bound state is a prerequisite to be able to derive a structural model. The DEER experiments described in chapter 3.3.6.3 clearly show that colicin A is oligomeric in the lipid bilayer but the obtained modulation depth values (see table 3.5) and corresponding numbers of interacting spins do not allow unambiguous determination of the oligomerisation degree in such way as long as reliable values for e.g. the dissociation constant of oligomerisation and consequently the ratio between monomers and oligomers in the samples are unknown. Titration experiments like that described in chapter 3.3.6.3 can in principle be used to provide this data, but analysis of the titration data in terms of binding or dissociation constants in turn also requires knowledge about the oligomerisation state. Consequently, the experimental data presented so far does not allow distinguishing between colicin A dimers or higher oligomers. A coarse analysis of the binding constant for ColA oligomerisation in membranes was carried out by a protein-lipid dilution experiment on ColA-77R1^{H4}. Based on the average surface area on the membrane per lipid molecule of 72 Å^2, the protein/surface ratio for each protein/lipid ratio was calculated. The surface area including a ColA monomer was analysed and the dimer dissociation constant K_d in molecules/μm^2 briefly calculated (data not shown). This analysis for ColA reveals protein densities of 5000 molecules/μm^2. This result is in agreement with the dimer dissociation constant K_d for the lipid anchored GTPase RAS which was found to be in a range of about 1000 to 4000 molecules/μm^2 (Lin et al., 2014). Such high local concentration and therefore the physiological relevance of ColA oligimerisation might be explanainable by the translocation mechanism. Colicin A uses two different membrane proteins to traverse the outer membrane, the vitamin B12 receptor BtuB and the porin OmpF (Lazzaroni et al., 2002) (Lazdunski et al., 2000). Entry of ColA into the cell starts with binding to its putative receptor, the vitamin B12 receptor BtuB (Di Masi, 1976) (James et al., 1996), whereas the second putative receptor is the non-selective trimeric porin OmpF (Bourdineaud et al., 1990 (Cowan et al., 1992).

Kurisu et al. (2003) suggest for ColE3 that binding of the receptor binding domain to BtuB concentrates the colicin on the surface area. Afterwards the translocation domain binds to the secondary receptor and the translocation domain and the pore-forming domain translocate with the help of the porin OmpF, while the receptor-binding domain is thought to be still attached to its receptor (Kurisu et al., 2003). This indicates an important role for the "linker-or spacer" region presented in numerous colicins. In colicin Ia a long helix in the translocation domain is proposed to function as a spacer region (Wiener et al., 1997). For colicin A it has also been proposed that this helix region could act a a spacer domain (Bouveret et al., 1998) (Journet et al., 2001). Thus, 2-3 colicin molecules can be translocated by the OmpF–trimer, and if the receptor-binding domain remains attached to its receptor BtuB after translocation of the translocation and pore-forming domains, free diffusion of the ColA pore-forming domain appears strongly limited, leading to local concentrations of several 1000 ColA molecules/μm^2 (assuming an area for ColA diffusion of ~ 100 nm^2, as an Ompf trimer occupies a surface area of about 60 nm^2).

Furthermore, also based on the observed spin numbers higher oligomers than trimers appear to be unlikely, leaving the question, whether ColA forms dimers or trimers in the membrane bound state. Therefore, in the following additional information about the putative structure of ColA-mem and especially the degree of oligomerisation will be deduced from comparison with structurally and functionally related proteins. For many pore-forming toxins like α-hemolysin, diphteriatoxin and the Bcl-2 family members it is known that these proteins are also secreted as soluble molecules and inserted into the inner membrane to form oligomeric pores (Mechaly et al., 2011). Especially the Bcl-2 like proteins, being key players in programmed cell death, i.e. apoptosis, like Bcl-2 itself, Bcl-xL and Bax show remarkable sequence identity to ColA (see Figure 3.39), and furthermore exhibit significant structural similarities with the pore-forming colicins (Figure 3.40) in the soluble state. For these proteins it has been shown that they form dimers after insertion into the membrane (Suzuki et al., 2000) (Annis et al., 2005). The results obtained by DEER spectroscopy also provide evidence for a dimeric assembly of ColA in the membrane. Comprehensive studies on proteins of the Bcl-2 family identified conserved so-called Bcl-2 homology domains, BH1, BH2, BH3 and BH4 (Suzuki et al., 2000), being important for their function. Bcl-2 and Bcl-xL contain all 4 BH domains and have antiapoptotic function, whereas Bax and Bak contain only BH1, BH2 and BH3 domains - and have a proapoptotic effect (Garcia-Saez et al., 2004). For Bcl-2 and Bax it was shown that these proteins dimerize *via* the BH domains (Bcl-2 homology), and that these dimers can also form higher oligomeric structures to constitute larger channels (Shimizu et al., 2000), proposedly leading to, e.g., cytochrome c release in the course of apoptosis. Strikingly, interpretation of the electron densities observed for membrane bound Col Ia (Greig et al., 2009, see chapter 3.1.5) as trimers of dimers provides further evidence for the functional and structural similarities between the Bcl-2 and pore forming colicin protein families.

Closer inspection of the sequence alignment between colicin A and the Bcl-2 like proteins reveals that the most conserved regions correspond to the BH domains of the Bcl-2 members. The highest sequence identities are observed for the BH1 and BH4 domains and to a lesser extent also for BH3. The BH2 domains show only minor similarities between the Bcl-2 proteins and colicin A. In Bcl-xL and Bcl-2 both

the BH1 and BH3 domains are thought to be responsible for dimerisation. Bax and Bak only seem to dimerize via their BH3 domains as both proteins do not have BH1 domains. As being responsible for dimerisation of the proteins hydrophobic residues leucine and isoleucine seem to be of particular importance (Suzuki et al., 2000). Interestingly, in all proteins compared here, including colicin A, the leucine residues in the BH3 domain are highly conserved. Moreover, isoleucine is also found in colicin A, Bax and Bak at the same positions in the BH3 domains. These observations provide further evidences that ColA and Bcl-2 proteins exhibit similar structural properties.

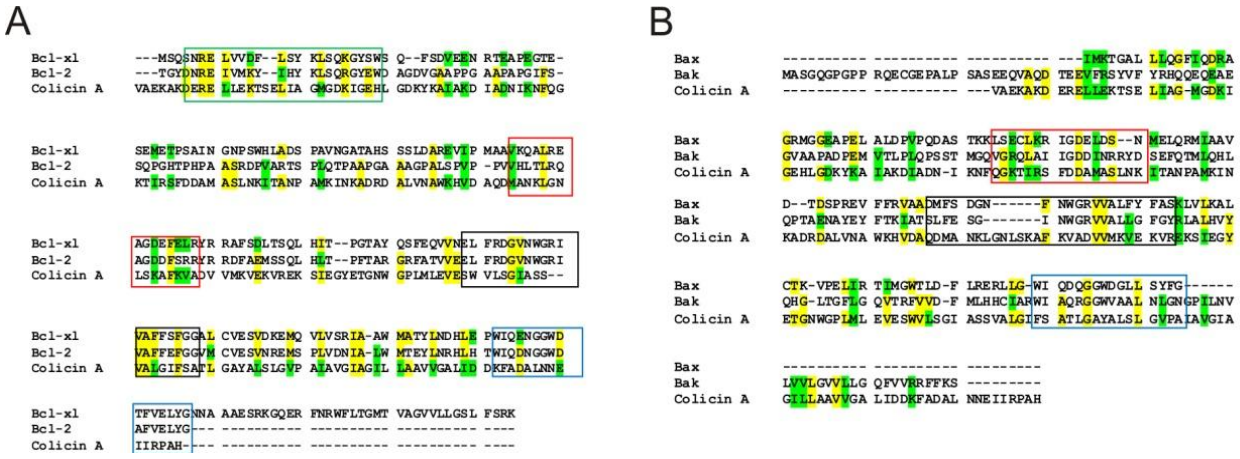

Figure 3.39: (A) and (B): Sequence-alignment of colicin A with different proteins of the Bcl-2 family. Identical amino acid residues are colored in yellow, similar amino acids are colored in green. The different BH-homology domains are colored, blue: BH4, red: BH3, yellow: BH1 and green: BH2.

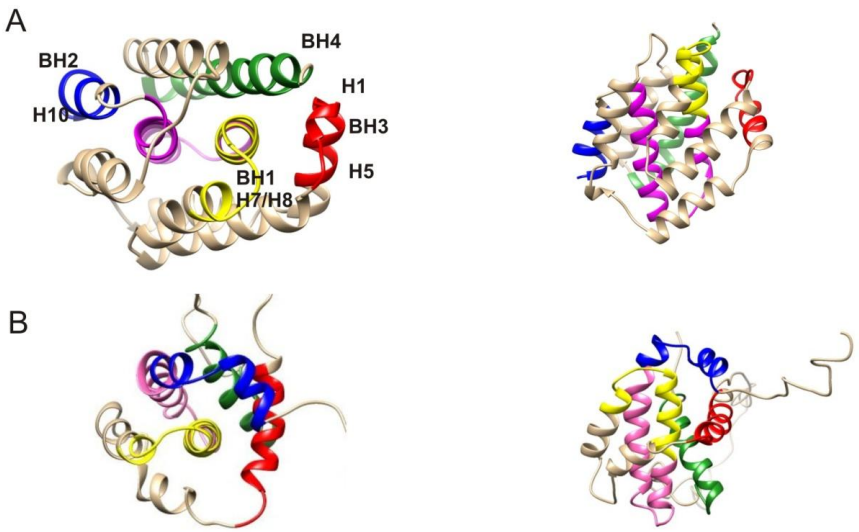

Figure 3.40: (A) X-ray crystal structure of water-soluble pore-forming domain of colicin A (1COL.pdb), concerning the sequence-homology the potential BH domains are colored, green: BH4, red: BH3, yellow: BH1 and blue BH2. (B) In Bcl-xL these domains are also in close proximity and form a hydrophobic cleft (1LXL.pdb)

As already mentioned, the BH2 domain is less conserved in colicin A. This domain is only present in Bcl-2 and Bcl-xL but not in Bax and Bak, and represents the so-called tail anchor domain. Bax and Bak have no tail-anchored region and are consequently predominantly soluble in the cytoplasm before membrane insertion, analogous to colicin A.

Comparison of the primary sequeneces with secondary structure predictions and structural data for the soluble form (see Figure 3.40) reveals that the BH4 domain in Bcl-2 and Bcl-xL comprises helix 1. This helix is also present in ColA, albeit the helix in colicin A is longer by 8 residues. The BH3 domains in the Bcl proteins comprise H2, corresponding to H5 in colicin A, being of almost the same length. Protein dimerization thus could take place in colicin A *via* helix 5. According to the cw EPR data obtained by accessibility measurements in this work, H5 in the closed channel state of colicin A is located within the membrane bilayer, most likely in an orientation parallel to the membrane surface. The BH1 domain, proposed to be in addition to BH3 responsible for dimerisation of Bcl-xL and Bcl-2, in these proteins located between H4 and H5, in colicin A is located between helices 7 and helix 8, the latter being part of the hydrophobic helical hairpin H8-H9. Noteworthy, dimerisation *via* the helical hairpin to form a bundle of four putatively transmembrane helices could, together with H4 and H5 being the voltage sensor, rationalize how ColA can form a pore of ~ 1 nm diameter, corresponding to ≥ 6 transmembrane helices.

Based on the above mentioned findings from the sequence alignment, i.e. striking similarities between ColA and the Bcl-2 family members, especially in terms of conservation of regions comprising the dimerisation interfaces in the Bcl-2 proteins, and the DEER data obtained in this work, it seems to be well justified to assume that ColA also dimerises in the membrane bound state. Taking into account the high similarities in the BH1 and BH3 domains, it can also be proposed that dimerisation of colicin A takes place *via* helices H5 (BH3 domain) and H8 (BH1 domain).

As described in the introduction in more detail, the hypothesis of a multimeric colicin A channel has already been brought up in several publications, for example a study on the colicins A and E1 using CD spectroscopy (Pattus et al., 1985), that supported a possible oligomerisation of the channel domains. In Pattus et al. (1985) two possible models are postulated, each requiring six helices to form the pore. The first model assumes a dimerisation of colicin A by the helices H4, H5 and H6, whereas a second model describes the channel as a trimer, in which the pore is formed by helices H5 and H6. The evidence for the dimer model can furthermore be promoted with the results in the study of Baty et al. (1987). Measuring the colicin A activity *in vivo* on sensitive cells and *in vitro* in planar lipid bilayers supported more the dimer model because deletion mutations in helices 4-6 abolish ColA channel formation (Baty et al., 1987). Strikingly, in the background of the findings presented in this study, these two models could correspond to dimer formation and formation of trimers of dimers, respectively, as observed by Greig et al. (2009). At this point, an obvious contradiction of a dimeric ColA form with some experimental data should be mentioned again. Electrophysiological studies by Martinez et al. (1983), Slatin et al. (1994), Kienker et al. (2008), and Sippach (2009) concluded that functional channels formed by the colicins A, Ia and E1 are comprised of a single monomer. Remarkably, the study by Sippach also revealed that large molecules such

as calcein or tetraethylammonium are able to pass the colicin A channel and a pore diameter > ~10 Å was estimated (Sippach, 2009), later confirmed by Slatin et al. (2010), who proposed furthermore that a selective proton pathway exists through the channel of ColA. Combining these results provides a basis for the assumption that a proton conductive monomeric form of colicin A can cause lethal effects already at low colicin concentrations in the medium, and that oligomeric forms appear at higher ColA concentrations, allowing the diffusion of larger molecules. Therein, a dimeric form, and, putatively not of physiological relevance, trimers or even higher oligomers of such dimers at very high concentrations, seem to exist. Conclusively, a dimeric form of ColA most likely appears to be the state of physiological relevance and for the construction of a molecular model of colicin A in the closed channel state it was assumed that it is a dimer.

3.3.7.2 Conformational arrangement of the ColA pore-forming domain

The accessibility and polarity measurements described in chapter 3.3.3 revealed that the hydrophobic helical hairpin H8/H9 has a transmembrane orientation like it is proposed according to the umbrella model for ColA in the membrane bound state. Furthermore, based on the present polarity and accessibility data sets, H5 and H6, and also parts of H2 and H3, are also at least partly embedded in the membrane.

Besides the immersion depths obtained from cw experiments, the distance constraints from the DEER measurements (chapter 3.3.6) and the information obtained from comparison with the Bcl-2 proteins (see previous paragraph), further conclusions concerning the tertiary structure of ColA in the membrane can be drawn from the room temperature cw EPR spectra (Fig. 3.18). All the spectra of colicin A reveal the presence of at least two spectral components characterized by different mobilities. In general, this can arise from either two different protein conformations for ColA, what has been proven to be the case for at least some positions using temperature dependent measurements and by analysis of the influence of paramagnetic quenchers on the spectral features. In addition, two-component EPR spectra can result from close interactions of the spin label side chains with nearby groups, and it has been shown that in this case the two spectral components (immobile and mobile) can be clearly distinguished from each other (Kronke et al., 2010). Considering this criterion, the cw EPR spectra of the colicin mutants 62R1^{H3}, 77R1^{H4}, 91R1^{H5}, 140R1^{H7}, 150R1^{H8}, 155R1^{H8}, 169R1^{H9}, 192R1^{H10} and 198R1^{H10} might indicate such interactions between the label side chains and nearby secondary structure elements, providing evidence that these positions might represent contact points to other helices (Kronke et al., 2010). In this case, this would be contacts either between helices within a colicin A protomer or between helices of two colicin A molecules in the putative dimer. Considering also the sequence alignment with the Bcl-2 protein family, that suggests that the BH homology domains BH1, BH3 and maybe also BH2 are important for function and interaction within the dimer, this analysis might further support the structural similarities between the

protein families, as 91R1^{H5} (BH3), 140R1^{H7} (BH1), 150R1^{H8} (BH1), 155R1^{H8} (BH1), 192R1^{H10} (BH2), and 198R1^{H10} (BH2), are located in those domains. Consequently, the cw data might indicate that these positions are at contact points between the two molecules in the dimer.

Based on these conclusions, the assumption of a dimeric conformation for the colicin A closed channel state, and sets of inter- and intramolecular distance constraints from the singly and doubly labeled ColA mutants (see tables 3.5 and 3.6) a structural model was developed. This will be described in the following chapter.

3.3.7.3 Molecular modeling of the closed channel state of ColA

Construction of a dimeric model for the closed channel state of ColA based on the experimental constrains described in the previous chapters was performed by the help of Dr. J.P. Klare. It is assumed that the secondary structure of the protein is largely conserved upon membrane insertion. Consequently, all helical segments present in the X-ray structure of the soluble form of ColA were extracted from the pdb file (1COL.pdb), then duplicated (one of the two copies of each helix will be denoted with a prime in the following, e.g.; H8 and H8') and all together used as building blocks for the dimer model. Modeling, i.e. arrangement of the helical building blocks, was performed with the free software package swiss-pdb-viewer 4.0.1 (http://spdbv.vital-it.ch/). Positioning of the helices was guided by (i) the putative helix-helix interactions predicted from comparison with the Bcl-2 proteins (ii) the immersion-depth parameters and (iii) the distance constrains obtained from the single and double mutants.

Comparison of interspin distances calculated from the model(s) with the experimental distance distributions was performed using the rotamer library analysis (RLA) implemented in the software package MMM 2013.2 (Multiscale Modeling of Macromolecules) from Y. Polyhach and G. Jeschke (ETH Zürich)(http://www.epr.ethz.ch/software/index). For details about the RLA approach see chapter 3.2.7.3 in the experimental section. Starting point for modeling was formation of a dimer of the hydrophobic hairpin H8 and H9 by means of contacts between helices H8 and H8'. Then pairwise the amphipathic helices 1 to 7 were (in reversed order, i.e. adding the pair of helices 1 in the end) individually placed around the dimeric hairpin. During all modeling steps a c2 symmetry of the complex was preserved. After initial placement of each helix pair, the RLA was performed and the data used to refine positioning of the helices to finally obtain minimal deviation between the calculated and experimental data. If necessary, helices positioned before were readjusted to obtain optimal agreement with the experiments.

After all helices have been positioned according to the experimental constraints and considering the similarity of ColA with Bcl-2 proteins, the loops between the helices were modeled. For this purpose the build-in functions 'BuildLoop' and 'OptimizeLoop' provided by the software package 'YASARA Structure' (www.yasara.org) have been used. In brief, the function 'BuildLoop' uses structural data from the protein database (pdb) that matches a given number of existing residues on both sides of the loop (or on one side if N- or C-termini are modeled), and inserts the best fitting structure into the model. If

necessary, the function can mutate amino acid side chains in the loop structures to match the given sequence (Canutescu and Dunbrack, 2003). This function was used to obtain a starting model for each loop/terminal region that was subsequently optimized using the function 'OptimizeLoop'. This function takes a given number of loop conformations from the PDB, considering the given start and end anchor atoms flanking the loop. Then each loop conformation is modelled, and the orientation of the side chains of the loop itself and in its surrounding are optimized (energy minimization). The final energy of the model is calculated according to the selected force field (YASARA2, this force field is, according to the program manual optimized for such tasks) including solvation. The final energies of all (optimized) loop conformations are compared and the lowest energy-model is selected. The Skript used to build and optimize the loop-regions and the N- and C-termini in the ColA-mem dimer model is given in the appendix of Chapter 3.

Figure 3.41 shows the resulting model viewed from along the normal of the membrane plane (a) and with view from the periplasmic side of the *E. coli* inner membrane. In panel c of Figure 3.41 a topological model corresponding to the model shown in A and B is shown in comparison with the topology model derived from the cw EPR data (shown as dotted frames for the helices see Figure 3.40 and 3.41). It can be seen that the experimentally based predictions are largely preserved in the model, except slightly increased immersion depths for helices H3, H5 and H6. H2 was modeled slightly more tilted than predicted before. Nevertheless, all these deviations are largely within the uncertainties arising from interpretation of the data by comparing with model systems like the one used in this study, bacteriorhodopsin. For example, depending on location of the spin label side chain either at the outside of the protein, i.e. pointing into the membrane bilayer or to the proton-conducting channel inside the protein, polarity and accessibility values can largely differ between two corresponding positions with the same immersion depth (Savitsky et al., 2004), (Bordignon and Steinhoff, 2007). For ColA – a pore forming toxin - in the membrane bound state it can be expected that even in the closed channel state observed here, and suggested by the structural model, water-accessible cavities might already extend significantly into the protein, thus increasing polarity and accessibility at the spin label position compared to the values expected from their real immersion depth.

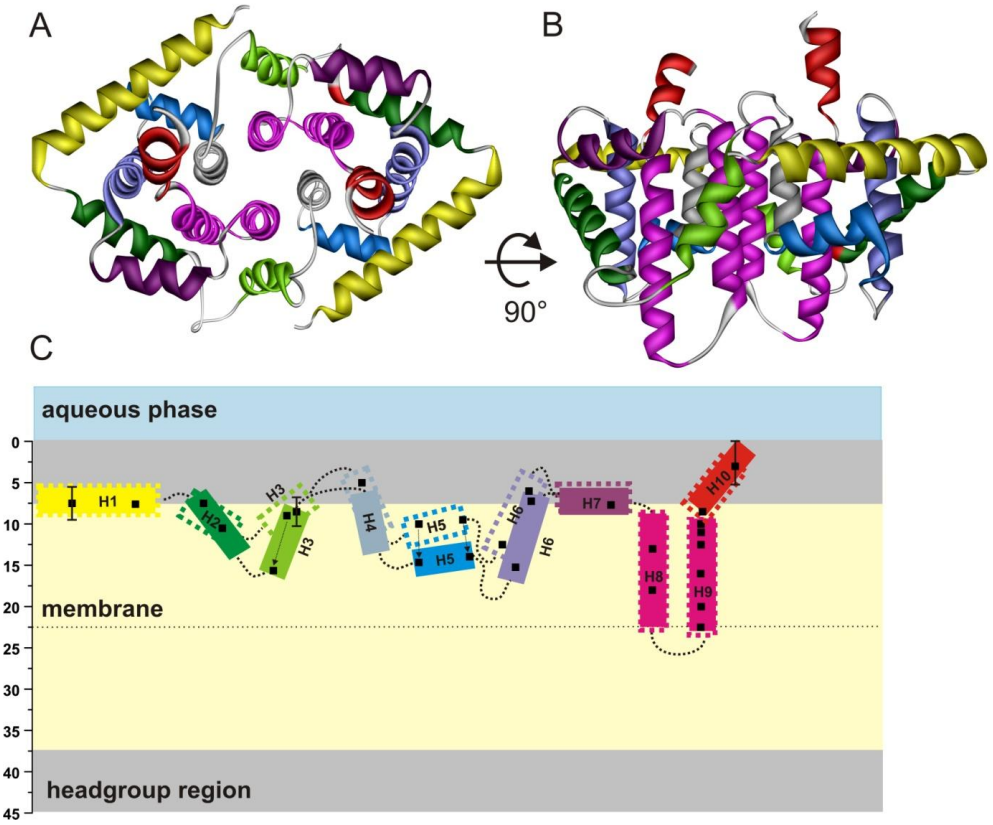

Figure 3.41: Putative model of colicin A. (A) top view (from periplasmic side), (B) side view (periplasm on top), (C) membrane insertion of the helices of the model compared to the topology model (dotted boxes), obtained from accessibility and polarity measurements (cf. Fig. 3.30).

Further evaluation of the model has been carried out by a RLA for the singly and doubly labeled ColA variants. Comparisons of the distance distributions calculated from the model with the RLA approach (blue distributions) with the experimental data (black distributions) are shown in Figure 3.43. It can be seen, that for some of the single label positions good or reasonable agreement between the model and the experimental data is already obtained with the manually build model, e.g. for T15R1^{H1}, A42R1^{H2}, I66R1^{H3}, A91R1^{H5}, E126R1^{H6}, A150R1^{H8}, A169R1^{H9}, G176R1^{H9}, A181R1^{H9}, V182R1^{H9}, and A192R1^{H10}. Some of the deviations observed can be related to the fact that the distance range accessible by the experiment (regions where no reliable distance data can be extracted from the experimental data are indicated by grey boxes in Figure 3.43) might not cover the inter spin distance range present for the respective ColA variant. Examples are I26R1^{H1}, K33R1^{H2}, F105R1^{H5}, and S155R1^{H8} (here the distance predicted from the model is > 5 Å, also not covered by the DEER experiment). For the remaining label positions calculated and experimental distance distributions mainly differ concerning their distribution width (e.g. for S62R1^{H3}), or show deviating mean distances (e.g. for V183R1^{H9}). The former cases can be easily explained by the fact that the RLA does not account for protein dynamics, as the protein structure is kept rigid. For the latter cases, where clear differences are observed concerning the mean distances, it has to be considered that in the *manually build model* yet no optimization of the side chain orientations has been carried out.

Furthermore, positioning of the α-helices to assemble the present model was performed without detailed inspection of the resulting helix-helix interactions, thus "fine-tuning" of the helix positions – especially with respect to a membrane bilayer - has also not been carried out. For the ColA double mutants (Figure 3.43 B) similar observations are made. Good agreement is here observed e.g. for A42R1/I187R1, V115R1/I187R1, A91R1/V115R1 and W140R1/A150R1. The other distance distributions exhibit deviations from the experimental ones similar to those described above for the single site mutants. Consequently, the initial model was refined by means of an *energy minimization* step in a lipid bilayer. This task has been performed using YASARA Structure (energy minimization represents one of the initial steps performed in the macro for (membrane) MD simulation described in the following section, step 4). The resulting model embedded in a lipid bilayer composed of phosphatidylethanolamine (PEA, 74 %) and phosphatidylglycerol (PGL, 26 %) is shown in Figure 3.42.

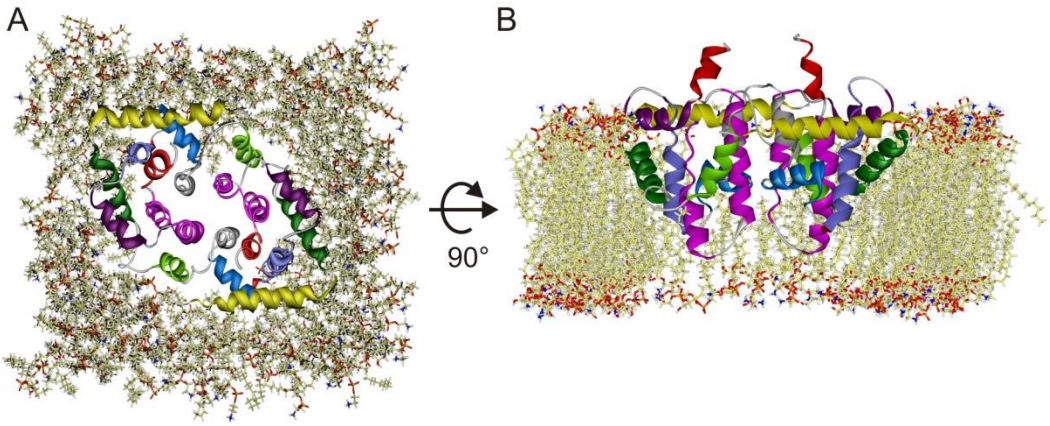

Figure 3.42: Membrane inserted ColA dimer model for MD simulation after energy minimization. (A) top view (from periplasmic side), (B) side view (periplasm on top). In the side view, several lipid molecules have been removed for a better view on the protein structure.

The resulting distance distributions from a RLA performed on the energy minimized model are shown in Figure 3.43 A in red. A significant improvement concerning agreement between the calculated and experimental distance distributions is found for several positions, e.g. F105R1, E126R1, S155R1, G176R1, and I187R1, whereas for the remaining single site mutants no improvement is obtained. Inspection of the comparison for the double mutants (Figure 3.43 B) reveals further improvement of the agreement of the energy minimized model with the experimental data for W140R1/A150R1, A42/I187R1, I26/A77R1, and V115R1/I187R1. Remarkably, summarizing the results after energy minimization of the initial model, mostly improvements and no clearly recognizable worsening of the agreement between experimental and calculated distance distributions is observed. This can be taken as an indication for a general validity of the dimer model constructed for membrane bound ColA in the closed channel state. Nevertheless, the overall agreement with the DEER distance constraints, especially concerning the distance distribution widths,

remains unsatisfactory for a significant number of single and double site mutants. As already mentioned before, this most likely results from the fact that protein dynamics have not been taken into account yet.

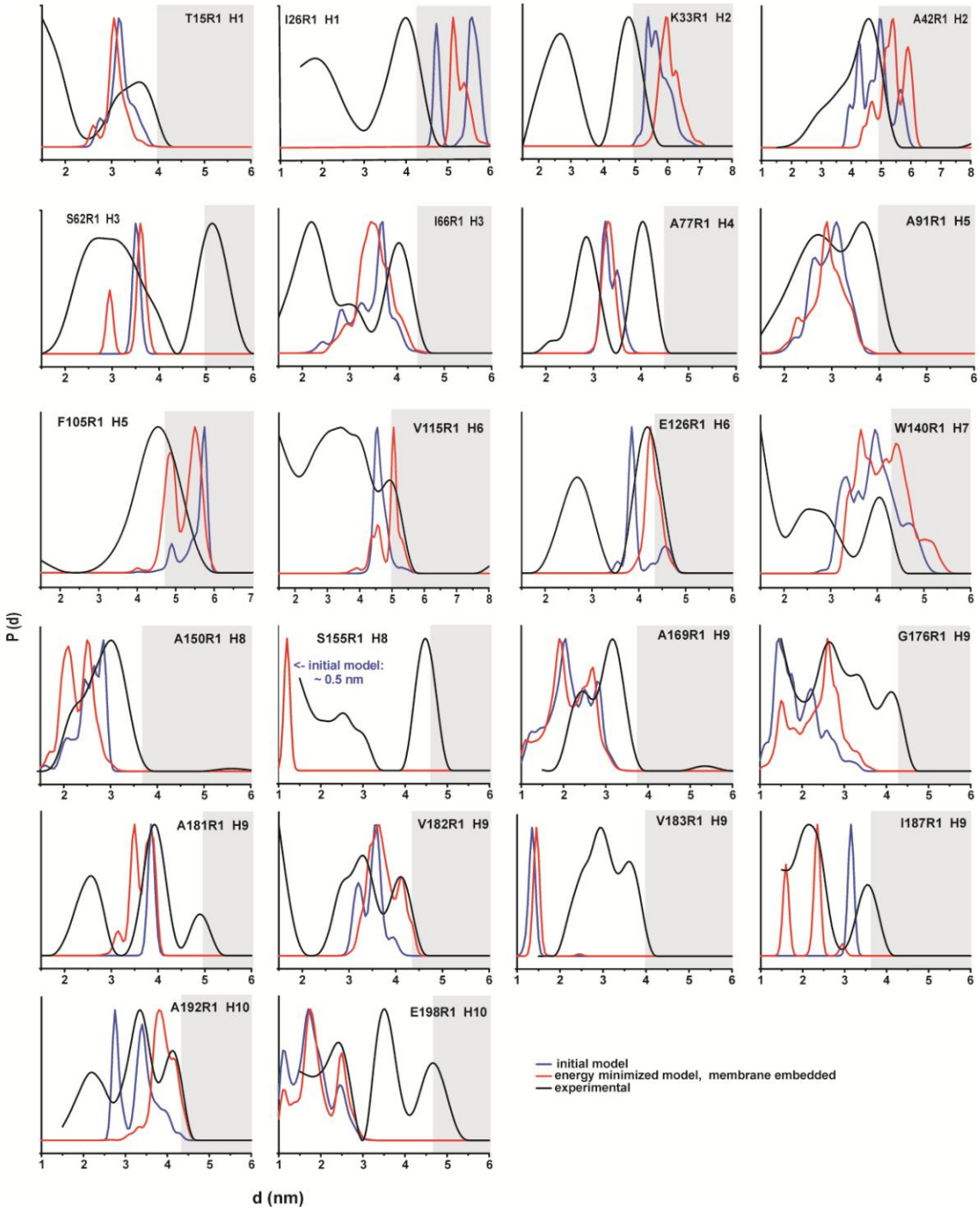

Figure 3.43 (A): Comparison of experimental distance distributions (black) obtained by DEER spectroscopy from singly labeled ColA with calculated distances from the initial model (blue) and the model after energy minimization in a lipid bilayer (red). All distance distributions have been normalized to to their maximum amplitudes. Grey boxes indicate regions in the distance distributions where no reliable distance data can be extracted from the experimental data.

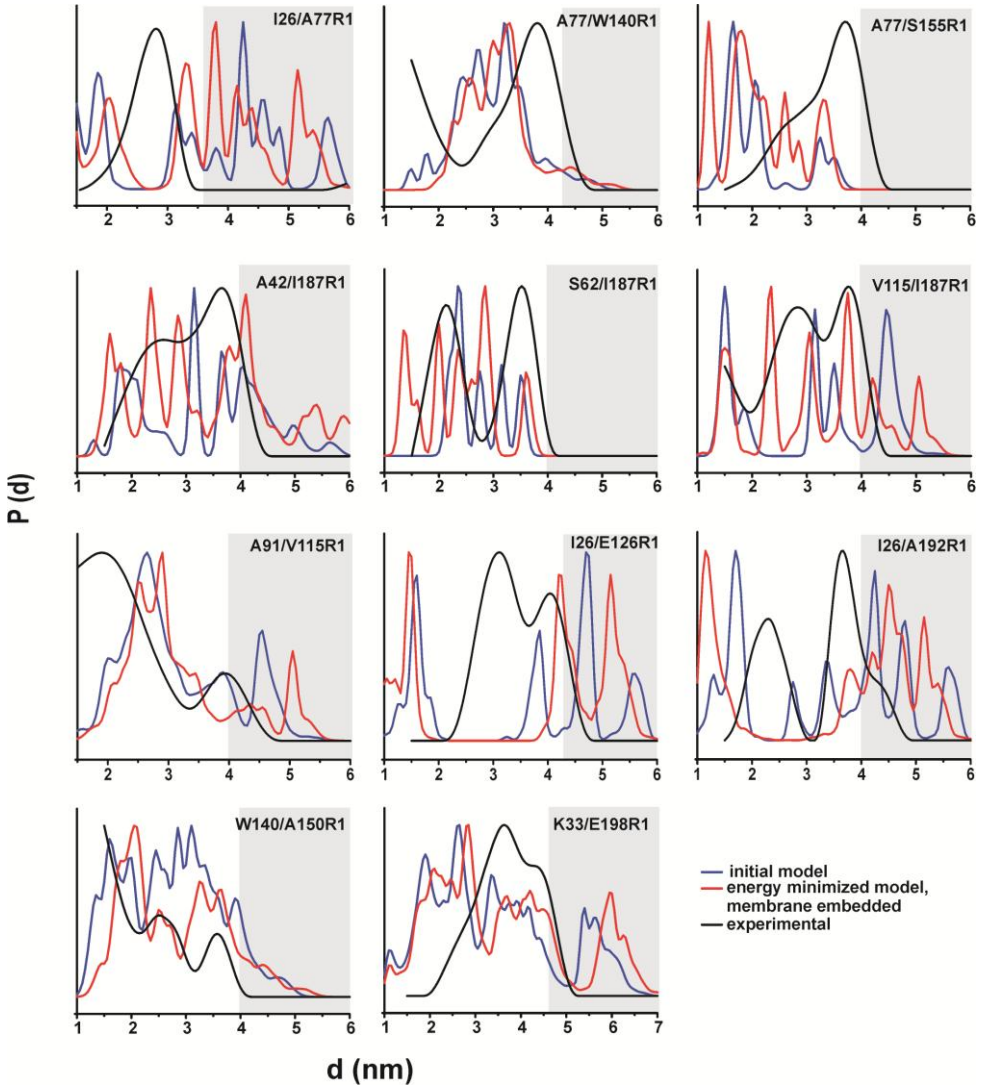

Figure 3.43 (B): Comparison of experimental distance distributions (black) obtained by DEER spectroscopy from doubly labeled ColA with calculated distances from the initial model (blue) and the model after energy minimization in a lipid bilayer (red). All distance distributions have been normalized to to their maximum amplitudes. Grey boxes indicate regions in the distance distributions where no reliable distance data can be extracted from the experimental data.

3.3.7.4 MD simulation of the ColA-mem dimer model in a lipid bilayer

A protein, independent of being a soluble or a membrane protein is a very dynamic entity (Frauenfelder et al., 1988) (Frauenfelder and Macmahon, 2004). The side chain orientations as well as the protein's backbone are continuously fluctuating between conformational substates separated by energy barriers < kT that can be easily overcome. Consequently, a protein's structure is insufficiently described by a static model like that presented above for the closed channel state of ColA. Thus, the RLAs performed to compare the model with the experimental distance constraints also do not reflect the distance distributions that have to be expected from the protein in the lipid bilayer appropriately. Thus, at least

some of the deviations observed between the RLA performed on the energy minimized model and the experimental data might be accountable to this fact. To overcome this problem, the dynamic behavior of a protein can be calculated by means of molecular dynamics (MD) simulations. In MD simulations the physical movements of atoms and molecules are calculated. In brief, the forces acting on all single atoms (described by the so called force field) are calculated based on the present structure and are – according to Newton's equations of motion - translated into atom velocities and directions of motions. New atom positions are calculated for the next time step of the simulation and again for the new structure the forces are calculated. The result of a MD simulation is a *trajectory* that describes the fluctuations of the system under investigation by means of snapshots, i.e. static structures of the protein at different time points of the simulation. The ensemble of such structures then should be able to describe the conformational space the protein samples at a given temperature. Consequently, for a better comparison between the model and the experimental distance distributions a MD simulation for the ColA-mem dimer model embedded in a lipid bilayer was performed by Dr. J.P. Klare (Physics Department, University of Osnabrück). For this purpose again the software package YASARA Structure was used, specifically by means of a script, '*md_runmembrane.mcr*', for the simulation of membrane proteins provided with the software package. This script has been modified before to include phosphatidylglycerol lipids to be able to reflect the composition of the *E. coli* inner membrane more appropriately. In brief, the script performs the following steps:

1. The program analyses the given protein structure to identify putative transmembrane segments and suggests, how it might be embedded in the membrane. The embedding can then be manually adjusted by moving the protein or membrane.

2. A membrane of the required size and composition is build and the protein is inserted into this membrane model in the way defined in step 1.

3. Water (explicit, PIP3P) and ions are placed around the membrane embedded protein to fill the simulation cell (usually, *periodic boundary conditions* are used to minimize the number of atoms in the simulation while no boundary effects have to be considered. In periodic boundary conditions each side of the unit cell loops back to the opposite side, i.e. when an atom passes through one face of the unit cell, it reappears on the opposite face with the same velocity, thereby mimicking a bulk phase).

4. A steepest descent energy minimization is performed to remove bumps and correct the covalent geometry.

5. A 250 ps equilibration simulation is performed, during which the membrane is artificially stabilized while it adapts to the protein.

6. A MD simulation at the given temperature is performed on the equilibrated system.

The results of a MD simulation over 30 ns in explicit water (PIP3P) and in a lipid bilayer as described in the previous section (74 % PEA, 26 % PGL) at 298 K (25°C) are summarized in Figure 3.44 by means of

the system's overall energy (Panel A), overall RMSD (panel B), and the time average structure calculated from the full trajectory (panel C). Please note that the apparent absence of α-helical structure in some regions of the average structure rather indicates high conformational flexibility than loss of secondary structure content, what can also be seen from the coloring according to the B-factors calculated from the root mean square fluctuations during the simulation (Figure 3.44 C, middle panel).

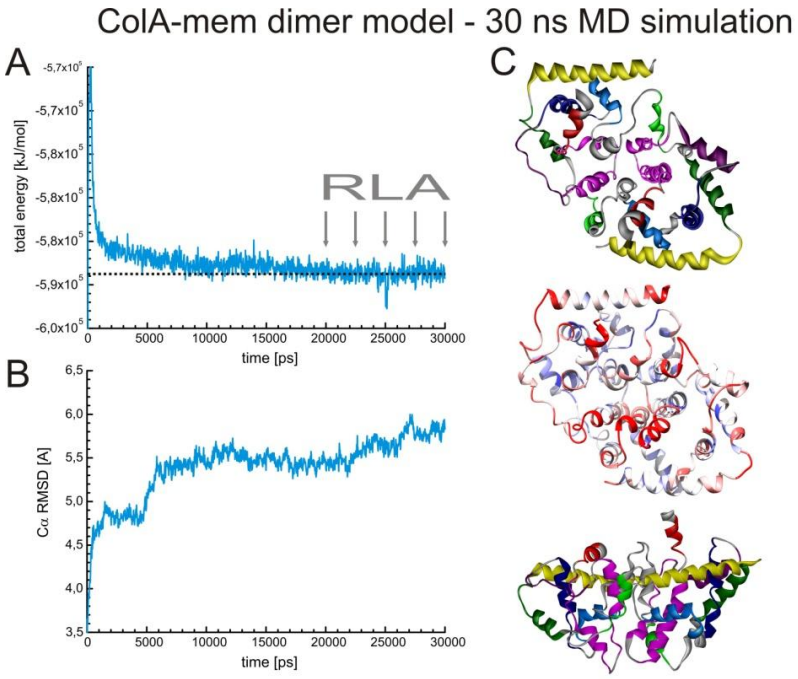

Figure 3.44: Results of the 30 ns MD simulation of the energy minimized ColA dimer model in a lipid bilayer (74 % PEA, 26 % PGL) at 298 K (A) Overall energy (kJ/mol) vs. time, (B) RMSD (Å) from energy minimized model vs. time, (C) time average structure calculated from the 30 ns MD trajectory. Helices in the upper and bottom panel (top and side view, respectively) are coloured according to the previously used color code. In the middle panel the structure is colored according to the B-factors calculated from the simulation (red: high B-factor; blue: low B-factor).

To compute distance distributions from the given MD trajectory, a simplified approach has been used, in which the RLA was performed on snapshots of the MD taken at 20.0, 22.5, 25.0, 27.5 and 30.0 ns (it was assumed, that 20 ns simulation time were sufficient for the protein to adapt to the presence of the lipid bilayer, as judged from the constant overall energy level; cf. Figure 3.44 A, dotted line, the respective time points are marked by arrows). In Figure 3.45 the sum of these distance distributions is compared to the experimental data. It can be seen that for most single (Figure 3.45 A) and double mutants (Figure 3.45 B) good agreement is achieved. Remarkably good agreement is found for a large number of ColA single mutants, i.e. T15R1^{H1}, S62R1^{H3}, A77R1^{H4}, A91R1^{H5}, F105R1^{H5}, A150R1^{H8}, S155R1^{H8}, G176R1^{H9}, A181R1^{H9}, I187R1^{H9}, and A192R1^{H10}, as well as for almost all doubly labeled ColA variants (exceptions are A77R1/S155R1, A42R1/I187R1, I26R1/E126R1 and K33R1/E198R1). For positions that still show

significant deviations between model and experiment, this can be either explained by the limited DEER distance range (e.g. for I26R1, W140R1 and I26R1/E126R1) or the simplified approach that still can not fully account for the dynamic fluctuations the protein undergoes in the membrane (e.g. for V115R1, V183R1 and A42R1/I187R1). A more sophisticated analysis of the MD trajectory - and also additional, longer MD simulations - should be carried out in the future for a full validation and putative refinement of the present ColA-mem dimer model. Nevertheless, the overall good agreement with the experimental data from cw and DEER EPR suggests that the present dimer model largely coincides with the structure of ColA in its membrane bound closed channel state.

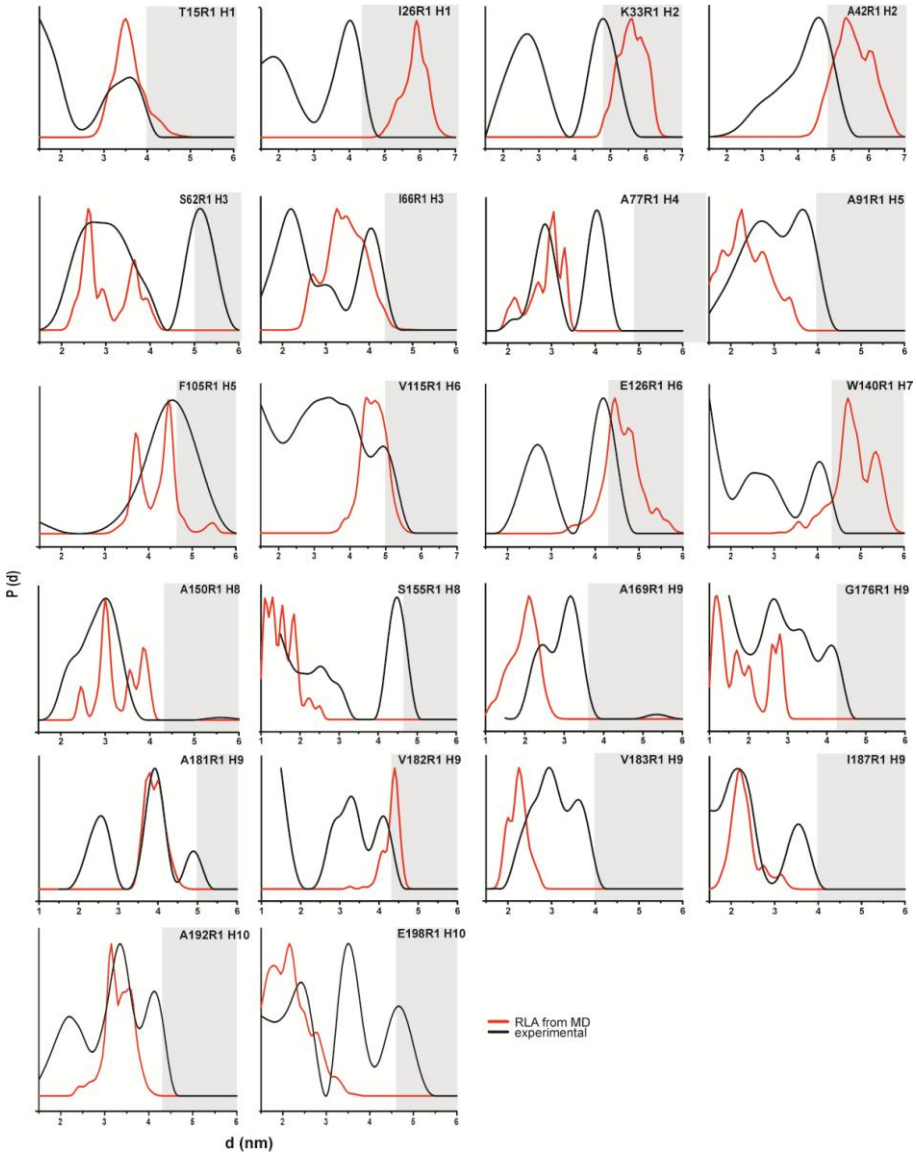

Figure 3.45 (A): Comparison of experimental distance distributions (black) obtained by DEER spectroscopy from singly labeled ColA with calculated distances from the MD simulation of the model after energy minimization in a lipid bilayer (red) Structural data from the 30 ns MD trajectory where extracted at 20.0, 22.5, 25.0, 27.5 and 30.0 ns and subjected to the RLA. The depicted distance distributions (red) represent the sum of the 5 calculated distributions that has been normalized to the maximum of the respective experimental distance distribution. Grey boxes indicate regions in the distance distributions where no reliable distance data can be extracted from the experimental data.

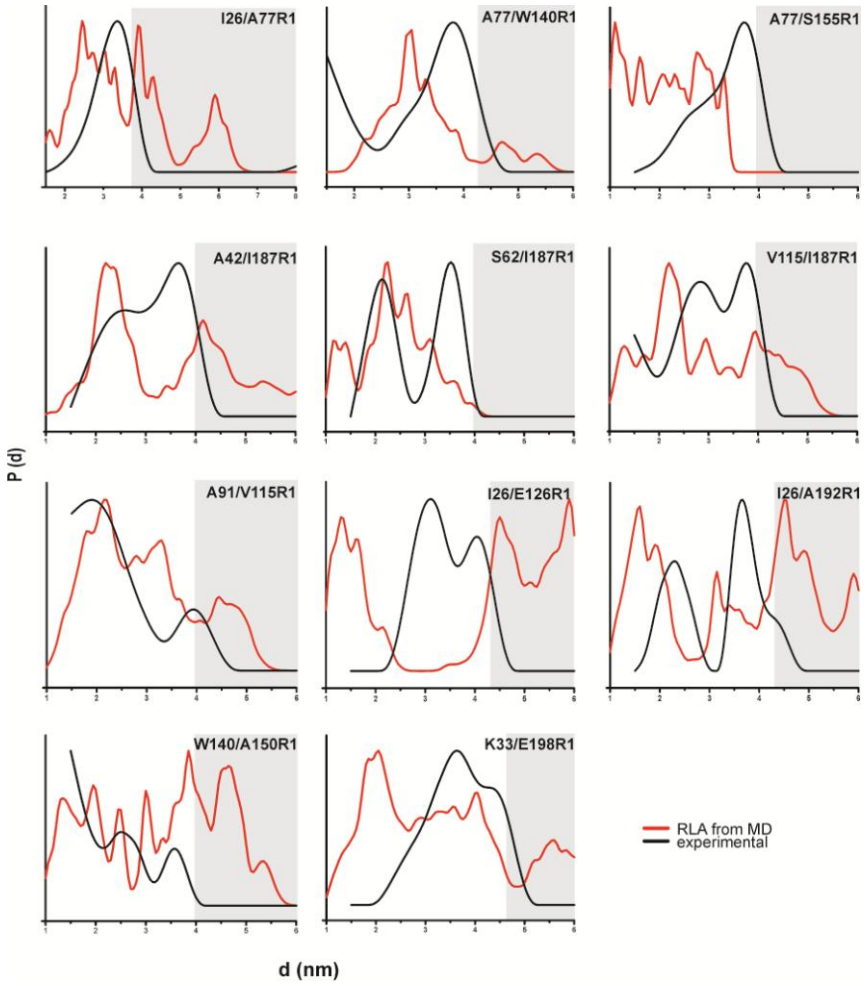

Figure 3.45 (B): Comparison of experimental distance distributions (black) obtained by DEER spectroscopy from doubly labeled ColA with calculated distances from the MD simulation of the model after energy minimization in a lipid bilayer (red) Structural data from the 30 ns MD trajectory where extracted at 20.0, 22.5, 25.0, 27.5 and 30.0 ns and subjected to the RLA. The depicted distance distributions (red) represent the sum of the 5 calculated distributions that has been normalized to the maximum of the respective experimental distance distribution. Grey boxes indicate regions in the distance distributions where no reliable distance data can be extracted from the experimental data.

3.3.7.5 Further evaluation and discussion of the dimer model of ColA-mem

In the previous chapter its has been shown that the dimer model constructed for the membrane bound closed channel state of ColA is in good agreement with the topological (mobility, polarity and accessibility) data as well as with the distance constraints obtained from the cw and pulsed EPR experiments, respectively. Besides comparison with the EPR data obtained in this work, further evaluation of the validity of the model can be done based on biochemical and structural data from the literature as well as by relating properties of the present model with characteristics that have been found or proposed for the membrane bound state of ColA. Based on structural investigations using CD spectroscopy, Pattus et al. (1985) already proposed formation of a dimer by helices H4, H5 and H6, of ColA. Figure 3.46 shows a view on the ColA-mem dimer model (energy minimized model), illustrating which helices form contacts to the other protomer. It can be seen that in agreement with this suggestion H4 (by interaction with H8'), H5 (by interaction with H1') and H6 (by interaction with H1' and H2') contribute to the dimer interface in the present model. As detailed above (chapter 3.3.7.1), from the high similarities to Bcl-2 family proteins in the BH1 and BH3 domains, it can also be proposed that dimerisation of colicin A takes place *via* helices H5 (BH3 domain) and H8 (BH1 domain). Also this proposal is satisfied by the dimer model.

Based on the results in the study by Baty et al. (1987), measuring the colicin A activity *in vivo* on sensitive cells and *in vitro* in planar lipid bilayers showed that deletion mutations in helices 4-6 abolished the ColA channel formation (Baty et al., 1987). Furthermore Nardi et al. (2001) implied that H5 and H6 play a role in forming the ColA channel (Nardi et al., 2001), (Slatin et al., 2004). They found that the colicin channel is built by only approximately half of the channel forming domain (Nardi et al., 2001) which implies the evidence of a colicin channel formed by multimers. Figure 3.46 also reveals that the ColA dimer can be classified as a so-called *domain-swapped dimer*, in which the two monomers undergo large conformational changes upon dimerisation by which helices/domains are "exchanged" between two protomers. Indeed, taking the long loop region between H3 and H4 into account, helices H1 – H3 of each protomer could also occupy the positions their counterparts have, thus forming two compact monomers with a "flat" interaction surface. Nevertheless, such topology would not be in line with the experimentally observed inter-spin distances for these helices. Furthermore, from an energetic point of view, the interaction surface in the domain-swapped dimer is significantly larger and thus the stability of this structure higher compared to a "classic" dimer.

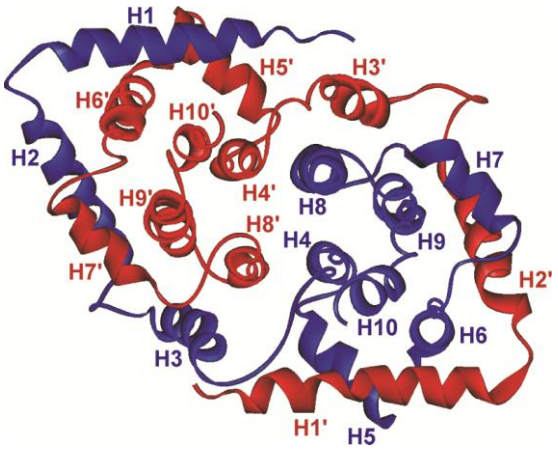

Figure 3.46: Membrane inserted ColA dimer model after energy minimization. Top view from the periplasmic side. The two protomers in the dimer are shown as red and blue ribbons, respectively. Helices are labeled and the helices in the "red protomer" are marked by a prime (').

The Voltage Sensor

According to several studies the putative voltage sensor of ColA comprises helices H4 and H5 (see Cascales et al. (2007) and references therein). Inspection of this region in the ColA-mem dimer model reveals a direct rationale how voltage-sensing and channel-opening upon a positive membrane potential could take place. As depicted in Figure 3.47 A, showing the respective region, numerous positive charges from Lys and Arg side chains (K87, K97, K103, K106, K113, K116, R118, K120) render this segment including helix H6 putatively sensitive towards such membrane potential. It can be easily envisioned, how helices H5 and H6 could be pulled towards the cytoplasmic side of the membrane (as indicated by the arrow in Figure 3.47 A), thereby forming two additional transmembrane helices per ColA molecule: (i) helix H5 prolongs H4 to form a transmembrane segment, and (ii) H6 might pull parts of H7 into the membrane to span the bilayer. Thus, the ColA dimer would comprise 8 transmembrane helices after channel opening, sufficient to form a pore with a diameter that could be in line with the observed properties. Interestingly, and as mentioned in chapter 3.3.7.1, the study by Pattus et al. (1985) also proposed the ColA channel to be formed by helices H5 and H6 ("of the trimer").

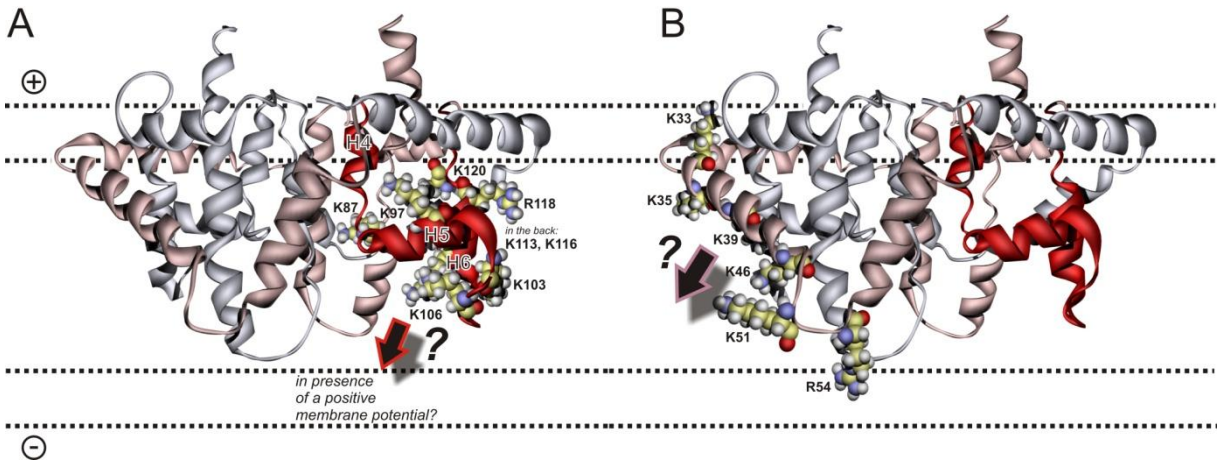

Figure 3.47: Putative voltage sensor(s) in the ColA-mem dimer model. Positively charged side chains (Lys, Arg) in helices (A) H4-H6 and (B) H2 and H3 are depicted in spacefill representation.

Besides helices H4, H5 and H6, a number of studies further identified H2 and H3 also to be translocated across the inner membrane upon voltage-gated channel-opening of ColA (see Cascales et al. (2007) and references therein). Furthermore Nardi et al. (2001) proposed that the voltage dependence of colicin A is obviously regulated by the first 4 α-helices, whereas Duché et al. (1999) suggest that the voltage responsive segment in ColA extends from helix 1 to helix 8. Strikingly, also helix H2 comprises numerous Lys (K33, K35, K39, K46, K51) and one Arg (R54) residues, rendering this helix also voltage-sensitive. In the presented model, H2 exhibits a tilted orientation (~ 60° with respect to the membrane normal), and it could be envisioned that a positive transmembrane potential could orient H2 parallel to the membrane normal, thus forming together with H3 an additional transmembrane segment comprising two helices.

Consequently, if both voltage sensors/translocatable regions predicted from the present model and being in line with numerous published reports would comprise two additional TM helices each, the dimeric open-channel state of ColA could exhibit an overall number of up to 12 transmembrane helices. Therefore, the current model can directly explain the experimentally observed voltage-dependency and pore-diameter for membrane-bound ColA.

Comparison with Cryo-EM data for oligomeric colicin Ia

As already described in the introduction of this chapter, besides numerous indications for and speculations about an oligomeric state of ColA in the membrane, Greig et al. (2009) succeeded to visualize oligomers of Col Ia in the membrane by cryo-electron microscopy. Although the sequence identity between ColA and Col Ia is not very high, the degree of amino acid sequence identity in the c-terminal domain is 24 % (Parker et al., 1992 and references therein), it is assumed that their secondary structure composition is highly conserved, and it can be expected that these two colicins share common structural

features also in their membrane bound state. Greig et al. (2009) speculated that, due to the observed C3 symmetry, either trimers or hexamers (as trimers of dimers) are the oligomeric units observed. Interestingly, the dimer model proposed in the present work from first sight provides a rationale to combine three of such dimers to form a hexameric assembly with a ring-like structure like that observed by cryo-EM. In Figure 3.48 an overlay of such ColA trimer of dimers is – scaled according to the scale bars given in the Figure – shown overlayed onto a 2-dimensional electron density map from Greig et al. (2009). Strikingly, the ColA trimer of dimer units seems to fit the observed electron density maps perfectly. The missing C2 symmetry in the dimers could easily be explained if the dimers appear slightly tilted with respect to the membrane plane in the trimer. Such packing effects might appear in the two-dimensional crystals formed by Col Ia, that are comparable to for example the purple membrane sheets in *H. salinarum*, a hexagonal lattice formed by trimers of bacteriorhodopsin, with a lipid content of only ~ 30 %.

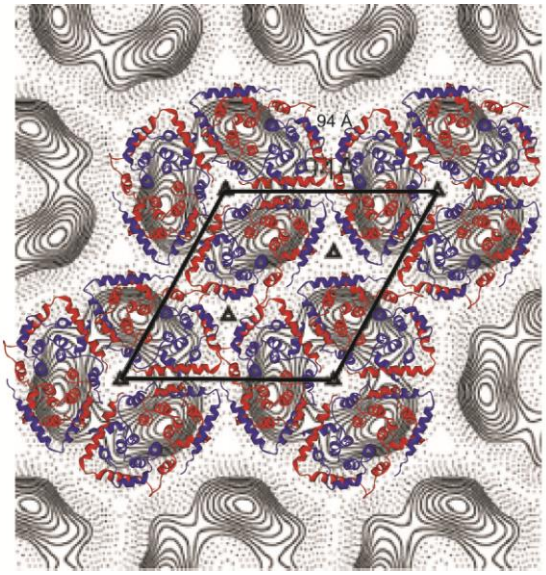

Figure 3.48: Trimer of dimer model for ColA projected onto an electron density map obtained for oligomeric Col Ia in a lipid bilayer (Greig et al., 2009). Both, model and electron density map have the same length scale (the sides of the rectangle in the center of the Figure correspond to 94 Å.

Although the physiological relevance of such hexamers and 2D crystals formed thereof is highly questionable (if ColA binding to host cells via BtuB, being present in ~ 200 copies per cell, is mandatory for import of the pore forming domain), formation of higher aggregates might be an intrinsic property of pore-forming colicins as well as also Bcl-2 family proteins and other related toxins, and the obvious compatibility of the ColA-mem dimer model presented here provides more evidence that the present dimer model is in good agreement with the structure of ColA-mem in the closed state.

3.4 Summary and Outlook

Colicin A (ColA) is a plasmid-encoded water-soluble pore-forming toxin produced by *E. coli* (Cascales et al., 2007). The protein kills unprotected cells of related strains by inserting specific helical segments of the pore-forming subdomain into the cytoplasmic membrane to form voltage-dependent ion channels. The crystal structure of the soluble form of the pore-forming domain has been solved, but detailed structural data for the membrane-bound channel, in the closed as well as in the open state, is still missing. Currently two models are discussed for the closed channel state, the "Umbrella-Model" and the "Pen-knife-Model". Furthermore, based on results of earlier studies, the channel was assumed to be formed by a single pore-forming domain, although the channel properties, i.e. an inner pore diameter of at least 1 nm, are difficult to explain in this way. Strong evidence for an oligomeric structure of the channel was already provided by an electron microscopy study on the closely related colicin Ia (Greig et al., 2009).

Previous EPR results already provided first evidence for the closed channel state being in agreement with the previously suggested "Umbrella-Model" (Pulagam et al., 2008) (Boehme et al., 2009). In the present study, various cw -and pulse EPR methods in combination with site-directed spin labeling under *in vitro* conditions have been performed. Furthermore, inter spin distances measurement under *in vivo* conditions have been carried out to confirm the physiological relevance of the results obtained by the *in vitro* experiments. The data and conclusions drawn thereof presented in this chapter provide further insights into the topology of the colicin A closed channel state.

First, the protocol for the colicin A expression and purification was optimized to increase the amount of purified colicin A for the EPR investigations. Preparation of colicin A from the membrane fraction leads to an increase of a factor of about 200 of the colicin A yield compared to previously published protocols, where ColA has only been isolated from the extracellular medium. Comparison of the proteins prepared by the new protocol established in this work revealed no differences in the ESR spectra for the labeled solubilized samples between the different preparation methods. Accordingly, all EPR investigations, including mobility, polarity, accessibility and inter spin distance measurements have been carried out on protein samples prepared by the newly developed protocol. Cysteine mutants of colicin A, each containing one or two cysteine residues, were labeled with a nitroxide (MTS) spin label and reconstituted into liposomes by a detergent-mediated reconstitution.

The results under *in vitro* conditions indicate that a larger fraction of the protein than previously suggested penetrates into the hydrophobic core of the membrane. Based on the results presented in this chapter the hydrophobic hairpin H8 and H9 is located deeply in the membrane, which is in agreement with previous accessibility data and also with other reports utilizing NMR and Trp fluorescence measurements. In addition, the data obtained in this work indicates that helices H1, H7 and H10 lie on the membrane surface, whereas parts of H2 (42R1) and H3 (62R1) are located in the hydrophobic part of the lipid bilayer. Moreover, residues located in helices H5 and H6 are also located deeply in the bilayer core,

supporting the idea that colicin A contributes more than two (H2/H3, H5/H6 and H8/H9) membrane segments in the membrane integrated state. These results are in good agreement with previous studies on Col Ia (Slatin et al., 1994) in which the possibility of a hydrophobic and an amphipathic hairpin for ColA and four transmembrane segments for Col Ia have been postulated.

All room temperature spectra of colicin A reveal the presence of at least two spectral components characterized by different mobilities. This could be either arising from different rotamer conformations or from different protein conformations. However, the probability that the two major spectral components of all 22 positions on rec-mem-ColA investigated here are caused by different rotamer conformations seems very unlikely. Temperature dependent cw EPR measurements and the influence of paramagnetic quenchers on the spectral features rather suggest the presence of a conformational equilibrium between two protein conformations. The presence of two conformations in a lipid- and reconstitution-dependent equilibrium for ColA in the closed channel-state appears to be in line with a mechanism of colicin E1 insertion proposed by Kienker et al. (1997, 2000), that was supported by MD-simulations (Prieto et al., 2011), in which one component might represent a precursor state for the umbrella model. According to this insertion mechanism, colicin A first is oriented with the hydrophobic hairpin parallel to the membrane plane (a so-called "adsorbed state"), than undergoes conformational changes to a penknife model-like structure as a precursor state for membrane insertion. Afterwards the orientation of the hydrophobic hairpin changes to the umbrella conformation. In order to characterize this putative conformational equilibrium in more detail, further investigations, for example by saturation recovery experiments, are needed.

So far the information available about colicin A suggests that one colicin molecule can already form a functional channel. Nevertheless, a significant number of indications exist for colicin channels being oligomeric, for example its putative channel diameter, but also direct evidences like the oligomeric structure observed for Col Ia by Cryo-EM (Greig et al., 2009). The distance measurements carried out in this work by pulse EPR spectroscopy on lipid-reconstituted colicin A provide the evidence that ColA in lipid bilayer membranes forms an oligomeric structure under *in vitro* conditions. This behavior is also known for other pore-forming toxins, like for example Aerolysin (Fivaz et al., 2001) and Bax (Minn et al., 1997) (Antonsson et al., 2000). Although based on the present data it appears to be difficult to define the degree of oligomerisation, especially to distinguish between ColA dimers or higher oligomers, several lines of evidence (spin numbers, inter spin distances, remarkable similarities to the Bcl-2 family proteins), support the assumption of a ColA-mem dimer.

Of course, the conformation of a protein and the dynamics strongly depend on the environmental conditions and an oligomeric state observed *in vitro* is not necessarily of physiological relevance *in vivo*. Accordingly, pulse EPR distance measurements have also been performed under *in vivo* conditions. Incubation of spin labeled colicin A with living *E. coli* cells and subsequent DEER distance measurements reveal clear indications for an oligomeric ColA structure also *in vivo*, proving that colicin A is organized as an oligomer in the membrane integrated state also under physiological conditions. Being confident, that a

colicin oligomer represents a physiological relevant state, the results of all EPR measurements, i.e. distance constraints form singly and doubly labeled ColA, mobility, accessibility and polarity data, were combined to construct a dimer model for the colicin A closed channel state conformation.

The ColA-mem dimer model constructed in this work is characterized by a membrane embedded core mainly build from the hydrophobic hairpin (H8/H9) and helices H4 and H6 that at least partially protrude into the hydrophobic core of the bilayer. The remaining helices form, as previously suggested (Boehme et al., 2009), a ring-like structure in the membrane headgroup region, wherein helices H1-H3 "embrace" the core of the other protomer in the dimer, thus forming a stable assembly similar to topologies that have been predicted for Bcl-2 family proteins like Bax and Bak.

Evaluation of the model by comparison with data and proposals from the literature largely confirms the ColA-mem dimer model presented here. Moreover, inspection of the model reveals for example a direct explanation for the observed voltage dependency of channel opening. For example, the formation of two (additional) transmembrane segments by TM-potential-mediated motion of helices H5 and H6 and possibly also H2 and H3 as described above can be directly predicted from the ColA-mem dimer model, thus providing the rationale for the observed channel diameter of > 1 nm.

The conformation of the open channel of colicin A and other colicins is still obscure. Although the model proposed in this work provides first insights also into how the open channel state might look like, to address the question of the topology of the colicin A open channel state, further investigations are needed. Channel opening of colicin A takes place in the presence of a *trans*-negative membrane potential, that could be mimicked for example using the K^+ ionophore valinomycin. Valinomycin creates a diffusion potential across the membrane, that could result in an opening of the channel. Development of a protocol based on the observed channel activity (Honigmann et al., 2012) to stabilize the open conformation could then provide the basis for EPR investigations on the open channel state.

3.5 Bibliography

Abrams et al., 1991 — Abrams C.K., Jakes K.S., Finkelstein A., Slatin S.L. (1991) Identification of a translocated gating charge in a voltage-dependent channel. Colicin E1 channels in planar phospholipid bilayer membranes. *J. Gen. Physiol.* **98**:77-93

Adams et al., 1998 — Adams, J. M., and Cory, S. (1998) The Bcl-2 protein family: Arbiters of cell survival. *Science* **281:**1322-1326

Annis et al., 2005 — Annis, M.G., Soucie, E.L., Dlugosz, PJ., Cruz-Aguado, J.A., Penn, L.Z., Leber, B. and Andrews D.W. (2005) Bax forms multispanning monomers to permeabilize membranes during apoptosis. *EMBO J.* **24**:2096-2103

Antonsson et al., 2002 — Antonsson B., Montessuit S., Lauper S., Eskes R., Martinou J.C., (2000) Bax oligomerisation is required for channel-forming activity in liposomes and to trigger cytochrome c release from mitochondria. *Biochem. J.* **15**:271-278

Bainbridge et al., 1998 — Bainbridge, G., Armstrong, G.A., Dover, L.G., Whelan, K.F., Lakey, J.H. (1998) Displacement of OmpF loop 3 is notrequired for the membrane translocation of colicins N andA *in vivo*. *FEBS Lett.* **432:**117–122

Barth et al., 2007 — Barth P, Schonbrun J, Baker D. (2007) Toward high-resolution prediction and design of transmembrane helical protein structures. *Proc Natl. Acad. Sci USA* **104**:15682–15687

Baty et al., 1987 — Baty, D., Knibiehler, M., Verheij, H., Pattus, F., Shire, D., Bernadac, A., Lazdunski, C. (1987) Site-directed mutagenesis of the COOH-terminal region of colicin A: effect on secretion and voltage-dependent channel activity. *Biochem. Proc. Natl. Acad. Sci.* **84**:1152-1156

Bleicken et al., 2009 — Bleicken, S., Classen, M., Padmavathi, P.V.L., Ishikawa, T., Zeth, K., Steinoff, H.-J., Bordignon, E. (2009) Molecular details of Bax activation, oligomerisation, and membrane insertion. *J.Biol.Chem.* **285**:6636-6647

Boehme et al., 2009 — Boehme S, Pulagam L. P., Holterhues J, Ouchni F, Klare JP, Steinhoff H.-J. (2009) Topology of the amphipathic helices of the colicin A pore-forming domain in E. coli lipid membranes studied by pulse EPR. *Chem Phys.* **31**:6770-6777

Bourdineaud et al., 1990, — Bourdineaud J.P., Fierobe H.P., Lazdunski C., Pagès J.M. (1990). Involvement of OmpF during reception and translocation steps of colicin N entry. *Mol. Microbiol.* **4**:1737-1743

Canutescu and Dunbrack, 2003 — Canutescu, A. A., Dunbrack R.L., Jr. (2003) Cyclic coordinate descent: A robotics algorithm for protein loop closure. *Protein Sci.* **12:**:963-72

Cascales et al., 2007 — Cascales, E. K., Buchanan S.K., Duché D., Kleanthous, C. Lloube's,R.Postle, K. Riley, M., Slatin,S. and Cavard, D. (2007) colicin Biology. *Microbiol. Mol. Biol. Rev.* **71**:158-229

Cascales et al., 2000 — Cascales E, Gavioli M, Sturgis J.N, Lloubès R. (2000). Proton motive force drives the interaction ofthe inner membrane TolA and outer membrane Pal proteins in *Escherichia coli*. *Mol. Microbiol.* **38**:904-915

Cavard, 2002 — Cavard, D. (2002) Assembly of colicin A in the outer membrane of producing Escherichia coli cells requires both phospholipase A and one porin, but phospholipase a is sufficient for secretion. *J. Mol. Biol.* **184**:3723-3733

Cavard, 2002 b — Cavard, D. (2002) Colicin A multimerizes when unfolded. *Biochemie* **84**:485-488

Cavard, 1997 — Cavard, D. (1997). Role of the colicin A lysis protein in the expression of the colicin A operon. *Microbiol.* **43**:2295-2303

Cavard et al., 1981 — Cavard, D., Bernadac, A, Lazdunski, C. (1981) Exclusive localisation of colicin A in the cellcytoplasm of producing bacteria. *Eur. J. Biochem.* **119**:2554-2562

Cavard et al., 1992 — Cavard, D. and Oudega, B. (1992) General introduction to the secretion of bacteriocins. Bacteriocins, Microcins and Lantibiotics. R. James, C. Lazdunski and F. Pattus, Springer-Verlag, Berlin**:** 297-305

Cramer et al., 1990 — Cramer, W.A., Cohen, F.S., Merrill, A.R., Song, H.Y. (1990) Structure and dynamics of the colicin E1 channel. *Mol. Microbiol.* **4**:519-26

Cramer et al., 1995 — Cramer, W.A., Heymann, J.B., Schendel, S.L., Deriy, B.N., Cohen,.FS., Elkins, P.A., Stauffacher, C.V. (1995) Structure-function of the channel forming colicins. *Ann. Rev. Biophys. Biomol. Struct.* **24**:611-641

Chou et al., 1999 — Chou, J.J., Li, H., Salvesen, G.S., Yuan, J., and Wagner, G. (1999) Structure Calculation Solution structure of BID, an intracellular amplifier of apoptotic signaling. *Cell* **96**:615–624

Cowan et al., 1992 — Cowan, S. W.; Schirmer, T.; Rummel, G.; Steiert, M.; Ghosh, R.; Pauptit, R..A.; Jansonius, J.N.; Rosenbusch, Jurg P. (1992) Crystal structures explain functional properties of two *E. coli* porins. *Nature* **358**:727-733

Dalton et al., 1987 — Dalton LA, McIntyre JO, Fleischer S., (1987) Distance estimate of the active center of D-beta-hydroxybutyrate dehydrogenase from the membrane surface. *Biochem.* **26**:2117-30

Di Masi et al., 1976 — Di Masi D.R, White J. C., Schnaitman C. A, Bradbeer, C. (1976) Transport of vitamin B12 in *Escherichia coli*: common receptor sites for vitamin B12 and the E colicins on the outer membrane of the cell envelope. *J. Bacteriol.* **115**: 506-513

Dekker et al., 1999 — Dekker N, Tommassen J, Verheij H.M. (1999) Bacteriocin Release Protein triggers dimerisation of outer Membrane Phospholipase A in vivo. *J. Bacteriol.* **181**:3281-3283

Doebber, 2009 — Doebber, M. (2009) EPR Analysis of a Two-State Conformational Equilibrium in an *N. pharaonis* HAMP Domain, PhD Thesis, University of Osnabrück.

Duché et al., 1994 — Duché D, Parker M.W, González-Mañas J.M, Pattus F, Baty D. (1994) Uncoupled steps of the colicin A pore formation demonstrated by disulfide bond engineering. *J. Biol. Chem.* **269**:6332-6339

Duché et al., 1995 — Duché D, Letellier L, Géli V, Bénédetti H, Baty D. (1995) Quantification of group A colicin import sites. *J. Bacteriol.* **177**:4935-4939

Duché et al., 1999 — Duché D, Corda Y, Géli V, Baty D. (1999) Integration of the colicin A pore-forming domain into the cytoplasmic membrane of *Escherichia coli. J. Mol. Biol.* **285**:1965-1975

Elkins et al., 1997 — Elkins, P., Bunker, A., Cramer, W.A., Stauffacher, C.V. (1997)A mechanism for toxin insertion intomembranes is suggested by the crystal structure of the channel-forming domain of colicin E1. *Structure* **5**:443-458

Farahbakhsh et al., 1992 — Farahbakhsh Z.T., Altenbach C., Hubbell W.L. (1992) Spin labeled cysteines as sensors for protein-lipid interaction and conformation in rhodopsin. *Photochem. Photobiol.* **56**:1019-1033

Fivaz et al., 2001 — Fivaz M, Abrami L, Tsitrin Y, van der Goot F.G. (2001)Aerolysin from *Aeromonas hydrophila* and related toxins. *Curr. Top. Microbiol. Immunol.* **257**:35-52

Frauenfelder et al., 1988 — Frauenfelder, H., Parak, F.G., Young, R.D. (1988) Conformational Substates in Proteins. *Ann. Rev. Biophys. Biophys. Chem.* **17**:451-479

Frauenfelder and Macmohan — Frauenfelder, H. and Macmohan, B.H. (2004) Energy landscape and fluctuations in proteins. *Ann.Phys.* **9**:655-667

Frenette et al., 1988 — Frenette, M., Knibiehler, M., Baty, D., Geli, V. Pattus, F., Verger, R. and Lazdunski, C. (1988) Interactions of colicin A domains with phospholipid monolayers and liposomes: relevance to the mechanism of action. *Biochim. Biophy. Acta* **947**:445-464

Fuska et al., 1979 — Fuska, J., Fusková A., Smarda J., Mach J. (1979) Effect of colicin E3 on leukemia cells P388 in vitro. *Experientia* **35**:406-407

Garcia-Saez et al., 2004 — Garcia-Saez A. J, Mingarro I, Perez-Paya E, Salgado J. (2004) Membrane insertion fragments of Bcl-xL, Bax, and Bid. *Biochem.* **43**:10930–10943

González-Mañaset al., 1992 — Gonzalez-Manas, J.M., Lakey, J.H. and Pattus, F. (1992) Brominated phospholipids as a tool for monitoring the membrane insertion of colicin A. *Biochem.* **31**:7294-300

González-Mañaset al., 1993 — Gonzalez-Manas, J.M., Lakey, J.H. and Pattus, F. (1993) Interaction of the colicin A pore-forming domain with negatively charged phospholipids. *Eur.J.Biochem.* **211**:625-633

Gouaux, 1997 — Gouaux, E. (1997) The long and short of colicin Action: the molecular basis for thebiological activity of channel-forming colicins. *Structure* **5**:313-317

Greig et al., 2009 — Greig, S.L., Radjainia, M. and Mitra, A.K. (2009) Oligomeric structure of colicin Ia channel in lipid bilayer membranes. *J. Biol. Chem.* **284**:16126-16134

Gross et al., 1999 — Gross, A., McDonnell, J. M., and Korsmeyer, S. J. (1999) BCL-2 family members and the mitochondria in apoptosis. *Genes De*v. **13**:1899-1911

Gu et al., 1999 — Gu YL, Kar T, Scheiner S., (1999) Fundamental properties of the CH center dot center dot center dot O interaction: Is it a true hydrogen bond? *J. Am. Chem. Soc.* **121**:9411–9422

Hilsenbeck et al., 2004 — Hilsenbeck J.L, Park H, Chen G, Youn B, Postle K, Kang C. (2004) Crystal structure of the cytotoxic bacterial protein colicin B at 2.5 A resolution. *Mol. Microbiol.* **51**:711-720.

Howard et al., 1991 — Howard, S.P., Cavard, D., Lazdunski, C. (1991) Phospholipase-A-independent damagecaused by the colicin A lysis protein during its assembly into the inner and outermembranes of *Escherichia coli*. *Gen. Microbiol.* **137**:81-89

Honigmann et al., 2012 — Honigmann, A., Pulagam, L.P., Sippach, M., Bartsch, P., Steinhoff, H.-J., Wagner, R. (2012) A high resolution electro-optical approach for investigating transition of soluble proteins to integral membrane proteins probed by colicin A. *Biochem. Biophys. Res. Commun*. **427**:385-91

Hubbell et al., 1994 — Hubbell, W.L., Altenbach, C. (1994) Investigation of strucutre and dynamics in membrane proteins using site-directed spin labeling. *Curr. Opin. Struct. Biol.* **4**:566-573

Hubbell et al., 1996 — Hubbell, W. L., McHaourab, H. S., Altenbach, C., and Lietzow, M.A. (1996) Watching proteins move using site-directed spin labeling. *Structure* **4**:779-783

James et al., 1996 — James R., Kleanthous, C., Moore, G.R. (1996) The biology of E colicins: paradigms and paradoxes. *Microbiol.* **142**:1569-1580

Jeanteur et al., 1994 — Jeanteur, D., Pattus, F. and Timmins, P.A. (1994) Membrane-bound form of the pore-forming domain of colicin A. A neutron scattering study. *J. Mol. Biol.* **235**:898-907

Jeschke et al., 2006 — Jeschke, G., Chechik, V., Ionita, P., Godt, A., Zimmermann, H., Banham, J., Timmel, C. R., Hilger, D., and Jung, H. (2006) DeerAnalysis2006 - a comprehensive software package for analyzing pulsed ELDOR data. *Appl. Magn. Reson.* **30**:473-498

Journet et al., 2001 — Journet, L., Bouveret, E., Rigal, A., Lloubès, R., Lazdunski, C., and Bénédetti, H. (2001) Import of colicins across the outer membrane of *Escherichia coli* involves multiple protein interactions in the periplasm. *Mol. Microbiol.* **42:**331–344.

Kienker et al., 1997 — Kienker, P.K, Qiu, X., Slatin, S.L., Finkelstein, A., Jakes, K.S. (1997) Transmembrane insertion of the colicin Ia hydrophobic hairpin. *J. Membr. Biol.* **157**:27-37

Kienker et al., 2000 — Kienker, P.K., Jakes, K.S. and Finkelstein, A. (2000) Protein translocation across planar bilayers by the colicin Ia channel-forming domain: where will it end*? J.Gen. Physiol.* **116**:587-598

Kienker et al., 2002 — Kienker, P. S. L. Slatin, and Finkelstein, A. (2002) Colicin channels have a shockingly high proton permeability. *Biophys. J.* **82**:555a

Kienker et al., 2008 — Kienker, P.K., Jakes, K.S., Finkelstein, A. (2008) Identification of channel-lining amino acid residues in the hydrophobic segment of colicin Ia. *J. Gen. Physiol.* **132**:693-707

Kim et al., 1998 — Kim Y., Valentine K., Opella S.J., Schendel S.L., Cramer W.A. (1998) Solid-state NMR studies of the membrane-bound closed state of the colicin E1 channel domain in lipid bilayers. *Protein Sci.* **7**:342-348

Koppelmann et al., 2001 — Koppelman, C.M., Den Blaauwen, T., Duursma, M.C., Heeren, R.M., Nanninga, N. (2001) *Escherichia coli* minicell membranes are enriched in cardiolipin. *J. Bacteriol.* **183:**6144-6147

Krasilnikov et al., 1998 — Krasilnikov, O.V., Da Cruz, J.B., Yuldasheva, L.N., Varanda, W.A. and Nogueira, R.A. (1998) A novel approach to study the geometry of the water lumen of ion channels. *J. Mol. Biol.* **161**:83-92

Krieger et al., 2002 — Krieger, E., Koraimann, G., and Vriend, G. (2002) Increasing the precision of comparative models with YASARA NOVA—a self-parameterizing force field. *Protein*s **47**:393–402

Kroncke et al., 2010 — Kroncke, B.M., Horanyi P.S. and Columbus L. (2010) Structural origins of nitroxide side chain dynamics on membrane protein α-helical sites. *Biochem.* **49**:10045–10060

Kurisu et al., 2003 — Kurisu, G.; Zakharov, S. D.; Zhalnina, M. V.; Bano, S.; Eroukova,V. Y., Rokitskaya, T. I.; Antonenko,Y. N.; Wiener, M. C.; Cramer,W. A. (2003) The structure of BtuB with bound colicin E3 R-domain implies a translocon. *Nat. Struct. Biol.* **10**:948-954

Kuwana et al., 2002 — Kuwana, T., Mackay, M.R., Perkins, G., Ellisman, M.H., Latterich, M., Schneiter, R., Green, D.R., Newmeyer, D.D. (2002) Bid, Bax, and Lipids Cooperate to Form Supramolecular Openings in the Outer Mitochondrial Membrane. *Cell* **111**:331-342

Kühn, 2003 — M. Kühn. (2003) Orientierung von Helix 9 in membrangebundenemcolicin A untersucht mit ESR Spektroskopie and SDSL. PhD Thesis, Ruhr-Universität Bochum

Lakey et al., 1994 — Lakey, J.H., van der Goot, F.G. and Pattus, F. (1994) All in the family: the toxic activityof pore-forming colicins. *Toxicology* **87**:85-108

Lakey et al., 1991 — Lakey, J.H, Massotte, D., Heitz, F., Dasseux, J.L., Faucon, J.F, Parker, M.W, Pattus, F. (1991) Membrane insertion of the pore-forming domain of colicin A. A spectroscopic study. *Eur. J. Biochem.* **196**:599-607

Lakey et al., 1992 — Lakey, J.H, González-Mañas, J.M, van der Goot, F.G., Pattus, F. (1992)The membrane insertion of colicins. *FEBS Lett.* **307**:26-29

Lazdunski et al., 1998 — Lazdunski, C.J, Bouveret, E., Rigal, A., Journet, L., Lloubès, R., Bénédetti, H. (1998) Colicin import into *Escherichia coli* cells. *J. Bacteriol.* **180**:4993-5002

Lazdunski et al., 2000 — Lazdunski C, Bouveret E, Rigal A, Journet L, Lloubès R, Bénédetti H. (2000) Colicin import into *Escherichia coli* cells requires the proximity of the inner and outer membranes and other factors. *Int. Med. Microbiol.* **290**:337-344

Lazzaroni,et al., 2002 — Lazzaroni, J.C., Dubuisson, J.F., and Vianney, A. (2002) The Tol proteins of *Escherichia coli* and their involvement in the translocation of group A colicins. *Biochem.* **84**:391–397

Lih et al., 2012 — Lih, C., Zhang, Y., Vankemmelbeke, M., Hecht, O., Aleanizy F.S., Macdonald C., Moore, G.R., James, R., Penfold C,N. (2012) Structural evidence that colicin A protein binds to a novel binding site of TolA protein in *Escherichia coli* periplasm. *J. Biol. Chem.* **287**:19048-19057

Lin et al., 2000 — Lin, J. H., and Baumgaertner A. (2000) Stability of a melittin pore in a lipidbilayer: a molecular dynamics study. *Biophys. J.* **78**:1714–1724

Lindeberg et al., 2000 — Lindeberg, M., Zakharov, S.D. and Cramer, W.A. (2000) Unfolding pathway of the colicin E1 channel protein on a membrane surface. *J. Mol. Biol.* **295**:679-692

Lopes et al., 2010 — Lopes, S., Neves, C.S., Eaton, P., Gameiro, P. (2010) Cardiolip in a key component to mimic the *E. coli* bacterial membrane in model systems revealed by dynamic light scattering and steady-state fluorescence anisotropy. *Anal. Bioanal. Chem.* **398**:1357-1366

Luirink et al., 1986 — Luirink, J., van der Sande, C., Tommassen, J., Veltkamp, E., De Graaf, F.K, Oudega, B. (1986) Effects of divalent cations and of phospholipase A on excretion of cloacin DF13 and lysis of host cells. *J. Gen. Microbiol.* **132**:825-834

Luirink et al., 1991 — Luirink, J., Duim, B., de Gier, J.W., Oudega, B. (1991) Functioning of the stable signal peptide of the pCloDF13-encoded bacteriocin release protein. *Mol. Microbiol.* **5**: 393-399

Luzzati, 1986 — Luzzati V., Biological Membranes (1986), Academic Press, New York.

Martinez et al., 1983 — Martinez, M. C., Lazdunski, C., Pattus, F. (1983) Isolation, molecular and functional properties of the C-terminal domain of colicin A. *EMBO J.* **2**:1501-1507

Massotte et al., 1993 — Massotte, D., Yamamoto, M., Scianimanico, S., Sorokine, O., van Dorsselaer, A., Nakatani, Y., Ourisson, G., Pattus, F. (1993) Structure of the membrane-bound form of the pore-formingdomain of colicin A: a partial proteolysis and mass spectrometry study. *Biochem.* **32**:13787-13794

Matsuzaki, 1998 — Matsuzaki, K. (1998) Magainins as paradigm for the mode of action of pore forming polypeptides. *Biochem. Biophys. Acta* **1376**:391–400

Matsuzaki et al., 1996 — Matsuzaki, K., O. Murase, N. Fujii, and Miyajima K. (1996) An antimicrobial peptide, magainin 2, induced rapid flip-flop of phospholipids coupled with pore formation and peptide translocation. *Biochem.* **35**:11361– 11368

McDonnell et al., 1999 — McDonnell, J.M., Fushman, D., Milliman, C.L., Korsmeyer, S.J., and Cowburn, D. (1999) Solution structure of the proapoptotic molecule BID: a structural basis for apoptotic agonists and antagonists. *Cell* **96**:625–634

Mchaourab et al., 1996 — Mchaourab, H.S., Lietzow, M.A., Hideg, K., Hubbell, W.L. (1996) Motion of spin-labeled side chains in T4 lysozyme. Correlation with protein structure and dynamics. *Biochem.* **35**:7692-7704

Mechaly et al., 2011 — Mechaly, A. E, Bellomio, A., Gil-Cartón, D., Morante, K., Valle, M., González-Mañas, J.M, Guérin, D.M. (2011) Structural insights into the oligomerisation and architecture of eukaryotic membrane pore-forming toxins. *Structure* **19**:181-191

Merill and Cramer, 1990 — Merrill A. R., and Cramer W. A. (1990) Identification of a Voltage-Responsive Segment of the Potential-Gated colicin El Ion Channel. *Biochem.* **29**:8529-8534

Minn et al., 2000 — Minn, A.J., Vélez, P., Schendel, S.L., Liang, H., Muchmore, S.W., Fesik, S.W., Fill, M., Thompson (1997) Bcl-x(L) forms an ion channel in synthetic lipid membranes. *Nature* **385**:353-357

Nardi et al., 2001 — Nardi, A., Slatin, S.L., Baty, D. and Duché D. (2001) The c-terminal half of the colicin A pore-forming domain is active *in vivo* and *in vitro*. *J. Mol. Biol.* **307**:1293-1303

Nechushtan et al., 1999 — Nechushtan, A., Smith, C.L., Hsu, Y.T., Youle, R. J. (1999) Conformation of the Bax C-terminus regulates subcellular location and cell death. *EMBO J.* **18**:2330–2341

Neidhardt et al., 1990 — Neidhardt, F. C.; Ingraham, J. L. and Schaechter, M. (1990). Physiology of the bacterial cell: A molecular approach. *Sinauer Associates Inc.*

Panchal et al., 2002 — Panchal, R.G, Smart, M.L, Bowser, D.N, Williamsm D.A, Petrou, S. (2002) Pore-forming proteins and their application inbiotechnology. *Curr. Pharm. Biotechnol.* **3**:99-115

Parker et al., 1989 — Parker, M.W., Pattus, F., Tucker, A. D., Tsernoglou, D. (1989) Structure of the membrane-pore-forming fragment of colicin A. *Nature* **337**:93-96

Parker et al., 1992 — Parker, M.W, Postma, J. P, Pattus, F., Tucker, A. D., Tsernoglou, D. (1992) Refined structure of the pore-forming domain of colicin A at 2.4 A resolution. *J. Mol. Biol.* **224**:639-657

Pattus et al., 1985 — Pattus, F., Heitz, F., Martinez, C., Provencher, S.W., Lazdunski, C. (1985) Secondary structure of the pore-forming colicin A and its C-terminal fragment. Experimental fact and structure prediction. *Eur. J. Biochem.* **152**:681-689

Pettersen et al., 2004 — Pettersen, E.F., Goddard, T.D., Huang, C.C., Couch, G.S., Greenblatt, D.M., Meng, E.C., Ferrinm T.E. (2004) UCSF Chimera--a visualization system for exploratory research and analysis. *J. Comput. Chem.* **25**:1605-1612

Polyhach and Jeschke, 2010 — Polyhach, Y., and Jeschke, G. (2010) Prediction of favourable sites for spin labeling of proteins. *Spectroscopy* **24**:651-659

Polyhach et al., 2011 — Polyhach Y., Bordignon, E., and Jeschke, G. (2011) Rotamer libraries of spin labeled cysteines for protein studies, *Phys. Chem. Chem. Phys.* **13**:2356-2366

Prieto et al., 2011 — Prieto, L. and Lazardis, T., (2011) Computational studies of colicin insertion into membranes: The closed channel. *Proteins* **79**:126-141

Pugsley, 1984 — Pugsley, A.P. (1984) The ins and outs of colicins. Part I: Production, and translocation across membranes. *Microbiol. Sci.* **1**:168-175

Pugsley et al., 1984 — Pugsley, A. P. and M. Schwartz (1984) colicin E2 release: lysis, leakage or secretion? Possible role of a phospholipase. *EMBO J.* **3**:2393-2397

Pulagam et al., 2008 — Pulagam, P., V., L. and Steinhoff, H.-J. (2008) Conformation of the closed channel state of colicin A in proteoliposomes: an umbrella model, *J. Mol. Biol.* **378**:204-214

Pulagam, 2007 — Pulagam, L. P. (2007) Structural analysis of colicin A: *in vitro, in vivo* and in silico studies PhD Thesis, Universität Osnabrück.

Pulagam and Steinhoff, 2013 — Pulagam LP, Steinhoff, H.J. (2013) Acidic pH-induced membrane insertion of colicin A into *E. coli* natural lipids probed by site directed spin labeling. *J. Mol. Biol.* **425**:1782-1794

Savitsky et al., 2004 — Savitsky, A., Kühn, M., Duché, D., Möbius, K. and Steinhoff, H.-J.(2004) Spontaneous refolding of the pore-forming colicin A toxin upon membrane association as studied by x-band and w-band high field electron paramagnetic resonance spectroscopy. *J. Phys. Chem.* **108**:9541–9548

Schägger et al., 1987 — Schägger, H., von Jagow, G. (1987) Tricine-sodium dodecyl sulfate-polyacrylamide gel electrophoresis for the separation of proteins in the range from 1 to 100 kDa. *Anal. Biochem.* **166**:368-379

Scheiner et al., 2001 — Scheiner, S., Kar, T., Gu, Y.L. (2001) Strength of the (CH)-H-alpha-O hydrogen bond of amino acid residues. *J. Biol. Chem.* **276**: 9832–9837

Shimizu et al., 2000 — Shimizu, S., Ide, T., Yanagida, T., ,Tsujimoto, Y. (2000) Electrophysiological study of a novel large pore formed by Bax and the voltage-dependent anion channel that is permeable to cytochrome c. *J. Biol. Chem.* **275**:12321-12325

Shin et al., 1993 — Shin Y.K, Levinthal C, Levinthal F, Hubbell W.L (1993) Colicin E1 binding to membranes: time resolved studies of spin-labeled mutants. *Science* **259**: 960-963

Sippach, 2009 — Sippach, M. (2009) Elektrophysiologische Charakterisierung von colicin A – Mutanten. Bachelor thesis, Universität Osnabrück.

Sippach, 2011 — Sippach, M. (2011) EPR-Untersuchungen zur Konformation von colicin A. Master thesis, Universität Osnabrück.

Slatin et al., 2004 — Slatin, S. L., Duché D., Kienker, P.K., Baty, D. (2004) Gating movements of colicin A and colicin Ia are different. *J. Membr. Biol.* **202**:73-83

Slatin et al., 1994 — Slatin, S.L., Qiu, X.-Q., Jakes, K.S., Finkelstein, A. (1994) Identification of a translocated protein segment in a voltage-dependent channel. *Nature* **371**: 158–161

Slatin et al., 2010 — Slatin, S.L., Duché, D., Baty, D. (2010) Determinants of the proton selectivity of the colicin A channel. *Biochem.* **49**:4786-4793

Smarda et al., 1998 — Smarda, J., and Smajs, D. (1998) Colicins exocellular lethal proteins of *Escherichia coli*. *Folia Microbiol. (Praha)* **43**:563-582

Smarda et al., 2001 — Smarda, J., Fialova, M. and J. Smarda, Jr. (2001) Cytotoxic effects of colicins E1 and E3 on v-myb-transformed chicken monoblasts. *Folia Biol. (Praha)* **47**: 11-13

Snijder et al., 1999 — Snijder, H.J., Ubarretxena-Belandia, I., Blaauw, M., Kalk, K.H., Verheij, H.M., Egmond, M.R., Dekker, N., Dijkstra, B.W. (1999) Structural evidence for dimerisation-regulated activation of an integral membrane phospholipase. *Nature* **401**:717-721

Steinhoff et al., 2000 — Steinhoff, H.J., Müller, M., Beier, C., Pfeiffer, M. (2000) Molecular dynamics simulation and EPR spectroscopy of nitroxide side chains in bacteriorhodopsin. *J. Mol. Liquids* **84**:17-27

Suzuki et al., 2000 — Suzuki, M., Youle, R.J., Tjandra, N. (2000) Structure of Bax: coregulation of dimer formation and intracellular localization. *Cell* **103**:645–654

Tory et al., 1999 — Tory, M. C., and Merrill, A. R. (1999) Adventures in membrane protein topology. A study of the membrane-bound state of colicin E1. *J. Biol. Chem.* **274**:24539-2449

van der Goot et al., 1994 — van der Goot, F.G, González-Mañas, J.M, Lakey, J.H, Pattus, F. (1994) A 'molten globule' membrane-insertion intermediate of the pore-forming domain of colicin A. *Nature* **354**:408-410

van der Wal et al., 1995 — van der Wal F.J, Luirink J, Oudega B. (1995) Bacteriocin release proteins: mode of action, structure, and biotechnological applications. *FEMS Microbiol. Rev.* **17**:381-399

Vargas et al., 2000 — Vargas, R., Garza, J., Dixon, D.A., Hay, B.P. (2000) How strong is the C-alpha-H-O=C hydrogen bond? *J. Am. Chem. Soc.* **122**:4750–4755

Vetter et al., 1998 — Vetter, I.R, Parker, M.W., Tucker, A.D., Lakey, J.H., Pattus, F., Tsernoglou, D. (1998) Crystal structure of a colicin N fragment suggests a model fortoxicity. *Structure* **6**:863-874

Walker et al., 1992 — Walker, B., Krishnasastry, M. Zorn, L., and Baley, H. (1992) Assembly of the oligomeric membrane pore formed by Staphylococcal alpha-hemolysin examined by truncation mutagenesis. *J. Biol.Chem.* **267**:21782-21786

Walker et al., 1995 — Walker, B. Braha, O., Cheley, S.and Baley, H. (1995) An intermediate in the assembly of a pore-forming protein trapped with a genetically-engineerred switch. *Chem. Biol.* **2**:99-105

Walker et al., 2004 — Walker, B, Lancaster, L., James, R., Kleanthous, C. (2004) Identification of the catalytic motif of the microbial ribosome inactivating cytotoxin colicin E3. *Protein Sci.* **13**:1603-1611

Wang et al., 1998 — Wang, K., Gross, A., Waksman, G., and Korsmeyer, S.J. (1998) Mutagenesis of the BH3 domain of BAX identifies residues critical for dimerisation and killing. *Mol. Cell. Biol.* **18**:6083–6089

Wiener et al., 1997 — Wiener, M., Freymann, D., Ghosh, P., Stroud, R.M. (1997) Crystal structure of colicin Ia. *Nature* **385**:461-464

Wegener, 2002 — Wegener, C. (2002) Multifrequenz (9 GHz and 95 GHz) ESR Spektroskopie zur Analyse der Dynamik and Polarität von ortsspezifisch spinmarkiertem Bakteriorhodopsin. PhD Thesis, Ruhr-University Bochum.

Yeaman et al., 2003 — Yeaman, M. R., and Yount, N.Y. (2003) Mechanism of antimicrobial peptide action and resistance. *Pharmacol. Rev.* **55**:27-55

Zhang et al., 1993 — Zhang, Y.L. and Cramer, W.A. (1993) Intramembrane helix-helix interactions as the basis of inhibition of the colicin E1 ion channel by its immunity protein. *J. Biol. Chem.* **268:**10176-84

Zjang et al., 2010 — Zhang, Li, C., Vankemmelbeke, M. N. Bardelang, P., Paoli, M., Penfold C. N. and James R. (2010) The crystal structure of the TolB box of colicin A in complex with TolB reveals important differences in the recruitment of the common TolB translocation portal used by group A colicins. *Mol. Microbiol.* **75**:623–636

Zakharov et al., 1996 — Zakharov, S.D., Heymann, J.B., Zhang, Y.L., Cramer, W. A. (1996) Membrane binding of the colicin E1 channel: activity requires an electrostatic interaction of intermediate magnitude. *Biophys. J.* **70:**2774-2783

Zakharov et al., 2002 — Zakharov, S.D., Rokitskaya, T.I, Shapovalov, V.L, Antonenko, Y.N, Cramer, W.A. (2002) Tuning the membrane surface potential for efficient toxin import. *Proc. Natl. Acad. Sci.* **99**:8654-8659

Zakharov and Cramer 2002 — Zakharov, S.D., Cramer, W.A. (2002) Colicin crystal structures: pathways and mechanism for colicin insertion into membranes. *Biochem.Biophys. Acta* **1565**:333-346

3.6 Appendix

```
ForceField YASARA2,SetPar=Yes
Cell Auto,Extension=10

# Chain A

ShowMessage "Optimizing loop between helices H1 and H2 in Chain A"
OptimizeLoop (anchorAH1C),(anchorAH2N),Samples=200
HideMessage

ShowMessage "Optimizing loop between helices H2 and H3 in Chain A"
OptimizeLoop (anchorAH2C),(anchorAH3N),Samples=200
HideMessage

ShowMessage "Optimizing loop between helices H3 and H4 in Chain A"
OptimizeLoop (anchorAH3C),(anchorAH4N),Samples=200
HideMessage

ShowMessage "Optimizing loop between helices H4 and H5 in Chain A"
OptimizeLoop (anchorAH4C),(anchorAH5N),Samples=200
HideMessage

ShowMessage "Optimizing loop between helices H5 and H6 in Chain A"
OptimizeLoop (anchorAH5C),(anchorAH6N),Samples=200
HideMessage


ShowMessage "Optimizing loop between helices H6 and H7 in Chain A"
OptimizeLoop (anchorAH6C),(anchorAH7N),Samples=200
HideMessage

ShowMessage "Optimizing loop between helices H7 and H8/9 in Chain A"
OptimizeLoop (anchorAH7C),(anchorAH89N),Samples=200
HideMessage

ShowMessage "Optimizing loop between helices H8/9 and H10 in Chain A"
OptimizeLoop (anchorAH89C),(anchorAH10N),Samples=200
HideMessage

# Chain B

ShowMessage "Optimizing loop between helices H1 and H2 in Chain B"
OptimizeLoop (anchorBH1C),(anchorBH2N),Samples=200
HideMessage

ShowMessage "Optimizing loop between helices H2 and H3 in Chain B"
OptimizeLoop (anchorBH2C),(anchorBH3N),Samples=200
HideMessage

ShowMessage "Optimizing loop between helices H3 and H4 in Chain B"
OptimizeLoop (anchorBH3C),(anchorBH4N),Samples=200
HideMessage
```

```
ShowMessage "Optimizing loop between helices H4 and H5 in Chain B"
OptimizeLoop (anchorBH4C),(anchorBH5N),Samples=200
HideMessage

ShowMessage "Optimizing loop between helices H5 and H6 in Chain B"
OptimizeLoop (anchorBH5C),(anchorBH6N),Samples=200
HideMessage

ShowMessage "Optimizing loop between helices H6 and H7 in Chain B"
OptimizeLoop (anchorBH6C),(anchorBH7N),Samples=200
HideMessage

ShowMessage "Optimizing loop between helices H7 and H8/9 in Chain B"
OptimizeLoop (anchorBH7C),(anchorBH89N),Samples=200
HideMessage

ShowMessage "Optimizing loop between helices H8/9 and H10 in Chain B"
OptimizeLoop (anchorBH89C),(anchorBH10N),Samples=200
HideMessage
```

Table 3.7: ColA mutant list: Preparation and measurements of the mutants in previous and recent studies

ColA mutant	cloning	purification and labeling	Reconstitution and EPR measurements
T15C	*this study*	*this study*	*this study*
L19C		*this study*	*this study*
I26C		Pulagam et al., 2008	Pulagam et al., 2008 and *this study*
K33C		Pulagam et al., 2008	Pulagam et al., 2008 and *this study*
A42C		Pulagam et al., 2008	Pulagam et al., 2008 and *this study*
S62C		Pulagam et al., 2008	*this study*
I66C	*this study*	*this study*	*this study*
A77C	*this study*	*this study*	*this study*
A91C		Pulagam et al., 2008	Pulagam et al., 2008 and *this study*
F105C		Pulagam et al., 2008	Pulagam et al., 2008 and *this study*
V115C		Pulagam et al., 2008	Pulagam et al., 2008 and *this study*
E126C		*this study*	*this study*
W140C		*this study*	*this study*
A150C		*this study*	*this study*
S155C		Pulagam et al., 2008	Pulagam et al., 2008 and *this study*
G166C		*this study*	*this study*
A169C		Pulagam et al., 2008	Pulagam et al., 2008 and *this study*
G176C		Pulagam et al., 2008	Pulagam et al., 2008 and *this study*
A181C		Pulagam et al., 2008	Pulagam et al., 2008 and *this study*
V182C	*this study*	*this study*	*this study*
V183C		Pulagam et al., 2008	Pulagam et al., 2008 and *this study*
G184C		Pulagam et al., 2008	Pulagam et al., 2008 and *this study*
I187C	*this study*	*this study*	*this study*
A192C		Pulagam et al., 2008	Pulagam et al., 2008 and *this study*
E198C		*this study*	*this study*
L19C/I187C		*this study*	*this study*
A42C/I187C		Boehme et al., 2009 and *this study*	Boehme et al., 2009 and *this study*
S62C/I187C		Boehme et al., 2009 and *this study*	Boehme et al., 2009 and *this study*
A91C/I187C		Boehme et al., 2009 and *this study*	Boehme et al., 2009 and *this study*
V115C/I187C		Boehme et al., 2009 and *this study*	Boehme et al., 2009 and *this study*
A91C/G184C		*this study*	*this study*
A91C/V115C		*this study*	*this study*
L19C/A42C		*this study*	*this study*
I26C/A77C	*this study*	*this study*	*this study*
A77C/W140C	*this study*	*this study*	*this study*
A77C/S154C	*this study*	*this study*	*this study*
W140C/A150C		*this study*	*this study*
I26C/A192C		*this study*	*this study*
I26C/E126C		*this study*	*this study*
K33C/E198C		*this study*	*this study*

CHAPTER 4

Structure of the colicin A pore-forming domain under influence of the immunity protein Cai. The topology of the colicin A/Cai complex

4. Structure of the colicin A pore-forming domain under influence of the immunity protein Cai. The topology of the colicin A/Cai complex

4.1 Introduction

4.1.1 Colicin Immunity proteins

As described in detail in the introduction of the previous chapter, two classes of colicins exist regarding the basic mechanism of their cytotoxic activity. They can either form voltage-gated ion channels in the inner membrane, like colicin A, Ia, E1, K, N, U and B do, or they can have endonuclease activity, i.e. either cleaving the bacterial DNA (colicins E2, E7, E8 and E9), transfer RNA's (colicin E5), or the cell's ribosomal RNA (colicins E3 and E6). Independent of the underlying mechanism of cytotoxicity, all colicin-producing cells have to protect themselves from the lethal effects of their own colicin-mediated "defense-mechanism", as all colicins target closely related bacterial strains. For this purpose, specific host immunity proteins are encoded on the same plasmid where the colicin gene is located (Figure 4.1) that protects the cells against the toxic activity only of their own toxin (Benedetti et al., 1991) (Schramm et al., 1988). In contrast to the colicin genes, whose expression is triggered by, e.g. the SOS response of the host cell, expression of the immunity proteins is under the control of constitutive promoters (Soong et al., 1994), meaning that the immunity protein ist always present in the cell, even under conditions when no colicin expression takes place. Most colicin plasmids contain only a single immunity protein, but for some enzymatic colicins like E3, E6 (Chak et al., 1984) and E9 (James et al., 1987) it could be shown that they possess a second immunity gene. Interestingly, in such cases both immunity proteins have their own promoters that are independent of the SOS promoter of the colicin structural gene (Chak et al., 1985) and both are constitutively expressed under normal conditions.

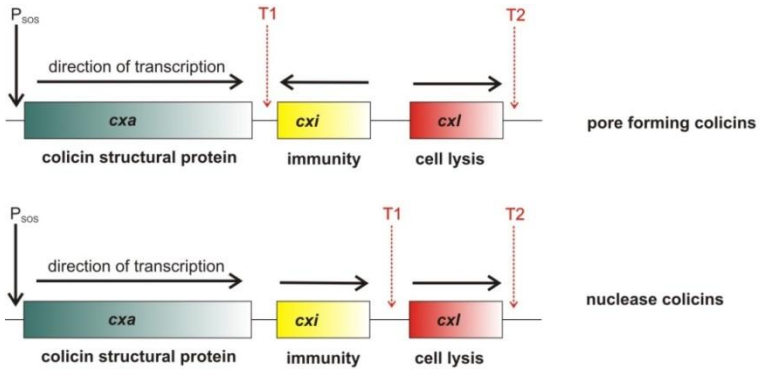

Figure 4.1: Organization of the genes in the colicin operon. The immunity protein is localized between the structural and the lysis gene. In the case for pore forming colicins the immunity protein is transcribed in the opposite direction. The transcription terminators are also indicated as arrows. The Figure was modified and adopted from Cascales et al., 2007.

4.1.2 The immunity proteins of pore-forming colicins

The immunity proteins mediating host-protection from pore-forming colicins are membrane proteins with a size of 11-18 kDa (Lazdunski et al., 1988). They are highly specific and usually only provide full protection against their "own" toxin (Song et al., 1991). However, for the immunity protein of colicin A, (Cai), it could be shown that it can partially protect cells also against colicin B when overexpressed in the cells, i.e. encoded on a high-copy-number plasmid (Géli et al., 1992). The pore-forming immunity proteins are located in the cytoplasmatic membrane of the producing cell and therefore not released into the extracellular medium as the colicins are (Song et al., 1991) (Duché, 2002) (Géli et al., 1988) (Bishop et al., 1985). This "immune system" of the cell is of remarkable efficiency, as only approximately 100-1000 immunity protein molecules present in the inner membrane mediate protection of the cells against colicin concentrations being 10^4 – 10^7 times higher than necessary to kill a nonimmune cell (Cascales et al., 2007). This high efficiency has, for example in the case of the immunity protein for ColE1, been attributed to the high diffusion rate constant of the relatively small immunity protein in the membrane of 10^{-9}–10^{-10} cm^2s^{-1}, corresponding to a possible migration length of at least 500 nm within 10 seconds, thus leading to a high probability that interaction between the colicin and the immunity protein takes place before the cell is harmed (Song et al., 1991). It should be also mentioned that immunity proteins are only required to protect the cell against exogenous colicin, i.e. produced by neighbouring cells and inserted into the inner membrane from the periplasmic space. Colicin molecules expressed by the host cell itself (internal colicin) can also insert into the inner membrane rather then being released, but for those molecules the transmembrane potential is opposite to that required to open the pore (Cascales et al., 2007).

The immunity proteins of pore-forming colicins can be divided into two groups, likewise to the colicins. According to sequence similarities, immunity proteins against colicins A, B, N and U belong to the so-called A-type, whereas those for colicins E1, E5, K, Ia and Ib are E1 type immunity proteins (Schramm et al., 1988). Secondary structure predictions and topology analyses of immunity proteins for colicin A, Cai, and colicin U, Cui, indicate the presence of 4 transmembrane segments, and both its N- and C-termini are located in the cytoplasm (Géli et al., 1989) (Pilsl et al., 1998). Contrarily, the immunity protein for colicin E1 seems to consist of only 3 transmembrane helices, with the N-terminus located in the cytoplasm and the C-terminus in the periplasm (Géli et al., 1989) (Song et al., 1991) (Pilsl et al., 1995) (Pilsl et al., 1998). In general, the mechanism of protection is to prevent opening of the voltage-gated ion channel rather than to inhibit insertion of the colicin's pore forming domain. For this, by fast diffusion within the inner membrane (see above) the immunity protein approaches and interacts with the helices of the colicin pore-forming domain, and it has been shown that these interactions occur mostly between the hydrophobic helical hairpin of the pore forming domain and the transmembrane helices of the immunity proteins (Bénédetti et al., 1991b) (Cramer et al., 1995) (Espesset et al., 1994/1996) (Zhang et al., 1993).

Nevertheless, also interactions between other parts of the pore forming domain and the immunity proteins might take place. For example, for the colicin E1 immunity protein, Cei, interactions with the N-terminus of H6 and the C-terminus of H7 of ColE1 have been shown (Zhang et al., 1993). Also interaction of the immunity proteins with the colicin pore-forming domain upon voltage-gating has been proposed, for example, that displacement of H6 and H7 into a transmembrane orientation upon gating enables the interaction with the transmembrane helices of the immunity protein (Lindeberg et al., 2001). For the colicin A immunity protein it appears most likely that the interaction between the pore-forming domain and the immunity protein takes place in the closed channel state, as the hydrophobic helical hairpin inserts into the inner membrane already in the closed channel state – according to the "umbrella-model", as it has been shown in the previous chapter of this thesis. Thus, interaction with the immunity protein does not require the open channel state (Espesset e al., 1996) (Nardi et al., 2001).
From these findings it has been proposed that A-type immunity proteins inactivate colicins in the closed channel state, whereas E1-type immunity proteins inactivate colicins in the open channel state or just prior to channel opening (Cascales et al., 2007 and references therein).

4.1.3 The colicin A immunity protein Cai

Colicin A-producing cells constitutively express the specific host immunity protein Cai. In contrast to the colicin A protein and the lysis protein Cal, the immunity protein Cai is encoded on the antisense DNA-strand and synthesized at low levels of about 10^2 to 10^3 molecules per cell (colicin A 10^7 molecules per cell) (Cascales et al., 2007).

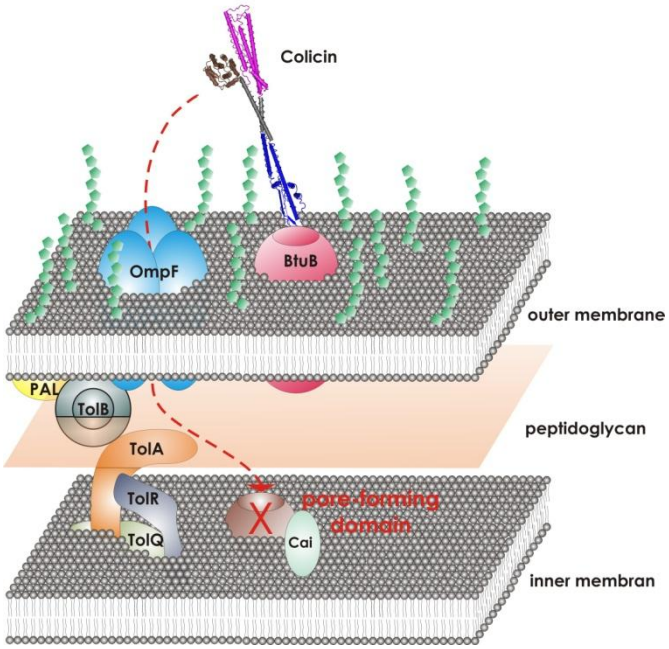

Figure 4.2: Translocation mechanism for colicin A, indicating how Cai might interact with ColA in the inner membrane. The Figure was taken and modified from M. Sippach, Master Thesis, 2011.

The colicin A immunity protein Cai is an integral membrane protein of 178 amino acids with a size of 21 kDa, comprising four transmembrane helices with both its N- and C-termini located in the cytoplasm, see Figure 4.3 A (Geli et al., 1992) (Song et al., 1991).

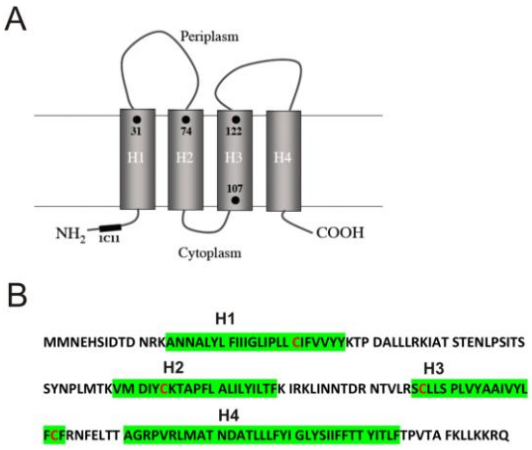

Figure 4.3: (A) Topological model of Cai in the cytoplasmatic membrane of *E. coli*. The four cysteine residues present in the primary sequence (panel B) are shown as black dots labeled with corresponding residue numbers. The picture in panel a has been taken from Zhang et al. (2010). In the the amino acid sequence (B) the 4 putative transmembrane helices are indicated by green boxes. The cysteine residues are shown in red.

Furthermore, cysteine cross-linking experiments with Cai revealed indications for homodimer formation, in which dimerisation takes place by means of the third transmembrane segment as depicted in Figure 4.4 (Zhang et al., 2010). This study also revealed that the interaction of ColA with the Cai dimer modifies both the Cai dimer interaction and the arrangement of the helices inside the two protomers. Furthermore it was shown, that mutation of the four Cys residues present in the sequence of Cai leads to significant impairment of Cai's protective function (Zhang et al., 2010)

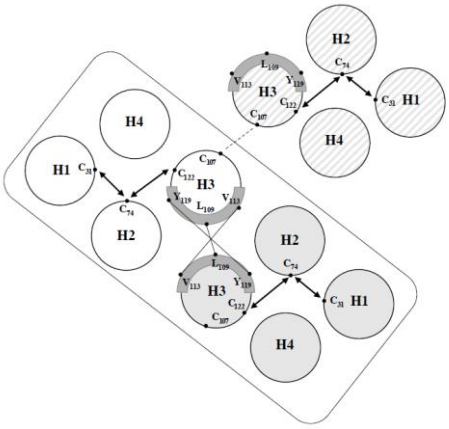

Figure 4.4: Model of Cai helix packing and the dimerisation *via* the third transmembrane segment. The Figure has been adopted from Zhang et al., 2010.

Several studies already indicated that interaction between colicin A and Cai takes place most likely *via* the hydrophobic helical hairpin of the colicin A C-terminal domain (Geli et al., 1992) (Pilsl et al., 1998) Espesset et al., 1996). The sequence that determines the ColA/Cai interaction is localized between residues L530 and D577 (Geli et al., 1992), correspondinf to residues L142 and D189 in the colicin A pore-formin domain (see chapter 3). Thus, H8 and H9 together carry the localization information for Cai, as it also has been shown by co-immunoprecipitation that neither H8 or H9 on their own interact with Cai (Nardi et al., 2001). Additionally, the study by Nardi et al., (2001), indicates that not only the hydrophobic helical hairpin interacts with the immunity protein, but as also H10 of ColA. The transmembrane helices of the immunity protein are thought to interact with the hydrophobic hairpin in order to block the conformational changes necessary for channel opening (Pilsl et al., 1995) (Zhang et al., 1993). However, there are in principle two possibilities of neutralizing the pore forming ability of colicin A: either by stabilization of the closed channel state conformation, or by inducing a colicin A conformation that is not competent for channel opening.

4.1.4 Aim of the study

In the present study the interaction between Cai and colicin A, especially the influence of Cai on the structure of membrane bound colicin A, is investigated by EPR spectroscopic methods like mobility, polarity and inter spin distance measurements, in order to gain more insights into this poorly understood interaction. So far, investigations using EPR spectroscopy on colicin immunity proteins have only been performed on Im9, conferring immunity towards the endonuclease colicin E9 (White et al., 2007).

This study is supposed to contribute to understanding the influence of the immunity protein Cai on colicin A. Various cw- and pulse EPR methods are used to address the pertinent questions: What is the conformation of colicin A in the presence of Cai, and how does Cai inhibits channel opening. Furthermore, initial experiments are performed to reveal if the conformation of the immunity protein Cai changes in the absence and presence of colicin A. The results presented in this chapter will contribute to a more detailed understanding of how proteins conferring immunity to pore forming colicins work in general.

4.2 Materials and Methods

If not stated otherwise, all chemicals and reagents used in this study were purchased from the following manufacturers. AppliChem (Darmstadt) , Avanti Polar Lipids Inc. (Alabaster, USA), BioRad Laboratories GmbH (Munich, Germany), Carl Roth GmbH + Co. KG (Karlsruhe, Germany), Eppendorf AG (Hamburg, Germany), Fermentas GmbH (St. Leon-Roth, Germany), GE Healthcare Europe GmbH (Munich, Germany), Merck KGaA (Darmstadt, Germany), Millipore GmbH (Eschborn, Germany), NEB GmbH (Frankfurt am Main, Germany), Qiagen GmbH (Hilden, Germany), Roche Diagnostics GmbH (Mannheim, Germany, Whatman GmbH (Dassel, Germany).

4.2.1 Bacterial strains and plasmids

Table 4.1 summarizes the bacterial strains and plasmids used in this work with their respective genetic properties.

Table 4.1: *E. coli* strains used in this work with their respective genotypes, and plasmids with the respective antibiotic resistances

bacterial strain	**genotype**
E. coli DH5α	F- *f80dlacZM15 D(lacZYA argF)U169* Hanahan (1983) *deo*R *phoA supE44 hsdr17(rK-, mK+)*
E. coli BL21(DE3)	*fhuA2 [lon] ompT gal (λ DE3) [dcm]* Δ*hsdS λ DE3 = λ sBamHIo* Δ*EcoRI-B int::(lacI::PlacUV5::T7 gene1) i21* Δ*nin5*
E. coli C41(DE3)	*F– ompT gal dcm hsdS$_B$(r_{B^-} m_{B^-})(DE3)*
vector	**description**
pET28a	Kan^R expression-vector, T7-promotor
pET28a_Cai	Kan^R expression-plasmid 10His-Xa-Cai, T7-promotor

4.2.2 Constructs used for overexpression of Cai in *E. coli*

The gene *cai* has been synthesized by the company GeneArt (http://www.lifetechnologies.com/de/de/home/life-science/cloning/gene-synthesis/geneart-gene synthesis.html). The construct carries a N-terminal 10x His-tag coding sequence for purification purposes, and furthermore a factor Xa cleavage site to be able to remove the affinity tag. The whole construct was finally subcloned using the NcoI and XhoI restriction sites into a pET28a expression vector using the strain *E. coli* DH5α. DNA sequencing verified correctness of the 10His-Xa_Cai gene sequence. For the isolation of plasmid DNA, 5 ml *E. coli* DH5α overnight culture was cultivated and the „QIAprep Spin Miniprep Kit" (Qiagen, Hilden) was used as recommended by the manufacturer. Chemically competent *E. coli* cells (BL21 (DE3)) suitable for transformation and protein expression were transformed with the plasmid pET28a_Cai by heatshock using the standard transformation protocol recommended by the manufacturer (Finnzymes; NEB).

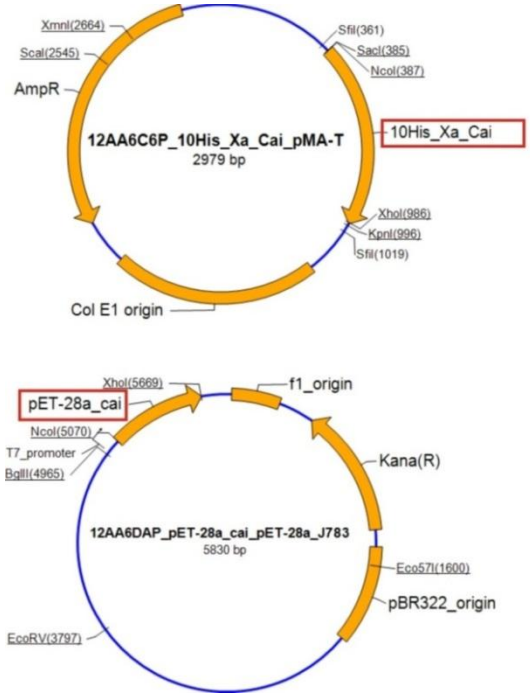

Figure 4.5: Plasmid maps for the initial 10His-Xa-Cai construct provided by GeneArt (top), and of pET28A_Cai.

4.2.3 Biochemical approaches

4.2.3.1 Media and cultivation conditions

The cultivation of *E. coli* cells was performed in rich medium, LB (Lysogeny Broth, "Luria broth"), with 10 g/L Bacto-tryptone (Difco, Detroit, USA), 5 g/L yeast extract and 10 g/L NaCl (Sambrook et al., 1989) at 37°C under aerobic conditions at 162 rpm. If appropriate, the medium was supplemented with

the corresponding antibiotic kanamycin to a final concentration of 50 mg/ml. For agar plates 15 g/L Bacto-Agar was added before autoclaving.

4.2.3.2 Expression and cell harvesting

The growth of the bacterial cultures was followed by determining the optical density (OD) of the medium at 600 nm. *E. coli* BL21 (DE3) cells transformed with the plasmid pET28a_Cai were cultivated overnight in LB medium containing kanamycin to obtain a pre-culture for inoculation of the main expression cultures. Subsequently, the main cultures (1 L LB medium) were inoculated with the overnight culture to obtain an optical density OD_{600} = 0.1, and grown to reach an optical density of OD_{600} = 0.5-0.7. The heterologous overexpression of Cai was induced by the addition of IPTG for BL21-pET28a_Cai with a final concentration of 400 μM and for C41_pET28a_Cai in a final concentration of 1 mM. As a control samples were taken for SDS-Page analysis before and after induction with IPTG. After 3-5 hours of induction the cells were harvested at 4500 rpm at 4°C for 20 min, using a Sorvall centrifuge equipped with a SLA 3000 rotor.

4.2.3.3 Protein isolation

For the isolation of Cai the cell pellets were resuspended in buffer A (Table 4.2) and treated with DNase. Subsequently, cells were disrupted by sonification and the crude extract was centrifuged for 1 h at 50000 x g and 4°C to separate the cell debris. After centrifugation the corresponding cell pellet was resuspended in buffer B (Table 4.2) complemented with 2 % DDM for membrane protein solubilization, and stirred overnight at 4°C. Aterwards, cell membranes were removed by centrifugation at 50000 x g for 1.5 h and 4°C. For further use the supernatant was treated with 10 mM imidazole, 150 mM NaCl and 0.5 mM PMSF.

4.2.3.4 Protein purification by Ni-NTA affinity chromatography

The supernatant containing solubilized N-terminal His-tagged Cai was incubated with pre-equilibrated (Ni-NTA buffer A, see Table 4.2) Ni-NTA affinity matrix under gentle stirring for 60 min at 4°C. After incubation the Ni^{2+}-NTA-protein complex was filled in a glass column and washed with Ni-NTA buffer A (5-fold column volume, see table 4.2) to remove unbound protein from the affinity matrix. Furthermore, to remove nonspecifically bound molecules two washing steps with Ni-NTA buffer B (5-fold column value) containing 20 mM and 35 mM imidazole were performed. The purified protein was then eluted from the column with a 5-fold column volume of the Ni-NTA buffer B containing 135 mM

imidazole. Finally, the column was washed with 5 column volumes of buffer B containing 250 mM imidazole to assure that the protein was eluted completely from the column. The corresponding fractions were collected in fractions of 1 ml and the presence of purified Cai was verified by SDS-PAGE (according to Schägger et al., 1987). The fractions containing Cai were pooled and concentrated by ultrafiltration using centrifugal filter devices with a MWC (molecular weight cutoff) of 10 kDa (Amicon/Millipore, Carringtwohill, Co. Cork, Ireland; Vivascience, Lincoln, USA), that have been saturated two times with BSA in a concentration of 1 mg/ml and washed two times with buffer (50 mM sodium potassium buffer, pH 6.8) before use. The concentrated samples were subsequently subjected to size exclusion chromatography.

4.2.3.5 Further purification by size exclusion chromatography

For size exclusion chromatography 500 µl of the concentrated protein solution were loaded onto a gel filtration column Superdex 200 MR 10/300 (Amersham Pharmacia Biotech) and purified based on their size at a flow rate of 0.5 ml/minute with 10 mM sodium potassium buffer, pH 6.8. The eluted protein fractions containing Cai were concentrated (see 4.5.4). The concentrated protein solutions were frozen in liquid nitrogen and stored at -80°C.

Table 4.2: Buffer composition

Buffer A	**Buffer B**	**Ni-NTA buffer (A)**	**Ni-NTA buffer (B)**
50 mM NaP_i pH 6.8	50 mM NaP_i pH 6.8	50 mM NaP_i pH 6.8	50 mM NaP_i pH 6.8
1 mM DTT	1 mM DTT	150 mM NaCl	150 mM NaCl
2 mM EDTA	0.5 mM PMSF	0.1 % DDM	0.1 % DDM
0.5 mM PMSF		10 mM imidazole	250 mM imidazole
		0.5 mM PMSF	0.5 mM PMSF

4.2.3.6 Determination of protein concentrations

To measure the protein concentration of Cai in solution, absorption of the protein was determined at 280 nm with an UV-VIS spectrophotometer (UV-2450, Shimadzu Corporation, Kyoto, Japan). Protein concentrations have been calculated using Lambert-Beer's law. The extinction coefficient of Cai has been calculated by Expasy protparam (web.expasy.org/protparam) (extinction coefficient: 16390 M^{-1} cm^{-1}, at 280 nm).

4.2.3.7 Spin labeling (SDSL)

For the purpose of labeling with the MTS spin label ((1-oxy-2,2,5,5-tetramethyl-pyrrolinyl-3-methyl) methanethiosulfonate) first freshly prepared 1 M DTT stock solution (DiThioThreitol DTT; Sigma-Aldrich, Munich, Germany) was added to Cai in a final concentration of 10 mM (1:100 v/v) and incubated overnight at 4°C. The reducing agent DTT was removed by exchanging the buffer 5 times with 50 mM potassium phosphate buffer (pH 6.8) by using 10K BSA saturated (see 4.5.4) Amicon Ultra-4 centrifugal filter devices (Millipore). Subsequently, a MTS spin label stock solution (100 mM) in acetonitrile was added to the protein solutions (1 mM final concentration of MTSSL, 1:100 v/v) and incubated overnight at 4°C. Unbound spin label was removed by exchanging the buffer (10 mM potassium phosphate buffer pH 6.8) 5 times using 10 kDA BSA saturated Amicon Ultra-4 centrifugal filter devices, and the spin-labeled Cai was concentrated and stored at -80°C.

4.2.3.8 Liposome preparation and detergent-mediated reconstitution

The liposome preparation and detergent reconstitution was carried out as described in chapter 3.2 for colicin A (chapters 3.2.4.10 and 3.2.4.11). Proteoliposomes have been prepared with Cai alone or with colicin A and Cai. The lipid: protein ratio was 1:500. For samples containing spin labeled colicin A and wt-Cai reconstitution was carried out with a ColA: Cai ratio of 1:4 to assure "saturation" of ColA with Cai, or at a ratio of 4:1, if spin labeled Cai and Wt-ColA was used. The resulting samples were resuspended in 50 µl buffer (50 mM NaPi, pH 6.8), frozen in liquid nitrogen applying 3 freeze-thaw cycles and finally stored at – 80°C until they were used for the EPR experiments.

4.2.4 EPR Methods

To address the question what conformational changes colicin A might undergo in the presence of its immunity protein Cai and *vice versa*, mobility and polarity data as well as inter spin distance data have been collected for spin labeled ColA in the presence of wt-Cai, and for labeled Cai alone and in the presence of ColA, respectively. To identify conformational changes of ColA induced by Cai, the data has been compared to that described in chapter 3. EPR measurements and data analyses have been carried out also as described in chapter 3.

4.3 Results and Discussion

According to current knowledge interaction of Cai with colicin A takes place *via* ColA's hydrophobic helical hairpin. As already mentioned, in principle two possibilities exist, how Cai might prevent ColA channel opening upon association of the two proteins: either by stabilisation of the closed channel state, or by inducing a conformation of colicin that is not competent for channel opening. Accordingly, two questions arise that will be addressed in the following:

a) What is the conformation of colicin A in the presence of Cai? To address this question the existing subset of the colicin A mutants described in chapter 3 were investigated in the presence of saturating concentrations of wt-Cai.

b) What is the conformation of Cai in the absence and in the presence of colicin A? For this purpose, initial experiments have been carried out using wt-Cai that possesses four native cysteine residues. Wt-Cai was labeled with MTSSL as described above and (i) the mobility of the R1 side chain from room temperature cw EPR spectra, quantified by means of the reciprocal width of the central resonance line (ΔH_0^{-1}) and inverse spectral second moment ($\langle H^2 \rangle^{-1}$), (ii) the polarity of the spin label microenvironment, determined via the hyperfine coupling tensor element A_{zz}, obtained from low temperature (160 K) cw-EPR spectra, and (iii) distance data have been recorded in the absence and in the presence of saturating concentrations of ColA. Experiments using only singly or doubly labeled Cai have not been performed in this study, as it was shown, that mutation of these Cys residues leads to significant impairment of Cai's protective function (Zhang et al., 2010). Thus, orthogonal labeling strategies that were not accessible during the time this study has been carried out, e.g. applying click chemistry, have to be applied for site-specific labeling of Cai.

4.3.1 Biochemical results

4.3.2 Protein purification

The first step of purification was performed by Ni-NTA affinity chromatography. After incubation of Cai on the surface of the Ni-NTA affinity matrix unspecifically bound proteins have been removed by washing the loaded Ni-NTA material with buffer containing 20 mM and 35 mM imidazole. The protein was eluted with 135 mM imidazole. Figure 4.6 shows the SDS PAGE analysis of the elution fraction.

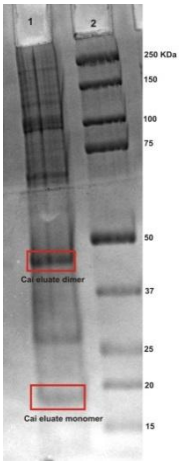

Figure 4.6: SDS-Page analysis of the elution fraction (135 mM imidazole) from Ni-NTA affinity chromatography (lane 1). The second lane shows a molecular weight marker (Precision Plus Protein WesternC Standards, BioRad).

SDS PAGE analysis of the main elution fraction from the affinity column reveals one weak band at an apparent molecular mass of about 20 kDa, most likely corresponding to a monomeric form of Cai. Nevertheless, the major band on the gel is observed at a molecular weight of ~ 45 kDa that should correspond to a dimeric form of the protein. These results are in good agreement with crosslinking studies (Zhang et al., 2010) that clearly indicated that Cai forms homo-dimers in the inner membrane of *E. coli*. The appropriate Ni-NTA fractions were pooled, concentrated, and subjected to size exclusion chromatography. For this step 500 µl of the concentrated elution fraction were loaded on a gel filtration column Superdex 200 MR 10/300 (Amersham Pharmacia Biotech) and eluted at a flow rate of 0.5 ml/minute using 50 mM sodium potassium buffer, pH 6.8, 0.1 % DDM. The elution profile is shown in Figure 4.7.

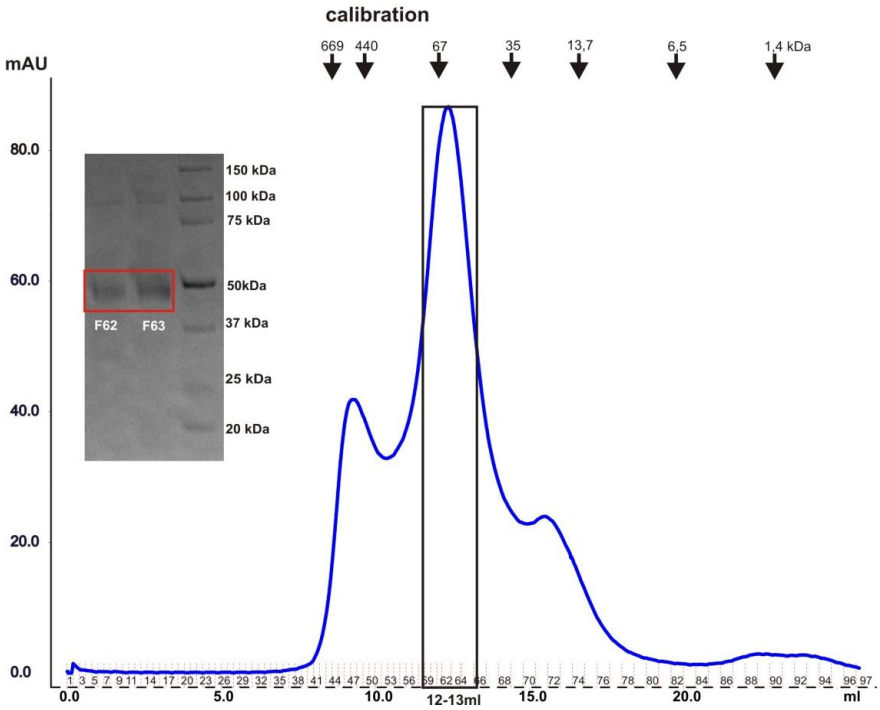

Figure 4.7: Size exclusion elution profile of the second purification step for Cai. Calibration of the column is given on the top. The inset on the left side shows a SDS PAGE of the two major elution fractions (F62 and F63, corresponding to an elution volume of 12-13 ml)

Calibration of the column with a set of reference proteins (see Figure 4.7) allows for estimating the approximate size of the proteins eluted from the column. According to this calibration for Cai in the monomeric form with a size of about 21 kDa a retention volume of ~ 15 ml is expected, whereas a dimeric form (~ 42 kDa) should appear at ~ 13 ml. As evident from the elution profile three peaks at retention volumes of about 9-10 ml, 12-13 ml (major peak) and ~ 16 ml are detected, corresponding to a small fraction (~ 10 %) of monomeric Cai, about 70 % of the dimeric form and approximately 20 % of higher oligomers. Nevertheless, due to the use of DDM for solubilization of the membrane protein Cai, the resulting protein-detergent micelle complex might exhibit significantly larger hydrodynamic radii (DDM micelles have a size of ~ 50 kDa) than expected from the size of the protein itself. Thus, it cannot be excluded that monomeric Cai (in a DDM micelle) is the predominant form and that at retention volumes of 9-10 ml a dimeric form elutes from the column. In this case, the highest volume peak could correspond to a denatured, monomeric form. Therefore, size exclusion chromatography cannot clearly confirm that Cai preferentially forms dimers. Nevertheless, SDS PAGE analysis of the two major fractions (number F62 and F63, see inset in Figure 4.7) reveals a molecular weight of ~ 45 kDa, identical to the major band observed after affinity chromatography. As it can be assumed that under the denaturing conditions in SDS PAGE the DDM molecules are largely substituted by SDS, the molecular weight of the species observed on the gel should reflect its real size. Thus, it can be concluded that indeed Cai dimers are the major species in DDM and the Cai fractions corresponding to an elution volume of 12-13 ml were pooled and concentrated for further use.

4.3.3 Spin labeling of Cai

The purified and concentrated samples were subjected to spin labeling as described in chapter 3.2 (Material and Methods, 3.2.4.8). As in this work only native Cai containing 4 Cysteine residues ($C31^{H1}/C74^{H2}/C107^{H3}/C122^{H3}$) was used, and no reliable information about the fold of the protein is available, it has to be expected that after labeling up to 4 positions in the protein carry a spin label side chain. The calculated labeling efficiency of about 91 % suggests that most of the 4 cysteine residues were hardly accessible, e.g. buried inside of the protein. The room temperature EPR spectrum (Figure 4.8) indicates strong spin-spin interaction by dipolar broadening and increased linewidths. Indicating that at least two spin label side chains are located in a distance < 1.5 nm.

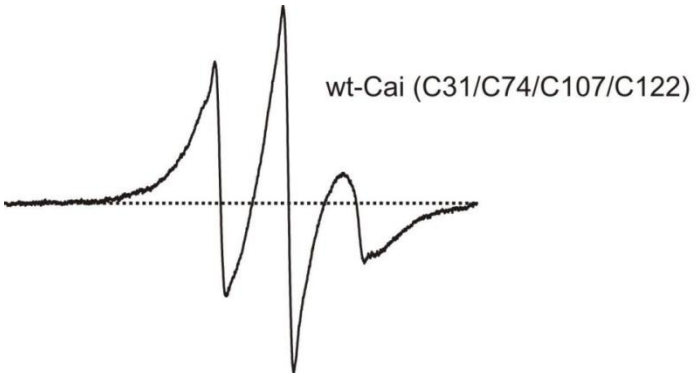

Figure 4.8: Room temperature EPR spectrum of spin labeled wt-Cai in DDM containing 4 putatively labeled Cysteine residues.

4.3.4 Colicin A single mutants in the presence of its immunity protein

The room temperature EPR spectra obtained from the ColA single spin label mutants $T15R1^{H1}$, $A42R1^{H2}$, $I66R1^{H3}$, $A91R1^{H5}$, $V115R1^{H6}$, $W140R1^{H7}$, $S155R1^{H8}$, $A181R1^{H9}$, $V182R1^{H9}$ and $E198R1^{H10}$ (see Figure 4.9, where these positions are indicated on the ColA-mem dimer model, cf. chapter 3.3.7) reconstituted in liposomes (rec-ColA) in the absence (black spectra) and in the presence of saturating concentrations of wt-Cai (rec-ColA/Cai, red spectra)-wt are shown in Figure 4.10.

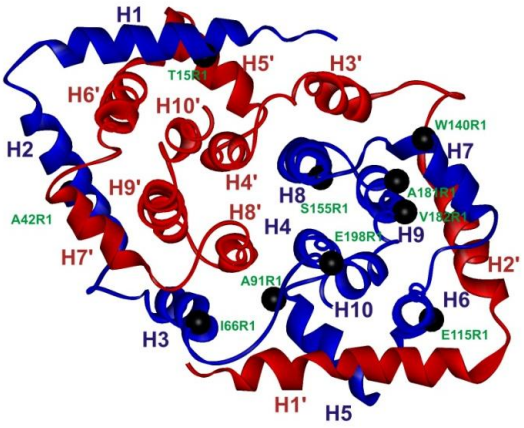

Figure 4.9: Spin label positions on ColA used for investigations in the presence of the immunity protein Cai shown on the ColA-mem dimer model developed in chapter 3.3.7.

Figure 4.10: Comparison between room temperature EPR spectra of R1 labeled rec-ColA (black spectra) and rec-ColA in the presence of wt-Cai (red spectra). All spectra are normalized by their amplitudes.

As already discussed in chapter 3 (3.2.5.2 and 3.3.4.2), all RT cw EPR spectra are characterized by the presence of at least two components representing spin label side chain populations with different rotational freedom. Interestingly, in about half of the cases where spectral changes are observed upon interaction with Cai, these changes cannot - or not only - be described by a shift between the two major components. This indicates either a direct interaction of the region were the R1 side chain is located with Cai, or – assuming no direct interaction with Cai – a significant conformational change of ColA upon Cai binding. Figure 4.10 shows that positions 42R1^{H2} and 66R1^{H3} seem not to exhibit changes of their spin label side chain mobility in the presence of Cai and also the inverse of the central line width (ΔH_0^{-1}), as shown in Figure 4.11, reveals no differences. For positions 15R1^{H1} and 91R1^{H5} changes in the mobility after treatment with the immunity protein Cai are visible already from visual inspection of the EPR spectra. The spin labels at position 15R1 become more immobile (by means of a shift between the two spectral components), whereas 91R1 shows a slightly higher mobility in the presence of Cai. More significant spectral changes upon addition of Cai are observed for 115R1^{H6}, 155R1^{H8}, 181R1^{H9}, 182R1^{H9} and 198R1^{H10}. This suggests that helices H7-H10 are either directly involved in the interaction with Cai – being in line with the literature (see chapter 4.1), or that Cai binding induces significant conformational changes – also suggesting that the binding interface is in close proximity. Interestingly, although the changes are of different nature for the different positions, in general an increase in spin label mobility can be observed (except for position 15R1), as deduced from visual inspection of the spectra shown in Figure 4.10.

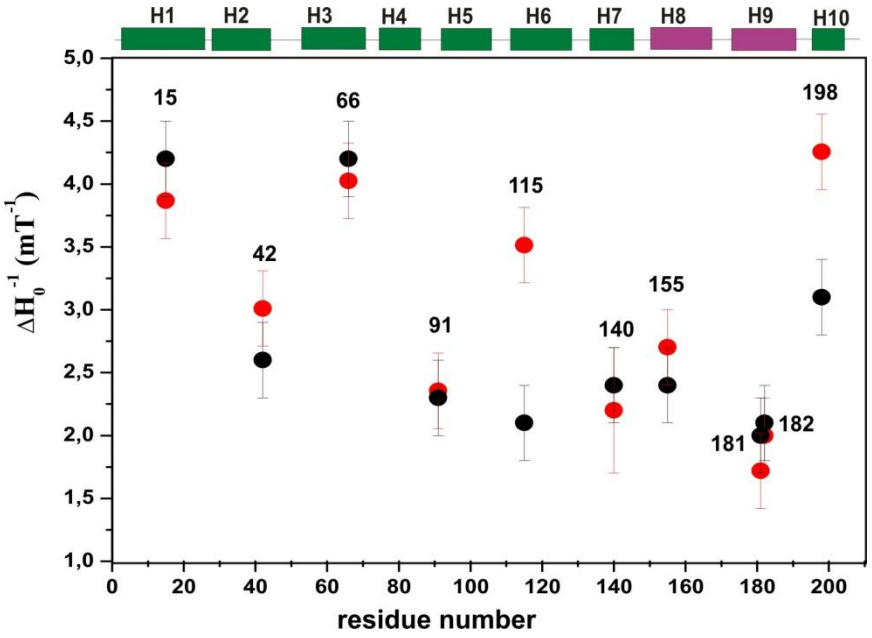

Figure 4.11: The inverse of the central line width (ΔH_0^{-1}) for the R1 sites of rec-mem-ColA with and without Cai were determined from the EPR spectra shown in Figure 4.10 by using the program *unispec*. The values for rec-mem-ColA are colored in black and rec-mem-ColA with Cai are colored in red.

Nevertheless, this trend is not reflected in the inverse of the central line width (ΔH_0^{-1}), as for most of the positions the difference for ΔH_0^{-1} in the presence and absence of Cai are within the error margins. For positions 115R1^{H6} and 198R1^{H10} the increase in spin label mobility visible from Fig. 4.10 is also reflected in ΔH_0^{-1} and could be interpreted as a destabilization of the structure of H6 and H10.

Nevertheless, the ΔH_0^{-1} values for these two positions should be treated with caution, because - as visible from Figure 4.10 - after addition of Cai the spectra for these positions reveal the presence of an increased amount of free spin label. As already mentioned before, for two component spectra the inverse of the central line width strongly biased by the more mobile component. Thus, for a more precise interpretation of the spin label dynamics under the influence of Cai a two-dimensional plot of the inverse spectral second moment ($\langle H^2 \rangle^{-1}$) *versus* the inverse central line width (ΔH_0^{-1}) (Hubbell et al., 1996) (Mchaourab et al., 1996) is shown in Figure 4.12. The inverse second moment reflects the influence of the immobile component rather than of the mobile component.

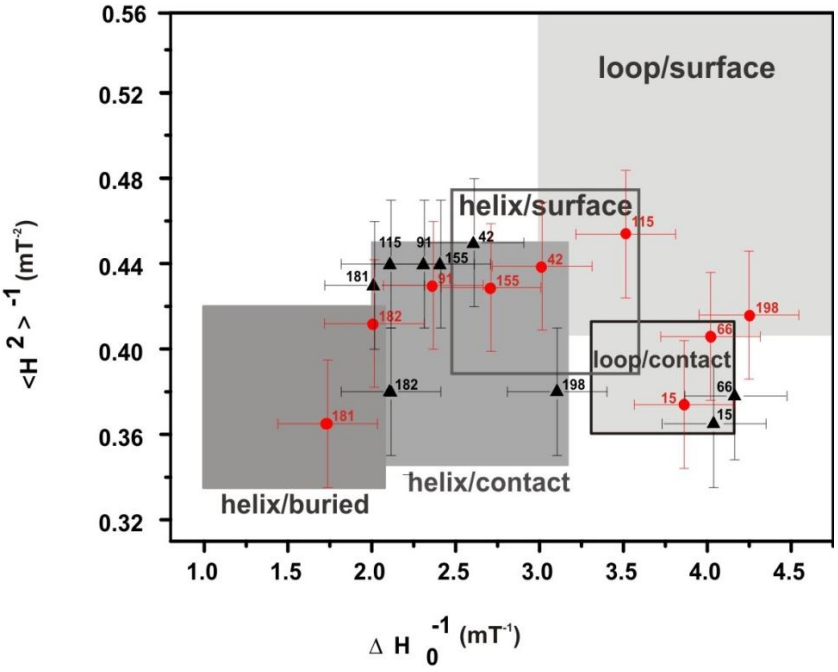

Figure 4.12: Classification of colicin A side chain localizations with (red filled circles) and without Cai (black triangles) with regard to the protein structure by plotting the inverse spectral second moment ($\langle H^2 \rangle^{-1}$) versus the inverse central line width (ΔH_0^{-1}). The parameters were calculated from cw X-band EPR spectra at room temperature (see Figure 4.10).

The strongest effects upon Cai binding are observed for positions 115R1^{H6}, 181R1^{H9} and 198R1^{H10}. Position 115R1, belonging to the helix/contact region in the absence of Cai, moves to the helix/surface – loop/surface region. A spin label at position 181R1 becomes more buried on interaction with Cai. Keeping in mind the assumption that the helical hairpin H8-H9 interacts directly with the Cai transmembrane helices, this observation can support this notion. The other positions in the hydrophobic hairpin, like 155R1 and 182R1, exhibit a slight mobilization. Nevertheless, the former stays within the helix/contact region and the latter remains at the border between the helix/contact and helix/surface

regions of the plot, and the changes are within the error margins. In contrast, position 198R1 becomes more mobile, being situated largely within the loop/surface region of the 2D plot in the presence of Cai, being an indication for increased dynamics of the small C-terminal helix H10. For the remaining positions only slight differences in both mobility parameters are observed. These residues largely remain in the topology regions in the mobility plot. All positions investigated here, evenly distributed over 9 of the 10 ColA helices, exhibit no significant differences in the mobility of spin labels attached to them. However, we cannot assume or exclude from these findings that Cai binding to ColA influences the structure of the whole protein. Remarkably, positions 115R1^{H6}, 181R1^{H9} and 198R1^{H10} demonstrate a clear influence of Cai binding in terms of the protein's topology characterization. As mentioned before, the notion that an interaction of the immunity protein with colicin A occurs most likely via the hydrophobic hairpin (Espesset et al., 1996) has been already brought up. This notion is supported by the mobility analysis presented here for position 181R1^{H9}.

4.3.5 Polarity measurements on colicin A single mutants in the presence of its immunity protein

The hyperfine coupling tensor element A_{zz}, reflecting the local polarity at the position of the spin label side chain, has been determined in the presence of Cai for the ColA positions mentioned in the previous chapter. The results are shown in Figure 4.13 in comparison to the values obtained in the absence of Cai (see chapter 3.3.3.2). They indicate slight changes for 91R1^{H5}, 115R1^{H6}, 140R1^{H7}, 155R1^{H8}, 181R1^{H9}, and 198R1^{H10}. A spin label attached at position 15R1^{H1} shows no significant changes in the cw low temperature spectra, being in line with the observations from the cw room temperature spectra. Also for position 182R1^{H9} no changes in polarity are observed, but here the room temperature spectra with and without Cai were found to be slightly different. Thus, for this position in the hydrophobic hairpin the conformational changes that can be deduced from the observed mobility changes (Fig 4.11) do not lead to a change of the local polarity. This means for example that it is unlikely that H9 of the hairpin largely changes its immersion depths in the lipid bilayer, indicating that the protein remains in an "umbrella"-like structure. For all other positions investigated here, except 15R1^{H1}, 182R1^{H9} and 198R1 on H10, association with Cai leads to increased polarity values, what might indicate that the helices where the spin labels are located move more towards the aqueous phase. Indeed, keeping the ColA dimer structure model (see Figure 4.9) in mind, it could easily be envisioned that Cai interacting with the helical hairpin of ColA might displace some of the surrounding helices.

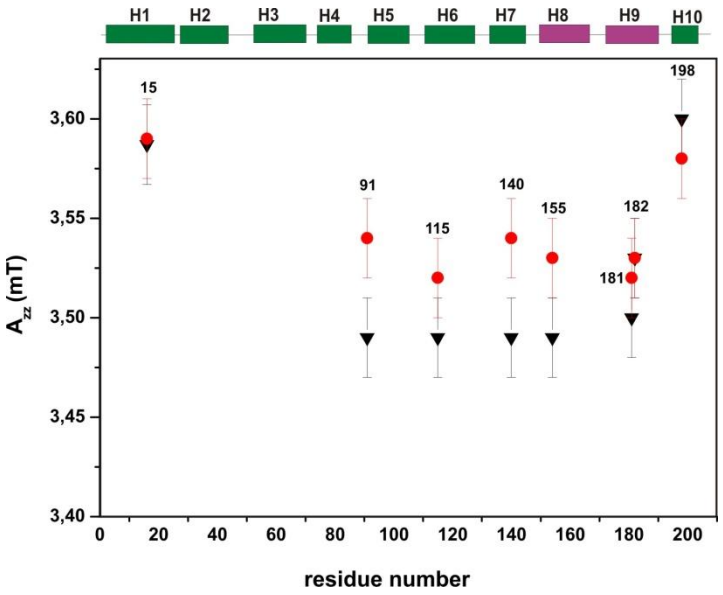

Figure 4.13: Hyperfine coupling tensor elements A_{zz} determined by polarity measurements at 160 K for rec-mem-ColA (black) and rec-mem-ColA in presence of unlabeled wt-Cai (red).

In summary, the immunity protein seems to interact or at least influence colicin A helices H5, H6, H8, H9 and H10. Figure 4.14 visualizes on the dimer model, which helices according to the results of the mobility and polarity measurements might be directly or indirectly involved in the interaction with Cai. A possible mode of action could be for example an interaction of Cai with helices H6 and H9 in the membrane and direct or indirect influence on the conformation of helices H5, H8 and H10. Nevertheless, also other scenarios can be envisioned that would explain the observed mobility and polarity changes upon Cai binding to ColA.

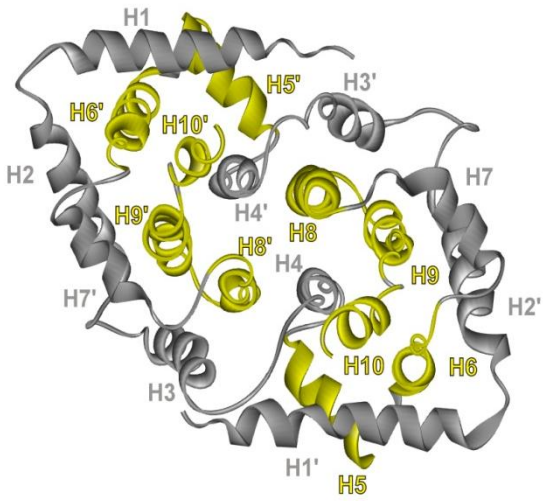

Figure 4.14: ColA-mem dimer model, indicating by yellow ribbons which helices are, according to the mobility and polarity data, influenced by Cai binding.

4.3.6 Distance determination on colicin A single mutants in the presence of its immunity protein

In order to get insights into possible structural changes upon interaction between colicin A and Cai, inter spin distance measurements on singly labeled ColA, thus determination of intermolecular distances within the putative ColA-mem dimer, in the presence of Cai have been performed using cw-EPR and pulsed EPR (DEER) methods. The distance distributions (Fig. 4.15 A and B, right panels) obtained by Tikhonov regularization from the background corrected DEER time domain data (Fig. 4.15 A and B left panels). For position 15R1^{H1} no significant changes could be observed. The broad distance distribution centered around ~ 3.5 nm in the absence of Cai changes to two definite peaks at 2.6 nm and 4.1 nm in the presence of Cai. Only minor changes in the inter spin distance distributions are observed for positions 155^{H8}, 182^{H9} and 198^{H10}, suggesting that the core of the dimer structure comprised by ColA's hydrophobic hairpin largely persists in the presence of the immunity protein. The distance distribution for position 91R1^{H5} is also largely preserved , although the short distance peak appears less pronounced and shifted by about 0.5 nm to shorter distances. Thus, H5 seems to be slightly displaced or rotated upon interaction with Cai, being in line with the observed changes in polarity.

More significant differences are observed for 115R1^{H6} and 181R1^{H9}. Especially 115R1^{H6} reveals significant narrowing of the distance distributions, indicating reduced conformational flexibility of helices H1 and H6 in der ColA dimer structure. For position 181R1^{H9} the major distance peak is shifted from ~3.9 nm to ~3.2 nm in the presence of Cai. Nevertheless, in conjunction with the observation that the inter spin distance for the neighboring residue 182R1^{H9} remains largely unchanged, it appears more likely that the local environment of the labels at position 181R1 changes upon Cai binding rather than that the helix is displaced. This would be in line with the above mentioned presumption that Cai interacts with ColA by binding to helices H6 and H9 within the membrane, as schematically shown in Figure 4.16.

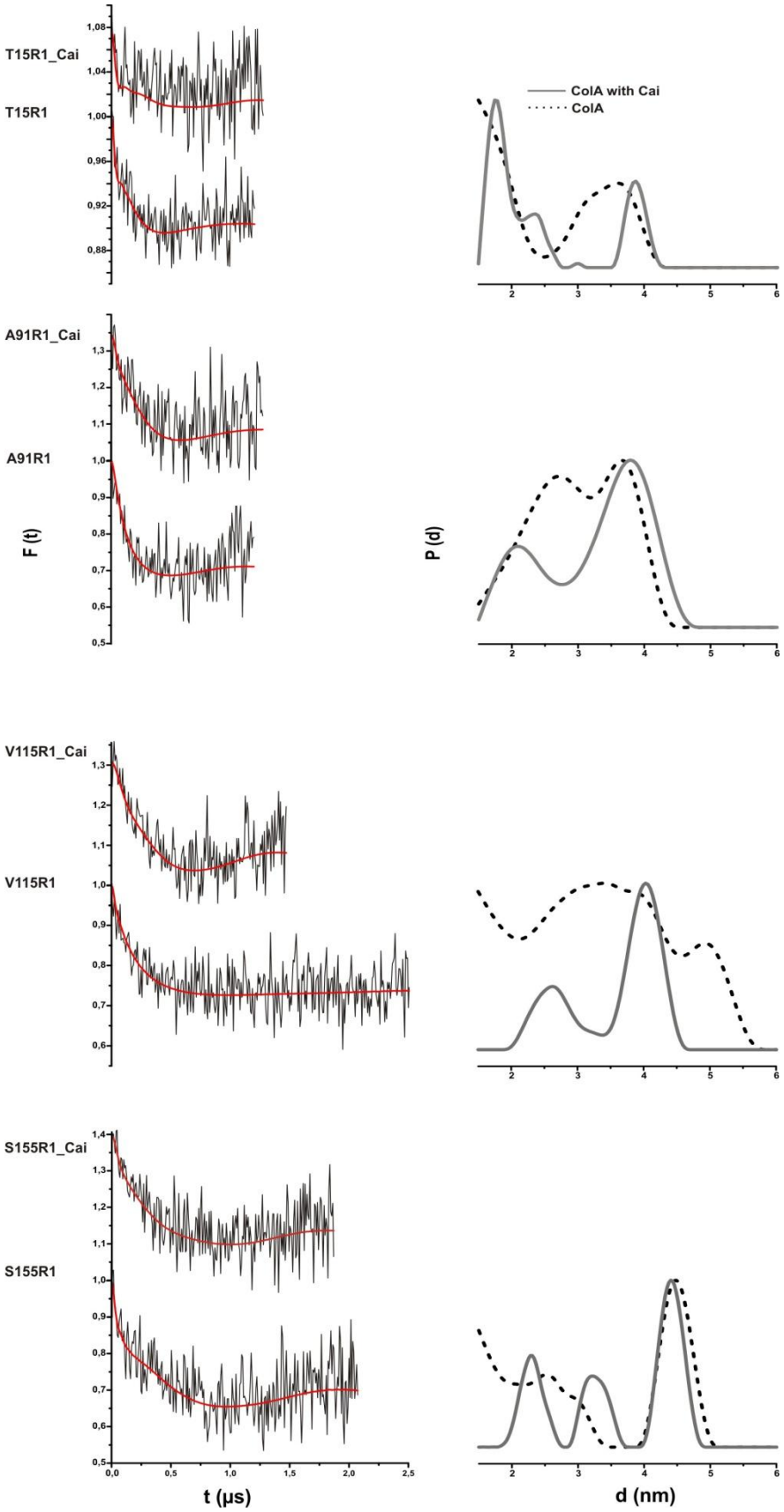

Figure 4.15 (A): DEER spectroscopy results for ColA-mem single mutants T15R1, A91R1, V115R1 and S155R1 in the presence (solid lines) and in the absence Cai (dotted lines). Left: The dipolar evolution functions are shown as black lines and the corresponding fits calculated with DeerAnalysis are indicated as red lines. Right: Resulting DEER distance distributions obtained by Tikhonov regularization.

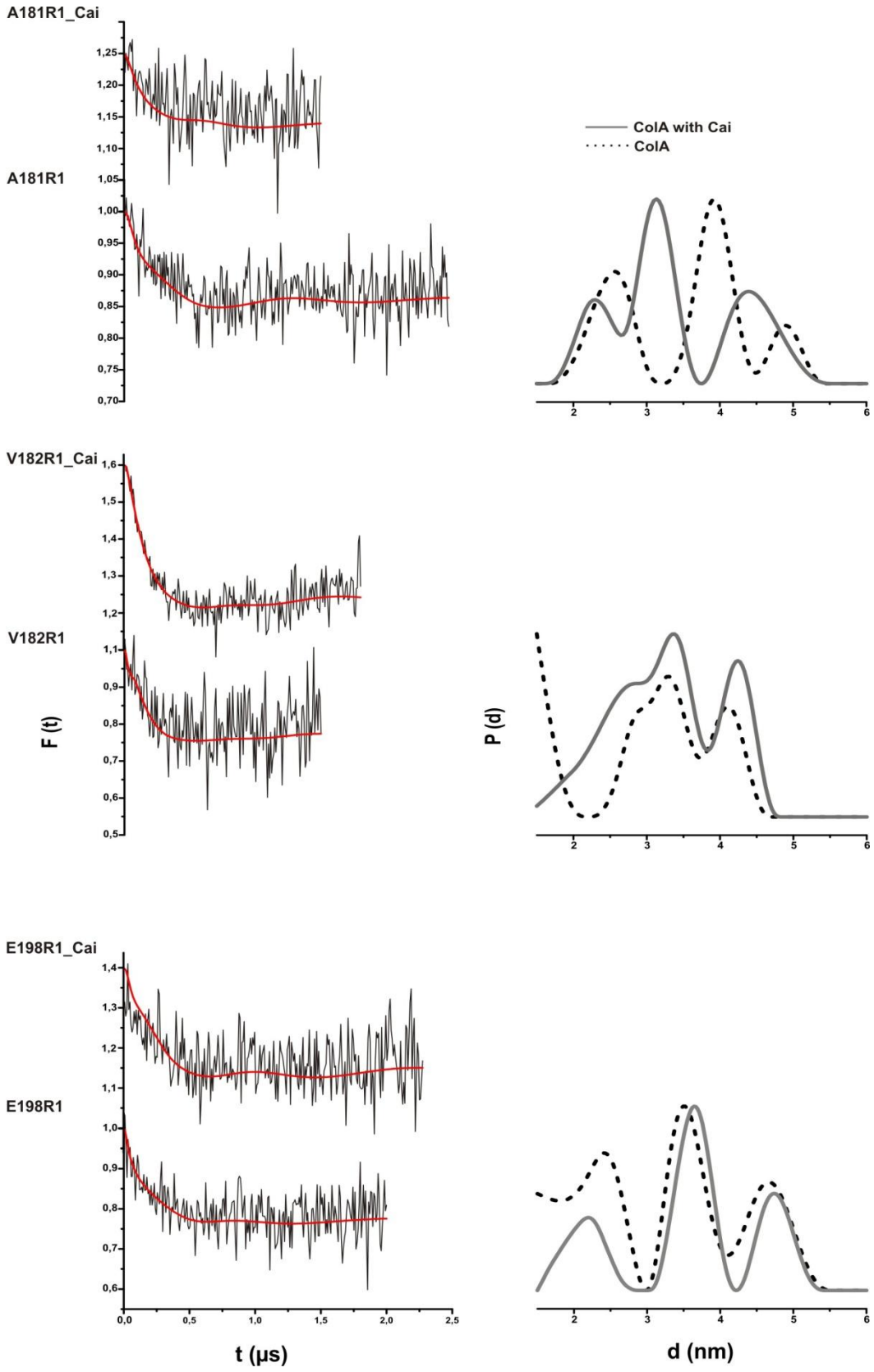

Figure 4.15 (B): DEER spectroscopy results for ColA-mem single mutants A181R1, V182R1 and E198R1 in the presence (solid lines) and in the absence Cai (dotted lines). Left: The dipolar evolution functions are shown as black lines and the corresponding fits calculated with DeerAnalysis are indicated as red lines. Right: Resulting DEER distance distributions obtained by Tikhonov regularization.

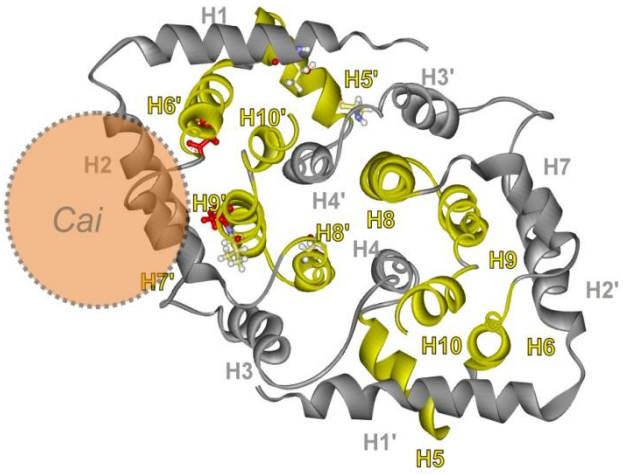

Figure 4.16: ColA-mem dimer model, indicating the putative Cai binding site deduced from cw mobility and polarity data and the changes in inter spin distances observed *via* DEER. The side chains where spin labels have been attached to ColA for DEER are shown in ball and stick representation. The two positions exhibiting the strongest influence of Cai binding are colored in red.

These data provide first insights into conformational changes colicin A undergoes in the presence of its immunity protein. The changes in the protein backbone structure could either be caused by direct interaction with Cai (see Figure 4.16) or by allosteric influence what has also been postulated for example for the endonuclease immunity protein Im9 (Wallis et al., 1995) (van den Bremer et al., 2004). Based on the observed reduction of the conformational flexibity of parts of ColA induced by Cai binding it can be speculated that the immunity protein stabilizes an inactive channel conformation, thereby largely increasing the energy barrier for transmembrane potential-mediated channel opening. This assumption is well in line with the notion that one of the interaction sites with Cai identified here, 115R1^{H6}, is part of the voltage sensor domain (see Chapter 3.3.7.5).

In summary, the results from the cw and DEER experiments on singly labeled ColA give evidence that the interaction of the immunity protein with the pore-forming domain already takes place in the closed channel state, what has been previously proposed (Espesset et al., 1996) (Pilsl et al., 1998). The data obtained in this work furthermore implies the idea that the immunity protein induces and/or stabilizes a ColA conformation that is – probably by direct interaction with H6 of the voltage sensor domain - not able to respond to the transmembrane potential by channel opening. Nevertheless, the available data for the ColA-Cai complex is still limited, and for a more detailed analysis additional spin labels at positions on all ColA helices as well as doubly labeled variants should be examined.

4.3.7 Mobility analysis of spin labels attached to Cai in the presence and absence of colicin A

As mentioned before, the four cysteine residues present in wt-Cai cannot be removed without significant impairment of the proteins protective function on cells treated with ColA (Zhang et al. 2010). Thus, orthogonal labeling strategies are required for site-specific spin labeling of the ColA immunity protein. To obtain first insights into possible structural changes Cai undergoes upon interaction with ColA, spin labeling of wt-Cai was performed. Consequently, up to four spin label side chains can be expected to be attached to the protein, i.e. the resulting EPR spectra represent a superposition of up to four single site spectra. The room temperature X-band cw EPR spectra obtained for spin labeled wt-Cai in the absence (black) and presence of unlabeled colicin A-wt (red spectrum) are shown as an inset in Figure 4.17. It is evident that spin labels attached to Cai become partly immobilized upon interaction with ColA in the membrane bilayer.

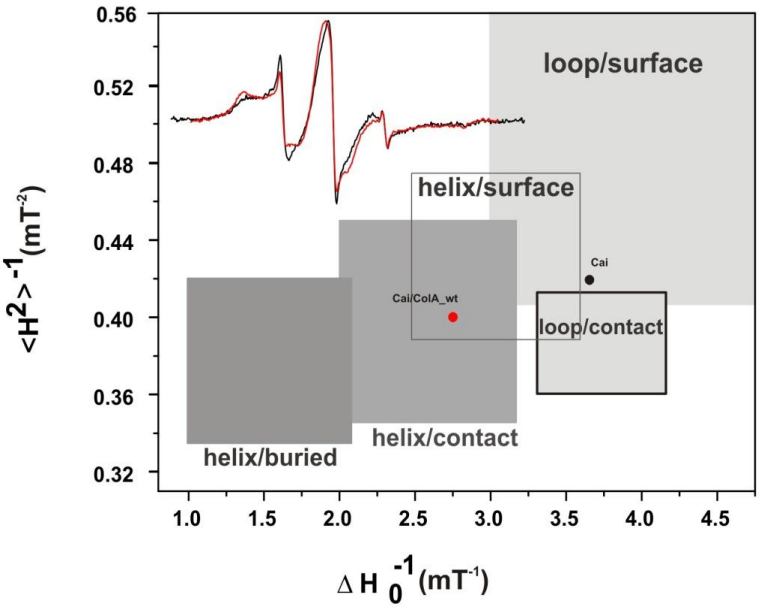

Figure 4:17: Classification of spin labeled rec_Cai with and without colicin A with regard to the protein structure by plotting the inverse spectral second moment ($\langle H^2 \rangle^{-1}$) versus the inverse central line width (ΔH_0^{-1}). Picture modified from (Bordignon et al., 2007). Rec-mem-Cai is colored in black and rec-mem_Cai with ColA_wt is colored in red. The cw-EPR room temperature spectra of rec-mem-Cai (black) and rec-mem-Cai with ColA-wt (red) are shown as an inset in the Figure.

Although an analysis of the inverse spectral second moment and the inverse of the central line width does not appear to be straightforward in this case, where wt-Cai carrying all four native cysteine was used for spin labeling and reconstitution, a 2-dimensional plot of the two parameters (Figure 4.17) like it has been used before, can allow for a general statement about the overall mobility of the protein in the absence and in the presence of ColA. This analysis reveals stronger tertiary interactions for the ColA-Cai complex

compared to Cai alone. This shows that (i) Cai with spin labels attached to the native cysteines is still able to bind ColA, and that (ii) either one or more of the cysteine residues are involved in protein-protein contacts, or/and Cai becomes more rigid when bound to the ColA pore forming domain. Notably, the first assumption would be in line with the observed impairment of ColA inhibition when the cysteine residues are mutated, whereas the second notion is in good agreement with crosslinking studies showing a more mobile arrangement of the Cai transmembrane helices in the absence of ColA (Zhang et al., 2010).

4.3.8 Polarity measurements on spin labeled wt Cai in the presence and absence of colicin A

The mean environmental polarity of spin labels attached to Cai has been determined in the absence and presence of unlabeled colicin A-wt from cw spectra obtained at 160 K (Figure 4.18). The mean A_{zz} value increases from ~ 3.54 mT to ~ 3.58 mT upon binding to ColA, indicating that at least one of the four native cysteine residues is moved to a more polar environment. Of course, it is not possible to draw more detailed conclusions from this data, and at the current stage it cannot be concluded that the conformation of Cai is different in the presence and absence of colicin as suggested before (Zhang et al., 2010), as the changes observed for the polarity are within in the error margins.

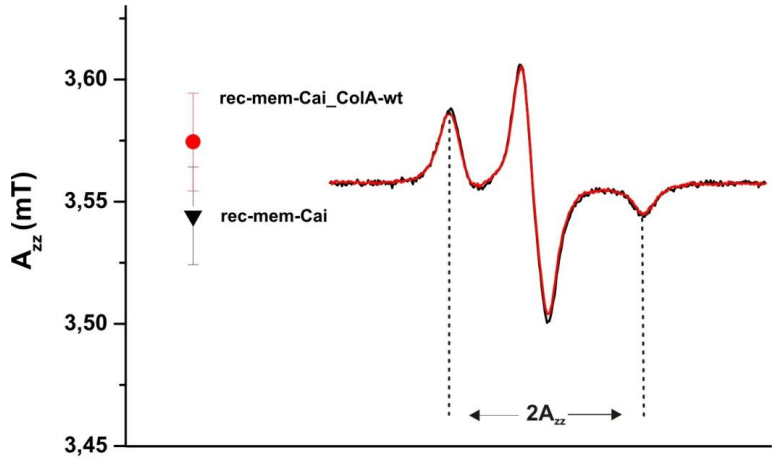

Figure 4.18: Hyperfine coupling tensor elements A_{zz} determined by polarity measurements for rec-mem-Cai (black) and rec-mem-Cai in presence of unlabeled ColA-wt (red) including the low temperature (160K) EPR spectra of Cai. Spectra of rec-mem-Cai are colored in black and rec-mem-Cai with ColA-wt colored in red.

4.3.9 Distance determination on rec-mem-Cai in the presence of colicin A

To further probe the influence of ColA-wt on the structure of Cai, DEER distance measurements have been performed on spin labeled wt-Cai (Figure 4.19). The distance distribution obtained by Tikhonov regularization for the background corrected DEER time domain trace for rec-mem-Cai without ColA exhibits two peaks centered at 2.3 nm and 3.6 nm. In the presence of ColA the DEER form factor, despite the low signal to noise-ratio, as well as the resulting distance distribution exhibit significant changes. In the presence of ColA-wt the ratio between the two peaks changes and the distances appear to be shifted to smaller values (2 nm and 3.2 nm).

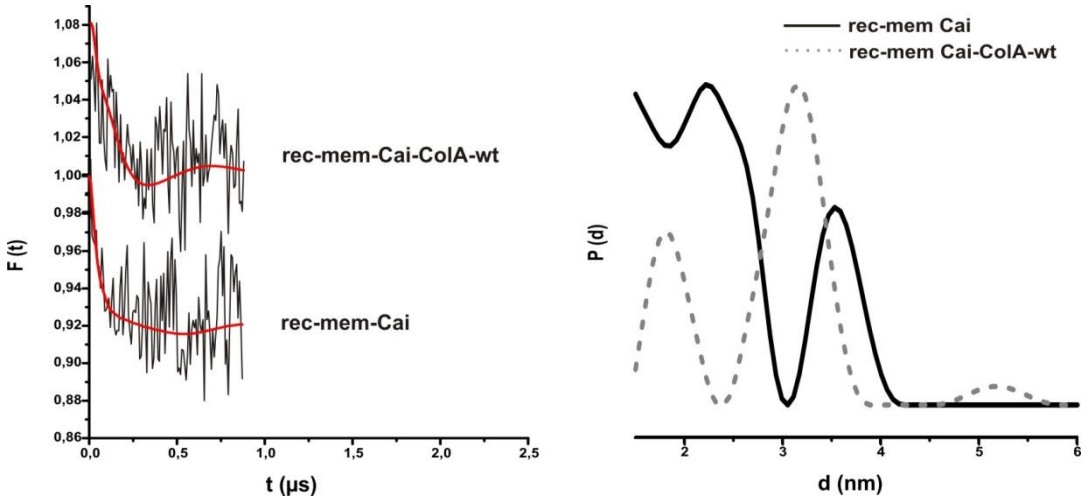

Figure 4.19: DEER spectroscopy results for spin labeled rec-mem Cai (solid line) and rec-mem Cai in the presence of ColA-wt (dotted line). Left: The dipolar evolution functions (black) and the corresponding fits calculated with DeerAnalysis indicated as red lines. Right: The resulting DEER distance distribution obtained from DeerAnalysis by Tikhonov regularization.

Due to the fact that the DEER data has been obtained from spin labeled wt-Cai containing four cysteine residues, the distance distributions cannot be analysed in terms of definite structural properties and/or structural changes induced by ColA binding. Nevertheless, this data can clearly confirm the above mentioned notion that Cai exhibits different conformations, e.g. concerning the arrangement of the helices in a putative Cai dimer, in the presence and absence of colicin A as suggested before (Zhang et al., 2010). Moreover, assuming that not only *intra*-molecular but also *inter*-molecular interactions within the dimer contribute to the DEER signal, the almost unaffected modulation depths of the two DEER traces allow to assume that Cai interacts with ColA as a dimer. Thus, depending on the abundance of Cai in the membrane, the ColA: Cai complex might have a 2:2 or 2:4 stoichiometry.

4.4 Summary and Outlook

The immunity protein Cai, an integral inner membrane protein, protects the producing *E. coli* cell from the cytotoxic activity of its corresponding toxin, colicin A. The protein diffuses in the inner membrane to interact with the pore-forming domain of ColA and prevents channel opening by a yet unknown mechanism. In general, to prevent opening of the colicin A channel, two possible scenarios can be envisioned. Either the ColA closed channel state is stabilized by Cai such that the energy barrier to reach the open state is largely increased, or by inducing a conformation of colicin that is not competent for channel opening. The data presented in this chapter provides more insights into the mechanism and influence of the immunity protein Cai on the colicin A.

Mobility, polarity and interspin distances measurements for single spin label probes attached to ColA in the presence and absence of the immunity protein Cai reveal a clear influence on the ColA helices of the pore-forming domain in the presence of Cai. Previously it was postulated that the main region recognized by the immunity protein Cai is the hydrophobic helical hairpin (H8, H9) (Geli et al., 1992) (Pilsl et al., 1998) (Nardi et al., 2001). Based on the here observed mobility and polarity data it becomes clear that the interaction between Cai and ColA takes mainly place *via* the helical hairpin as suggested. Furthermore, a clear influence on the mobility and polarity is here also observed for H6 and H10, strikingly indicating interactions of Cai also directly with parts of the putative voltage sensor of ColA (H6). An interaction of Cai with H6 was also suggested before by Espesset et al. (1996) for colicin E1, for which H6 has also been proposed to act as voltage-responsive segment.

Inter spin distance measurements on singly labeled ColA furthermore suggest that the relative arrangement of helices H1, H5, H8, H9 and H10 largely persist in the closed channel state upon interaction with Cai. In contrast, for ColA helix 6 DEER spectroscopy reveals a strong influence of Cai binding, providing a first hint for how Cai might prevent channel opening. It could be envisioned that Cai induces a conformational change in/for the voltage sensor helix H6 of ColA forming a "locked" inactive channel conformation that is not capable of voltage sensing and channel opening. Thus, the mechanism by which Cai acts on ColA might be both, stabilization of the closed channel state by "trapping" most ColA helices in the closed conformation and deactivation of the voltage responsive segment H6, thereby inducing a ColA conformation that is not competent for channel opening.

Initial experiments with spin labeled wt-Cai in the presence and absence of unlabeled ColA reveal first insights also into the immunity protein's properties. Mobility, polarity and inter spin distance measurements reveal (i) reduced structural flexibility in the presence of ColA-wt, (ii) increased polarity most likely resulting from replacing Cai-lipid interactions with Cai-ColA contacts, and (iii) shorter inter- and/or intramolecular distances, suggesting a more compact structure in the presence of ColA, thus further supporting notion (i). Nevertheless, it has to be kept in mind that in this case wild-type Cai with

four putative labeling positions was used for spin labeling and reconstitution. Thus, these result and conclusions drawn thereof allow only a very general statement about the immunity protein Cai itself.

In summary, the results obtained in this thesis are in very good agreement with previous studies on Cai and could confirm for the first time experimentally some of the assumptions made before. Moreover, the data give rise for a mechanism how Cai can prevent channel opening. Nevertheless, this work represents only an initial step in analysis of the ColA-Cai interaction. To get more insights into the structure of the immunity protein, especially the three-dimensional arrangement of the transmembrane helices in the absence and presence of ColA, it will be necessary to prepare a set of Cai single site spin label mutants for example by using the nonsense codon suppressor methodology (Chin et al., 2002) in conjunction with "Click" labeling (Hong et al., 2009). This approach is currently under development in our group and can therefore in the near future be applied for investigations on Cai and its interaction with the pore forming domain of ColA.

4.5 Bibliography

Benedetti et al., 1991 — Benedetti, H., Frenette, M., Baty, D., Knibiehler, M., Pattus, F. and. Lazdunski, C. (1991) Individual domains of colicins confer specificity in colicin uptake in pore-properties and in immunity requirement. *J. Mol. Biol.* **217**:429–439

Benedetti et al., 1991b — Benedetti, H., Lazdunski, C., and Lloube`s, R. (1991) Protein import into *E. coli*: colicins A and E1 interact with a component of their translocation system. *EMBO J.* **10:**1989–1995

Bishop et al., 1985 — Bishop, L.J, Bjes, E.S, Davidson, V.L, Cramer, W.A. (1985) Localization of the immunity protein-reactive domain in unmodified and chemically modified COOH-terminal peptides of colicin E1. *J. Bacteriol.* **164**:237-244

Bordingon et al., 2007 — Bordignon, E., and Steinhoff, H.-J., ESR spectroscopy in membrane biophysics, in: M.A. Hemminga, L.J. Berliner (Eds.), Biological Magnetic Resonance, Vol. 27, Springer, Heidelberg, 2007, pp. 129–164.

Cascales et al., 2007 — Cascales, E. K., Buchanan, S.K., Duché, D., Kleanthous, C. Lloube`s, R.Postle, K. Riley, M. Slatin, S. and Cavard, D. (2007) Colicin Biology. *Microbiol. Mol. Biol. Rev.* **71**:158-229

Chin et al., 2002 — Chin, J.W., Santoro, S.W., Martin, A.B., King, D.S., Wang, L., and Schultz, P.G. (2002) Addition of p-azido-L-phenylalanine to the genetic code of *Escherichia coli*. *J. Am. Chem. Soc.* **124**:9026–9027

Cramer et al., 1983 — Cramer W.A., Dankert J.R., Uratani Y. (1983) The membrane channel-forming bacteriocidal protein, colicin E1. *Biochem. Biophys. Acta* **737**:173-193

Cramer et al., 1995 — Cramer, W.A., Heymann, J.B., Schendel, S.L., Deriy B.N., Cohen F.S., Elkins P.A., Stauffacher C.V. (1995) Structure-function of the channel forming colicins. *Ann. Rev. Biophys. Biomol. Struct.* **24**:611-641

Chak et al., 1984 — Chak, K.-F., and James R., (1984) Localization and characterization of a gene on the ColE3-CA38 plasmid that confers immunity to colicin E8. *Gen. Microbiol.* **132**:61-71

Chak et al., 1985 — Chak, K.-F., and James, R., (1985) Analysis of the promoters for the two immunity genes present in the ColE3-CA38 plasmid using two new promoter probe vectors. *Nu.c Acids Res.* **13**:2519-2531

Duché, et al., 2002 — Duché, D. (2002) The pore-forming domain of colicin A fused to a signal peptide: a tool for studying pore-formation and inhibition. *Biochem.* **84**:455-464

Espesset et al., 1996 — Espesset, D., Duché, D., Baty, D., and Geli, V. (1996) The channel domain of colicin A is inhibited by its immunity protein through direct interaction in the *Escherichia coli* inner membrane. *EMBO J.* **15**:2356-2364

Espesset et al., 1994 — Espesset, D., Y. Corda, K. Cunningham, H. Benedetti, R. Lloubes, C. Lazdunski, and Geli, V. (1994) The colicin A pore-forming domain fused to mitochondrial inter membrane space sorting signals can be functionally inserted into the *Escherichia coli* plasma membrane by a mechanism that passes the Tol proteins. *Mol. Microbiol.* **13**:1121–1131

Geli et al., 1992 — Geli, V., and Lazdunski, C. (1992) An α-helical hydrophobic hairpin as a specific determinant in protein-protein interaction occurring in *Escherichia coli* colicin A and B immunity systems. *J. Bacteriol.* **174**:6432–6437

Geli et al., 1989 — Geli, V., D. Baty, F. Pattus, and Lazdunski. C. (1989) Topology and function of the integral membrane protein conferring immunity to colicin A. *Mol. Microbiol.* **3**:679–687

Hubbell et al., 1996 — Hubbell, W. L., McHaourab, H. S., Altenbach, C., and Lietzow, M.A. (1996) Watching proteins move using site-directed spin labeling. *Structure* **4**:779-783

Hong et al., 2009 — Hong, V., Presolski, S. I., Ma, C., and Finn, M. G. (2009) Analysis and optimization of copper-catalyzed azide-alkyne cycloaddition for bioconjugation *Angew. Chem. Int. Ed.* **48**:9879-9883

James et al., 1987 — James, R., Jarvis, M., Barker, D.F. (1987) Nucleotide sequence of the immunity and lysis region of the ColE9-J plasmid. *Gen. Microbiol.* **133**:1553-1562

Lazdunski et al., 1998 — Lazdunski, C.J., Bouveret, E., Rigal, A., Journet, L., Lloubès R., Bénédetti H. (1998) Colicin import into *Escherichia coli* cells. *J. Bacteriol.* **180**:4993-5002

Lin et al., 2014 — Wan-Chen Lin, Lars Iversen, Hsiung-Lin Tu, Christopher Rhodes, Sune M. Christensen, Jeffrey S. Iwig, Scott D. Hansen, William Y. C. Huang, Jay T., Groves (2014) H-Ras forms dimers on membrane surfaces via a protein–protein interface. *Proc. Natl. Acad. Sci.* U S A **111**:2996–3001

Mchaourab et al., 1996 — Mchaourab H.S, Lietzow M.A, Hideg K, Hubbell W.L. (1996) Motion of spin-labeled side chains in T4 lysozyme. Correlation with protein structure and dynamics. *Biochem.* **35**:7692-7704

Nardi et al., 2001 — Nardi A., Corda Y., Baty D., Duché D. (2001) Colicin A Immunity Protein Interacts with the Hydrophobic Helical Hairpin of the colicin A Channel Domain in the *Escherichia coli* Inner Membrane. *J. Bacteriol.* **183**:6721-6725

Pilsl et al., 1998 — Pilsl, H., Smajs, D. and Braun, V. (1998) The tip of the hydrophobic hairpin of colicin U is dispensable for colicin U activity but is important for interaction with the immunity protein. *J. Bacteriol.* **180**:4111–4115

Pilsl et al., 1995 — Pilsl, H., and Braun, V. (1995) Evidence that the immunity protein inactivates colicin 5 immediately prior to the formation of the transmembrane channel. *J. Bacteriol.* **177**:6966–6972

Sambrook et al., 1989 — Sambrook, J., Fritsch, E. F., and Maniatis, T. (1989) Molecular Cloning. A laboratory manual. Second edition. *Cold Spring Harbor Press*, New York.

Schägger et al., 1987 — Schägger, H., von Jagow, G. (1987) Tricine-sodium dodecyl sulfate-polyacrylamide gel electrophoresis for the separation of proteins in the range from 1 to 100 kDa. *Anal. Biochem.* **166**:368-379

Schramm et al., 1988 — Schramm, E., Olschlager, T., Troger, W. and Braun, V. (1988) Sequence, expression and localization of the immunity protein for colicin *B. Mol. Gen. Genet*. **211**:176–182

Song et al., 1991 — Song, H. Y., and. Cramer, W. A. (1991) Membrane topography of ColE1 gene products: the immunity protein. *J. Bacteriol.* **173**:2935–2943

Soong et al., 1994 — Soong B.W., Hsieh S.Y., Chak K.F. (1994) Mapping of transcriptional start sites of the *cea* and *cei* genes of the ColE7 operon. *Mol. Gen. Genet.* **243**:477-481

van den Bremer et al., 20004 — van den Bremer E.T., Keeble A.H., Visser A.J., van Hoek A., Kleanthous C., Heck A.J., Jiskoot W. (2004) Ligand-induced changes in the conformational dynamics of a bacterial cytotoxic endonuclease. *Biochem.* **43**:4347-4355

Wallis et al., 1995 — Wallis R., Moore G.R., James R., Kleanthous C., (1995) Protein-protein interactions in colicin E9 DNase-immunity protein complexes. 1. Diffusion controlled association and femtomolar binding for the cognate complex. *Biochem.* **34**:13743-13750

White et al., 2007 — White, G.F., Ottingnon, L.,Georgiou, T., Kleanthous, C., Moore, G.R., Thomson, A.J. and Oganesyan, V.S. (2007) Analysis of nitroxide spin label motion in a protein-protein complex using multiple frequency EPR spectroscopy. *J. Magn. Reson.* **185**:191-203

Zhang et al., 2010 — Zhang, Y. L, Lloubes R. and Duché, D. (2010) Channel domain of colicin A modifies the dimeric organization of its immunity protein. *J. Biol. Chem.* **285**:38053-38061

Zhang et al., 1993 — Zhang, Y. L., and. Cramer, W. A. (1993) Intra membrane helix-helix interactions as the basis of inhibition of the colicin E1 ion channel by its immunity protein. *J. Biol. Chem.* **268**:10176–10184

CHAPTER 5

Structure and functional dynamics of Extracellular Loop eL4 of the *E. coli* Na^+/proline symporter PutP

Parts of this chapter have already been published:

Michael Raba*, Sabrina Dunkel*, Daniel Hilger, Kamila Lipiszko, Yevhen Polyhach, Gunnar Jeschke, Susanne Bracher, Johann P. Klare, Matthias Quick, Heinrich Jung, and Heinz-Jürgen Steinhoff

Extracellular Loop 4 of the Proline Transporter PutP Controls the Periplasmic Entrance to Ligand Binding Sites

Structure **22**:769-780 (2014)

*These authors contributed equally to this work

5. Structure and functional dynamics of Extracellular Loop eL4 of the *Escherichia coli* Na^+/proline symporter PutP

5.1 Introduction

5.1.1 Membrane transport diversity

Biological membranes represent a permeability barrier and separate the cell interior from the environment. The exchange of components between the two compartments for small and uncharged molecules takes place by free diffusion. On the other hand small polar and apolar molecules like ions, organic acids, peptides and sugars cannot pass the membrane barrier by free diffusion due to their hydrophilic nature. To allow the selective uptake and excretion of these components, biological membranes exhibit passive or active transport systems. Passive transport through the membrane by free diffusion needs no energy, whereas the active transport of a solute against its concentration gradient requires energy. Based on that, the transport systems can be divided into four different classes (see Figure 5.1): (i) channels, (ii) primary transporters, (iii) secondary transporters and (iv) the phosphoenolpyruvate:carbohydrate phosphotransferase system (PTS).

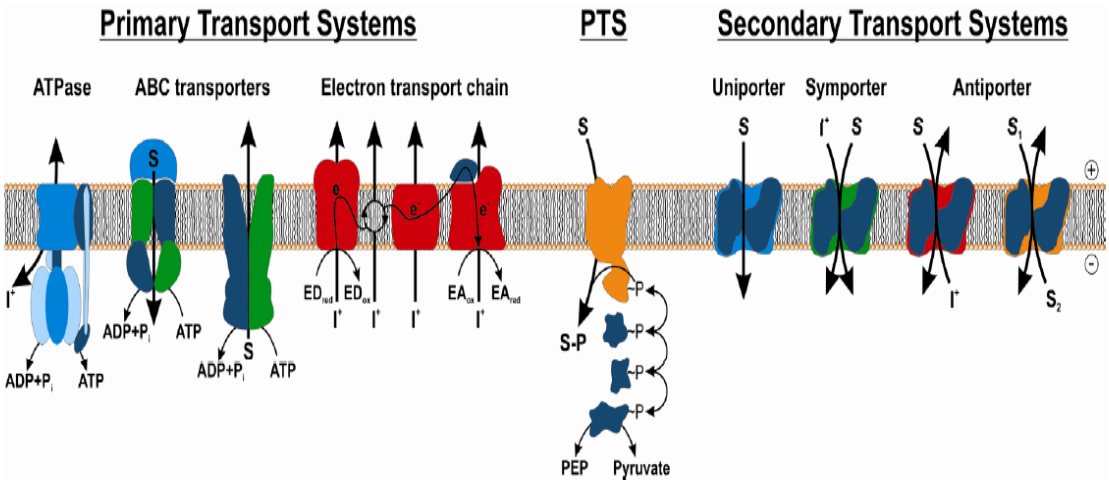

Figure 5.1: Classification of the different active transporter systems. According to the utilized energy source the transporter systems can be classified into three classes: primary transport systems, secondary transport systems, and the phosphoenolpyruvate:carbohydrate phosphotransferase system (PTS). **I^+:** ion most likely H^+ or Na^+, **S**: solute, **ED**: electron donor, **EA**: electron acceptor, **PEP**: phosphoenolpyruvate. The Figure was adopted from D. Hilger, PhD Thesis, 2010.

Channels are regulated by an opening and closing mechanism which can be triggered by different stimuli, like for example voltage, ligands or mechanical forces (Kung et al., 2010) (Catterall, 2010) (Corringer et al., 2010).

Primary transporters use energy to transport molecules across the membrane. The sources of this energy can be either redox potentials, chemical energy – e.g. stored in molecules like ATP - light or electrochemical gradients, that in turn can be established utilizing chemical energy. An example for primary transporters using light as an energy source are the light-driven ion pumps bacterio- and halorhodopsin (Lanyi, 2006) (Essen, 2002). Another example for primary transporters are the ATP-driven transport systems. ATP-binding cassette (ABC) transporters are members of the large superfamily of transporters which utilize the energy of ATP hydrolysis to drive the import of various substrates across the membrane.

Secondary transport systems use the energy to transport solutes and ions across the lipid bilayer against their concentration gradients and can be further divided into three sub-groups, (i) uniporter, (ii) antiporter and (iii) symporter. Uniporters are integral membrane proteins that couple the transport of molecules with the solute gradient, and that are not coupled to other compounds. One example for an uniporter is the sugar transporter Glf of *Zymomonas mobilis* (Weisser et al., 1995). Antiporters pump two species of ions or solutes in opposite direction across the membrane, like the Na^+/H^+ antiporter NhaA of *E. coli* (Padan et al., 2004). In contrast to antiporters, symporters catalyze the transport of two compounds in the same direction across the membrane. The transport principle is to use the "downhill" transport of one solute (from high to low concentration) to "drive" another molecule uphill against its electrochemical gradient. Well characterized examples are the human Na^+/glucose cotransporter SGLT1 (Wright et al., 1992) and the Na^+/proline symporter PutP of *Escherichia coli* (Jung et al., 1998 b). The last group of secondary transporters is the so called phosphoenolpyruvate: carbohydrate phosphotransferase system (PTS), which is only known for bacteria. This multi-component system catalyzes the phosphorylation of substrates during their translocation by phosphoenolpyruvate (PEP), thus providing the energy for the transport process.

5.1.2 Secondary transport systems

Secondary transporter systems form the largest and wide spread group of transporters, and can be found in all three kingdoms of life. They transport a broad range of substrates across biological membranes like sugars, amino acids, ions, nucleosides, organic acids, compatible solutes, vitamins, neurotransmitters, peptides, urea, heavy metals, autoinducers, and tRNAs (Saier, 1999). Due to this high diversity of the transported substrates, secondary transporters play a major role in numerous cellular processes. One example facilitating catabolic as well as anabolic pathways is the proline transporter PutP of *E. coli* (Mueckler, 1994), (Guan and Kaback 2006) (Jung, 2001). The most common energy source for uphill

transport of substrates used by secondary transporters in bacteria is the electrochemical proton gradient ($\Delta\mu_{H+}$) across the cytoplasmatic membrane. In most cases the proton gradient is built by primary proton pumps, which use the energy of electrons provided by an electron carrier to pump protons out across the membrane. The proton motive force (*pmf* or Δp) resulting from the proton gradient is composed of a pH gradient (ΔpH) – due to the difference in proton concentration on both sides of the membrane - and an electrical potential across the membrane ($\Delta\Psi$). The *pmf* is responsible for the movement of protons across the membrane downhill the electrochemical gradient and this gradient can be used for osmotic, mechanical and chemical work. One example is the F_1F_0-ATP synthase which uses the energy stored in the proton gradient to synthesize ATP from ADP and phosphate (Junge et al., 1997). A popular example for a H^+- dependent transport system is the *E. coli* multidrug resistance protein EmrE that belongs to the small multidrug resistance (SMR) family of transporters (Grinius and Goldberg, 1994) (Paulsen et al., 1996). Besides the H^+- dependent transport systems, a related class of transporters exists that uses Na^+ instead of H^+ as the coupling ion. These Na^+-dependent transporters, constituting the sodium/solute symporter family (SSSF) of transport proteins, like the above mentioned *E. coli* Na^+/proline symporter PutP or the *Aquifex aeolicus* Na^+/leucine symporter LeuT (Jung, 1998) (Yamashita et al., 2005), use the sodium motive force (*smf*), that depends on ΔpNa^+ rather than ΔpH and is produced by specific Na^+ pumps.

The basic mechanism underlying the function of all secondary transporters, independent of the gradient used to drive the transport process, involves conformational changes induced by substrate binding occuring during passage through a translocation pathway for the solutes inside the transporter protein (Mitchell, 1991) (West, 1997). Another key determinant of function based on these transporter movements is that the translocation pathway is accessible for the solutes only from one side of the lipid bilayer in contrast to channels and pores that provide only passive transport driven by the gradient of the substrate itself. A more detailed mechanistic model for active transport of solutes across the membrane by transporter proteins is the *alternating access mechanism* (West, 1979) (Maloney, 1994) (Jardetzky, 1966). According to this mechanism, the transport protein can exist in two different major conformations, an outward-facing conformation (C_O) and an inward-facing conformation (C_I). After binding and during transport of the solutes, the transporter can also adopt a number of additional states, representing transition states between the two major conformations. A scheme describing this mechanism is shown in Figure 5.2. The transport cycle starts in the absence of ligands, the so called apo-state, in which the symporter exists in an outward-facing open conformation (C_O). Binding of the periplasmatic ion (I) to the binding site results in a binary complex (C_OI), leading to structural rearrangement of the symporter. This conformational change increases the affinity to the co-transported substrate (S), and binding of the substrate generates a ternary complex (C_OIS). Substrate binding induces other conformational changes and specific protein domains, so called *gates,* shield the binding site from the outside of the ternary complex, leaving the transporter in an outward-facing occluded conformation ($C_{Ooc}IS$). Further conformational rearrangements of the ternary complex lead from the outward-facing occluded conformation to the inward-facing orientation. First, the extracellular cavity is closed - the transporter protein adopts a transient occluded state ($C_{oc}IS$). Afterwards, the intracellular cavity opens, but the intracellular gate still

remains closed ($C_{Ioc}IS$). When the gate opens (C_IIS), the subsequent release of the ion and the substrate takes place and the transporter molecule adopts the inward-facing open apo-state (C_I). The transporter reorientates back from the inward-facing to the initial outward-facing state (C_O), passing the substrate free occluded state (C_{oc}), finally ending up in the apo state again being able to start the next transport cycle.

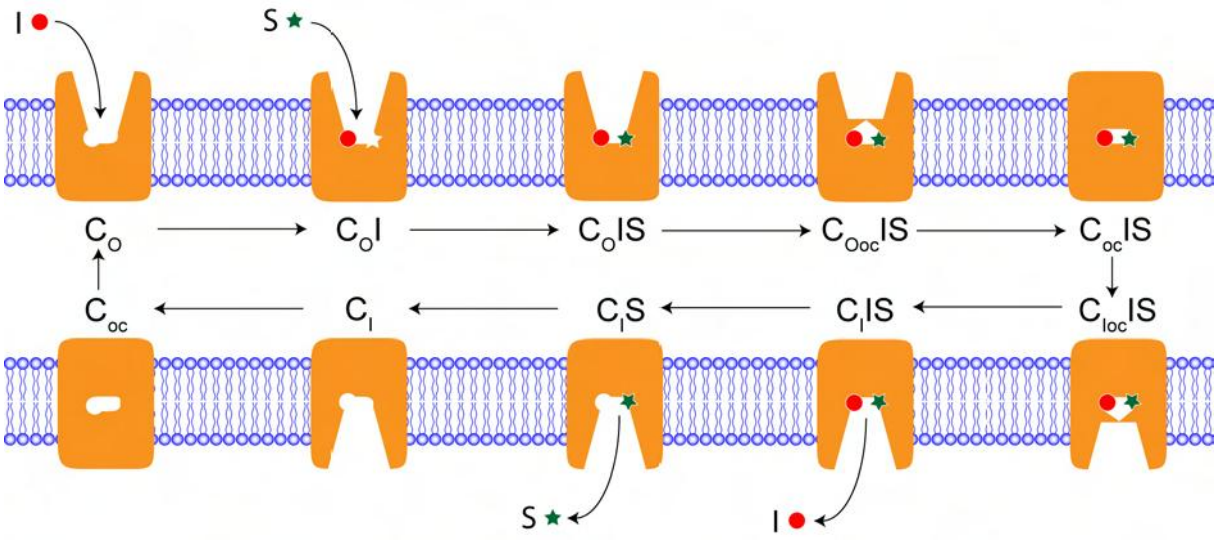

Figure 5.2: Schematic presentation of the reaction cycle of a secondary ion-coupled solute symporter. The Figure is based on Forrest et al., 2011 and was adopted from M. Raba, PhD Thesis 2012. For details see text.

Most secondary transporters share common structural features: hydrophobic, α-helical domains or transmembrane domains (TMs) - connected by hydrophilic loops. Currently, three-dimensional structures of such transporters are available for AcrB (Murakami et al., 2002), AAC (Pebay-Peyroula et al., 2003), CLC (Dutzler et al., 2002), EmrD (Yin et al., 2006), EmrE (Chen et al., 2007), GlpT (Huang et al., 2003, Glt_{Ph} (Yernool et al., 2004); LacY (Abramson et al., 2003), (Guan et al., 2007) $LeuT_{Aa}$, (Yamashita et al., 2005) and NhaA, (Hunte et al., 2005). Nevertheless, only some of them have been crystallized in different conformations.

5.1.3 PutP - a member of the sodium substrate symporter family

The sodium/solute symporter family (SSSF; TC 2.A.21; SLC5) comprises several hundred representatives in all three kingdoms of life (Jung et al., 2012). Members of this group of transporters use a preexisting Na^+ gradient to drive the uphill transport of various solutes such as amino acids, vitamins or ions across the membrane (Jung, 2002). The human Na^+/I^- symporter (NIS) and the Na^+/glucose transporter (SGLT1) were shown to be involved in diseases such as iodide transport defect (Reed-Tsur et al., 2008) or glucose-galactose malabsorption (Wright et al., 2007). Moreover, PutP-mediated proline uptake in bacteria

plays an important role in human infectious diseases. In *Staphylococcus aureus*, the proline permease contributes to the survival of the pathogen in the host organism (Bayer et al., 1999), and a knock out of the homologous gene in *Helicobacter pylori* abolished its ability to colonize the stomach of model organisms (Kavermann et al., 2003).

To understand the molecular principles of Na^+-coupled transport, here the Na^+-dependent proline permease PutP of *Escherichia coli* was used, the functionally best-characterized member of the SSSF. Previous studies showed that this symporter is functioning according to an ordered binding mechanism and that Na^+-coupled proline uptake is mediated with a stoichiometry of 1:1 (Yamato, 1992) (Yamato and Anraku, 1990). For PutP a topology model comprising 13 TMs was proposed with the N-terminus facing the periplasm and a C-terminus found in the cytoplasm (Wegener et al., 2000) (Jung et al., 1998 a). A secondary structure model for PutP is shown in Figure 5.3.

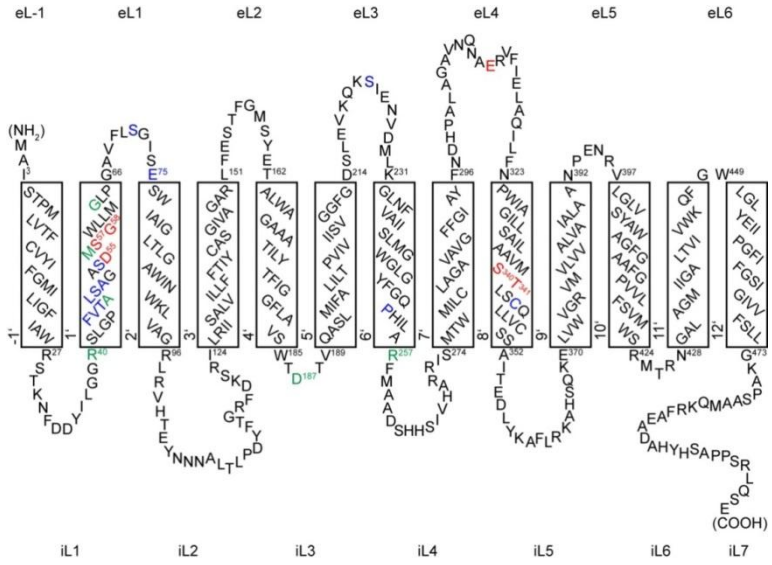

Figure 5.3: Secondary-structure model of the Na^+/proline symporter PutP. (Jung et al., 1998) (Wegener et al., 2000) The topology comprises a 13 transmembrane motif with the N-terminus facing the periplasm and the C-terminus facing the cytoplasm. For a better understanding the transmembrane segments of all members of the LeuT structural family are numbered from 1' to 10'. Therefore the N-terminal transmembrane segment of PutP is numbered as -1' and the C-terminal transmembrane segments as 11' and 12'. eL: extracellular loops, iL: intracellular loops. Residues involved in alteration are colored: Red: ligand involved, blue: ligand dependent conformational dynamics, green: structural and or functional importance.

Biochemical and spectroscopic analyses gave detailed insights into PutP's tertiary structure in which TM1' and TM8' seem to be involved in formation of a hydrophilic inward-facing cavity (Pirch et al., 2003) (Hilger et al., 2008). Cysteine labeling experiments with TM1' were carried out, which provided the first evidence for ligand dependent opening and closing of the cytoplasmic vestibule. Furthermore, it could be shown that TM1' and TM8' are located close to each other, whereas TM8' contains residues which are significant for Na^+ and proline binding (S340 and T341). These findings are in good agreement with

studies on the three-dimensional structure of the leucine transporter $LeuT_{Aa}$, which contains comparable polar residues (T354 and S355) important for Na^+ binding (Yamashita et al., 2005).

With *in vitro* and *in vivo* transport analyses, the role of amino acids for the transporter function could also be analysed. Some positions in TM1', D55, S57 and G58, suggested the involvement in Na^+ and/or proline binding (Pirch et al., 2002) (Quick et al., 1996) (Quick and Jung, 1997). In addition, it forms part of a water filled cleft that is open to the cytoplasm in the absence of ligands and closes induced by proline binding in the presence of Na^+ (Pirch et al., 2003). Furthermore, Pirch et al., (2003) identified two additional amino acids, A48 and G63, to be fundamental for transporter function. Taken together these results suggest that residues in TM1' and TM8' were involved in the translocation pathway of PutP, and important for ion and substrate binding. Moreover, residues which are located halfway across the membrane, like S340 and T341, seem to be necessary for transporter function and suggest participation in formation of the Na^+ and/or proline binding pocket.

In addition, by site directed mutagenesis further residues in the hydrophilic loop domains (iL, eL) could be identified to be of importance. Arginine R40 in the intracellular loop iL1 is suggested to be localized in close proximity to the ion binding site and to represent a residue being of major importance for Na^+ coupling to proline transport (Quick et al., 1999). On the other hand residue D187 in the intracellular loop domain iL3 might be involved in release of Na^+ into the cytoplasm (Quick and Jung, 1998). Finally, if the negatively charged residue E311 in extracellular loop eL4 is substituted by Gln or Arg, this eliminates the transporter function of PutP completely, suggesting an involvement in transporter dynamic function rather than in ligand binding (M. Raba, PhD Thesis, 2012: Bracher and Jung, unpublished results). The conformational dynamics upon ligand-binding could be observed at specific PutP sites by various spectroscopic and biochemical analyses (Wegener et al., 2000) (Jeschke et al., 2004) (Pirch et al., 2003) (Pirch et al., 2002). Effects upon ligand binding could be identified in iL1 (L37) and TM1' (F45). Binding of proline induces conformational changes in both of these regions of PutP, whereas Na^+ only has an effect on the intracellular loop (Wegener et al., 2000). Later, interspin distances measurements between positions L37 (iL1) and D187 (iL3) supported this notion by revealing an increase of the main distances upon Na^+ binding (Jeschke et al., 2004). Other parts of the protein that also have been identified to be effected by ligand binding are TM6' (P252), iL4 (R257), eL4 (D298, I315, L318) and TM8' (C344) (M. Raba, PhD Thesis, 2012; Pirch and Jung, unpublished information; Imrich and Jung, unpublished results).

Information about the tertiary structure of PutP is limited. Mainly spin labeling EPR studies contributed to todays understanding of the structural features of PutP. For example, interspin distances measurements confirmed that iL2 and eL4 are located on opposite sides of the membrane bilayer, and that iL1, iL2 and iL3 are found on the same side (Jeschke et al., 2004), in agreement with the proposed secondary structure model for PutP shown in Figure 5.3 (Jung et al., 1998) (Wegener et al., 2000).

Crystallization of vSGLT of *Vibrio parahaemolyticus* revealed first insights into the structure of SSSF transporters at atomic resolution (Faham et al., 2008). The structure implies that the SSSF shares the same fold with the LeuT structural family, a group of unrelated transporters that turned out to have a common core architecture (Abramson et al., 2003) (Yernool et al., 2004) (Schulze et al., 2010) (Faham et al., 2008) (Weyand et al., 2008) (Murakami et al., 2002) (Ressl et al., 2009) (Yamashita et al., 2005). The available structural information on vSGLT was used to compute a homology model of PutP (Olkhova et al., 2010) that is shown in Figure 5.4 A.

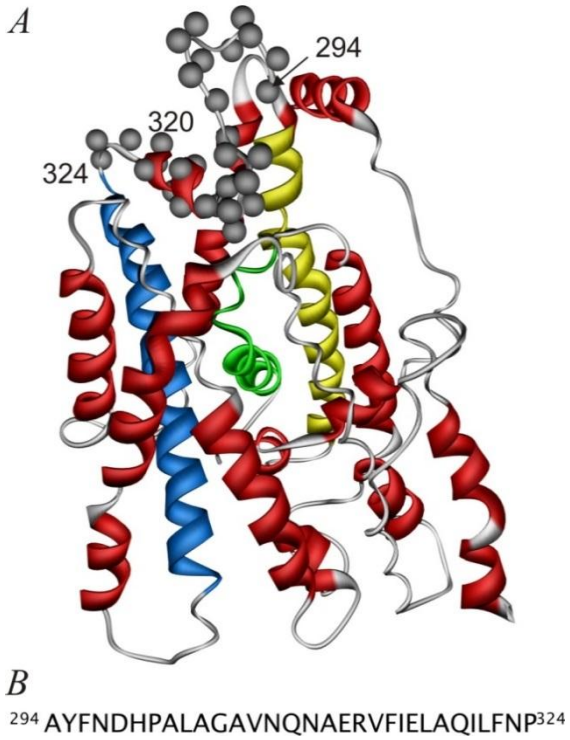

Figure 5.4: (A) PutP homology model based on the crystal structure of the sodium/galactose transporter vSGLT (Olkhova et al., 2010) in ribbon representation. Positions in eL4 are marked by spheres at the positions of the respective Cα atoms. Helices TM1' (green), TM7' (yellow), and TM8' (blue) are highlighted. (B) eL4 sequence.

Despite the increasing number of available transporter crystal structures with LeuT-like core architecture, detailed information on the protein dynamics during the translocation cycle is still quite limited. Based on the available structural information for LeuT, a molecular mechanism of function was proposed (Forrest et al., 2008) (Forrest and Rudnick, 2009). According to this model the reciprocal opening and closing of an outward- and an inward-facing cavity is achieved by a 'rocking bundle' motion of two domains formed by topologically inverted repeats, and movements of transmembrane helices (TMs) were predicted. Recently, LeuT structures in the outward- and inward facing conformation (Krishnamurthy and Gouaux, 2012) revealed major conformational alterations for TMs 1', 2', 5', 6', and 7'. Interestingly, it was shown that closing of the outward-facing cavity is not exclusively achieved by movements of transmembrane helices. In Mhp1, an α-helical domain in eL4 connecting TMs 7 and 8, contributes to the formation of a 'thick gate' that occludes the substrate binding site (Shimamura et al., 2010). The general importance of

this loop structure for the molecular mechanism of function of LeuT-like transporters was also supported by biophysical measurements in LeuT (Claxton et al., 2010). EPR spectroscopic analyses demonstrated that eL4 regulates the access from the extracellular milieu to the ion and substrate binding sites upon Na^+ and/or leucine binding. These data were supported by the comparison of crystal structures of LeuT in the outward-open and the inward-open conformation (Krishnamurthy and Gouaux, 2012). The transition of an outward-facing open to an inward-facing open conformation comes along with a substrate dependent movement of eL4 into the outward-facing cavity that occludes the binding site from the extracellular space. Furthermore, a functional role of eL4 is also described for eukaryotic representatives of this structural family, e.g. for the serotonine transporter SERT (Mitchell et al., 2004) and the γ-aminobutyric acid transporter GAT-1 (Zomot and Kanner, 2003).

5.1.4 Aim of the work

In order to provide experimental information on the structure, dynamics and functional role of the homologous loop eL4 of members of the sodium/solute symporter family (SSSF), a cysteine-scanning mutagenesis of the respective domain in PutP was performed, followed by site-directed spin labeling (SDSL) (Altenbach et al., 1989) (Altenbach et al., 1990) (Bordignon and Steinhoff, 2007) (Klare and Steinhoff, 2009) and electron paramagnetic resonance (EPR) spectroscopy. Single mutant spin label side chain's mobility, polarity and accessibility for paramagnetic quencher molecules together with inter-spin distances for a double mutant have been obtained to unravel the structure of the extracellular loop eL4 and possible structural changes thereof induced by ligand binding (Na^+ and Na^+ and proline) to PutP reconstituted into liposomes (Raba et al., 2014).

5.2 Material and Methods

Cloning, expression and purification of PutP mutants, spin labeling and reconstitution were done by the group of H. Jung at the LMU Munich, Department Biologie I, Ber. Mikrobiologie and kindly provided for EPR experiments by Dr. Michael Raba. The following single spin-labeled derivatives were analysed: A294R1, Y295R1, F296R1, N297R1, D298R1, H299R1, P300R1, A301R1, L302R1, A303R1, G304R1, A305R1, V306R1, N307R1, Q308R1, N309R1, A310R1, E311R1, R312R1, V313R1, F314R1, I315R1, E316R1, L317R1, A318R1, Q319R1, I320R1, L321R1, F322R1, N323R1, and P324R1. Double spin labeled derivate: H299R1/A318R1

5.2.1 EPR Methods

To determine the influence of the ligands on the EPR spectra, after thawing the respective proteoliposomes were supplemented with 50 mM NaCl or 50 mM NaCl and 10 mM proline, incubated over night at 4°C, centrifuged and resuspended in the appropriate buffer to yield a PutP concentration of 100 – 250 μM. As negative controls, measurements were also performed in the presence of 50 mM KCl or 50 mM KCl and 10 mM proline.

5.2.2 Mobility measurements

Spin label mobility and ligand dependent changes thereof in the EPR spectra for the different PutP R1 mutants were determined from room temperature X-band cw EPR spectra, recorded using a homemade X-band (~ 9.5 GHz) EPR spectrometer equipped with a Bruker dielectric resonator (MD5). All spectra were obtained at 0.5 mW incident microwave power and 0.15 mT B-field modulation in 0.9 mm diameter Glass capillaries loaded with 10 μl of the sample.

5.2.3 Temperature dependent measurements

Temperature dependent cw EPR spectra were analysed in terms of an equilibrium between two components with different mobilities present in the spectra at ambient temperature. The EPR spectra were recorded in the temperature range from 273 K to 303 K. The first derivative spectra were normalized to their amplitudes and compared to each other. The relative contributions of the two components were determined by means of the amplitudes in the low field region. The logarithm of the ratio of the two components was analysed in terms of the free energy ΔG by means of a van´t Hoff plot.

5.2.4 Polarity measurements

Low temperature cw-EPR measurements were carried out at 160 K on a homemade X-band EPR spectrometer equipped with a Super High Sensitivity Probehead (Bruker Biospin GmbH, Rheinstetten, Germany). The magnetic field was measured with a RMN-2 B-field meter (Drusch, Germany). A continuous flow cryostat Oxford ESR900 (Oxford Instruments, Oxfordshire, UK) was used in combination with an Intelligent Temperature Controller (ITC 4; Oxford Instruments), allowing the stabilization of the sample temperature to 160 K. The microwave power was set to 0.2 mW and the B-field modulation amplitude to 0.25 mT. EPR quartz capillaries (3 mm inner diameter) were filled with sample volumes of 40 µl. The hyperfine tensor component values A_{zz} as a measure for the polarity were determined from a detailed line shape analysis using the program Dipfit (Steinhoff et al., 1997).

5.2.5 Accessibility measurements

Accessibilities were determined for the collision reagents gaseous oxygen and NiEDDA (Ni(II)ethylenediamine diacetate) by the EPR power saturation method (Altenbach et al., 2005). 6.3 µl of sample solution were filled into gas permeable TPX (Polymethylpenten) capillaries (Rototec Spintec GmbH, Biebesheim, Germany) and the EPR spectra were recorded using a homebuilt cw EPR spectrometer equipped with a loop gap resonator. The B-field modulation was set to 0.15 mT and the applied microwave power was varied in the range from 0.1 to 50 mW. For reference measurements the sample was deoxygenated by fluxing the resonator permanently with nitrogen gas to determine the saturation behaviour in the absence of any exchange reagents. In order to obtain the accessibilities for the hydrophobic oxygen molecule, nitrogen was replaced by 100 % O_2 and the samples equilibrated before recording the EPR spectra. For determination of the spin label side chain accessibility from the aqueous phase NiEDDA with a final concentration of 20 mM was used. During the measurements a nitrogen gas flux was applied. Before each experiment the sample was fluxed with the respective gas for at least 30 min. Heisenberg exchange frequencies, W_{ex}, were calculated using the program powerfit written by Martin Kühn (Kühn, 2003).

5.2.6 Pulsed EPR spectroscopy

Pulse EPR experiments (double electron electron resonance, DEER) were performed at X-band frequencies (9.3–9.4 GHz) on a Bruker Elexsys 580 spectrometer equipped with a Bruker Flexline split-ring resonator ER 4118X-MS3. 2.4 mm inner diameter EPR quartz capillaries were loaded with 30-40 µl protein with a final concentration of 10% deuterated glycerol. For temperature control a continuous flow helium cryostat CF935 (Oxford Instruments) regulated by an Oxford temperature controller ITC 503S was used. All measurements were performed using the four-pulse DEER sequence: $\pi/2(\upsilon_{obs})$ - τ_1 – π (υ_{obs}) – t' – π (υ_{pump}) – $(\tau_1 + \tau_2 - t')$ – π (υ_{obs}) - τ_2 – echo (Martin et al., 1998) (Pannier et al., 2000). For the DEER pulses at the observer frequency the ‹x› channels were used. A two-step phase cycling (+ ‹x›, - ‹x›) was performed on $\pi/2(\upsilon_{obs})$. Time t' was varied, whereas τ_1 and τ_2 are kept constant, and the dipolar evolution time is given by $t = t' - \tau_1$. Data were analysed only for $t > 0$. The resonator was overcoupled to $Q \sim 100$; the pump frequency υ_{pump} was set to the center of the resonator dip and coincided with the maximum of the nitroxide EPR spectrum, whereas the observer frequency υ_{obs} was ~67 MHz higher and coincided with the low field local maximum of the spectrum. All measurements were performed at a temperature of 50 K with observer pulse lengths of 16 ns for $\pi/2$ and 32 ns for π pulses and a pump pulse length of 12 ns. Proton modulation was averaged by adding traces at eight different τ_1 values, starting at $\tau_{1,0}$ = 200 ns and incrementing by $\Delta\tau_1$ = 8 ns. Analysis of the DEER traces was performed with the software DeerAnalysis 2011 (Jeschke et al., 2006). Briefly, the phase corrected dipolar evolution data was background corrected assuming a homogeneous 2D background, and distance distributions were obtained by Tikhonov regularization with the regularization parameter α chosen based on the L curve criterion.

All resulting EPR datasets were handled and analysed as described in chapter 3.2.5 and 3.2.6

5.3 Results and Discussion

First insights into the architecture of the SSSF proteins were gained by the X-ray crystal structure of the sodium-coupled galactose symporter vSGLT of *Vibrio parahaemolyticus* (Faham et al., 2008). This structure was used to compute a homology model of PutP (Olkahova et al., 2011). Examination of this model together with data from several EPR studies (Wegener et al., 2000) (Hilger et al., 2008) (Hilger et al., 2009), as well as recent crystallographic and EPR investigations on the cognate bacterial homolog of a neurotransmitter: sodium symporter, LeuT (Claxton et al., 2010), lead to the proposal that helices VIII and IX as well as the interconnecting loop eL4 determine the accessibility of the periplasmic cavities which bind sodium and proline.

To elucidate the structure and ligand-induced dynamics of eL4, we performed a cysteine scanning mutagenesis and subsequent site-directed spin labeling with each individual loop position in combination with EPR spectroscopy. Analyses of spin label mobility and polarity as well as accessibility to paramagnetic quenchers will allow to refine this region in the present homology model, especially concerning the extent of an α-helical segment oriented approximately perpendicular to the transmembrane helices.

5.3.1 Structural features of eL4 in the absence of ligands

A detailed analysis of the structural features of eL4 was carried out using four parameters: (i) the mobility of the R1 side chain from room temperature cw EPR spectra, quantified by means of the reciprocal width of the central resonance line, ΔH_0^{-1}, (ii) the polarity of the spin label microenvironment, determined via the hyperfine coupling tensor element A_{zz} obtained from low temperature (160 K) cw-EPR spectra, (iii) the accessibility towards molecular oxygen (by means of the exchange frequency W_{ex}), reflecting the accessibility to the membrane lipids; and (iv) the accessibility towards the nickel complex NiEDDA, quantifying the accessibility of the spin label side chain from the aqueous phase.

5.3.1.1 Analysis of the spin label mobility in the apo state

The mobility of the R1 nitroxides can provide information about the protein's structure. Residues attached to a helix surface or located in loop regions reveal a high mobility. In contrast, R1 side chains bound in the protein's interior are strongly immobilized. In a first set of experiments, X-band cw EPR spectra of all spin labeled PutP variants have been recorded at 298 K (Fig. 5.5). All room temperature cw EPR spectra of PutP carrying spin labels in eL4 reveal the presence of at least two spectral components characterized by different mobilities (indicated by i = immobile and m = mobile for A294R1). This can be a result of inhomogeneous structural constraints in the microenvironment of the spin label leading to different stable spin label conformations (Hubbell et al., 1996) (Langen et al., 2000) or different protein conformations in equilibrium. This issue will be discussed later.

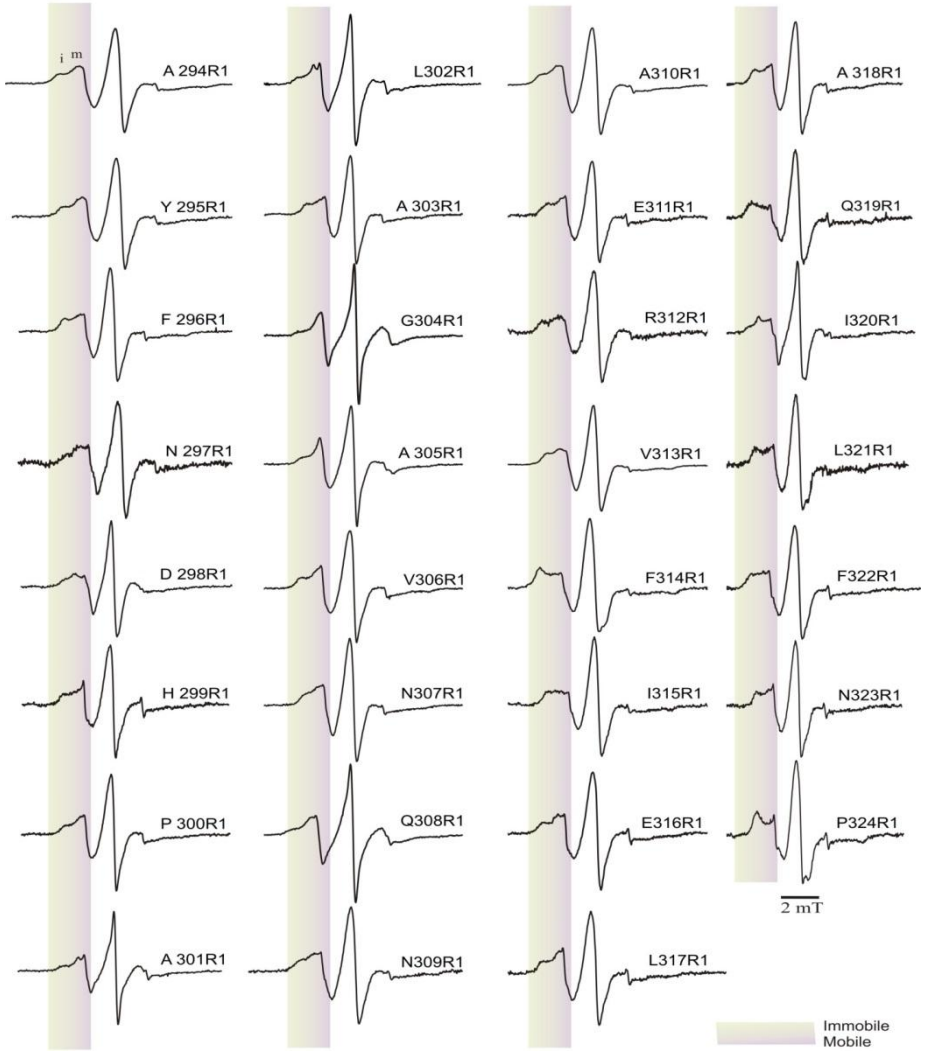

Figure 5.5: X band room temperature cw EPR spectra of eL4 in the ligand-free (apo) state. The spectra were normalized by their amplitudes. Residue number is given on the right side for each spectrum. Bars are placed at the low field spectral line to visualize the mobile and immobile components.

As a measure for the mobility of the spin probe attached to the respective thiol group, the reciprocal width of the central resonance line is shown in Fig. 5.6 as a function of sequence position. Inspection of the mobility profile reveals two distinct subdomains. The most mobile R1 side chains (ΔH_0^{-1} = ~ 2.8-4.3 mT^{-1}) in the absence of any ligand are found at positions 298-302, 304-306, and 308. For all other label positions similar, intermediate mobilities characterized by ΔH_0^{-1} values between 2.0 and 2.7 mT^{-1} are observed, indicating tertiary contacts. Furthermore, the mobility values for of the more mobile region 298-308 display a clear periodical pattern with a periodicity ~ 3.6 (indicated by the thick grey line in Fig. 5.6), taken together indicative for a surface exposed α-helix. A similar periodicity pattern, although much less expressed, can also be found in the region flanked by positions 310 and 318. Mobility values and pattern are in line with an α-helix involved in several tertiary contacts. An α-helical secondary structure for this part of eL4 (residues 313 to 317) has already been proposed from the vSGLT-based PutP homology model (Olkhova et al. 2010).

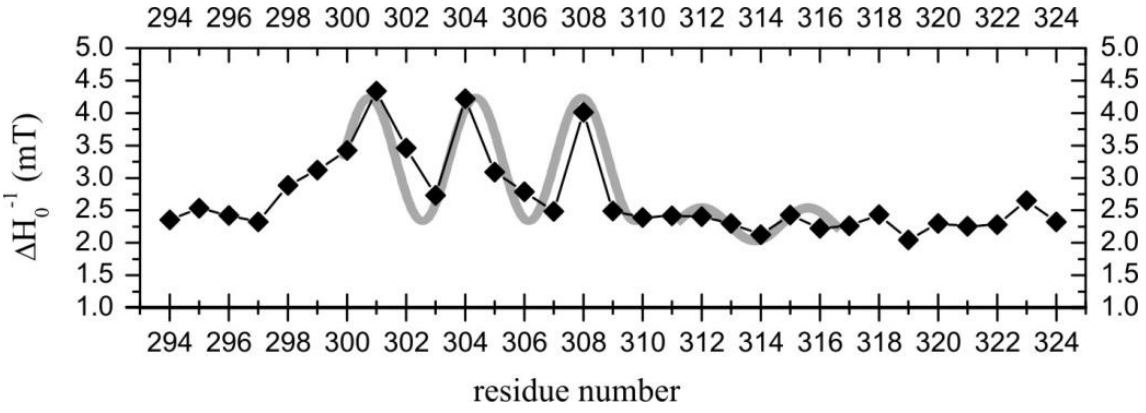

Figure 5.6: Cw EPR analysis of eL4 in the ligand-free (apo) state. Mobility parameter ΔH_0^{-1}; the estimated error is ±0.01 mT^{-1} due to uncertainties of the line width determination in the presence of multiple components (cf. Fig. 5.5).

5.3.1.2 Analysis of the spin label polarity in the Apo state

In the next part of this study the hyperfine coupling tensor element A_{zz} as a measure for the polarity of the R1 side chain's environment has been obtained from low temperature (160 K) cw-EPR spectra (Fig. 5.13). The resulting polarity profile for eL4 in the absence of ligands is shown in Figure 5.7. Only position 298 exhibits an A_{zz} value characteristic for residues fully exposed to the bulk water phase (A_{zz} = 3.6-3.7 mT) (Steinhoff et al., 2000) (Plato et al., 2002). The polarity profile displays strong variations with A_{zz} values ranging from 3.37 mT (pos. 319) to 3.64 mT (pos. 298), and reveals two subdomains with different mean polarities. The N-terminal part of eL4 (294-305) is located in a more polar environment ($\bar{A}_{zz}$ = 3.52 mT) than the C-terminal part (306-324, $\bar{A}_{zz}$ = 3.46 mT). Furthermore, as already observed in the mobility analysis, periodical patterns are also observed in the polarity profile. Both subdomains exhibit clear

patterns with periodicities of ~ 3.6 as indicated by the harmonic graphs in Figure 5.7. In the N-terminal region, the periodicity is not as pronounced as in the succeeding part. Consequently, the polarity analysis indicates the presence of two α-helical segments with different environmental polarity and involvement in tertiary contacts.

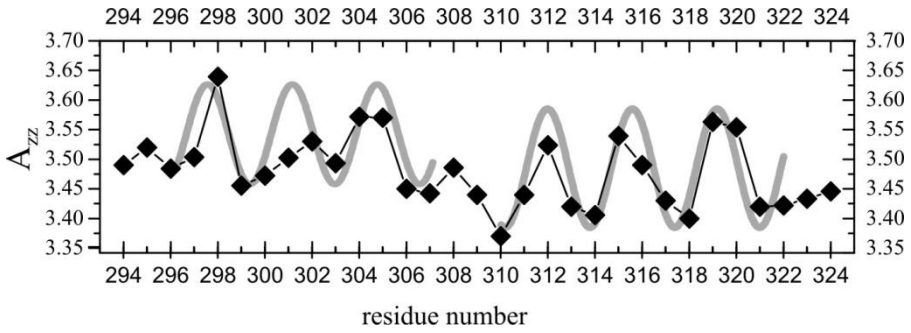

Figure 5.7: Cw EPR analysis of eL4 in the ligand-free (apo) state). Polarity parameters A_{zz} determined from the fitting of simulated spectra to the experimental ones obtained at 160 K.

5.3.1.3 Analysis of the spin label accessibility in the Apo state

In the third set of experiments, accessibility measurements have been carried out to supplement the interpretation of the mobility and polarity data. The Heisenberg exchange frequencies W_{ex} have been determined in the presence of oxygen (100 %) and 20 mM NiEDDA by cw EPR power saturation measurements. A spin label at a water exposed site is associated with a large exchange frequency with NiEDDA and a low accessibility for oxygen, whereas a higher accessibility for oxygen indicates a spin label located in the membrane interior. Buried sites are characterized by low collision frequencies for both quenchers. The accessibility profiles for oxygen and Ni are shown by means of the respective W_{ex} values in Figure 5.8. The Ni-accessibility profile reveals the same two-subdomain organization of eL4 as the mobility and polarity profiles. The two regions of α-helical periodicity are characterized by different Ni-accessibilities and thus different exposure to the bulk water phase. The same periodical patterns are observed in the oxygen-accessibility profile, where the different environments of the two subdomains are also reflected in different mean oxygen accessibilities, but less expressed compared to Ni.

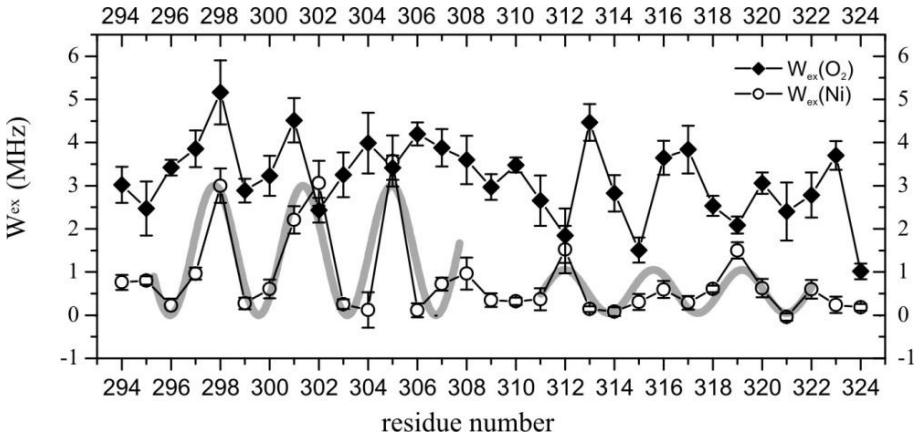

Figure 5.8: Cw EPR analysis of eL4 in the ligand-free (apo) state). Accessibilities for oxygen (100 %) and NiEDDA (20 mM) in terms of the Heisenberg exchange rates, W_{ex}.

The combined results from the mobility, polarity and accessibility analyses provide strong indications that eL4 comprises two α-helical segments, one in the N-terminal half (residues 295/296-306/307, in the following denoted eL4a) and one in the C-terminal half (residues 311/312-321/322, eL4b). Furthermore, eL4b appears to be significantly more closely associated to the rest of the protein than eL4a. As already described all of these spectra reveal the presence of two spectral components and it has to be taken into account that the peak-to peak line width is dominated by the mobile component even though it is the minor one.

5.3.2 Structural changes upon binding of Na^+ and/or proline

5.3.2.1 Analysis of the spin label mobility upon ligand binding

To track the dynamics of eL4 during the transport cycle, the influence of Na^+ and/or proline binding on spin label mobility, polarity and accessibility were tested. Room temperature cw EPR spectra recorded in the presence of Na^+ and/or proline reveal only slight changes in the EPR spectral shape (Fig 5.9) and therefore small changes in ΔH_0^{-1} (Fig 5.10). Significant changes in spin label side chain mobility upon ligand binding are only observed for positions 298 (Na^+/P: ΔH_0^{-1} = + 0.57 mT^{-1}), 300 (Na^+/P: + 0.48 mT^{-1}), 305 (Na^+/P: + 0.43 mT^{-1}), 306 (Na^+/P: + 0.47 mT^{-1}), and most expressed for positions 314 (Na^+: -0.85 mT^{-1}, Na^+/P: - 0.94 mT^{-1}) and 320 (Na^+/P: + 0.79 mT^{-1}) in eL4b. In general, the mobility of the spin label side chains was less affected by binding of Na^+ alone compared to the influence of Na^+ and proline. Furthermore, addition of Na^+ alone causes weak and unsystematic changes of spin label mobility in both directions, whereas Na^+/proline resulted with few exceptions (295, 302 and 314) in increased mobilities of the spin labels.

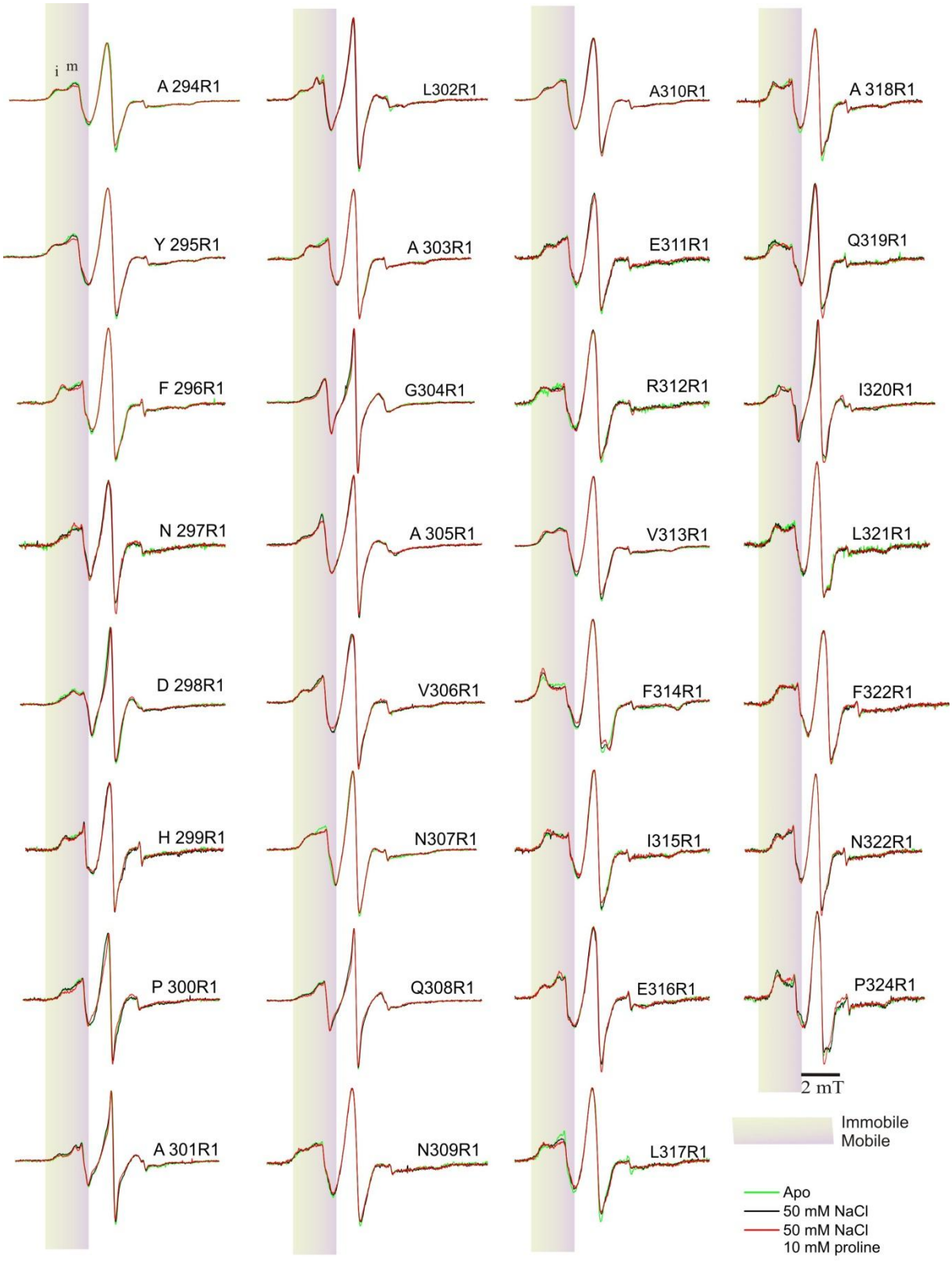

Figure 5.9: X band room temperature cw EPR spectra of eL4 in the presence of ligands (50 mM Na^+ and 50 mM Na^+/10 mM proline). The spectra were normalized by their amplitudes. Residue numbers are given on the left side for each spectrum. Bars are placed at the low field spectral line to visualize the mobile and immobile components.

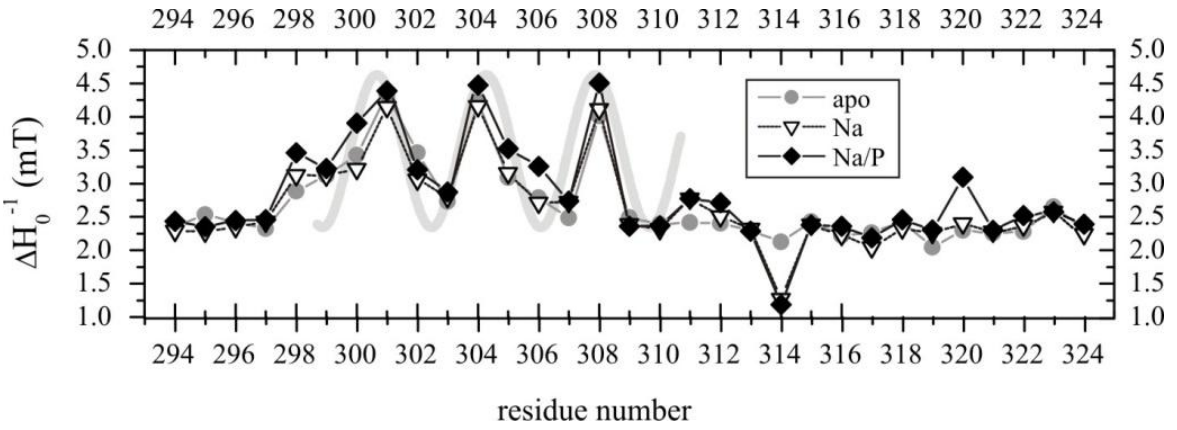

Figure 5.10: Cw EPR analysis of eL4 in the presence of ligands (50 mM Na^+ and 50 mM Na^+/10 mM proline). Mobility parameter ΔH_0^{-1}, the estimated error is ±0.01 mT^{-1} due to uncertainties of the line width determination in the presence of multiple components.

Most cw RT EPR spectra of spin labeled PutP variants, exhibit at least 2 components characterized by different mobilities. Since the reciprocal central line width is strongly biased by the mobile component of the spectrum, for a more precise interpretation of spin label dynamics the inverse of the spectral breadth (second moment, $<H^2>^{-1}$) was calculated from all cw RT EPR spectra. In contrast to the inverse central linewidth, the inverse second moment reflects the influence of the immobile component rather than the mobile component.

In Figure 5.11, the spectral second moment is plotted *versus* the inverse linewidth for each position in the apo state (Fig. 5.11 A), and in the presence of Na^+ (Fig. 5.11 B) and Na^+/proline (Fig. 5.11 C). The correlation between these two parameters allows a general classification of regions accommodating buried, surface-exposed, or loop residues as indicated in Figure 5.11 (Bordignon and Steinhoff, 2007).

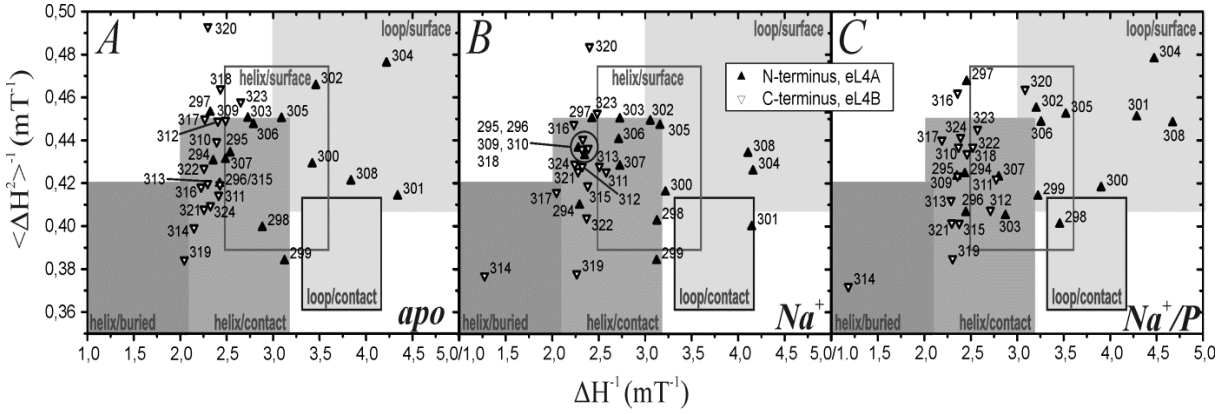

Figure 5.11: Two-dimensional mobility plot of the inverse of the second moment *versus* the inverse of the central linewidth for eL4 in the absence (A) and presence of ligands (50 mM Na^+ (B) and 50 mM Na^+/10 mM proline (C)). Topological regions of the protein according to (Isas et al., 2002) and (Mchaourab et al., 1996) are indicated by boxes.

The 2-dimensional mobility plots reveal most residues to be located in helix/contact and helix/surface regions. Exceptions are positions 300-302, 304 and 308 on eL4a. These residues show significantly higher mobilities and are also most affected by substrate binding. Strikingly, immobilization of spin label side chains at these positions imposed by sodium binding seems to be largely reverted by additional binding of proline. Another striking feature visible from the 2D plots is the behavior of position 314. In the apo state it is located in the borderline area between the helix/buried and helix/contact regions. Upon addition of sodium it exhibits, as already seen from the mobility plot in Fig. 5.10, strong immobilization that is even enhanced in the additional presence of the second substrate proline. In line with these observations are the very low accessibilities for the spin label at this position towards both oxygen and NiEDDA, indicating this side chain to be deeply buried in the protein interior (Fig. 5.14 A, B).

Interestingly, this residue, F314, appears to be "locked" in a hydrophobic pocket in the PutP homology model (Olkhova et al., 2010), suggesting that the homology model might represent PutP in a substrate bound form and furthermore that F314 might play a key role in stabilizing the substrate bound conformations of eL4.

5.3.2.2 Analysis of the spin label polarity upon ligand binding

In Figure 5.12 the results of the polarity measurements in the presence of ligands are shown. In general, addition of Na^+ causes only slight changes in A_{zz} (max. - 0.06 mT for position 305). The N-terminus (295-298, in eL4a) experiences a slightly less polar environment, but for H299R1 the environmental polarity increases. Contrarily, the stretch 306-314 (mostly eL4b), succeeding residue 305, that exhibits the most expressed shift towards a more apolar environment is shifted to a more polar region. The additional presence of the substrate proline leads to an overall shift for almost all residues (exceptions are D298R1, A305R1 and I320R1) to a more polar, i.e. more surface-exposed region.

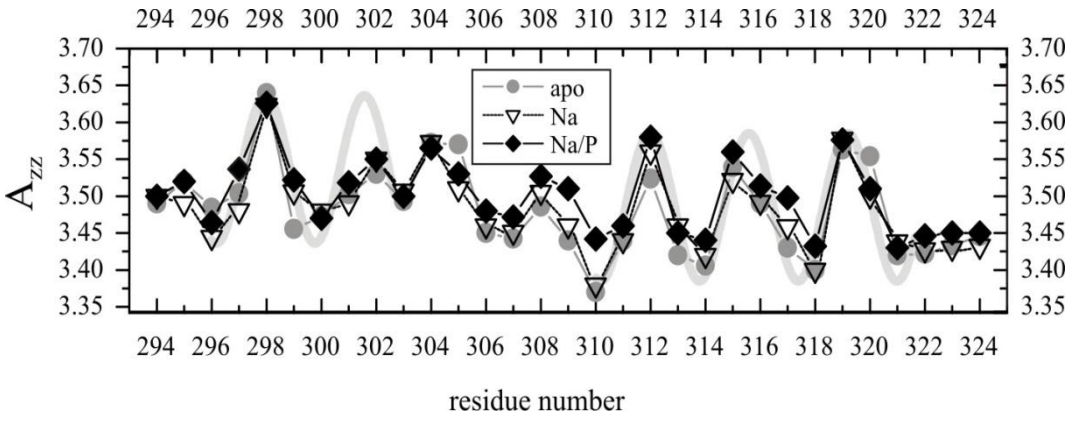

Figure 5.12: Cw EPR analysis of eL4 in the presence of ligands (50 mM Na^+ and 50 mM Na^+/10 mM proline). Polarity parameters A_{zz} determined from the fitting of simulated spectra to the experimental ones obtained at 160 K.

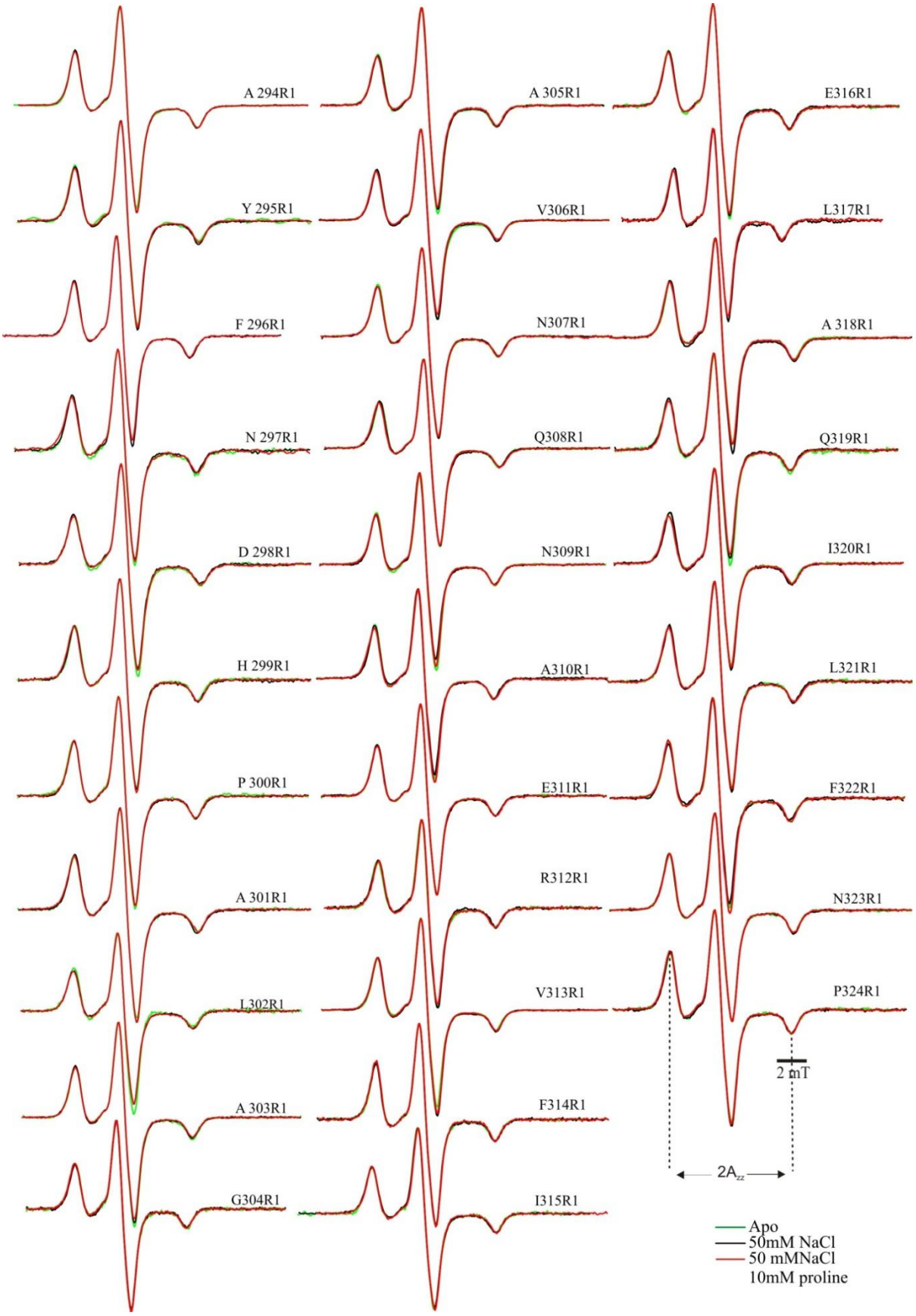

Figure 5.13: Low temperature (160 K) EPR spectra of eL4 in the apo state and in the presence of ligands (50 mM Na^+ and 50 mM Na^+/10 mM proline). Residue numbers are given on the left side for each spectrum.

5.3.2.3 Analysis of the spin label accessibility upon ligand binding

Accessibility measurements with spin labeled PutP derivatives in the presence of Na^+ reveal a strong increase in oxygen accessibility (Fig. 5.14) for residues in eL4b (positions 309-311, 313, 315-322 and 324), but much weaker and less systematic changes for eL4A ($\Delta W_{ex}(O_2) < 0$: 294-301, 303; $\Delta W_{ex}(O_2) > 0$: 302, 304-308). The additional presence of the second substrate proline had a largely contrary impact on the oxygen accessibilities. In the N-terminal part, eL4a, positions 297-300 now experience increased oxygen accessibilities, whereas for the remaining positions either no changes compared to Na^+ alone or only slight further changes in the same direction are observed. In the C-terminal part, eL4b, addition of proline leads to oxygen accessibilities more similar to the apo state, although most W_{ex} values tend to be slightly reduced in the presence of both substrates. The accessibilities towards the water-soluble NiEDDA complex are in general more affected by Na^+ alone, leading to increased W_{ex} values in most cases. Exceptions are D298R1, A305R1 and A318-I320, being those residues that already showed an exceptional behavior in the polarity analysis. In the presence of both ligands either no additional changes in Ni accessibility are observed, or the W_{ex} values are more similar to those in the apo state. Exceptions are positions 299-301 and 308 that show a significant further increase in Ni accessibility in the presence of proline.

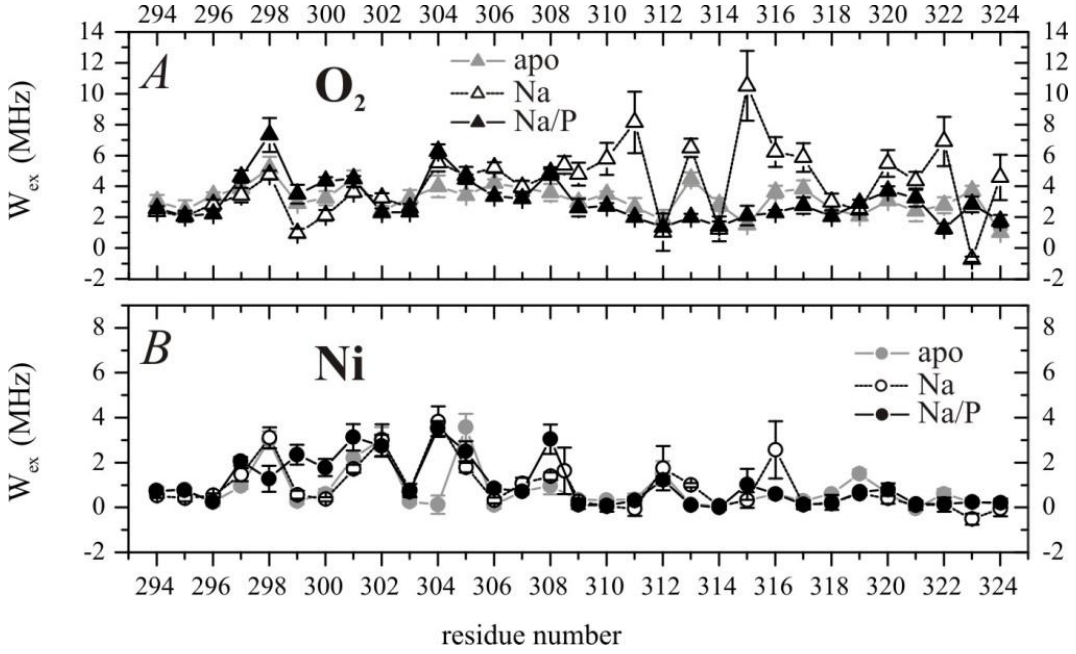

Figure 5.14: Cw EPR analysis of eL4 in the presence of ligands (50 mM Na^+ and 50 mM Na^+/10 mM proline). (A) Accessibilities for oxygen (100 %) in terms of the Heisenberg exchange rates, W_{ex}. (B) Accessibilities (W_{ex}) for NiEDDA (20 mM).

Interpretation of the accessibility data in terms of localization of the respective side chain with respect to the rest of the protein is not straightforward, as the accessibility of a spin label side chain is influenced not only by steric aspects, i.e. here the close interaction of eL4 with the rest of the protein, limiting oxygen and NiEDDA diffusion around the side chain under investigation. PutP is a membrane spanning protein and therefore the vicinity of the hydrophobic core of a lipid bilayer has also strong influence on the local oxygen and NiEDDA concentrations. In case of possible motions of eL4 perpendicular to the membrane plane these two effects might counteract each other and mask conformational changes to a certain extent.

Inspection of the mobility, polarity and accessibility traces in in terms of secondary structure reveals that the periodical patterns characteristic for α-helical structures persist also in the presence of substrates. Even though the addition of Na^+ and/or proline led to changes in the mobility, polarity and most expressed in oxygen accessibility, no structural rearrangements within the putative α-helical structures seem to take place. The data rather suggest ligand-induced movements of eL4 as a rigid body and that the observed changes are due to changes in the interaction between eL4 and the rest of the protein.

5.3.3 Probing structural changes of eL4 with DEER spectroscopy

To further probe the influence of substrate binding on the structure and function of eL4, a double-cysteine mutant was measured comprising cysteine substitution for residues H299 and A318, predicted to be located in the second helical turn of eL4a and the second-last helical turn of eL4b, respectively, to monitor the relative alignment of the two predicted α-helices in the absence and in the presence of substrate(s). After spin labeling pulsed EPR interspin distance measurements applying the double electron-electron resonance (DEER) technique have been carried out. The distance distribution (Fig. 5.15 B) obtained by Tikhonov regularization of the background corrected DEER time domain trace (Fig. 5.15 A) exhibits two populations centered at 2.7 and 3.8 nm. Even though the oligomeric state of PutP still remains to be elucidated, previous EPR studies applying DEER spectroscopy revealed no evidence for intermolecular spin-spin interactions (Jeschke et al., 2006). Therefore both distance populations have to result from intramolecular spin-spin couplings and the observed bimodal distance distribution must result either from two protein conformations in equilibrium or from two discrete rotamer populations imposed by strongly anisotropic secondary and tertiary contacts for the spin label side chain at least at one of the two labeled sites.

The addition of the substrates Na^+ or Na^+ and proline causes only minor changes in the DEER traces and resulting distance distributions (Fig. 5.15).

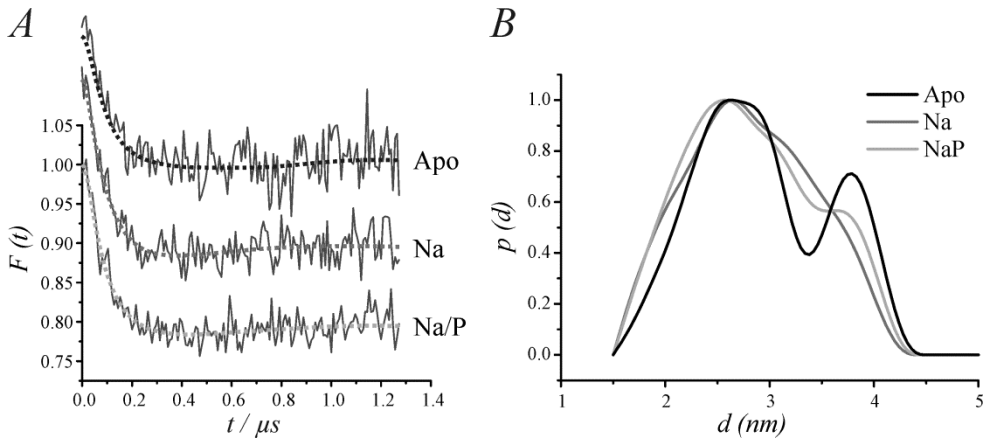

Figure 5.15: DEER PutP299/318, apo, Na^+ and Na^+P. (A) Background corrected DEER time traces. Background correction has been performed assuming a 2-dimensional distribution of the PutP molecules on the unilamellar vesicles. The fits to the experimental data (dotted lines) have been performed by Tikhonov regularization (B) Distance distributions obtained by Tikhonov regularization corresponding to the fits shown in (A).

This observation implies that the relative arrangement of the two helices largely persists during the conformational changes induced by substrate binding. The minor changes observed in the distance distributions, namely a slight decrease of both distances in the bimodal distribution by 1-2 Å and a change in their relative contributions could be caused by changes of the spin label side chain environment and consequently its motional freedom induced by substrate-induced motions of eL4 as a rigid body.

In the present study mobility, polarity and accessibility parameters were determined for spin label probes attached at all positions within the extracellular loop eL4 of membrane-reconstituted PutP for the apo and substrate bound states. Based on the observed clear periodicity of 3.6 residues found for almost all of the EPR parameters determined we identified, contrary to the homology model of PutP, that predicted just one α-helical domain from V313 to G319 (Olkhova et al., 2010), two α-helical regions within eL4. The first helix spans residues 295/296-306/307 (eL4a) and the second helix is found to include residues 311/312-321/322 (eL4b). This observation further links the sodium/proline symporter PutP to other members of the SSSF, namely the sodium/glucose transporter vSGLT, where two such α-helices (EL8a and EL8b) in the homologous loop domain were identified (Faham et al., 2008). Furthermore, crystal structures of LeuT, a member of a family of unrelated transporters that share the same fold with the SSSF, showed the presence of two short α-helices also named eL4a and eL4b (Abramson et al., 2003) (Yernool et al., 2004) (Schulze et al., 2010) (Faham et al., 2008) (Weyand et al., 2008) (Murakami et al., 2002) (Ressl et al., 2009) (Yamashita et al., 2005), indicating that two α-helices are a common feature in the corresponding loop domains, except for Mhp1 and BetP in which only one secondary structural element was observed. Also biochemical studies on the homologous loop in the serotonin transporter SERT, a

eukaryotic representative of this structural family, identified two α-helical domains, connected by a hinge (Mitchell et al., 2004).

A functional role of eL4 has been described for almost all representatives of this structural family. A cysteine-accessibility analysis of SERT supports the idea that eL4 undergoes conformational alterations during the transport cycle (Mitchell et al., 2004). As observed for LeuT and Mhp1, a direct participation of any residue of eL4 in substrate binding could not be shown, but it has been proposed that this region together with the two flanking transmembrane helices determine the accessibility of the periplasmic cavities which bind the substrates. For LeuT such a functional role for eL4 has been proposed based on the results of another SDSL EPR study (Claxton et al., 2010), where motions of eL4 during transport have been identified *via* inter spin distance measurements. Furthermore, recently obtained crystal structures of LeuT in different states of the transport cycle (Krishnamurthy and Gouaux, 2012), provided valuable insights into the putative function of eL4 as part of an extracellular gate determining substrate accessibility. The transition of an outward-facing open to an inward-facing open conformation comes along with a substrate dependent movement of eL4 into the outward-facing cavity that occludes the leucine binding site from the extracellular space. A similar mechanistic role of the corresponding loop was also proposed for the eukaryotic γ-aminobutyric acid transporter GAT-1 (Zomot and Kanner, 2003). The authors found that at least parts of eL4 are involved in structural rearrangements during transport, but in contrast to SERT, LeuT and Mhp1, a direct or indirect participation in GABA interaction has been suggested.

The data obtained for PutP in the presence of the substrates sodium and sodium/proline further supports this functional role of eL4 in the transport cycle. Analysis of the changes observed in mobility, polarity and accessibility upon substrate binding unambiguously reveals structural alterations without significant disturbance of secondary structure, namely the two helical segments eL4a and eL4b. Furthermore, inter spin distance measurements between two positions located on eL4a and eL4b, respectively, suggest that not only the secondary structure of eL4 is largely preserved during transport, but also the relative arrangement of the two α-helices remains largely unaltered.

5.3.4 Analysis of the spectral two-component system for PutP

As already mentioned and visible from Figures 5.5 and 5.9, all room temperature spectra of PutP carrying the spin label in eL4 reveal the presence of at least two spectral components characterized by different mobilities. The presence of two resolved components, a mobile and an immobile one, could also be observed for specific residues of other membrane proteins like KcsA, Rhodopsin (Kroncke et al., 2010) and Bacteriorhodopsin (Steinhoff et al., 2000). As an example position 165R1 in BR exhibits an equilibrium between two spinlabel populations with different mobilities (Steinhoff et al., 2000). Therefore the presence of these spectral components in eL4 of PutP can be a result of inhomogeneous structural

constraints in the microenvironment of the spin label leading, to different stable spin label conformations (Hubbell et al., 1996) (Langen et al., 2000) or different protein conformations in equilibrium. As also mentioned for colicin A in chapter 3, it seems very unlikely that the spectral components are only caused by different rotamer conformations in all 30 examined PutP derivates.

5.3.4.1 Influence of the temperature on the spectral features in the Apo state

In order to get more insights, temperature effects on the spectral features of 14 specific residues of eL4 in PutP in the absence of ligands were analysed by cw EPR. The cw EPR spectra were recorded in the temperature range from 273 K to 303 K. As already visible from Figure 5.16, lowering the temperature leads to an increase of the immobile (i) component and a concomitant decrease of the mobile (m) component, thereby shifting the equilibrium between the two conformations.

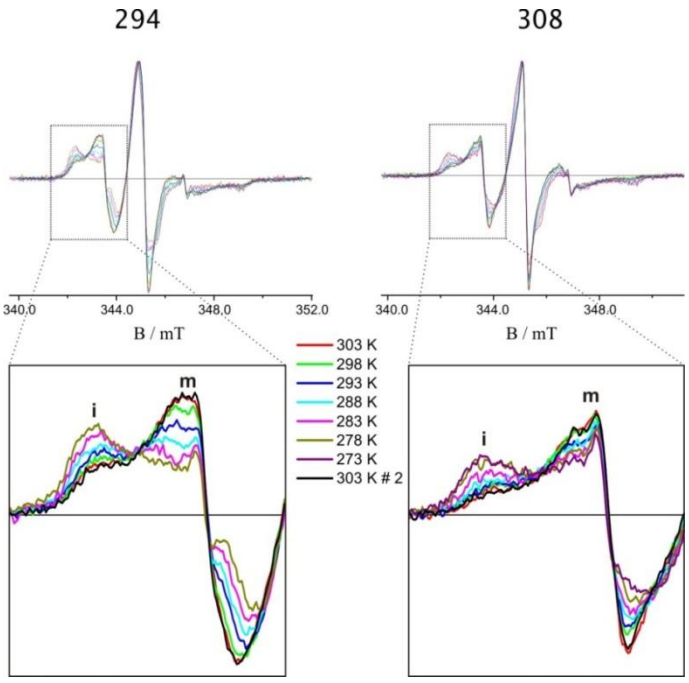

Figure 5.16: Temperature influence on spectral features of the reconstituted eL4 residues in PutP. The spectra were recorded in the temperature range from 273 K to 303 K. As example for the cw spectra the residues 294 and 308 are presented. Lowering the temperature leads to an increase of the immobile (i) component and a concomitant decrease of the mobile (m) component.

From the temperature dependent spectra the ratios between the mobile and immobile components have been determined by means of their amplitudes, as it could be shown by fitting selected spectra (data not shown) with the program multicomponent (Altenbach, Altenbach/labview-programs/epr-programs/multicomponent) that the amplitude ratios are equal to the spin number ratios.

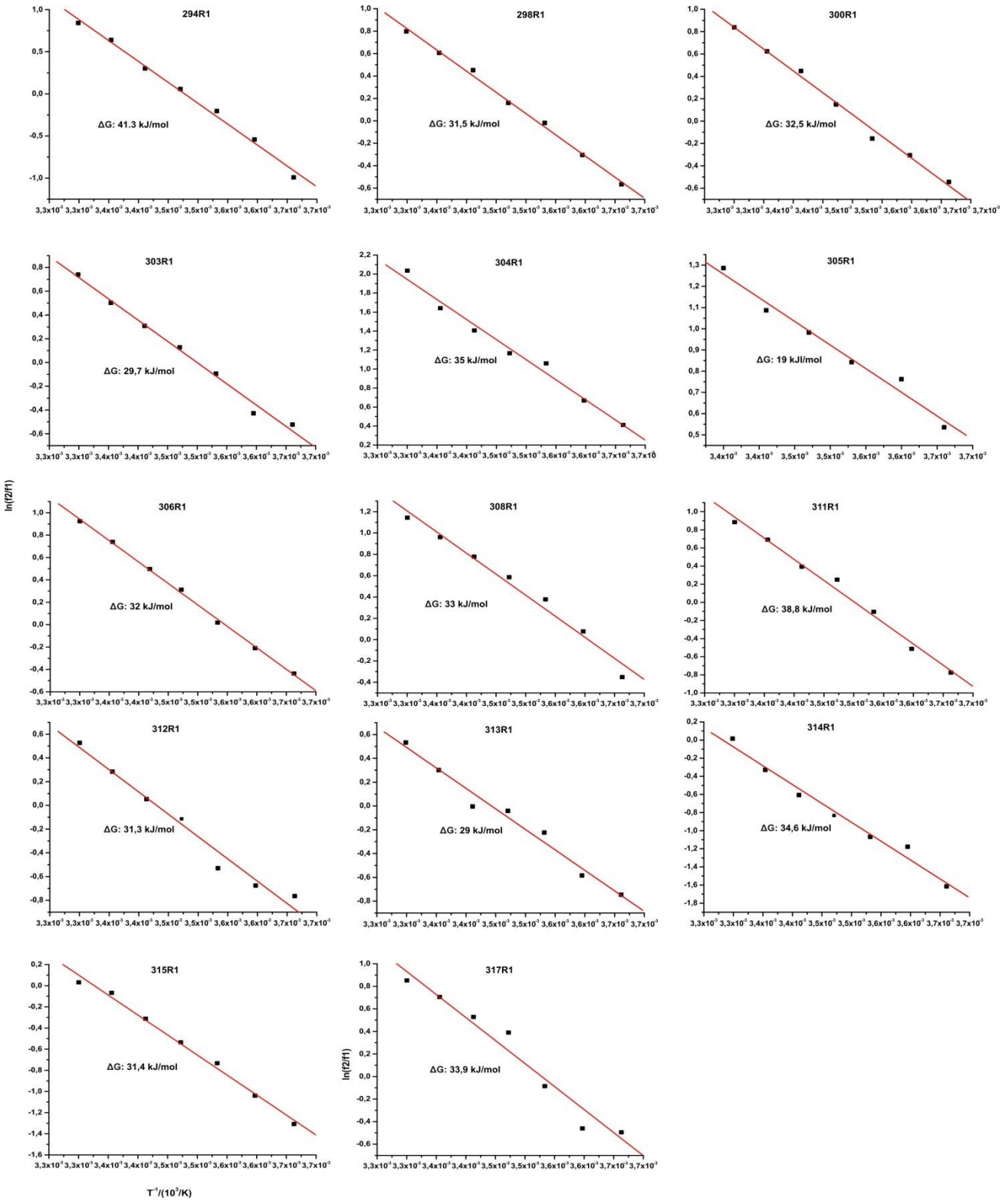

Figure 5.17: Plots of the natural logarithm of the ratio of the two conformations represented by the two spectral components, ln f_2/f_1 (determined from the amplitudes of the components in the temperature dependent cw EPR spectra), *versus* the inverse of the temperature (van´t Hoff plots) for the investigated PutP variants. The resulting ΔG values in kJ/mol are given in the respective plots.

Plots of the natural logarithm of the ratio of the two conformations represented by the two spectral components, in f_2/f_1, versus the inverse of temperature (van´t Hoff plots, Figure 5.17) provide the ΔG values for the transition between the two states representing the two components in thermodynamic equilibrium (Figure 5.18).

The ΔG values for positions in eL4 vary between 29.0 – 41.3 kJ/mol (7-10 kcal/mol) with the only exception for position 305 whith a ΔG value of about 19 kJ/mol (4.5 kcal/mol). Kroncke et al. (2010) suggested that ΔG values of about 4 kcal/mol correspond to different side chain rotamers at a helical site, explained by the observed nontraditional hydrogen bond contributing approximately 2 kcal/mol, and the stability of the conformer in the crystal structure due to the buried surface area another ~2 kcal/mol (Kroncke et al., 2010). For position I204R1 of LeuT a ΔG value of 7 kcal/mol was observed and the authors suggested that this energetic difference between the two populations is closer to the expected value of side chain rotamers, although they do not exclude that secondary or tertiary changes of LeuT takes place which could also be contribute to the population enthalpy difference.

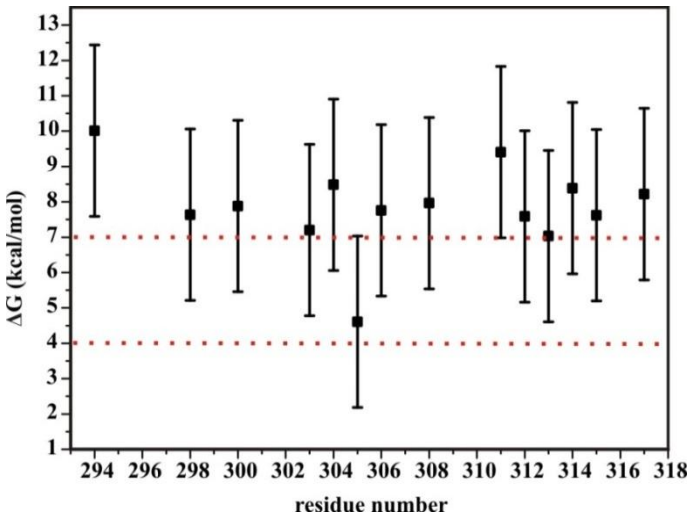

Figure 5.18: ΔG values in kcal/mol for the different PutP positions. The range corresponding to the value for different side chain rotamers is marked with red dotted lines (Kroncke et al., 2010).

The predominately identical ΔG values of about 29.0- 41.3 kJ/mol (7-10 kcal/mol) for positions on eL4 determined in this study, being significantly larger than 4 kcal/mol, thus imply that the two spectral components may arise from an equilibrium between different protein conformations rather than from a spin label side chain rotamer equilibrium. However, the existence and contribution of the latter cannot be completely excluded. For position 305, showing an exceptional low ΔG value, the presence of both equilibria with opposing energy trends for the conformational transition of the protein and the resulting label side chain rotamer transition can be assumed.

5.4 Summary

PutP is an integral membrane protein located in the cytoplasmic membrane of *Escherichia coli*, being responsible for the coupled transport of Na^+ and proline in a 1:1 stoichiometry. It belongs to the family of sodium solute symporters (SSSF). Three dimensional structural data for PutP are at the moment not available, but a homology model has been developed based on the crystal structure of another member of this protein family, the Na^+/galactose symporter vSGLT of *Vibrio parahaemolyticus* (Olkhova et al., 2011). In this chapter a site directed spin labeling electron paramagnetic resonance investigation on the sodium/proline symporter PutP part eL4 is described that was carried out to elucidate its structural and functional features. A series of spin-labeled mutants (kindly provided by Dr. Michael Raba, LMU Munich) was engineered to analyse the structure of eL4 in PutP, and its functional relevance compared with other members of this protein family.

The results obtained in this work reveal a clear periodicity of 3.6 residues corresponding to an α-helix for almost all of the EPR parameters like mobility, polarity and accessibility for two region. The first helix of eL4 in the N-terminal part, eL4a, spans positions 296-306, whereas the second, C-terminal helix, eL4b, comprises positions 312-321. Therefore eL4 in PutP forms a helix-loop-helix structure. This observation is in agreement with observations for other members of the of the SSSF, like the sodium/glucose transporter vSGLT, which contains two such α-helices (EL8a and EL8b) in the homologous loop domain (Faham et al., 2008) (Watanabe et al., 2010). Furthermore, crystal structures of LeuT, a member of a family of unrelated transporters that share the same fold with the SSSF, showed the presence of two short α-helices also named eL4a and eL4b (Abramson et al., 2003) (Yernool et al., 2004) (Faham et al., 2008; Murakami et al., 2002). An α-helical structure like eL4b in PutP seems to exist in all protein structure with the LeuT-fold (Schulze et al., 2010) (Yamashita et al., 2005) (Weyand et al., 2008) (Ressl et al., 2009) Schulze et al., 2010). The mobility and polarity data show furthermore that the two α-helical segments are involved to different extents in tertiary contacts and also exhibit different environmental polarities. The polarity profiles indicates the location of the N-terminal part (eL4a) in a more polar environment than the C-terminal part (eL4b) and the mobility profile for eL4a exhibits values for the inverse line width typical for a surface exposed label in an α-helical region, whereas eL4b seems to be more involved in tertiary contacts due to a closer contact to other protein components in PutP.

All room temperature spectra for PutP reveal the presence of two spectral components characterized by different mobilities. In order to investigate and verify the origin of the two spectral components, temperature-dependent (273 K to 303 K) cw X-band EPR measurements were carried out on different PutP variants in the absence of ligands. Lowering of the temperature leads to an increase of the immobile (i) component and a concomitant decrease of the mobile (m) component, thereby shifting the equilibrium between the two conformations. From the determination of this temperature dependency on the spectral

features compared to results obtained for LeuT (Kroncke et al., 2010) the ΔG values imply the idea that eL4 is involved in a protein conformational equilibrium at room temperature.

The cw EPR data obtained for PutP in the absence and presence of the ligands Na^+ and Na^+/proline further imply the idea of eL4 functioning as an external gate to the SSSF. The ligand-induced changes observed in mobility, polarity and accessibility upon substrate binding are small, but indicate significant structural alterations without large disturbance of secondary structure. Only two spin-label positions, where hydrophobic residues have been substitited, F314R1 and F310R1, demonstrate large substrate-dependent changes in mobility and polarity. A special case appears to be position F314, this residue exhibits low accessibility to both quencher molecules, O_2 and NiEDDA, and shows very low mobility and environmental polarity, indicating that this side chain is deeply buried in the protein interior. Careful inspection of the homology model and comparison to other transporter structure with the LeuT fold lead to the conclusion that Phe314 in eL4b of PutP anchors the loop in the core of the protein and is in hydrophobic contact with the extracellular terminus of cTM1 (Raba et al., 2014).

5.5 Bibliography

Abramson et al., 2003 — Abramson, J., Smirnova, I., Kasho, V., Verner, G., Kaback, H. R., and Iwata, S. (2003) Structure and mechanism of the lactose permease of *Escherichia coli*. *Science* **301**:610-615

Altenbach et al., 1989 — Altenbach, C., Flitsch, S.L., Khorana, H.G., and Hubbell, W.L. (1989) Structural studies on transmembrane proteins. 2. Spin labeling of bacteriorhodopsin mutants at unique cysteines. *Biochem.* **28**:7806–7812

Altenbach et al., 1990 — Altenbach, C., Marti, T., Khorana, H.G., and Hubbell, W.L. (1990) Transmembrane protein structure: spin labeling of bacteriorhodopsin mutants. *Science* **248**:1088–1092

Altenbach et al. 2005 — Altenbach, C., Froncisz, W., Hemker, R., McHaourab, H., and Hubbell, W. L. (2005) Accessibility of nitroxide side chains: absolute Heisenberg exchange rates from power saturation EPR. *Biophys. J.* **89**:2103–2112

Amann et al. 1988 — Amann, E., Ochs, B., and Abel, K. J. (1988) Tightly regulated tac promoter vectors useful for the expression of unfused and fused proteins in *Escherichia coli*. *Gene* **69**:301-315

Bayer et al., 1999 — Bayer, A. S., Coulter, S. N., Stover, C. K., and Schwan, W. R. (1999) Impact of the high-affinity proline permease gene (putP) on the virulence of Staphylococcus aureus in experimental endocarditis. *Infect. Immun.* **67**:740-744

Bordignon and Steinhoff, 2007 — Bordignon E., and Steinhoff, H.-J., *ESR spectroscopy in membrane biophysics*, in: M.A. Hemminga, L.J. Berliner (Eds.), Biological Magnetic Resonance, Vol. 27, Springer, Heidelberg, 2007, pp. 129–164

Catterall, 2010 — Catterall, W. A. (2010) Ion channel voltage sensors: structure, function, and pathophysiology. *Neuron* **67**:915-928

Chen et al., 1985 — Chen, C.C., Tsuchiya, T., Yamane, Y., Wood, J.M., and Wilson, T.H. (1985) Na^+ (Li^+)-proline cotransport in *Escherichia coli*. *J. Membrane. Biol.* **84**:157-164

Chen et al., 2007 — Chen, Y. J., Pornillos, O., Lieu, S., Ma, C., Chen, A. P., and Chang, G. (2007) X-ray structure of EmrE supports dual topology model. *Proc. Natl. Acad. Sci. U. S. A.* **104**:18999-19004

Claxton et al. 2010 — Claxton, D. P., Quick, M., Shi, L., de Carvalho, F. D., Weinstein, H., Javitch, J. A., and McHaourab, H. S., (2010) Ion/substrate-dependent conformational dynamics of a bacterial homolog of neurotrans-mitter:sodium symporters. *Nat. Struct. Mol. Biol.* **17**:822-829

Corringer et al., 2010 — Corringer, P. J., Baaden, M., Bocquet, N., Delarue, M. Dufresne, V., Nury, H., Prevost, M., Van Renterghem, C. (2010) Atomic structure and dynamics of pentameric ligand-gated ion channels: new insight from bacterial homologues. *J. Physiol.* **588**:565-572

Dutzler et al., 2002 — Dutzler, R., Campbell, E. B., Cadene, M., Chait, B. T., and MacKinnon R. (2002) X-ray structure of a ClC chloride channel at 3.0 Å reveals the molecular basis of anion selectivity. *Nature* **415**:287-294

Essen, 2002 — Essen, L. O. (2002) Halorhodopsin: light-driven ion pumping made simple? *Curr. Opin. Struct. Biol.* **12**:516-522

Faham et al. 2008 — Faham, S., Watanabe, A., Besserer, G. M., Cascio, D., Specht, A., Hirayama, B. A., Wright, E. M., and Abramson, J. (2008) The crystal structure of a sodium galactose transporter reveals mechanistic insights into Na^+/sugar symport. *Science* **321**:810-814

Forrest et al., 2008 — Forrest, L. R., Zhang, Y. W., Jacobs, M. T., Gesmonde, J., Xie, L., Honig, B. H., and Rudnick, G. (2008) Mechanism for alternating access in neurotransmitter transporters. *Proc. Natl. Acad. Sci. USA* **105**:10338-10343

Forrest and Rudnick, 2009 — Forrest, L. R., and Rudnick, G. (2009) The rocking bundle: a mechanism for ion-coupled solute flux by symmetrical transporters. *Physiology (Bethesda)* **24**:377-386

Grinius and Goldberg, 1994 — Grinius, L. L. and Goldberg, E. B. (1994) Bacterial multidrug resistance is due to a single membrane protein which functions as a drug pump. *J. Biol. Chem.* **269**:29998–30004

Guan and Kaback — Guan, L., and Kaback, H. R. (2006) Lessons from lactose permease. *Annu. Rev. Biophys. Biomol. Struct.* **35**:67-91

Guan et al., 2007 — Guan, L., Mirza, O., Verner, G., Iwata, S., and Kaback, H. R. (2007) Structural determination of wild-type lactose permease. *Proc. Natl. Acad. Sci. U. S. A.* **104**:15294-15298

Huang et al., 2003 — Huang, Y., Lemieux, M. J., Song, J., Auer, M., and Wang, D. N. (2003) Structure and mechanism of the glycerol-3-phosphate transporter from *Escherichia coli*. *Science* **301**:616-620

Hubbell and Altenbach, 1994 — Hubbell, W.L., and Altenbach C. (1994) Investigation of structure and dynamics in membrane proteins using site-directed spin labeling. *Curr. Opin. Struct. Biol.* **4**:566–573

Hubbell et al. 1996 — Hubbell, W. L., McHaourab, H. S., Altenbach, C., and Lietzow, M.A. (1996) Watching proteins move using site-directed spin labeling. *Structure* **4**:779-783

Hunte et al., 2005 — Hunte, C., Screpanti, E., Venturi, M., Rimon, A., Padan, E., and Michel, H. (2005) Structure of a Na^+/H^+ antiporter and insights into mechanism of action and regulation by pH. *Nature* **435**:1197-1202

Hilger et al. 2008 — Hilger, D., Böhm, M., Hackmann, A., Jung, H. (2008) Role of Ser-340 and Thr-341 in Transmembrane Domain IX of the Na^+/Proline Transporter PutP of Escherichia coli in Ligand Binding and Transport. *J. Biol. Chem.* **283**:4921-4929

Hilger et al. 2009 — Hilger, D,, Polyhach, Y., Jung, H., Jeschke, G. (2009) Backbone Structure of Transmembrane Domain IX of the Na^+/Proline Transporter PutP of *Escherichia coli. Biophys. J.* **96**:217-225

Hilger, 2010 — Hilger, D. PhD Thesis, (2010) Electron paramagnetic resonance spectroscopic analyses of membrane transport proteins, Fakultät für Biologie der Ludwig-Maximilians-Universität München

Isas et al., 2002 — Isas J, M., Langen R, Haigler H.T., Hubbell W.L. (2002) Structure and dynamics of a helical hairpin and loop region in annexin 12: a site-directed spin labeling study. *Biochem.* **41**:1464-1473.

Jardetzky, 1966 — Jardetzky, O. (1966) Simple allosteric model for membrane pumps. *Nature* **211**:969-970

Jeschke et al. 2006 — Jeschke, G., Chechik, V., Ionita, P., Godt, A., Zimmermann, H., Banham, J., Timmel, C. R., Hilger, D., and Jung, H. (2006) DeerAnalysis2006 - a comprehensive software package for analyzing pulsed ELDOR data. *Appl. Magn. Reson.* **30**:473-498

Jeschke et al., 2004 — Jeschke, G., Wegener, C., Nietschke, M., H. Jung and Steinhoff, H. J. (2004) Interresidual distance determination by four-pulse double electron-electron resonance in an integral membrane protein: the Na^+/proline transporter PutP of *Escherichia coli. Biophys J* **86**:2551-2557

Jung et al., 1998a — Jung, H., Rübenhagen, R., Tebbe, S., Leifker, K., Tholema, N., Quick, M., and Schmid, R. (1998) Topology of the Na^+/proline transporter of *Escherichia coli. J. Biol. Chem.* **273**:26400-26407

Jung et al., 1998b — Jung, H., Tebbe, S., Schmid, R., and Jung, K. (1998) Unidirectional reconstitution and characterization of purified Na^+/proline transporter of *Escherichia coli. Biochem.* **37**:11083-11088

Jung, 2001 — Jung, H. (2001) Towards the molecular mechanism of Na^+/solute symport in prokaryotes. *Biochim. Biophys. Acta* **1505**:131-143

Jung, 2002 — Jung, H. (2002) The sodium/substrate symporter family: structural and functional features. *FEBS Lett.* **529**:73-77

Jung et al., 2012 — Jung, H., Hilger, D., and Raba, M. (2012) The Na^+/L-proline transporter PutP. *Front. Biosci.* **17**:745-759

Junge et al., 1997 — Junge, W., Lill, H., and Engelbrecht, S. (1997) ATP synthase: an electrochemical transducer with rotatory mechanics. *Trends. Biochem. Sci.* **22**:420-423

Kavermann et al., 2003 — Kavermann, H., Burns, B. P., Angermuller, K., Odenbreit, S., Fischer, W., Melchers, K., and Haas, R. (2003) Identification and characterization of *Helicobacter pylori* genes essential for gastric colonization. *J. Exp. Med.* **197**:813-822

Klare and Steinhoff, 2009 Klare, J.P., and Steinhoff, H.-J. (2009) Spin labeling EPR. *Photosynth. Res.* **102**:377–390

Krishnamurthy and Gouaux, 2012 Krishnamurthy, H., and Gouaux, E. (2012) X-ray structures of LeuT in substrate-free outward-open and apo inward-open states. *Nature* **481**:469-474

Kroncke et al., 2010 Kroncke, B.M., Horanyi P.S., and Columbus L. (2010) Structural origins of nitroxide side chain dynamics on membrane protein α-helical sites. *Biochem.* **49**:10045–10060

Kung et al., 2010 Kung, C., Martinac, B., Sukharev, S. (2010) Mechanosensitive channels in microbes. *Annu. Rev. Microbiol.* **64**:313-329

Kühn, 2003 Kühn, M. (2003) Orientierung von Helix 9 in membrangebundenem colicin A untersucht mit ESR Spektroskopie and SDSL. PhD Thesis, Ruhr-Universität Bochum.

Langen et al. 2000 Langen, R., Oh, K. J., Cascio, D., and Hubbell, W. L. (2000) Crystal structures of spin labeled T4 lysozyme mutants: implications for the interpretation of EPR spectra in terms of structure. *Biochem.* **39**:8396-8405

Lanyi, 2006 Lanyi, J. K. (2006) Proton transfers in the bacteriorhodopsin photocycle. *Biochim. Biophys. Acta* **1757**:1012-1018

Maloney, 1994 Maloney, P. C. (1994) Bacterial transporters. *Curr. Opin. Struct. Biol.* **6**:571-582

Martin et al. 1998 Martin, R.E., Pannier, M., Diederich, F., Gramlich, V., Hubrich, M., and Spiess, H.W. (1998) Determination of End-to-End Distances in a Series of TEMPO Diradicals of up to 2.8 nm Length with a New Four-Pulse Double Electron Electron Resonance Experiment. *Angew. Chem. Int. Ed.* **37**:2833-2837

Mchaourab et al., 1996 Mchaourab H.S., Lietzow M.A., Hideg K., Hubbell, W.L. (1996) Motion of spin-labeled side chains in T4 lysozyme. Correlation with protein structure and dynamics. *Biochem.* **35**:7692-7704

Mitchell et al. 2004 Mitchell, S. M., Lee, E., Garcia, M. L., and Stephan, M. M. (2004) Structure and function of extracellular loop 4 of the serotonin transporter as revealed by cysteine-scanning mutagenesis. *J. Biol. Chem.* **279**:24089-24099

Mitchell, 1991 Mitchell, P. (1991) Foundations of vectorial metabolism and osmochemistry. *Biosci. Rep.* **11**:297-344

Muchmore et al., 1996 Muchmore S.W., Sattler M., Liang H., Meadows, R.P., Harlan, J.E., Yoon, H.S., Nettesheim, D., Chang, B.S., Thompson, C.B., Wong, S.L., Ng, S.L., Fesik, S.W. (1996) X-ray and NMR structure of human Bcl-xL, an inhibitor of programmed cell death. *Nature* **381**:335-41

Mueckler, 1994 Mueckler, M. (1994) Facilitative glucose transporters. *Eur. J. Biochem.* **219**:713-725

Murukami et al., 2002 — Murakami, S., Nakashima, R., Yamashita, E., and Yamaguchi, A. (2002) Crystal structure of bacterial multidrug efflux transporter AcrB. *Nature* **419**:587-593

Olkhova et al., 2010 — Olkhova, E., Raba, M., Bracher, S., Hilger, D., and Jung, H. (2010) Homology Model of the Na^+/Proline Transporter PutP of *Escherichia coli* and Its Functional Implications. *J. Mol. Biol.* **406**:59-74

Padan et al., 2004 — Padan, E., Tzubery, T., Herz, K., Kozachkov, L., Rimon, A., and Galili L. (2004) NhaA of *Escherichia coli*, as a model of a pH-regulated Na^+/H^+ antiporter. *Biochim. Biophys. Acta* **1658**:2-13

Pannier et al. 2000 — Pannier, M., Veit, S., Godt, A., Jeschke, G., and Spiess, H.W. (2000) Dead-time free measurement of dipole-dipole interactions between electron spins. *J. Magn. Reson.* **142**:331–340

Paulsen et al., 1996 — Paulsen, I. T., Skurray, R. A., Tam, R., Saier, M. H., Jr, Turner, R. J., Weiner, J. H. et al. (1996). The SMR family: a novel family of multidrug efflux proteins involved with the efflux of lipophilic drugs. *Mol. Microbiol.* **19**:1167–1175

Pebay-Peyroula et al., 2003 — Pebay-Peyroula, E., Dahout-Gonzalez, C., Kahn, R., Trézéguet, V., Lauquin, G. J., and Brandolin, G. (2003) Structure of mitochondrial ADP/ATP carrier in complex with carboxyatractyloside. *Nature* **426**:39-44

Pfeiffer et al., 1999 — Pfeiffer, M., Rink, T., Gerwert, K., Oesterhelt, D., and Steinhoff, H.J. (1999) Site-directed spinlabeling reveals the orientation of the amino acid side-chains in the E–F loop of bacteriorhodopsin. *J. Mol. Biol.* **287**:163–171

Pirch et al., 2003 — Pirch, T., Landmeier, S., and Jung, H. (2003) Transmembrane domain II of the Na^+/proline transporter PutP of Escherichia coli forms part of a conformationally flexible, cytoplasmic exposed aqueous cavity within the membrane. *J. Biol. Chem.* **278**:42942-42949

Pirch et al., 2002 — Pirch, T., Quick, M., Nietschke, M., Langkamp, M., and Jung, H. (2002) Sites important for Na^+ and substrate binding in the Na^+/proline transporter of Escherichia coli, a member of the Na+/solute symporter family. *J .Biol. Chem.* **277**:8790-8796

Plato et al., 2002 — Plato, M., Steinhoff, H.-J., Wegener, C., Törring, J. T., Savitsky, A., and Möbius, K. (2002) Molecular orbital study of polarity and hydrogen bonding effects on the g and hyperfine tensors of site directed NO spin labeled bacteriorhodopsin. *Mol. Phys.* **100**:3711–3721

Quick et al., 1996 — Quick, M., Tebbe, S. and Jung, H. (1996) Ser57 in the Na^+/proline permease of Escherichia coli is critical for high-affinity proline uptake. *Eur. J. Biochem.* **239**:732-736

Quick et al., 1999 — Quick, M., Stolting, S., and Jung, H. (1999) Role of conserved Arg40 and Arg117 in the Na^+/proline transporter of Escherichia coli. *Biochem.* **38**:13523-13529

Quick and Jung, 1997 — Quick, M. and Jung, H. (1997) Aspartate 55 in the Na^+/proline permease of *Escherichia coli* is essential for Na^+-coupled proline uptake. *Biochem.* **36**:4631-4636

Quick and Jung, 1998 — Quick, M., and Jung, H. (1998) A conserved aspartate residue, Asp187, is important for Na^+- dependent proline binding and transport by the Na^+/proline transporter of Escherichia coli. *Biochem.* **37**:13800-13806

Raba, 2012 — Raba, M., PhD Thesis (2012) Sites involved in ligand binding and translocation in the Na^+/proline symporter PutP of *Escherichia coli*. Fakultät für Biologie der Ludwig-Maximilians-Universität München

Raba et al., 2014 — Raba M., Dunkel, S., Hilger, D., Lipiszko, K., Polyhach, Y., Jeschke, G., Bracher, S., Quick M., Klare· J.P., Jung H., and Steinhoff H.-J. (2014) Extracellular loop 4 of the proline transporter PutP controls the periplasmic entrance to ligand binding sites. *Structure* **22**:769-780

Reed-Tsur et al., 2008 — Reed-Tsur, M. D., De la Vieja, A., Ginter, C. S., and Carrasco, N. (2008) Molecular characterization of V59E NIS, a Na^+/I^- symporter mutant that causes congenital I- transport defect. *Endocrinology* **149**:3077-3084

Ressl et al., 2009 — Ressl, S., Terwisscha van Scheltinga, A. C., Vonrhein, C., Ott, V., and Ziegler, C. (2009) Molecular basis of transport and regulation in the $Na^{(+)}$/betaine symporter BetP. *Nature* **458**:47-52

Saier, 1999 — Saier, M. H. Jr. (1999) Classification of transmembrane transport proteins in living organisms. In *Biomembrane Transport* (VanWinkle, L., ed.) pp. 265-276, *Academic Press*, San Diego, CA.

Shimamura et al., 2010 — Shimamura, T., Weyand, S., Beckstein, O., Rutherford, N. G., Hadden, J. M., Sharples, D., Sansom, M. S., Iwata, S., Henderson, P. J., and Cameron, A. D. (2010) Molecular basis of alternating access membrane transport by the sodium-hydantoin transporter Mhp1. *Science* **328**:470-473

Schulze et al., 2010 — Schulze, S., Koster, S., Geldmacher, U., Terwisscha van Scheltinga, A. C., and Kühlbrandt, W. (2010) Structural basis of $Na^{(+)}$-independent and cooperative substrate/product antiport in CaiT. *Nature* **467**:233-236

Stalmach et al. 1983 — Stalmach, M. E., Grothe, S., and Wood, J. M. (1983) Two proline porters in *Escherichia coli* K-12. *J. Bacteriol.* **156**:481-486

Steinhoff et al., 1997 — Steinhoff, H.-J., Radzwill, N., Thevis, W., Lenz, V., Brandenburg, D., Antson, A., Dodson, G.G., and Wollmer, A. (1997) Determination of interspin distances between spin labels attached to insulin: comparison of electron paramagnetic resonance data with the X- ray structure. *Biophys. J.* **73**:3287–3298

Steinhoff et al., 2000 — Steinhoff, H.-J., Savitsky, A., Wegener, C., Pfeiffer, M., Plato, M., and Möbius, K. (2000) High-field EPR studies of the structure and conformational changes of site-directed spin labeled bacteriorhodopsin. *Biochim. Biophys. Acta* **1457**:253–262

Watanabe et al. 2010 — Watanabe, A., Choe, S., Chaptal, V., Rosenberg, J.M., Wright, E.M., Grabe, M., and Abramson, J. (2010) The mechanism of sodium and substrate release from the binding pocket of vSGLT. *Nature* **468**:988-991

Weisser et al., 1995 — Weisser, P., Kramer, R., Sahm, H., and Sprenger, G. A. (1995) Functional expression of the glucose transporter of Zymomonas mobilis leads to restoration of glucose and fructose uptake in Escherichia coli mutants and provides evidence for its facilitator action. *J. Bacteriol.* **177**:3351-3354

West, 1997 — West, I. C. (1997) Ligand conduction and the gated-pore mechanism of transmembrane transport. *Biochim. Biophys. Acta* **1331**:213-234

Wegener et al. 2000 — Wegener, C., Tebbe, S., Steinhoff, H.-J., and Jung, H., (2000) Spin labeling analysis of structure and dynamics of the Na^+/proline transporter of Escherichia coli. *Biochem.* **39**:4831-4837

Wegener et al., 2001 — Wegener, A.A., Klare, J.P., Engelhard, M., and Steinhoff, H.J. (2001) Structural insights into the early steps of receptor–transducer signal transfer in archaeal phototaxis. *EMBO J.* **20**:5312–5319

Weyand et al., 2008 — Weyand, S., Shimamura, T., Yajima, S., Suzuki, S., Mirza, O., Krusong, K., Carpenter, E. P., Rutherford, N. G., Hadden, J. M., O'Reilly, J., Ma, P., Saidijam, M., Patching, S. G., Hope, R. J., Norbertczak, H. T., Roach, P. C., Iwata, S., Henderson, P. J., and Cameron, A. D. (2008) Structure and molecular mechanism of a nucleobase-cation-symport-1 family transporter. *Science* **322**:709-713

Wright et al., 2007 — Wright, E. M., Hirayama, B.A., and Loo, D. F. (2007) Active sugar transport in health and disease. *J. Intern. Med.* **261**:32-43

Yamato, 1992 — Yamato, I. (1992) Ordered binding model as a general mechanistic mechanism for secondary active transport systems. *FEBS Lett.* **298**:1-5

Yamato and Anraku, 1993 — Yamato, I., and Anraku, Y. (1993) Alkali Cation Transport Systems in Prokaryotes. E.P. Bakker (ed), Boca Raton, FL: CRC Press, pg. 464

Yamashita et al., 2005 — Yamashita, A., Singh, S. K., Kawate, T., Jin, Y., and Gouaux, E. (2005) Crystal structure of a bacterial homologue of Na^+/Cl^--dependent neurotransmitter transporters. *Nature* **437**:215-223

Yin et al., 2006 — Yin, Y., He, X., Szewczyk, P., Nguyen, T., and Chang, G. (2006) Structure of the multidrug transporter EmrD from *Escherichia coli*. *Science* **312**:741-744

Yernool et al., 2004 — Yernool, D., Boudker, O., Jin, Y. and Gouaux, E. (2004) Structure of a glutamate transporter homologue from *Pyrococcus horikoshii*. *Nature* **431**:811-818

Zomot and Kanner, 2003 — Zomot E., and Kanner B.I. (2003) The interaction of the gamma-aminobutyric acid transporter GAT-1 with the neurotransmitter is selectively impaired by sulfhydryl modification of a conformationally sensitive cysteine residue engineered into extracellular loop IV. *J. Biol. Chem.* **278**:42950-42958

6. Acknowledgements

First of all I would like to thank my supervisor Prof. Dr. Heinz-Jürgen Steinhoff for giving me the opportunity to work on this fascinating biophysical project. I am deeply grateful for his encouragement and support, guidance and excellent advice throughout this study. I would like to express my sincere gratitude for the trust he has put in me and it is a pleasure to be part of your group.

My sincere thanks also go to Prof. Dr. Dr. Heinrich Jung for his willingness to provide the second opinion. With this I would like to thank my collaborators Prof. Dr. Dr. Heinrich Jung and Dr. Michael Raba for the opportunity for this great and interesting cooperation project.

My special gratitude to Dr. Johann Klare for being my tutor during the last years. Your motivation, multiple help, advice and wide knowledge was an immense help for me. I incredibly thank you for lots of discussion and for starting measurements on weekend morning hours. I am indebted to you for everything.

I would like to extend my thanks to each member of our working-group. Thanks for the great help and many, not only subject-specific, discussions and the familiar atmosphere. Especially, I am very thankful to Marion Landsberg. I am indeed thankful to my „first" office colleagues: Christoph for helping me with the first very confusing EPR measurements and the amusing smoking sessions. Micha, Vitali and Dorith for kindly help and answering all my questions, as especially for the tremendously funny moments in and outside of the lab. Thank you a lot for these special atmosphere and plenty of fun.

I dedicate many thanks to all my friends for their encouragement and moral support and ensure that they have put up with me even in hard times. Friendship needs no words, thank you.

An dieser Stelle ein riesengroßes Dankeschön an meinen Mann Carsten der mir immer Rückhalt bot and mich trotzt all meiner Launen mit großer Geduld ertragen and unterstützt hat. Worte können dies kaum beschreiben. Danke für Deine jahrelange and liebevolle Unterstützung, für Deine Geduld and Fürsorge. Zu guter Letzt möchte ich meiner gesamten Familie danken, insbesondere meinen Eltern, ohne die diese Arbeit nicht möglich gewesen wäre. Danke für Eure Unterstützung und für die stete Hilfsbereitschaft in allen Lebenslagen. Danke Ihr seid die Besten.

7. Declaration

I declare that the submitted work has been completed by me the undersigned and that I have not used any other than permitted reference sources or materials. All references and other sources used by me have been appropriately acknowledged in the work. I further declare that this work has not been submitted for the purpose of academic examination, either in its original or similar form, anywhere else.

Osnabrück, Germany

Sabrina Dunkel